UNIVERSITY OF THESSALY
SCHOOL OF ENGINEERING
DEPARTMENT OF MECHANICAL ENGINEERING

STRUCTURAL DYNAMICS LABORATORY

# DESIGN OPTIMIZATION OF STRUCTURES SUBJECTED TO STOCHASTIC EXCITATIONS

Thesis by

KYRIAKOS K. PERROS

Diploma in Mechanical Engineering, University of Thessaly, 2004

M.Sc. in Mechanical Engineering, University of Thessaly, 2009

In partial fulfillment of the requirements

for the degree of

Doctor of Philosophy

**2010**

ΠΑΝΕΠΙΣΤΗΜΙΟ ΘΕΣΣΑΛΙΑΣ
ΠΟΛΥΤΕΧΝΙΚΗ ΣΧΟΛΗ
ΤΜΗΜΑ ΜΗΧΑΝΟΛΟΓΩΝ ΜΗΧΑΝΙΚΩΝ

ΕΡΓΑΣΤΗΡΙΟ ΔΥΝΑΜΙΚΗΣ ΣΥΣΤΗΜΑΤΩΝ

# ΒΕΛΤΙΣΤΟΣ ΣΧΕΔΙΑΣΜΟΣ ΚΑΤΑΣΚΕΥΩΝ ΥΠΟΒΑΛΛΟΜΕΝΩΝ ΣΕ ΣΤΟΧΑΣΤΙΚΕΣ ΔΙΕΓΕΡΣΕΙΣ

Διδακτορική Διατριβή

ΚΥΡΙΑΚΟΣ Κ. ΠΕΡΡΟΣ

Διπλωματούχου Μηχανολόγου Μηχανικού, Π.Θ., 2004
Μ.Δ.Ε. Μηχανολόγου Μηχανικού, Π.Θ., 2009

Υπεβλήθη για την εκπλήρωση μέρους των
απαιτήσεων για την απόκτηση του
Διδακτορικού Διπλώματος

**2010**



Η παρούσα διδακτορική διατριβή συγχρηματοδοτήθηκε κατά:

- 75% της Δημόσιας Δαπάνης από την Ευρωπαϊκή Ένωση - Ευρωπαϊκό Κοινωνικό Ταμείο
- 25% της Δημόσιας Δαπάνης από το Ελληνικό Δημόσιο

  Υπουργείο Ανάπτυξης - Γενική Γραμματεία Έρευνας και Τεχνολογίας
- και από τον Ιδιωτικό Τομέα

στο πλαίσιο του Μέτρου 8.3 του Ε.Π. Ανταγωνιστικότητα - Γ' Κοινοτικό Πλαίσιο Στήριξης.



This research is part of the 03-ED-524 project, implemented within the framework of the "Reinforcement Programme of Human Research Manpower" (PENED) and co-financed 25% from the Greek Ministry of Development (General Secretariat of Research and Technology), 75% from E.U. (European Social Fund) and the private sector, in the context of measure 8.3 of the Operational Program Competitiveness (3rd Community Support Framework Program).

Η έγκριση της διδακτορικής διατριβής από το Τμήμα Μηχανολόγων Μηχανικών Βιομηχανίας της Πολυτεχνικής Σχολής του Πανεπιστημίου Θεσσαλίας δεν υποδηλώνει αποδοχή των απόψεων του συγγραφέα (Ν. 5343/32 αρ. 202 παρ. 2).

**Εγκρίθηκε από τα Μέλη της Επταμελούς Εξεταστικής Επιτροπής:**

| | |
|---|---|
| Πρώτος Εξεταστής (Επιβλέπων) | Δρ. Κώστας Παπαδημητρίου<br>Καθηγητής, Τμήμα Μηχανολόγων Μηχανικών<br>Πανεπιστήμιο Θεσσαλίας |
| Δεύτερος Εξεταστής | Δρ. Νικόλαος Αράβας<br>Καθηγητής, Τμήμα Μηχανολόγων Μηχανικών,<br>Πανεπιστήμιο Θεσσαλίας |
| Τρίτος Εξεταστής | Δρ. Σωτήριος Νατσιάβας<br>Καθηγητής, Τμήμα Μηχανολόγων Μηχανικών<br>Αριστοτέλειο Πανεπιστήμιο Θεσσαλονίκης |
| Τέταρτος Εξεταστής | Δρ. Αλέξιος Κερμανίδης<br>Λέκτορας, Τμήμα Μηχανολόγων Μηχανικών,<br>Πανεπιστήμιο Θεσσαλίας |
| Πέμπτος Εξεταστής | Δρ. Αναστάσιος Σταμάτης<br>Επίκουρος Καθηγητής, Τμήμα Μηχανολόγων Μηχανικών,<br>Πανεπιστήμιο Θεσσαλίας |
| Έκτος Εξεταστής | Δρ. Νικόλαος Πελεκάσης<br>Αναπληρωτής Καθηγητής, Τμήμα Μηχανολόγων<br>Μηχανικών, Πανεπιστήμιο Θεσσαλίας |
| Έβδομος Εξεταστής | Δρ. Παναγιώτης Τσόπελας<br>Αναπληρωτής Καθηγητής, Τμήμα Πολιτικών Μηχανικών,<br>Πανεπιστήμιο Θεσσαλίας |

# Ευχαριστίες

Η παρούσα διδακτορική διατριβή εκπονήθηκε στο Εργαστήριο Δυναμικής Συστημάτων του τμήματος Μηχανολόγων Μηχανικών στο Πανεπιστήμιο Θεσσαλίας.

Πρώτα απ' όλα, θα ήθελα να ευχαριστήσω τον επιβλέποντα της διατριβής μου, Καθηγητή κ. Κώστα Παπαδημητρίου, για την πολύτιμη βοήθεια και καθοδήγησή του κατά τη διάρκεια της διδακτορικής μου διατριβής. Επίσης, ευχαριστώ τα υπόλοιπα μέλη της τριμελούς συμβουλευτικής επιτροπής της διδακτορικής διατριβής μου, Καθηγητές κκ. Νικόλαο Αράβα και Σωτήρη Νατσιάβα, καθώς και τα υπόλοιπα μέλη της επταμελούς επιτροπής για την προσεκτική ανάγνωση της εργασίας μου και για τις πολύτιμες υποδείξεις τους. Ευχαριστίες οφείλω σε όλους τους μεταπτυχιακούς και προπτυχιακούς φίλους και φοιτητές του Εργαστηρίου Δυναμικής Συστημάτων για την άριστη συνεργασία που είχαμε κατά τη διάρκεια της εκπόνησης της παρούσας διδακτορικής διατριβής.

Πάνω απ' όλα, είμαι ευγνώμων στους γονείς μου, Κωνσταντίνο και Αικατερίνη Πέρρου, για την ολόψυχη αγάπη και υποστήριξή τους όλα αυτά τα χρόνια. Αφιερώνω αυτή την διατριβή στην μητέρα μου και στον πατέρα μου.

Κυριάκος Πέρρος

*Στους γονείς μου,*

*Κωνσταντίνο και Αικατερίνη*

## SUMMARY

This thesis focuses on the optimal design of structures under the influence of stochastic dynamic loads, with applications to the sizing and topology optimization of truss structures. Furthermore, the study investigates the fatigue lifetime prediction of structures under stochastic dynamic loading. Finally, the design optimization framework is extended to incorporate performance functions related to fatigue lifetime of structures subject to stochastic dynamic loading.

Specifically, an innovative methodology for optimizing structures under stochastic dynamic excitations is proposed. The objective function related to the performance of the structure is constructed as a weighted sum of the variance of the structural response quantities of interest. Such response quantities are selected to be the displacements at the nodes of the system, stresses or strains developed in the structural parts, drift ratios etc. The excitations are modeled by white noise or filtered white noise processes. The variance of the response quantities are very efficiently estimated by solving the Lyapunov equation for the system. The adjoint method is developed to analytically estimate the sensitivities of the objective function with respect to the design parameters. This substantially increases the computational efficiency of the proposed methodology. The required computational effort for estimating the derivatives of the objective function is shown to be independent of the number of the design variables. Furthermore, the proposed methodology is extended to handle in the optimization the formulation of the response in the modal space. This exploits the benefits of using limited number of modes for the estimation of the system response

The proposed design optimization of dynamic systems is applied for addressing the problem of size and topology optimization of truss structures. A specific class of two dimensional truss structure subject to Gaussian white noise excitation is considered to demonstrate the theoretical developments. Using different types of performance functions, such as the weighted sum of the nodal displacements and the weighted sum of the stresses developed in the truss members, the structures is optimized in size and topology in order to find the optimal configuration that optimizes the performance. The results are compared to available design optimization results of the truss structures subject to deterministic static loading. The analysis in modal space is also applied on the truss structure, in order to explore the effect of using limited number of contributing modes in the estimation of the response and finally investigate their effect on optimal design.

A novel methodology for the fatigue reliability assessment of randomly vibrating multi-degree of freedom systems is also proposed within the coupled response-degradation model. The fatigue process in the system components is quantified by the fatigue crack growth equations which - via the stress range - are coupled with the system response. Simultaneously, the system dynamics are affected by the fatigue process through its stiffness degradation, so that it provides the actual stress values to the fatigue crack growth equation. In addition to the general coupled response-degradation analysis, its special case of non-coupled fatigue crack growth is treated as well, for the wide-band stationary applied stress by the use of its first four spectral moments and the approximate, empirically motivated, Dirlik's probability distribution for the stress range. The proposed methodology is applied on multi degree of freedom spring mass chain like structure and the results for the different approaches are compared. Both, the general analysis and the illustrating examples elaborated provide the route to the fatigue reliability estimation in complex–hierarchical vibratory systems under random loading.

Finally, the proposed methodologies for optimal design and fatigue lifetime prediction for structure subjected to stochastic dynamic excitations are combined, in order to form an innovative framework for design optimization of structures based on fatigue lifetime related performance function. In particular, the performance function for the optimization problem is defined as the weighted sum of the fatigue lifetimes of the structural parts. The adjoint method is extended to handle the new performance function for the computationally efficient and accurate estimation of the sensitivities of the objective function with respect to the design variables. The proposed methodology is applied for addressing the problem of size and topology optimization of truss structures subjected to stochastic dynamic loads. The optimal configurations obtained are compared to the results of the design optimization based on displacement and stress related performance functions. Similarities and differences between the fatigue-based and stress-based performance functions are discussed.

## Περιληψη

Η παρούσα διδακτορική διατριβή επικεντρώνεται στο βέλτιστο σχεδιασμό κατασκευών υπό την επιρροή στοχαστικών δυναμικών φορτίων, με εφαρμογές στη βελτιστοποίηση της τοπολογίας δικτυωμάτων και των διαστάσεων των διατομών των μελών. Επιπλέον, μελετάται η πρόβλεψη της διάρκειας ζωής κατασκευών σε κόπωση υπό στοχαστικές δυναμικές διεγέρσεις. Τέλος, η μεθοδολογία βέλτιστου σχεδιασμού κατασκευών επεκτείνεται για να ενσωματώσει συναρτήσεις απόδοσης που σχετίζονται με τη μέγιστη διάρκεια ζωής κατασκευών σε κόπωση, υποβαλλόμενων σε στοχαστικές δυναμικές φορτίσεις.

Συγκεκριμένα, προτείνεται μια καινοτόμα μεθοδολογία για τη βελτιστοποίηση κατασκευών που υποβάλλονται σε στοχαστικές δυναμικές διεγέρσεις. Η αντικειμενική συνάρτηση σχετιζόμενη με την απόδοση της κατασκευής επιλέγεται ως ένα σταθμισμένο άθροισμα της μεταβλητότητας της απόκρισης. Σαν αποκρίσεις θεωρούνται οι μετατοπίσεις των κόμβων του συστήματος, οι τάσεις και οι παραμορφώσεις που αναπτύσσονται στο δομικά στοιχεία. Οι διεγέρσεις μοντελοποιούνται σαν λευκός θόρυβος ή σαν φιλτραρισμένος λευκός θόρυβος. Η μεταβλητότητα των αποκρίσεων υπολογίζεται πολύ αποτελεσματικά μέσω της επίλυσης της εξίσωσης Lyapunov για το σύστημα. Η μέθοδος adjoint αναπτύσσεται για τον αναλυτικό υπολογισμό των παραγώγων της αντικειμενικής συνάρτησης ως προς τις παραμέτρους σχεδιασμού. Αυτό αυξάνει την υπολογιστική αποτελεσματικότητα της προτεινόμενης μεθοδολογίας. Αποδεικνύεται ότι η απαιτούμενη υπολογιστική ισχύς για την εκτίμηση των παραγώγων της αντικειμενικής συνάρτησης είναι ανεξάρτητη από τον αριθμό των σχεδιαστικών παραμέτρων. Επιπλέον, η προτεινόμενη μεθοδολογία επεκτείνεται ώστε να διαχειρίζεται τον υπολογισμό της απόκρισης των κατασκευών στον χώρο των ιδιομορφικών συντεταγμένων. Έτσι αξιοποιούνται τα οφέλη από τη χρήση περιορισμένου αριθμού ιδιομορφών για την εκτίμηση της απόκρισης του συστήματος.

Η προτεινόμενη μεθοδολογία για την βελτιστοποίηση του σχεδιασμού δυναμικών συστημάτων εφαρμόζεται στη βελτιστοποίηση της τοπολογίας δικτυωμάτων και των διαστάσεων των διατομών των μελών χρησιμοποιείται για την επίδειξη των θεωρητικών μελετών. Συγκεκριμένα μια ειδική κατηγορία διδιάστατων δικτυωμάτων, υποβαλλόμενων σε Γκαουσσιανό λευκό θόρυβο. Χρησιμοποιώντας διαφορετικούς τύπους συναρτήσεων απόδοσης, όπως είναι το σταθμισμένο άθροισμα των μετατοπίσεων στους κόμβους και το σταθμισμένο άθροισμα των τάσεων που αναπτύσσονται στα στοιχεία, οι κατασκευή βελτιστοποιείται σε μέγεθος και τοπολογικά προκειμένου να βρεθεί η βέλτιστη διάταξη, ώστε να βελτιστοποιείται η συνάρτηση απόδοσης. Τα αποτελέσματα συγκρίνονται με διαθέσιμα αποτελέσματα βελτιστοποίησης του σχεδιασμού των δικτυωμάτων

υποβαλλόμενων σε ντετερμινιστικά στατικά φορτία. Η ιδιομορφική ανάλυση επίσης εφαρμόζεται στη βελτιστοποίηση της ειδικής κατηγορίας δικτυωμάτων, προκειμένου να διερευνηθεί η επίδραση της χρήσης περιορισμένου αριθμού ιδιομορφών που συνεισφέρουν στην εκτίμηση της απόκρισης του συστήματος και τέλος διερευνάται η επιρροή στον βέλτιστο σχεδιασμό.

Προτείνεται επίσης μια μεθοδολογία για την εκτίμηση της διάρκειας ζωής κατασκευών πολλών βαθμών ελευθερίας σε κόπωση, υπό στοχαστικές δυναμικές διεγέρσεις, λαμβάνοντας υπόψιν την σχέση απόκρισης – υποβάθμισης των κατασκευών. Η διαδικασία της κόπωσης στα κατασκευαστικά μέρη ποσοτικοποιείται μέσω των εξισώσεων ανάπτυξης των ρωγμών οι οποίες - μέσω του φάσματος των τάσεων - είναι συζευγμένες με την απόκριση του συστήματος. Ταυτόχρονα, η δυναμική του συστήματος επηρεάζεται από την διαδικασία της κόπωσης, μέσω της υποβάθμισης της ακαμψίας του, ώστε να παρέχονται οι πραγματικές τιμές των τάσεων στην εξίσωση ανάπτυξης της ρωγμής. Επιπρόσθετα με τη συζευγμένη γενική ανάλυση απόκρισης-υποβάθμισης, η ειδική περίπτωση της μη συζευγμένης ανάπτυξης ρωγμής αντιμετωπίζεται επίσης, για στάσιμες, ευρέως φάσματος τάσεις, με τη χρήση των πρώτων τεσσάρων φασματικών ροπών, και της προσεγγιστικής, εμπειρικής κατανομής πιθανοτήτων του Dirlik για το εύρος των τάσεων. Η προτεινόμενη μεθοδολογία εφαρμόζεται σε συστήματα πολλών βαθμών ελευθερίας και τα αποτελέσματα για τις διαφορετικές προσεγγίσεις συγκρίνονται μεταξύ τους. Τόσο η γενική ανάλυση, όσο και τα παραδείγματα που παρουσιάζονται, παρέχουν ένα πλαίσιο για την εκτίμηση της αξιοπιστίας κατασκευών σε κόπωση για πιο πολύπλοκες κατασκευές υπό στοχαστικά δυναμικά φορτία.

Τέλος, οι προτεινόμενες μεθοδολογίες για το βέλτιστο σχεδιασμό και την εκτίμηση της διάρκειας ζωής σε κόπωση για τα συστήματα υποβαλλόμενα σε στοχαστικές δυναμικές διεγέρσεις συνδυάζονται για να διαμορφωθεί ένα καινοτόμο πλαίσιο για τη βελτιστοποίηση του σχεδιασμού των κατασκευών για τη μέγιστη διάρκεια ζωής σε κόπωση υπό την επιρροή αβεβαιοτήτων. Η συνάρτηση απόδοσης για το πρόβλημα βελτιστοποίησης ορίζεται ως το σταθμισμένο άθροισμα της διάρκεια ζωής των δομικών στοιχείων σε κόπωση. Η μέθοδος adjoint επεκτείνεται ώστε να διαχειρίζεται την υπολογιστικά αποτελεσματική εκτίμηση των παραγώγων της αντικειμενικής συνάρτησης ως προς τις μεταβλητές σχεδιασμού. Η προτεινόμενη μεθοδολογία εφαρμόζεται στη βελτιστοποίηση της τοπολογίας δικτυωμάτων και των διαστάσεων των διατομών των μελών, υποβαλλόμενων σε στοχαστικά δυναμικά φορτία. Οι βέλτιστες δομές που αποκτήθηκαν συγκρίνονται με τα αποτελέσματα της βελτιστοποίησης του σχεδιασμού βασισμένου σε συναρτήσεις απόδοσης σχετιζόμενες με μετατοπίσεις ή τάσεις. Ομοιότητες και διαφορές μεταξύ των συναρτήσεων απόδοσης βασισμένες σε κόπωση και τάσεις αναλύονται.

# LIST OF CONTENTS

## LIST OF FIGURES

## LIST OF TABLES

# CHAPTER 1 Introduction

## 1.1 Research Context

### 1.1.1 Design Optimization of Structures

Design optimization of structures is a powerful tool for discovering new solutions for engineering problems. This tool can be used to optimize the size and/or the shape of a structure, which is subjected to different kinds of loads and support boundary conditions, within a given domain.

In engineering design, the knowledge about a planned system is never complete and it is not known in advance which design will lead to the optimal performance. Therefore, it is desirable to optimize the performance measure over the space of design variables that define the set of acceptable designs. Additionally, modeling uncertainty arises because no mathematical model can capture perfectly the behavior of a real system and its environment. In practice, a model is used that is most likely to adequately represent the behavior of the system, as well as its imposed excitation. However, there is always uncertainty about which values of the model parameters will give the best representation of the system, so this uncertainty of the parameters should be quantified. Furthermore, whatever model is chosen, there will always be an uncertain prediction error between the model and system responses. For an efficient engineering design, all these uncertainties,

associated with future excitation events, as well as the modeling of the system, must be explicitly accounted for.

Consequently, in modern research, it is widely accepted that the analysis of structures for structural safety and security should be based on stochastic dynamic methods, because they provide the desired accuracy of predicting the construction and security against different limit states such as direct functionality, crash prevention and total dynamic instability. It is also gradually recognized that the safety of construction is best valued using a stochastic (probabilistic) approach. Therefore, the stochastic system design is the most logical approach to planning, but implementation has been limited by the fact that the computational time required is prohibitively large.

### 1.1.2 Topology Optimization

Computer aided topology optimization of structures is a relatively new but rapidly expanding field of structural mechanics. Topology optimization is used in an increasing rate by, for example the car, machine and aerospace industries as well as in materials, mechanism and Micro Electro Mechanical Systems (MEMS) design. The reason for this is that it often achieves greater savings and design improvements than shape optimization.

The topology optimization problem solves the basic engineering problem of distributing a limited amount of material in a design space, where a certain objective function has to be optimized. The research in the structural topology optimization field is mainly focused on the solution of the determinist static case (Bendsoe and Sigmund 2002, Sigmund 1997, Bendsoe and Kikuchi 1988, Zhou and Rozvany 1991, Rozvany et. al. 1992, Sigmund and Petersson 1998, Xie and Steven 1993 and 1997, Wang et. al. 2003, Yang et. al. 1999), neglecting the dynamics and uncertainty which stems from the nature of the structure and the imposed excitation. A common objective in static problems is to minimize the compliance of the system (maximum global stiffness).

In the topology optimization of dynamic systems, the objective is usually related to eigenvalue optimization (Tenek and Hagiwara, 1994, Ma et. al., 1995, Kosaka and Swan, 1999, Pedersen, 2000, Du and Olhoff, 2007, Xie and Steven, 1997, Zhao et. al. 1997, Yang et. al. 1999). These problems are relevant for the design of machines and structures which are subjected to a dynamic load. A possible motivation for this type of problems is, for example, to keep the eigenfrequency of a structure away from the driving frequency of an attached vibrating machine with a given frequency of vibration. A common objective in dynamic topology

optimization is to maximize the fundamental eigenfrequency, for example to shift the fundamental eigenfrequency away from certain disturbing frequencies. Moreover, structures with a high fundamental frequency tend to be reasonable stiff for static loads.

### 1.1.3 Stochastic Fatigue Prediction

In the last years an increasing amount of research efforts has been directed towards stochastic modeling of various deterioration (or degradation) processes in mechanical/structural components. Because of the practical importance of fatigue damage and fracture in various engineering structures, stochastic models of fatigue accumulation have been a subject of special interest (Sobczyk and Spencer 1992 and references therein). It should be underlined, however that though the fatigue process is inherently associated with vibrations of mechanical/structural systems, the research in random vibration theory and in modeling of fatigue has been conducted without a proper mutual coupling. Stochastic analysis of dynamics of mechanical/structural systems has been focused on the characterization of the response (and its unsafe states, e.g. instability regions, first-passage probabilities), whereas the analysis of fatigue deterioration has been concentrated on the fatigue crack growth analysis assuming that the characteristics of the response (e.g. stresses) are given.

The problem of fatigue of materials subjected to time-varying loads is old, the first comprehensive treatment by Woehler (1870) who introduced the curves SN, stress (S) - lifetime (N), for alternating loads with fixed amplitude. But from the very beginning the great dispersion of the S-N curves was recognized due to the stochastic nature of fatigue, resulting in the adoption by Ravilly (1938) S-N-P families of curves with the survival probability parameter P. Weibull (1939) proposed the use of a probabilistic approach to model the distribution of cycles to fatigue failure of metal specimens, while Miner (1945) used statistical variation diagrams of cycles of failure to describe the failure of metal specimens in the presence of holes under fixed amplitude loads. Theories for describing the fatigue gradually evolved from models of linear accumulation of damage type Palmgren-Miner in nonlinear models, e.g. equations Marco-Starkey, Henry, modified Miner, Morrow (1986), and empirical crack propagation models as well, eg Paris-Erdogan equation and Forman (Sobczyk and Spencer, 1992). Subsequent developments included the influence of the plasticity of materials, application of multiaxial stress situation, and apparently the effect of memory during the enforcement of load cycles of varying amplitude (Sobczyk and Spencer, 1992).

Traditionally, to introduce the stochastic nature of the phenomenon of fatigue, two methods used in newer models are used (Bogdanoff and Kozin, 1985). Usually, the randomization of the basic differential equations governing the problem of fatigue is selected, considering the parameters of equations as random variables, independent or not. Recently, the a-priori stochastic foundation of the problem of fatigue using purely stochastic equations is gaining ground. Generally, the field of stochastic fatigue is evolving rapidly in recent years (Sobczyk and Spencer, 1992). Among other things, a variety of models of failure and spread of cracks in complex, heterogeneous, anisotropic and classic metal material have been proposed by Krajcinovic (1986), Shlyannikov and Braude (1992), Liou et al (1999), Sobczyk ( 1987), Sobczyk and Trebicki (1995).

An important element in the application of stochastic models of fatigue in real structures is the influence of uncertainties due to incomplete knowledge of the system and/or the excitation. Specifically, studies and analysis of reliability usually do not take into account the incomplete knowledge of the nature of the material, the actual size of the structure and the shape of the road profile that will truly address the vehicle, but also the imperfections of the analytical methods and models. Recently, it has been internationally recognized and documented (eg Baker and Cornell, 2003; Porter et al., 2002) the need to incorporate these uncertainties and to develop methods of analysis and design under their influence (Au, Papadimitriou and Beck, 1999; Papadimitriou, Katafygiotis and Au, 1997; Beck et al., 1999).

It is clear that a more adequate approach should account for the joint (coupled) treatment of both the system dynamics and deterioration process (e.g. fatigue accumulation). Such an analysis allows to account the effect of stiffness degradation during the vibration process on the response and, at the same time, gives the actual stress values for estimation of fatigue. It seems that in stochastic dynamics the coupled analysis of the response and degradation had been treated first in the context of elasto-plastic (hysteretic) systems (Roberts 1978, Wen 1986). In the articles cited a degradation of the system is defined in terms of the hysteretic energy dissipation. As far as the joint analysis of random vibrations and fatigue degradation is concerned, one should mention the paper (Grigoriu 1990) containing the model in which fatigue crack growth equation is coupled with the equation for the amplitude of the response (obtained via the averaging method – Sobczyk 1991, Soong and Grigoriu 1993), and more extensive studies published in papers (Sobczyk and Trebicki 1999, Sobczyk and Trebicki 2000).

In the papers cited above the analysis was presented for the Gaussian response and specific calculations were performed for a single degree of freedom system. one of the objectives of this thesis is to treat the response-degradation problem of random vibration in a more general setting for multi degree of freedom systems and multidimensional nature of degradation process. Such an analysis is inspired by the recently growing industrial interest in prediction of the response and degradation of large scale mechanical and structural systems; an important class of such systems includes an “hierarchy” of oscillatory subsystems with different fatigue degrading stiffnesses.

## 1.2 Organization of this Thesis

The research work presented in the thesis contributes to the design optimization and fatigue of structures subjected to uncertain dynamic loads. This uncertain variability of the dynamic loads is modeled using stochastic processes. The performance measures needed in the design of the structures are related to the second – order statistics of various response quantities, such as displacements, velocities, accelerations, strains, stresses, drift and fatigue lifetime. In particular, novel methods developed in this thesis for fatigue lifetime predictions of structures subjected to stochastic loads are conveniently incorporated in the design optimization framework. For demonstration purposes, the proposed framework is applied to the design of a class of two – dimensional truss structure.

Methodologies for design optimization of structures under stochastic dynamic excitations are presented in Chapter 2. Specifically, after a brief presentation of methodologies for optimizing systems under static deterministic and uncertain loading, an innovative methodology for design optimization of structures subjected to stochastic dynamic loading is presented. The design optimization is formulated as a constrained optimization problem with the objective function related to the structural performance measure, the inequality constrains related to cost measures and the equality constrains related to the governing equations of motion of the system. Specifically, for the stochastic excitation case the response is also stochastic and the performance measures are associated with the second – order statistics (e.g. variance) of various response quantities of interest, such as displacements and stresses. Assuming white noise or filtered white noise excitation models, these second order statistics of the response are conveniently obtained by solving the Lyapunov (differential or algebraic) matrix equations. The cost function is related to the total volume of the structure which is restricted to remain within a specified volume. An adjoint method is developed for the

calculation of the gradients of the objective function, in order to increase the computational efficiency of the proposed methodology for the case of large number of design variables. The proposed design optimization methodology is also extended to handle the case of estimating the response using modal coordinates, thus further reducing the computational effort by exploiting the fact that only a small fraction of modes in relation to the large number of DOFs contribute to the response. This analysis, in conjunction with the adjoint method for the calculation of the gradients of the objective function, substantially increases the efficiency of the proposed methodology.

In Chapter 3, the proposed methodologies are implemented on two – dimensional truss structures, for different performance functions such as the weighted sum of the nodal displacements and the weighted sum of the stresses, in order to demonstrate their applicability. The obtained results are compared to available design optimization results for truss structures subjected to deterministic static loads. Furthermore, the modal space approach for the design optimization is also applied on truss structures in order to investigate the effect of using limited number of contributing modes in the estimation of the response and therefore explore their effect on the optimal response.

In Chapter 4, an innovative methodology for the fatigue reliability assessment of randomly vibrating multi-degree of freedom systems is presented within the coupled response-degradation model. The fatigue process in the system components is quantified by the fatigue crack growth equations, which - via the stress range - are coupled with the system response. Simultaneously, the system dynamics are affected by fatigue process via its stiffness degradation (so, it provides the actual stress values to the fatigue growth equation). In addition to the general coupled response-degradation analysis, its special case of non-coupled fatigue crack growth is treated as well for the wide-band stationary applied stress by the use of its first four spectral moments and the approximate, empirically motivated, probability distribution. Both, the general analysis and the illustrating exemplary problems elaborated in this chapter provide the route to the fatigue reliability estimation in complex – hierarchical vibratory systems under random loading.

In Chapter 5, the aforementioned methodologies developed in Chapter 2 and 4 are combined in order to establish a framework for fatigue – based design optimization of structures subjected to stochastic excitations. The objective function is selected to maximize the expected fatigue lifetime of the system. Using the methods developed in Chapter 4, the expected fatigue lifetime is

calculated very efficiently using only the spectral moments of the stresses developed in the structure. Certain similarities between the fatigue – based performance function and the stress – based performance function in Chapter 2 are revealed. The proposed methodology is used for size and topology optimization of two – dimensional truss structures in order to demonstrate its applicability. The optimal designs obtained from the fatigue – based design optimization methodology are compared to the optimal designs obtained from the stress – based design optimization methodology in order to identify the differences in the final designs.

# CHAPTER 2 Optimization of Structures under Stochastic Excitations

## 2.1 Introduction

In the present chapter, the problem of the design optimization of dynamic systems under stochastic excitations is addressed. First, a short description is given for the methodologies used up to now, such as the “minimum compliance” method, which are mainly applied to structures subjected to static loads. Next, an innovative methodology is presented for the optimization of the performance of multi-degree-of-freedom, under stochastic excitations. The performance of the system response is quantified by using different measures of the response, such as the weighted sum of the nodal displacements or the weighted sum of the developed stresses in the structural parts. Additionally, the adjoint method is used in order to efficiently calculate the sensitivities of the objective function with respect to the design variables. Next, the proposed methodology is extended to incorporate in the design optimization, the formulation of the response in the modal space, in order to take advantage of the fact that only a few modes in relation to the number of DOFs of the structure contribute to the response. The adjoint method is also used in this case in order to calculate the derivatives of the

objective function. Finally, a very simple illustrative example is given, where the proposed methodology is applied on a 2-DOF bar – mass system.

## 2.2 Optimization of Structures under Static Loads

Consider a structural model with $n$ DOFs and a vector $\underline{\theta} \in \mathbb{R}^{N_\theta}$, where $N_\theta$ is the number of the parameters in $\underline{\theta}$, of the design variables associated with geometrical properties, material properties as well as variables accounting for the layout of the structure, such as nodal coordinates in a truss structure. Let $\underline{f} \in \mathbb{R}^n$ be the vector of external static loads applied to the structure and $\underline{u} \in \mathbb{R}^n$ be the vector of displacements.

### 2.2.1 Minimum Compliance Method

The optimization of the geometry and topology of structures can conveniently be formulated using the "minimum compliance" method (Bendsoe and Sigmund 2002, Sigmund 1997). In this approach the layout of a structure is found by allowing a certain set of connections between a fixed set of nodal points as potential structural or vanishing members. The minimum compliance method minimizes the compliance of the structure subject to weight or volume constrains. The problem of minimum compliance design is formulated as follows. Find $\underline{\theta}$ that minimizes

$$J(\underline{q}) = \underline{f}^T \underline{u}(\underline{q}) \tag{2.1}$$

subject to

$$K\underline{u} = \underline{f} \tag{2.2}$$

$$V \leq V_0 \tag{2.3}$$

$$\underline{q}_{\min} \leq \underline{q} \leq \underline{q}_{\max} \tag{2.4}$$

where $K$ is the stiffness matrix of the system and $\underline{q}_{\min}$ and $\underline{q}_{\max}$ are the lower and upper boundaries of the design parameters, $V$ is the volume of the structure and $V_0$ is a constant defining the maximum volume allowed for the optimal structure. Note that $J(\underline{q})$ is the norm of $K^{-1}$ or compliance.

The design optimization problem is thus formulated as a constrained optimization problem, involving equality constrains (2.2) and inequality constrains (2.3), along with constrains (2.4) on the upper and lower boundaries of the design variables. Gradient-based optimization algorithms can be applied to numerically solve the

constrained optimization problem. Such algorithms require the analytical evaluation of the gradients of the objective function in (2.1) and the gradient of the equality constraints in (2.2). The first derivatives of the objective function with respect to the design variables $\theta_j$, $j = 1,..., N_\theta$ are given by

$$\frac{\partial J}{\partial q_j} = f^T \frac{\partial \underline{u}}{\partial q_j} \tag{2.5}$$

whereas taking the first derivatives of the constraints in (2.2) lead to

$$K \frac{\partial \underline{u}}{\partial q_j} = - \frac{\partial K}{\partial q_j} \underline{u}, \quad j = 1, 2, ..., N_q \tag{2.6}$$

Thus the calculation of the derivatives of the objective function and the constraints require the numerical solution of $N_q + 1$ linear algebraic systems of dimension $n$.

The adjoint method can be used to reduce the number of linear algebraic systems to two, independently of the number of the design variables. The adjoint method is an efficient way for calculating the sensitivities for this type of constrained optimization problems, even for very large dimensional design space. According to the adjoint method, the objective function is augmented by the constraints equations (2.2) as follows

$$J^*(\underline{\theta}) = \underline{f}^T \underline{u}(\underline{\theta}) - \underline{\lambda}^T \left( K\underline{u} - \underline{f} \right) \tag{2.7}$$

where the arbitrary vector $\underline{\lambda}$ is to be selected conveniently. Given the constraints in (2.2) the function $J^*(\underline{\theta})$ is the same as $J(\underline{\theta})$ for admissible $\underline{\theta}$.

The derivatives of the new objective function with respect to the design variables $\underline{\theta}$, are now given by

$$\frac{\partial J^*}{\partial \theta_j} = \underline{f}^T \frac{\partial \underline{u}}{\partial \theta_j} - \underline{\lambda}^T \left( \frac{\partial K}{\partial \theta_j} \underline{u} + K \frac{\partial \underline{u}}{\partial \theta_j} \right) = \left( \underline{f}^T - \underline{\lambda}^T K \right) \frac{\partial \underline{u}}{\partial \theta_j} - \underline{\lambda}^T \frac{\partial K}{\partial \theta_j} \underline{u} \tag{2.8}$$

The idea in the adjoint method is to eliminate the terms involving $\frac{\partial \underline{u}}{\partial \theta_j}$ so that the estimation of these derivatives is avoided. This is done by selecting $\underline{\lambda}$ to satisfy the adjoint equation

$$\underline{\lambda}^T K - \underline{f}^T = 0 \ or \ K\underline{\lambda} = \underline{f} \tag{2.9}$$

where use was made of the fact that $K$ is symmetric ($K = K^T$).

Using the adjoint equation (2.9) the equation (2.8) yields

$$\frac{\partial J^*}{\partial \theta_j} = -\underline{\lambda}^T \frac{\partial K}{\partial \theta_j} \underline{u} \tag{2.10}$$

which is computed for all $j = 1, 2, ..., N_q$ by solving the adjoint equation (2.9) for $\underline{\lambda}$, independently of the number $N_q$ of the design variables.

It should be noted that for the special case of linear dependence between the global mass and stiffness matrices on the parameters in the set $\underline{q}$, that is, and

$$\begin{aligned} M(\underline{\theta}) &= M_0 + \sum_{j=1}^{N_\theta} M_j \theta_j \\ K(\underline{\theta}) &= K_0 + \sum_{j=1}^{N_\theta} K_j \theta_j \end{aligned} \tag{2.11}$$

the gradients of $M(\underline{q})$ and $K(\underline{q})$ are easily computed from the constant matrices $M_0$, $K_0$, $M_j$ and $K_j$, $j = 1, \cdots, N_q$. In order to save computational time, these constant matrices are computed and assembled once and, therefore, there is no need this computation to be repeated during the iterations involved in optimization algorithms. For the general case of nonlinear dependence between the global mass and stiffness matrices on the parameters in the set $\underline{q}$, the matrices $M_j$ and $K_j$ involved in the formulation can be obtained numerically at the element level and assembled to form the global matrices.

After the derivation of the equation (2.11), the derivatives of the stiffness matrix appearing in (2.10) can be readily obtained by

$$\frac{\partial K}{\partial \theta_j} = K_j \tag{2.12}$$

Also, note that the stiffness matrices $K_0$ and $K_i$ are only computed once before the optimization process and therefore the derivatives of the objective function given in (2.10) can be calculated directly by

$$\frac{\partial J^*}{\partial \theta_j} = -\underline{\lambda}^T K_j \underline{u} \tag{2.13}$$

avoiding the necessity of solving the system several times at each iteration of the optimization algorithm. This leads to a significant reduction of the computational cost of the methodology, simply by using the advantages of the adjoint method

and the fact that the stiffness matrix of the system is given by the representation (2.11).

Note that the Hessian of the objective function can also be computed analytically by differentiating equation (2.10)

$$\frac{\partial J^*}{\partial \theta_i \partial \theta_j} = -\frac{\partial \underline{\lambda}^T}{\partial \theta_i} K_j \underline{u} - \underline{\lambda}^T \frac{\partial^2 K}{\partial \theta_i \partial \theta_j} \underline{u} - \underline{\lambda}^T K_j \frac{\partial \underline{u}}{\partial \theta_i} \tag{2.14}$$

where use was made of the symmetry of $K$ and $K_j$ matrices.

For the special case of representation (2.11), the second term in (2.14) is equal to zero. Also, using the equations (2.2) and (2.9) one has $\underline{u} = \underline{\lambda}$. Therefore the second derivative of the objective function yields

$$\frac{\partial J^*}{\partial \theta_i \partial \theta_j} = -\frac{\partial \underline{u}^T}{\partial \theta_i} K_j \underline{u} - \underline{u}^T K_j \frac{\partial \underline{u}}{\partial \theta_i} = -2\underline{u}^T K_j \frac{\partial \underline{u}}{\partial \theta_i} \tag{2.15}$$

Additionally, by differentiating the equation (2.2) one has

$$\frac{\partial K}{\partial \theta_j} \underline{u} + K \frac{\partial \underline{u}}{\partial \theta_j} = 0 \Leftrightarrow \frac{\partial \underline{u}}{\partial \theta_j} = -K^{-1} \frac{\partial K}{\partial \theta_j} \underline{u} = -K^{-1} K_j \underline{u} \tag{2.16}$$

Using (2.6), solving for $\frac{\partial \underline{u}}{\partial \theta_i}$ and substituting in (2.15), the Hessian of the objective function takes the form

By substituting (2.16) in (2.15) Hessian of the objective function takes the form

$$\left[\nabla^2 J\right]_{ij} = \frac{\partial J^*}{\partial \theta_i \partial \theta_j} = -2\underline{u}^T K_j^T K^{-1} K_j \underline{u} \tag{2.17}$$

Introducing the matrices

$$\Psi = [\underline{\psi}_1 \; \underline{\psi}_2 \cdots \underline{\psi}_n] \tag{2.18}$$

$$\Delta = [\underline{\delta}_1 \; \underline{\delta}_2 \cdots \underline{\delta}_n] \tag{2.19}$$

where

$$\underline{\psi}_j = K_j \underline{u} \tag{2.20}$$

$$\underline{\delta}_j = K^{-1} \underline{\psi}_j \tag{2.21}$$

the components of the Hessian $H$ can equivalently be written in matrix form

$$H = \nabla^2 J = 2\Psi^T \Delta \tag{2.22}$$

### 2.2.2 Generalized Method

In general, the design optimization problem can be formulated as a constrained optimization. The objective and the constraints are associated with performance and cost-related criteria. Specifically, the design optimization problem is formulated as follows. Find the $\underline{\theta}$ values that minimize the objective

$$J(\underline{q}) = F(\underline{u}(\underline{q})) \tag{2.23}$$

subject to

$$K\underline{u} = \underline{f} \tag{2.24}$$

$$V \leq V_0 \tag{2.25}$$

$$\underline{q}_{\min} \leq \underline{q} \leq \underline{q}_{\max} \tag{2.26}$$

Herein, $J(\underline{q})$ is a general objective that relates to the performance of the system as this is measured by the response $\underline{u}(\underline{q})$ or functions of the responses $F(\underline{u}(\underline{q}))$. The function of the responses can be associated with strength and safety criteria of the structure. Examples of performance function $J(\underline{q})$ are given next. For design objectives related to the displacement, drift or stresses of the structure, one can define the objective to be

$$J(\underline{q}) = \left\|\underline{s}\right\|^2 \tag{2.27}$$

where $\|\square\|$ is a specific norm of the vector $\underline{u}$ and $\underline{\sigma}$ is a vector of responses that is related to the displacement response vector by $\underline{\sigma} = \Sigma' \underline{u}$. For the norm $\left\|\underline{s}\right\| = \underline{s}^T W \underline{s}$, the objective is written as

$$J(\underline{q}) = \underline{u}^T \mathrm{S}\, \underline{u} \tag{2.28}$$

where $\Sigma = \Sigma' W \Sigma$. For the norm $\left\|\underline{u}\right\| = \max\left|u_i\right|$, the objective is written as

$$J(\theta) = \max\left|\sigma_i\right| \tag{2.29}$$

which is $C^0$ continuous.

For the general case of (2.23) the derivatives of the objective function can be efficiently computed using the adjoint formulation. The objective function is augmented by the constrains equation (2.24) as follows

$$J^* = \underline{u}^T \Sigma \underline{u} - \underline{\lambda}^T \left( K\underline{u} - \underline{f} \right) \tag{2.30}$$

where the arbitrary vector $\underline{\lambda}$ is to be selected conveniently.

The derivatives of the new objective function with respect to the design variables in $\underline{\theta}$, are now given by

$$\begin{aligned}\frac{\partial J^*}{\partial \theta_j} &= \underline{\nabla}_{\underline{u}}^T F(\underline{u}) \frac{\partial \underline{u}}{\partial \theta_j} - \underline{\lambda}^T \left( K \frac{\partial \underline{u}}{\partial \theta_j} + \frac{\partial K}{\partial \theta_j} \underline{u} \right) = \\ &= -\underline{\lambda}^T \frac{\partial K}{\partial \theta_j} \underline{u} + \left( \underline{\nabla}_{\underline{u}}^T F(\underline{u}) - \underline{\lambda}^T K \right) \frac{\partial \underline{u}}{\partial \theta_j}\end{aligned} \tag{2.31}$$

Selecting $\underline{\lambda}$ to eliminate the last term, the adjoint equation takes the form

$$K\underline{\lambda} = \underline{\nabla}_{\underline{u}} F(\underline{u}) \tag{2.32}$$

and the derivative of the objective function simplifies to

$$\frac{\partial J^*}{\partial \theta_j} = -\underline{\lambda}^T \frac{\partial K}{\partial \theta_j} \underline{u} \tag{2.33}$$

which is qualitatively the same as in equation (2.10). The only difference is the right hand side vector (RHS) of the adjoint equation which affects the value of the vector $\underline{\lambda}$. Note that for the special case of objective function (2.28), the RHS of the adjoint equation takes the form $\underline{\nabla}_{\underline{u}}^T F(\underline{u}) = 2\Sigma\underline{u}$. Also it is worth noting that for the special case of objective function (2.29) which is $C^0$ continuous, the derivatives contain jumps at some values of $\underline{\theta}$

### 2.2.3 Method Accounting for Static Loading Uncertainties

Uncertainties in a variable are quantified by a probability distribution as means of specifying the plausibility of each possible value of the variable. In the case that the static load vector $\underline{f}$ is considered to be uncertain and a distribution with probability density function $p(\underline{f})$ is introduces to quantify the uncertainty. The minimum compliance method can be formulated as follows. Find $\underline{\theta}$ that minimizes

$$J(\underline{\theta}) = E\left[\underline{f}^T \underline{u}(\underline{\theta})\right] \tag{2.34}$$

where $E[\square]$ denotes mathematical expectation.

This case has been formulated and presented in the work by Christiansen et.al. (2001). In this study the mathematical modeling and solution of robust structural optimization of linear elastic structures, under uncertainty in the data describing the loading conditions and the material properties, is considered. This work has been extended by Guest and Igusa (2008) to handle the uncertainty in the nodal

coordinates of the system, demonstrating that the load and nodal uncertainties can have dramatic impact on the optimal design of the structures. Furthermore, Evgrafov et. al. (2003a and 2003b) have considered structural topology optimization problems including unilateral constraints arising from non-penetration conditions in contact mechanics or non-compression conditions for elastic ropes, whereas parameters such as loads are allowed to be stochastic in order to construct more realistic models and to hedge off possible failures or an inefficient behavior of optimal structures.

## 2.3 Optimization of Structures under Stochastic Dynamic Loads

The formulation for the design optimization of structures under static loads in next extended to handle the case of uncertain dynamic loads. The excitation of the structure is considered to vary with time and the value of the excitation at each time instant is uncertain. In fact, it is assumed that the uncertain excitation can be modeled by zero-mean Gaussian stochastic processes so that the second-order statistics of these processes fully describe the characteristics of the excitations (Lutes and Sarkani 2003). In addition, the structure is assumed to be linear so that the responses to Gaussian zero-mean excitations are also Gaussian zero-mean processes that are described by the second-order statistics. Herein, attention will be given to the covariance response at zero lag. Such response covariances are readily obtained by solving the Lyapunov matrix equations (Lutes and Sarkani 2003).

### 2.3.1 General Formulation

Similar to the static case, the design optimization problem can be formulated as a constrained optimization problem. The objective is related to the performance of the structure which is evaluated by the covariance of the response at zero lag. The constraints are associated as before with governing equations of motion of the system and the cost of the design. Specifically, the design optimization problem is formulated as follows. Find the $\underline{\theta}$ values that minimize the objective

$$J(\underline{q}) = F(Q(\underline{q})) \tag{2.35}$$

subject to constraints

$$g(Q(\underline{q})) = 0 \tag{2.36}$$

$$V(\underline{q}) \leq V_0 \tag{2.37}$$

$$\underline{q}_{\min} \leq \underline{q} \leq \underline{q}_{\max} \tag{2.38}$$

Herein, $Q(\underline{q})$ is the covariance of response quantities of interest such as displacements, velocities, acceleration, stresses, fatigue, etc., $J(\underline{q})$ is a general objective that relates to the performance of the system as this is measured by the function of the covariance responses $F(\cdot)$, and $g(\cdot)$ indicates the set of equations that the covariance response satisfies based on the governing equations of motion of the system. The covariance responses in $Q(\underline{q})$ are associated with second-order statistics of performance, strength and safety criteria of the structure.

### 2.3.2 Performance Functions

Examples of performance functions $F(Q(\underline{q}))$ are given next. For design objectives related to the displacement, drift or stress responses of the structure and for the case of Gaussian response, one can define the objective to be a measure of the intensity of the response. In the analysis that follows, the variances of the responses are considered as adequate measures of the intensity of the responses.

Let $Q_y \equiv Q_y(\underline{\theta}) = E[\underline{y}(t;\underline{\theta})\underline{y}^T(t;\underline{\theta})]$ be the covariance matrix of the Gaussian stochastic response vector $\underline{y}(t)$. For stationary response the covariance matrix is constant, independent of time $t$. The performance function is defined to be

$$F(Q(\underline{\theta})) = tr\left(W\ Q_y(\underline{\theta})\right) \tag{2.39}$$

where $W$ is a weight matrix. A special case is to select

$$W = \begin{bmatrix} w_1 & & 0 \\ & \mathrm{O} & \\ 0 & & w_{n_y} \end{bmatrix} = diag\left(\underline{w}\right) \quad \in \Re^{n_y \times n_y} \tag{2.40}$$

to be a diagonal matrix of weighting factors $\underline{w} = (w_1, \cdots, w_{n_y})^T$, chosen so that $\sum_{i=1}^{n_y} w_i = 1$. The performance function in this case takes the form

$$F(Q(\underline{\theta})) = \sum_{i=1}^{n_y} w_i E\left[Q_{ii}(\underline{\theta})\right] = \sum_{i=1}^{n_y} w_i E\left[y_i^2(t;\underline{\theta})\right] \tag{2.41}$$

which represents a weighted sum of the variances of the response quantities of interest. Using this general formulation, one can control the responses of the system that are needed to be optimized, separating the most important quantities from the less important by assigning higher or lower values to the corresponding weighting factors.

An alternative and equally important choice of the performance function is related to the response quantity of maximum intensity or variance, that is, to choose the performance to be

$$F(Q(\underline{\theta})) = \max[diag\{Q_y(\underline{\theta})\}] = \max[\underline{q}_y(\underline{\theta})] \tag{2.42}$$

where $\underline{q}_y(\underline{\theta}) = diag[Q_y(\underline{\theta})] = [Q_{11,y}(\underline{\theta}), \mathrm{L}\ , Q_{n_y n_y, y}(\underline{\theta})]^T$ contains the diagonal elements of the covariance matrix $Q_y(\underline{\theta})$. The performance function is this case is $C^0$ continuous.

### 2.3.3 Covariance Response Formulation

The covariance response matrix $Q_y(\underline{\theta})$ is readily obtained from the equation of motion of the linear structure subjected to zero-mean Gaussian excitations. The formulation for the covariance response is next presented and is used to define the constraint equations given by (2.36).

The equation of motion of a linear structure is

$$M\ddot{\underline{u}} + C\dot{\underline{u}} + K\underline{u} = R\underline{f}^*(t) = \underline{f}(t) \tag{2.43}$$

where $\underline{u}(t) \in \mathbb{R}^n$ is the displacement vector, $M \in \mathbb{R}^{n \times n}$, $K \in \mathbb{R}^{n \times n}$ and $C \in \mathbb{R}^{n \times n}$ are the mass, stiffness and damping matrices respectively, $\underline{f}^* \in \mathbb{R}^{n_f}$ is the vector of the independent excitations applied on the structure, and $R \in \mathbb{R}^{n \times n_f}$ is a matrix that defines the degrees of freedom on which the excitation is applied. Introducing the state vector

$$\underline{x}_s = \begin{bmatrix} \underline{u} \\ \dot{\underline{u}} \end{bmatrix} \in \mathbb{R}^{2n} \tag{2.44}$$

and the observation vector $\underline{y} \in \mathbb{R}^{n_y}$ to contain all the response quantities of interests that may depend linearly on the states of the system and the excitation, the equation of motion (2.43) can be written in state vector form

$$\begin{aligned} \dot{\underline{x}}_s &= A_s \underline{x}_s + B_s \underline{f}^* \\ \underline{y} &= \hat{C}\underline{x} + D\underline{f}^* \end{aligned} \tag{2.45}$$

where $A_s$, and $B_s$ are the system matrices that depend on the matrices $M$, $K$, $C$, $R$ as follows

$$A_s = \begin{bmatrix} 0_{nn} & I_{nn} \\ -M^{-1}K & -M^{-1}C \end{bmatrix} \tag{2.46}$$

$$B_s = \begin{bmatrix} \underline{0}_{nn_f} \\ M^{-1}\underline{R} \end{bmatrix} \tag{2.47}$$

and $\hat{C}$ and $D$ define the dependence of the observation vector $\underline{y}$ on the state and excitation vectors. For the case for which the vector $\underline{y}$ includes displacement, velocity, strain and stress quantities, the observation vector depends only on the state vector $\underline{x}$ and the matrix $D = 0$ in (2.45). In this case, the response vector is given by

$$\underline{y} = \hat{C}\underline{x} \tag{2.48}$$

Using (2.48) the covariance matrix $Q_y(\underline{\theta}) \in \mathbb{R}^{n_y \times n_y}$ of the observation matrix $\underline{y}$ is related to the covariance response $Q_x(\underline{\theta})$ of the state vector $\underline{x}$ as follows

$$Q_y(\underline{\theta}) = E\left[\underline{y}(t)\,\underline{y}^T(t)\right] = \hat{C}\,E\left[\underline{x}(t)\,\underline{x}^T(t)\right]\hat{C}^T = \hat{C}Q_x(\underline{\theta})\hat{C}^T \tag{2.49}$$

The covariance response $Q_x(\underline{\theta})$ of the state vector $\underline{x}(t)$ can readily be obtained from the aforementioned formulation as a function of the covariance of the excitation vector and the properties of the linear system (Lutes and Sarkani 2003). Two special cases are next considered depending on the type of the excitation used. The first case assumes that the excitation is white noise and the second case assumes that the excitation is filtered white noise generated by passing white noise through a filter described by a set of linear differential equations. In both cases, the covariance response can be obtained in the time domain by solving the Lyapunov system of differential equations. In the stationary case, the Lyapunov system is a system of linear algebraic equations. More general types of Gaussian stochastic excitations that are specified in the frequency domain by power spectral densities can also be handled. Specifically, the variances of the responses are obtained in the frequency domain by one-dimensional integrals involving as integrands the product of transfer functions of the linear system and the power spectral density of the excitation processes.

Next, the formulation for the covariance response for the white noise and the filtered white noise excitations are presented.

#### 2.3.3.1 White noise excitations

For the case for which the components of the excitation vector $\underline{f}^*$ are white noise processes, the covariance response $Q(\underline{\theta}) \equiv Q_x(\underline{\theta}) = E[\underline{x}(t;\underline{\theta})\underline{x}^T(t;\underline{\theta})] \in \mathbb{R}^{2n \times 2n}$ of the state vector satisfies the Lyapunov system of equations, given by

$$\dot{Q} = AQ + QA^T + BS^*B^T \tag{2.50}$$

where

$$A = A_s, \quad B = B_s \quad \text{and} \quad S^* = E\left[\underline{f}^*\underline{f}^{*T}\right] \tag{2.51}$$

Since the input excitation is considered to be stationary, the transient term of the Lyapunov equation is equal to zero

$$\dot{Q} = \mathbf{0} \tag{2.52}$$

In this case for the stationary response, the Lyapunov equation takes the form:

$$AQ + QA^T + BS^*B^T = \mathbf{0} \tag{2.53}$$

which consists of $2n \times 2n$ linear algebraic equations. Taking advantage of the symmetry of $Q$, the number of equations is reduced to $n(2n+1)$

### 2.3.3.2 Filtered white noise excitations

It is next assumed that the excitation vector $\underline{f}^*$ is generated by passing white noise through e filter. The filter equations are written in state space form

$$\begin{aligned} \dot{\underline{x}}_f &= A_f \underline{x}_f + B_f \underline{w} \\ \underline{f}^* &= C_f \underline{x}_f + D_f \underline{w} \end{aligned} \tag{2.54}$$

where $\underline{x}_f \in \mathbb{R}^{n_f}$ is the filter state vector and $\underline{w}$ is a Gaussian white noise vector process with PSD equal to $S_w$.

The filter equations can be solved simultaneously with the system equation for the system given in (2.45), simply by augmenting the states of the system to include the states of the filter. Specifically, introducing the augmented state vector

$$\underline{x} = \begin{Bmatrix} \underline{x}_s \\ \underline{x}_f \end{Bmatrix} \in \mathbb{R}^{n_s+n_f} \tag{2.55}$$

consisting of the system states and the input filter states, using the system and filter state space formulations (2.45) and (2.54), the state space equations for the augmented state vector are given by

$$\dot{\underline{x}} = \begin{Bmatrix} \dot{\underline{x}}_s \\ \dot{\underline{x}}_f \end{Bmatrix} = \begin{Bmatrix} A_s\underline{x}_s + B_sC_f\underline{x}_f + B_sD_f\underline{w} \\ A_f\underline{x}_f + B_f\underline{w} \end{Bmatrix} = \begin{bmatrix} A_s & B_sC_f \\ 0 & A_f \end{bmatrix} \begin{Bmatrix} \underline{x}_s \\ \underline{x}_f \end{Bmatrix} + \begin{bmatrix} B_sD_f \\ B_f \end{bmatrix} \underline{w} \tag{2.56}$$

or alternatively

$$\dot{\underline{x}} = A\underline{x} + B\underline{w} \tag{2.57}$$

where

$$A = \begin{bmatrix} A_s & B_s C_f \\ 0 & A_f \end{bmatrix} \tag{2.58}$$

and

$$B = \begin{bmatrix} B_s D_f \\ B_f \end{bmatrix} \tag{2.59}$$

The response quantity of interest $\underline{y}$ may be related to both the system state $\underline{x}_s$ and the filter state $\underline{x}_f$ through the observation equation

$$\underline{y} = \hat{C}_s \underline{x}_s + \hat{C}_f \underline{x}_f = \hat{C}\underline{x} \tag{2.60}$$

where

$$\hat{C} = \begin{bmatrix} C_s & C_f \end{bmatrix} \tag{2.61}$$

The covariance $Q_{\underline{y}}$ of the response vector $\underline{y}$ is given by (2.49) with $\hat{C}$ is given by (2.61), $Q_{\underline{x}}$ is given by (2.50) and $A$ and $B$ are given by (2.58) and (2.59).

**2.3.3.3 Second-order filter dynamics**

A special case of a stochastic model of dynamic excitation is the uni-modal second-order filter white-noise excitation. The characteristics of this type of excitation are given by the second order filter equation

$$\ddot{q}_f(t) + 2z_f w_f \dot{q}_f(t) + w_f^2 q_f(t) = aw(t) \tag{2.62}$$

$$f(t) = \ddot{q}_f(t) = -2z_f w_f \dot{q}_f(t) - w_f^2 q_f(t) + aw(t) \tag{2.63}$$

The characteristics of the excitation depend on the values of the filter parameters: the dominant frequency $\omega_f$ and the damping ratio $\zeta_f$. Alternatively, introducing the filter state vector

$$\underline{x}_f = \begin{bmatrix} q_f \\ \dot{q}_f \end{bmatrix} \tag{2.64}$$

the second order filter equation can be expressed in state space (2.54), where

$$A_f = \begin{bmatrix} 0 & 1 \\ -\omega_f^2 & -2\zeta_f \omega_f \end{bmatrix} \tag{2.65}$$

$$B_f = \begin{bmatrix} 0 \\ a \end{bmatrix} \tag{2.66}$$

$$C_f = \begin{bmatrix} -\omega_f^2 & -2\zeta_f \omega_f \end{bmatrix} \tag{2.67}$$

$$D_f = 0 \tag{2.68}$$

If needed, the Lyapunov equation for the filter is given by

$$\begin{aligned} A_f Q_f + Q_f A_f^T + B_f S_n B_f^T &= 0 \\ Q_{\underline{f}^*} &= C_f Q_f C_f^T \end{aligned} \tag{2.69}$$

where $S_w$ is the power spectral density of the Gaussian white noise $w(t)$.

Introducing the augmented state vector

$$\underline{x} = \begin{bmatrix} \underline{u} \\ \dot{\underline{u}} \\ q_f \\ \dot{q}_f \end{bmatrix} \tag{2.70}$$

the state space equations are given by (2.57) with the matrices $A$ and $B$ given by (2.58) and (2.59), while the observation matrix $\hat{C}$ is given by (2.61). Specifically, using the state space description of the system dynamics given by (2.45) with $A_s$ and $B_s$ given by (2.46) and (2.47), respectively, the matrices $A$ and $B$ are readily obtained by

$$A = \begin{bmatrix} 0_{nn} & I_{nn} & 0_{n1} & 0_{n1} \\ -M^{-1}K & -M^{-1}C & -\omega_g^2 M^{-1}R & -2\zeta_g \omega_g M^{-1}R \\ 0_{1n} & 0_{1n} & 0 & 1 \\ 0_{1n} & 0_{1n} & -\omega_f^2 & -2\zeta_f \omega_f \end{bmatrix} \tag{2.71}$$

$$B = \begin{bmatrix} 0_{m1} \\ \alpha M^{-1}R \\ 0 \\ \alpha \end{bmatrix} \tag{2.72}$$

### 2.3.4 Objective Function

Using the performance function (2.39) and relation (2.49) the objective function in (2.35) can be written in the form

$$J(\underline{\theta}) = tr\left(W\hat{C}Q(\underline{\theta})\hat{C}^T\right) \tag{2.73}$$

Noting that $tr\left(AB\right) = tr\left(BA\right)$, the objective function takes the form

$$J(\underline{\theta}) = tr\left(\Sigma Q(\underline{\theta})\right) \tag{2.74}$$

Where

$$\Sigma = \hat{C}^T W \hat{C} \tag{2.75}$$

Which depending on the definition of $\hat{C}$, it may also depend on $\underline{\theta}$.

At this point, it should be stressed that the choice of the matrix $\Sigma$ can control the optimization process by defining the nature of the objective function. That is, one can control whether the quantity to be optimized would be the variance of the displacement in one node or the sum of the displacement variance in all the nodes or any other combination of the response quantities.

Apart from the general formulation for the matrix $\Sigma$, one can use more specific formulation in order to define different objective functions. A very simple case is to choose

$$\Sigma = \mathrm{I} \quad \in \Re^{2n\times 2n} \tag{2.76}$$

then the initial objective function turns to

$$J = tr\left(\Sigma Q\right) = \sum_{i=1}^{n} E\left[u_i^2\right] + \sum_{i=1}^{n} E\left[\dot{u}_i^2\right] \tag{2.77}$$

that is the objective function is equal to the sum of the variances of the displacements and the velocities of the system. Another very simple case is to choose

$$\Sigma = W = diag\left(w_i\right) \quad \in \Re^{2n\times 2n} \tag{2.78}$$

In this case, the initial objective function turns to

$$J = tr\left(\Sigma Q\right) = \sum_{i=1}^{n} w_i E\left[u_i^2\right] + \sum_{i=1}^{n} w_i E\left[\dot{u}_i^2\right] \tag{2.79}$$

that is the objective function is equal to the weighted sum of the variances of the displacements and the velocities of the system.

#### 2.3.4.1 Similarity with minimum compliance method

Following the minimum compliance method in the case of white noise excitation, the objective function can be defined in a similar fashion as in (2.34) by

$$J(\underline{\theta}) = E\left[\underline{u}^2(\underline{\theta})\right] = E\left[\underline{f}^T(t)\underline{u}(\underline{\theta})\right] \tag{2.80}$$

The difference with (2.34) is that in (2.80) the variance of $f^T u$ instead of the mean is used. For zero-mean white noise excitation the mean of $u$ is zero, so an estimate of the response intensity is given by the variance of the response.

The objective function can also be expressed as

$$J(\underline{\theta}) = E\left[\left(\underline{f}^T\underline{u}\right)^2\right] = E\left[\underline{f}^T\underline{u}\underline{u}^T\underline{f}\right] = E\left[tr\left(\underline{f}^T\underline{u}\underline{u}^T\underline{f}\right)\right] \tag{2.81}$$

Noting that $tr(AB) = tr(BA)$,

$$tr\left(\underline{f}^T\underline{x}\underline{x}^T\underline{f}\right) = tr\left(\underline{f}^T X\underline{f}\right) = tr\left(\underline{f}\underline{f}^T X\right) = tr\left(\underline{f}\underline{f}^T\underline{x}\underline{x}^T\right) \tag{2.82}$$

The objective function simplifies to

$$J(\underline{\theta}) = E\left[tr\left(\underline{f}^T\underline{u}\underline{u}^T\underline{f}\right)\right] = E\left[tr\left(\underline{f}\underline{f}^T\underline{u}\underline{u}^T\right)\right] = tr\left(E\left[\underline{f}\underline{f}^T\underline{u}\underline{u}^T\right]\right) \tag{2.83}$$

Approximating the last equation, one can introduce the objective function

$$J(\underline{\theta}) = tr\left(E\left[\underline{f}\underline{f}^T\right]E\left[\underline{u}\underline{u}^T\right]\right) = tr(\Sigma Q) \tag{2.84}$$

Where

$$\Sigma = \begin{bmatrix} E\left[\underline{f}\underline{f}^T\right] & 0_{nn} \\ 0_{nn} & 0_{nn} \end{bmatrix} = \begin{bmatrix} R \\ 0_{nn_f} \end{bmatrix} E\left[\underline{f}^*\underline{f}^{*T}\right]\begin{bmatrix} R & 0_{nn_f} \end{bmatrix} \tag{2.85}$$

$R$ defines the degrees of freedom on which the excitation is applied and $S^* = E\left[\underline{f}^*\underline{f}^{*T}\right]$ is the power spectral density of the Gaussian white noise input. This formulation bears great resemblance to the minimum compliance formulation for the deterministic static case given in (2.1).

## 2.4 Optimization Using the Adjoint Formulation

The design optimization problem under stochastic excitations was formulated as a constrained optimization problem, involving equality constrains (2.53) and inequality constraints (2.37), along with constraints (2.38) on the upper and lower boundaries of the design variables. Gradient-based optimization algorithms can be applied to numerically solve the constrained optimization problem. Such

algorithms require the analytical evaluation of the gradients of the objective function in (2.35) and the gradient of the equality constraints in (2.53). Using the form (2.74), the first derivatives of the objective function with respect to the design variables $\theta_j$, $j=1,...,N_\theta$ are given by

$$\frac{\partial J}{\partial \theta_j} = tr\left(\frac{\partial \Sigma}{\partial \theta_j}\, Q(\underline{\theta})\right) + tr\left(\Sigma\, \frac{\partial Q(\underline{\theta})}{\partial \theta_j}\right) \tag{2.86}$$

whereas taking the first derivatives of the constraints in (2.53) lead to the following system of equations for $\frac{\partial Q}{\partial \theta_j}$

$$A\frac{\partial Q}{\partial \theta_j} + \frac{\partial Q}{\partial \theta_j}A^T + \frac{\partial A}{\partial \theta_j}Q + Q\frac{\partial A^T}{\partial \theta_j} + \frac{\partial B}{\partial \theta_j}S^*B^T + BS^*\frac{\partial B^T}{\partial \theta_j} = \mathbf{0} \tag{2.87}$$

$j=1,\cdots,N_\theta$. Thus, taking advantage of the symmetry of the matrices $Q$ and $\frac{\partial Q}{\partial \theta_j}$, the calculation of the derivatives of the objective function and the constraints require the numerical solution of $N_q+1$ linear algebraic systems of dimension $n(2n+1)$.

The adjoint method can be used to reduce the number of linear algebraic systems to only two, independently of the number $N_q$ of the design variables. The adjoint method is an efficient way for calculating the sensitivities for this type of constrained optimization problems, even for very large dimensional design space. According to the adjoint method, the objective function is augmented by the constraints equations (2.36) as follows

$$J^*\left(\underline{\theta}\right) = J\left(\underline{\theta}\right) - tr\left(\Lambda\Psi\right) = J\left(\underline{\theta}\right) - \sum_{i=1}^{2n}\sum_{j=1}^{2n}\lambda_{ij}\psi_{ji} \tag{2.88}$$

where the arbitrary matrix $\Lambda$ is to be selected conveniently, and the new matrix $\Psi$ has been introduced to denote the right hand side of (2.53) as follows

$$\Psi = AQ + QA^T + BS^*B^T \tag{2.89}$$

Given the constraints in (2.53) the function $J^*(\underline{\theta})$ is the same as $J(\underline{\theta})$ for admissible $\underline{\theta}$.

The derivatives of the new objective function with respect to the design variables $\underline{\theta}$, are now given by

$$\frac{\partial J^*}{\partial \theta_j} = tr\left(\frac{\partial \Sigma}{\partial \theta_j} Q\right) + tr\left(\Sigma \frac{\partial Q}{\partial \theta_j}\right) - \\ -tr\left(\Lambda\left(A\frac{\partial Q}{\partial \theta_j} + \frac{\partial Q}{\partial \theta_j}A^T + \frac{\partial A}{\partial \theta_j}Q + Q\frac{\partial A^T}{\partial \theta_j} + \frac{\partial B}{\partial \theta_j}S^*B^T + BS^*\frac{\partial B^T}{\partial \theta_j}\right)\right) \tag{2.90}$$

The gradient can be simplified to

$$\frac{\partial J^*}{\partial \theta_j} = tr\left(\Sigma\frac{\partial Q}{\partial \theta_j} - \Lambda A\frac{\partial Q}{\partial \theta_j} - \Lambda\frac{\partial Q}{\partial \theta_j}A^T\right) - tr\left(\Lambda\left(\frac{\partial A}{\partial \theta_j}Q + Q\frac{\partial A^T}{\partial \theta_j}\right)\right) - \\ -tr\left(\Lambda\left(\frac{\partial B}{\partial \theta_j}S^*B^T + BS^*\frac{\partial B^T}{\partial \theta_j}\right)\right) + tr\left(\frac{\partial \Sigma}{\partial \theta_j}Q\right) \tag{2.91}$$

Noting that $tr\left(AB\right) = tr\left(BA\right)$ then one has that

$$tr\left(\Lambda\frac{\partial Q}{\partial \theta_j}A^T\right) = tr\left(A^T\Lambda\frac{\partial Q}{\partial \theta_j}\right) \tag{2.92}$$

and the derivative of the objective function becomes

$$\frac{\partial J^*}{\partial \theta_j} = tr\left(\left(\Sigma - \Lambda A - A^T\Lambda\right)\frac{\partial Q}{\partial \theta_j}\right) - tr\left(\Lambda\left(\frac{\partial A}{\partial \theta_j}Q + Q\frac{\partial A^T}{\partial \theta_j}\right)\right) - \\ -tr\left(\Lambda\left(\frac{\partial B}{\partial \theta_j}S^*B^T + BS^*\frac{\partial B^T}{\partial \theta_j}\right)\right) + tr\left(\frac{\partial \Sigma}{\partial \theta_j}Q\right) \tag{2.93}$$

The idea in the adjoint method is to eliminate the terms involving $\frac{\partial Q}{\partial \theta_j}$, so that the estimation of these derivatives for each $\theta_j$ is avoided. This is achieved by selecting $\Lambda$ to satisfy the adjoint equation

$$\Sigma - \Lambda A - A^T\Lambda = 0 \\ \Lambda A + A^T\Lambda = \Sigma = BS^*B^T \tag{2.94}$$

Using the adjoint equation (2.94) the formulation for the derivative of the objective function becomes

$$\frac{\partial J^*}{\partial \theta_j} = -tr\left(\Lambda\left(\frac{\partial A}{\partial \theta_j}Q + Q\frac{\partial A^T}{\partial \theta_j}\right)\right) - tr\left(\Lambda\left(\frac{\partial B}{\partial \theta_j}S^*B^T + BS^*\frac{\partial B^T}{\partial \theta_j}\right)\right) + tr\left(\frac{\partial \Sigma}{\partial \theta_j}Q\right) \tag{2.95}$$

Note that the second term in (2.95) is equal to zero if the matrix $B$ is independent of the parameters $\underline{\theta}$. Similarly, for matrix $\Sigma$ that is independent of the parameters $\underline{\theta}$, the first term is equal to zero. In this case, the gradients of the objective function are given by the first term of the equation, that is

$$\frac{\partial J^*}{\partial \theta_j} = -tr\left(\Lambda\left(\frac{\partial A}{\partial \theta_j}Q + Q\frac{\partial A^T}{\partial \theta_j}\right)\right) \tag{2.96}$$

Thus, the gradient of the objective $J^*$ is computed for all $j = 1, 2, ..., N_\theta$ by solving a simple adjoint equation (2.94) for $\Lambda$ and the equation (2.53) for the covariance matrix $Q$.

### 2.4.1 Implementation Issues

The gradient of the objective $J^*$ requires the estimation of the derivative of the matrices $A$ and $B$. In the case of white noise excitation, $A = A_s$ and the derivatives are given by

$$\frac{\partial A}{\partial \theta_j} = -\begin{bmatrix} \mathbf{0} & \mathbf{0} \\ \dfrac{\partial M^{-1}}{\partial \theta_j}K + M^{-1}\dfrac{\partial K}{\partial \theta_j} & \dfrac{\partial M^{-1}}{\partial \theta_j}C + M^{-1}\dfrac{\partial C}{\partial \theta_j} \end{bmatrix} \tag{2.97}$$

$$\frac{\partial B}{\partial \theta_j} = \begin{bmatrix} \mathbf{0} \\ \dfrac{\partial M^{-1}}{\partial \theta_j}R \end{bmatrix} \tag{2.98}$$

Noting that

$$\frac{\partial M^{-1}}{\partial \theta_j} = -M^{-1}\frac{\partial M}{\partial \theta_j}M^{-1} \tag{2.99}$$

the equations (2.97) and (2.98) become

$$\frac{\partial A}{\partial \theta_j} = -\begin{bmatrix} \mathbf{0} & \mathbf{0} \\ -M^{-1}\dfrac{\partial M}{\partial \theta_j}M^{-1}K + M^{-1}\dfrac{\partial K}{\partial \theta_j} & -M^{-1}\dfrac{\partial M}{\partial \theta_j}M^{-1}C + M^{-1}\dfrac{\partial C}{\partial \theta_j} \end{bmatrix} =$$
$$= -\begin{bmatrix} M^{-1} & \mathbf{0} \\ \mathbf{0} & M^{-1} \end{bmatrix}\begin{bmatrix} \mathbf{0} & \mathbf{0} \\ -\dfrac{\partial M}{\partial \theta_j}M^{-1}K + \dfrac{\partial K}{\partial \theta_j} & -\dfrac{\partial M}{\partial \theta_j}M^{-1}C + \dfrac{\partial C}{\partial \theta_j} \end{bmatrix} \tag{2.100}$$

$$\frac{\partial B}{\partial \theta_j} = -\begin{bmatrix} \mathbf{0} \\ M^{-1}\dfrac{\partial M}{\partial \theta_j}M^{-1}R \end{bmatrix} \tag{2.101}$$

Assuming Rayleigh damping, the damping matrix can be written as

$$C = aM + bK \tag{2.102}$$

The derivative of the damping matrix, which appears in (2.97) and (2.100), can be calculated by the expression

$$\frac{\partial C}{\partial \theta_j} = \frac{\partial a}{\partial \theta_j}M + a\frac{\partial M}{\partial \theta_j} + \frac{\partial b}{\partial \theta_j}K + b\frac{\partial K}{\partial \theta_j} \tag{2.103}$$

The parameters $a$ and $b$ are chosen so that the damping coefficients for the $r$ and $s$ eigenmodes of the system are given by $\zeta_r$ and $\zeta_s$ respectively. These parameters can be computed by solving the linear system

$$\begin{aligned} a + \omega_r^2 b &= 2\zeta_r\omega_r \\ a + \omega_s^2 b &= 2\zeta_s\omega_s \end{aligned} \tag{2.104}$$

where $\omega_r$ and $\omega_s$ is the *r* and *s* eigenfrequencies of the system. The derivatives of these parameters can be easily computed by solving the $2\times 2$ linear system

$$\begin{aligned} \frac{\partial a}{\partial \theta_j} + \omega_r^2\frac{\partial b}{\partial \theta_j} &= 2\zeta_r\frac{\partial \omega_r}{\partial \theta_j} - b\frac{\partial \omega_r^2}{\partial \theta_j} \\ \frac{\partial a}{\partial \theta_j} + \omega_s^2\frac{\partial b}{\partial \theta_j} &= 2\zeta_s\frac{\partial \omega_s}{\partial \theta_j} - b\frac{\partial \omega_s^2}{\partial \theta_j} \end{aligned} \tag{2.105}$$

Finally, using Nelson method (Nelson, 1976), the derivatives of the natural frequency appearing in (2.105) can be computed by the relationships

$$\frac{\partial \omega_r^2}{\partial \theta_j} = \underline{\phi}_r^T\left(\frac{\partial K}{\partial \theta_j} - \omega_r^2\frac{\partial M}{\partial \theta_j}\right)\underline{\phi}_r \tag{2.106}$$

$$\frac{\partial \omega_r}{\partial \theta_j} = \frac{1}{2\omega_r}\frac{\partial \omega_r^2}{\partial \theta_j} \tag{2.107}$$

where $\underline{\phi}_r$ is the $r$ eigenmode of the system.

Finally, in the case of filtered white noise excitation the derivative of $A$ and $B$ with respect to $\theta_j$ are readily obtained from (2.71) and (2.72) in the form

$$\frac{\partial A}{\partial \theta_j} = -M^{-1}\begin{bmatrix} 0_{nn} & 0_{nn} & 0_{n1} & 0_{n1} \\ -\frac{\partial M}{\partial \theta_j}M^{-1}K + \frac{\partial K}{\partial \theta_j} & -\frac{\partial M}{\partial \theta_j}M^{-1}C + \frac{\partial C}{\partial \theta_j} & \omega_g^2\frac{\partial M}{\partial \theta_j}M^{-1}R & 2\zeta_g\omega_g\frac{\partial M}{\partial \theta_j}M^{-1}R \\ 0_{1n} & 0_{1n} & 0 & 0 \\ 0_{1n} & 0_{1n} & 0 & 0 \end{bmatrix} \tag{2.108}$$

$$\frac{\partial B}{\partial \theta_j} = \begin{bmatrix} 0_{m1} \\ -\alpha M^{-1}\frac{\partial M}{\partial \theta_j}M^{-1}R \\ 0 \\ 0 \end{bmatrix} \tag{2.109}$$

## 2.5 Optimization of Structures under Stochastic Dynamic Excitation: Modal Space Approach

For structures with large number of degrees of freedom, the response quantities of interest are often estimated accurately using only the contribution of the lowest modes. In this section, the design optimization problem is formulated in the modal space, considering the contribution of a number of modes in the response. In order to complete this formulation, one only needs to define the matrices $A$, $B$, $\hat{C}$ that define the state space form of the governing equations of motion in the modal space, as well as the matrices $\Sigma$, $\frac{\partial \Sigma}{\partial \theta_j}$, $\frac{\partial A}{\partial \theta_j}$, $\frac{\partial B}{\partial \theta_j}$ that are used in defining the objective function and estimating the gradient of the objective with respect to the design variables.

### 2.5.1 Formulation of Response in Modal Space

In the analysis that follows it is assumed that $K$ and $M$ are symmetric matrices. Let $\omega_r^2$, $r=1,2,\ldots,n$ be the eigenvalues and $\underline{\phi}_r$, $r=1,2,\ldots,n$ be the corresponding modeshapes obtained by solving the eigenvalues problem

$$\left(K-\omega_r M\right)\underline{\phi}_r=\underline{0} \tag{2.110}$$

Let also $\Phi=\left[\underline{\phi}_1\ \underline{\phi}_2\ \ldots\ \underline{\phi}_m\right]$ be the matrix of modeshapes containing the first $m\,(m\le n)$ modeshapes of the structure. The response $\underline{q}(t)$ of the structure in the modal space is given by

$$\underline{q}=\sum_{r=1}^{m}\underline{\phi}_r\xi_r(t)=\Phi\underline{\xi}(t) \tag{2.111}$$

where $\underline{\xi}=\left[\xi_1\ \xi_2\ \ldots\ \xi_m\ \right]^T$ and $\xi_r(t)$, $r=1,2,\ldots,m$ are the modal coordinates of the structure, satisfying the modal equations

$$\ddot{\xi}_r+2\zeta_r\omega_r\dot{\xi}_r+\omega_r^2\xi_r=\underline{\phi}_r^T R\underline{f}^*(t) \tag{2.112}$$

where $\zeta_r$, $r=1,2,\ldots,m$ are the modal damping ratios of the structure.

Let $\underline{x}_s\in\mathbb{R}^m$ be the state vector given by

$$\underline{x}_s=\begin{Bmatrix}\underline{\xi}\\ \dot{\underline{\xi}}\end{Bmatrix} \tag{2.113}$$

Using (2.112), the state vector satisfies the state space equation

$$\dot{\underline{x}}_s=A_s\underline{x}_s+B_s\underline{u} \tag{2.114}$$

where $A_s$ and $B_s$ are given respectively by

$$A_s=\begin{bmatrix}0_{mm} & I_{mm}\\ -\Omega^2 & -2Z\Omega\end{bmatrix} \tag{2.115}$$

$$\mathrm{B}_s=\begin{bmatrix}0_{mn_f}\\ \Phi^T R\end{bmatrix} \tag{2.116}$$

where $\Omega^2$ and $Z$ are the diagonal matrices of the eigenvalues and the modal damping ratios

$$\Omega^2 = \begin{bmatrix} \omega_1^2 & & 0 \\ & \ddots & \\ 0 & & \omega_m^2 \end{bmatrix} \tag{2.117}$$

$$Z = \begin{bmatrix} \zeta_1 & & 0 \\ & \ddots & \\ 0 & & \zeta_m \end{bmatrix} \tag{2.118}$$

where $0_{mn}$ denotes an $m \times n$ zero matrix and $I_{mn}$ denotes an $m \times n$ identity matrix.

Let $\underline{y}$ be a response quantity of interest that relates to $\underline{q}$ and $\dot{\underline{q}}$ through the observation equation

$$\underline{y} = R_1 \underline{q} + R_2 \dot{\underline{q}} = \begin{bmatrix} R_1 & R_2 \end{bmatrix} \begin{Bmatrix} \underline{q} \\ \dot{\underline{q}} \end{Bmatrix} \tag{2.119}$$

Using the transformation in (2.111), the vector $\underline{y}$ can be written as

$$\underline{y} = \begin{bmatrix} R_1 & R_2 \end{bmatrix} \begin{bmatrix} \Phi & 0_{mm} \\ 0_{mm} & \Phi \end{bmatrix} \begin{Bmatrix} \underline{\xi} \\ \dot{\underline{\xi}} \end{Bmatrix} = \begin{bmatrix} R_1 \Phi & R_2 \Phi \end{bmatrix} \underline{x} = \hat{C} \underline{x} \tag{2.120}$$

where $\hat{C}$ is given by

$$\hat{C} = \begin{bmatrix} R_1 \Phi & R_2 \Phi \end{bmatrix} \tag{2.121}$$

Thus, the matrices $A_s$, $B_s$, $\hat{C}$ that are needed in the state space formulation are given by (2.115), (2.116) and (2.121) respectively.

### 2.5.2 Gradient Estimation

Since the matrix $\hat{C}$ is given by (2.121), then the matrix $\Sigma$, given in (2.75), can be calculated by

$$\Sigma = \begin{bmatrix} \Phi^T R_1^T \\ \Phi^T R_2^T \end{bmatrix} W \begin{bmatrix} R_1 \Phi & R_2 \Phi \end{bmatrix} = \begin{bmatrix} \Phi^T R_1^T W R_1 \Phi & \Phi^T R_1^T W R_2 \Phi \\ \Phi^T R_2^T W R_1 \Phi & \Phi^T R_2^T W R_2 \Phi \end{bmatrix} \tag{2.122}$$

Therefore the gradient of $\Sigma$ can by calculated by

$$\frac{\partial \Sigma}{\partial \theta_j} = \begin{bmatrix} \frac{\partial \Phi^T}{\partial \theta_j} R_1^T W R_1 \Phi & \frac{\partial \Phi^T}{\partial \theta_j} R_1^T W R_2 \Phi \\ \frac{\partial \Phi^T}{\partial \theta_j} R_2^T W R_1 \Phi & \frac{\partial \Phi^T}{\partial \theta_j} R_2^T W R_2 \Phi \end{bmatrix} + \\ + \begin{bmatrix} \Phi^T R_1^T W R_1 \frac{\partial \Phi}{\partial \theta_j} & \Phi^T R_1^T W R_2 \frac{\partial \Phi}{\partial \theta_j} \\ \Phi^T R_2^T W R_1 \frac{\partial \Phi}{\partial \theta_j} & \Phi^T R_2^T W R_2 \frac{\partial \Phi}{\partial \theta_j} \end{bmatrix} \tag{2.123}$$

Introducing the new matrix $N$ by

$$N = \begin{bmatrix} \Phi^T R_1^T W R_1 \frac{\partial \Phi}{\partial \theta} & \Phi^T R_1^T W R_2 \frac{\partial \Phi}{\partial \theta} \\ \Phi^T R_2^T W R_1 \frac{\partial \Phi}{\partial \theta} & \Phi^T R_2^T W R_2 \frac{\partial \Phi}{\partial \theta} \end{bmatrix} \tag{2.124}$$

one has

$$\frac{\partial \Sigma}{\partial \theta} = N^T + N \tag{2.125}$$

Substituting in (2.90), the gradients of the objective function are given by

$$\frac{\partial J^*}{\partial \theta_j} = -tr\left( \Lambda \left( \frac{\partial A}{\partial \theta_j} Q + Q \frac{\partial A^T}{\partial \theta_j} + \frac{\partial B}{\partial \theta_j} S^* B^T + B S^* \frac{\partial B^T}{\partial \theta_j} \right) \right) + \\ + tr\left( \left( N + N^T \right) Q \right) \tag{2.126}$$

For the case of white noise excitation, $A = A_s$, $B = B_s$ and the derivatives of the matrices $A$ and $B$ can be obtained by (2.115) and (2.116) in the form

$$\frac{\partial A}{\partial \theta_j} = -\begin{bmatrix} \mathbf{0}_{mm} & \mathbf{0}_{mm} \\ \frac{\partial \Omega^2}{\partial \theta_j} & 2Z \frac{\partial \Omega}{\partial \theta_j} \end{bmatrix} \tag{2.127}$$

$$\frac{\partial B}{\partial \theta_j} = \begin{bmatrix} 0_{mn_f} \\ \frac{\partial \Phi^T}{\partial \theta_j} R \end{bmatrix} \tag{2.128}$$

The gradient of the modal frequencies and modeshapes can be calculated using Nelson's method (Nelson, 1976), specialized for symmetric mass and stiffness

matrices. This methodology computes the derivatives of the $r$-th eigenvalue and eigenvector with respect to a parameter $\theta_j$ in the parameter set $\underline{\theta}$ from the following formulas (Ntotsios and Papadimitriou, 2008)

$$\frac{\partial \omega_r^2}{\partial \theta_j} = \underline{\phi}_r^T (K_j - \omega_r^2 M_j) \underline{\phi}_r \tag{2.129}$$

$$\frac{\partial \omega_r}{\partial \theta_j} = \frac{1}{2\omega_r} \frac{\partial \omega_r^2}{\partial \theta_j} \tag{2.130}$$

and

$$\frac{\partial \underline{\phi}_r}{\partial \theta_j} = (I - \underline{\phi}_r \underline{\phi}_r^T M) A_r^{*-1} \underline{F}_r^* - \frac{1}{2} \underline{\phi}_r \underline{\phi}_r^T M_j \underline{\phi}_r \tag{2.131}$$

where

$$A_r = K - \omega_r^2 M \tag{2.132}$$

$$\underline{F}_{r,j} = -\frac{\partial A_r}{\partial \theta_j} \underline{\phi}_r = -(I - M \underline{\phi}_r \underline{\phi}_r^T)(K_j - \omega_r^2 M_j) \underline{\phi}_r \tag{2.133}$$

$$M_j \equiv M_j(\underline{\theta}) = \frac{\partial M(\underline{\theta})}{\partial \theta_j} \tag{2.134}$$

$$K_j \equiv K_j(\underline{\theta}) = \frac{\partial K(\underline{\theta})}{\partial \theta_j} \tag{2.135}$$

For notational convenience, the dependence of several variables on the parameter set $\underline{\theta}$ has been dropped. For an $n' \; n$ matrix $A_r$ referring to the formulation for the $r$-th mode, $A_r^*$ is used to denote the modified matrix derived from the matrix $A_r$ by replacing the elements of the $k$-th column and the $k$-th row by zeroes and the $(k, k)$ element of $A_r$ by one, where $k$ denotes the element of the modeshape vector $\underline{\phi}_r$ with the highest absolute value. Also, the vector $\underline{F}_r^*$ is used to denote the modified vector derived from $\underline{F}_r$ replacing the $k$-th element of the vector $\underline{F}_r$ by zero. More details can be found in the work by Nelson (Nelson, 1976).

For the case of filtered white noise excitation, the matrices $A$ and $B$ are given with respect to the system and filter matrices by (2.58) and (2.59). For the case of second order filter, $A$ and $B$ are given by (2.71) and (2.72). Thus, using (2.115) and (2.116), the matrices $A$ and $B$ take the form

$$A=\begin{bmatrix} 0_{mm} & I_{mm} & 0_{m1} & 0_{m1} \\ -\Omega^2 & -2Z\Omega & -\Phi^T R\omega_g^2 & -\Phi^T R2\zeta_g\omega_g \\ 0_{1m} & 0_{1m} & 0 & 1 \\ 0_{1m} & 0_{1m} & -\omega_g^2 & -\zeta_g\omega_g \end{bmatrix} \tag{2.136}$$

$$B=\begin{bmatrix} 0_{m1} \\ \alpha\Phi^T R \\ 0 \\ \alpha \end{bmatrix} \tag{2.137}$$

The derivatives of $A$ and $B$ can thus be obtained in the form

$$\frac{\partial A}{\partial\theta_j}=-\begin{bmatrix} 0_{mm} & 0_{mm} & 0_{m1} & 0_{m1} \\ \dfrac{\partial\Omega^2}{\partial\theta_j} & 2Z\dfrac{\partial\Omega}{\partial\theta_j} & \dfrac{\partial\Phi^T}{\partial\theta_j}R\omega_g^2 & \dfrac{\partial\Phi^T}{\partial\theta_j}R2\zeta_g\omega_g \\ 0_{1m} & 0_{1m} & 0 & 0 \\ 0_{1m} & 0_{1m} & 0 & 0 \end{bmatrix} \tag{2.138}$$

$$\frac{\partial B}{\partial\theta_j}=\begin{bmatrix} 0_{m1} \\ \alpha\dfrac{\partial\Phi^T}{\partial\theta_j}R \\ 0 \\ 0 \end{bmatrix} \tag{2.139}$$

## 2.6 Illustrative Example: 2-DOF System

In this section the sizing optimization of a two degrees of freedom bar - mass system is considered. A schematic diagram of such a system is shown in Figure 2.1. The equations of motion for the 2-DOF system is given by (2.43), where the mass and stiffness matrices $M$ and $K$ are given by

$$M=\begin{bmatrix} m_1+m & 0 \\ 0 & m_2+m \end{bmatrix} \tag{2.140}$$

$$K=\begin{bmatrix} k_1+k_2 & -k_2 \\ -k_2 & k_2 \end{bmatrix} \tag{2.141}$$

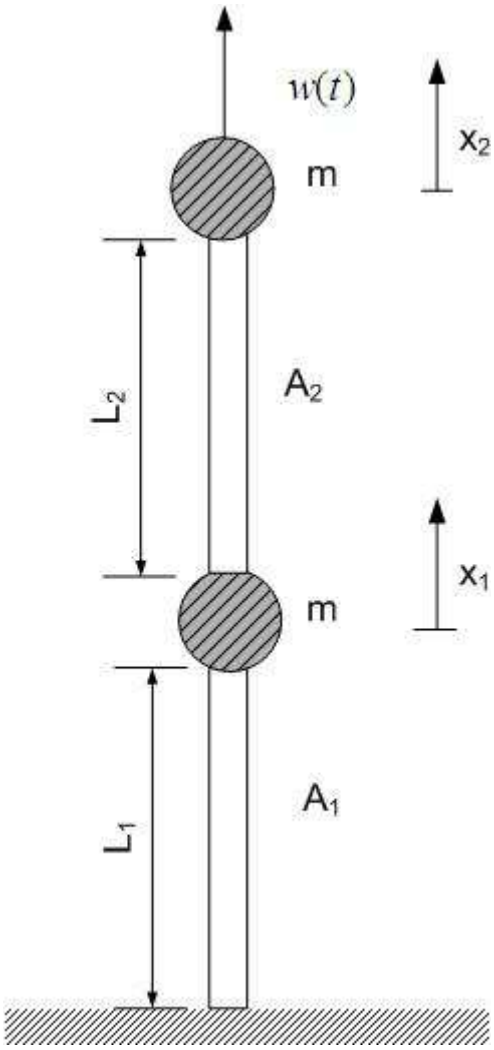


**Figure 2.1:** Two degrees of freedom bar – mass system

and $C$ is the damping matrix, which is assumed to be given by Rayleigh damping. Note that the quantity $m_j$, $j=1,2$ denotes the mass of the two bars which is lumped at the two nodes and are equal to

$$m_j = \rho A_j L_j \tag{2.142}$$

where $\rho$ is the density of the material, $A$ is the cross sectional area and $L$ is the length of the bar. Furthermore, additional masses $m$ can be added to the nodes of the structure. The quantities $k_j$, $j=1,2$ are the axial stiffnesses of the trusses, given by

$$k_j = \frac{EA_j}{L_j} \tag{2.143}$$

where $E$ is the Young modulus of the material. In order to investigate the response of this simple system and find the optimum distribution of the material at the two bars, the following assumptions are considered. The length and the material of the trusses are considered to be the same, whereas the cross sectional areas $A_j$ are the structural parameters to optimize. Since the only parameters that define the volume (mass) distribution are the cross sectional areas $A_1$ and $A_2$, the constrain given in (2.37) can be replaced by the constrain

$$A_1 + A_2 = c \tag{2.144}$$

where $c$ is constant which for the specific case is chosen to be equal to one. Furthermore, the value of the material density $\rho$ is chosen to be equal to 7850 kg/m$^3$, the length of the truss $L$ is chosen to be 1m, the Young modulus is equal to $2 \cdot 10^{11}$ and the damping ratio is chosen to be 2%.

In order to solve the optimization problem stated in equations (2.74), (2.53) and (2.144), the simple method of exhaustive search is used. That is, since there is a relationship between the two optimization parameters $A_1$ and $A_2$, given in (2.144) , then one can evaluate the objective function $J$ with respect to the optimization parameter $A_1$ and consequently find the optimum values of the parameters that minimize the value of the objective function.

Results are next presented separately for the static and dynamic case. Two performance functions are considered, one related to the edge displacement and one related to the stresses in the two bar elements.

### 2.6.1 Displacement – Based Optimal Design under Static Loads

The solution of the case that the excitation of the system is a static load at the second mass and the quantity to be minimized is the displacement of the second mass, is trivial. That is the values of the optimization parameters for the optimal solution are equal to 0.5, result which is clearly depicted in Figure 2.3.

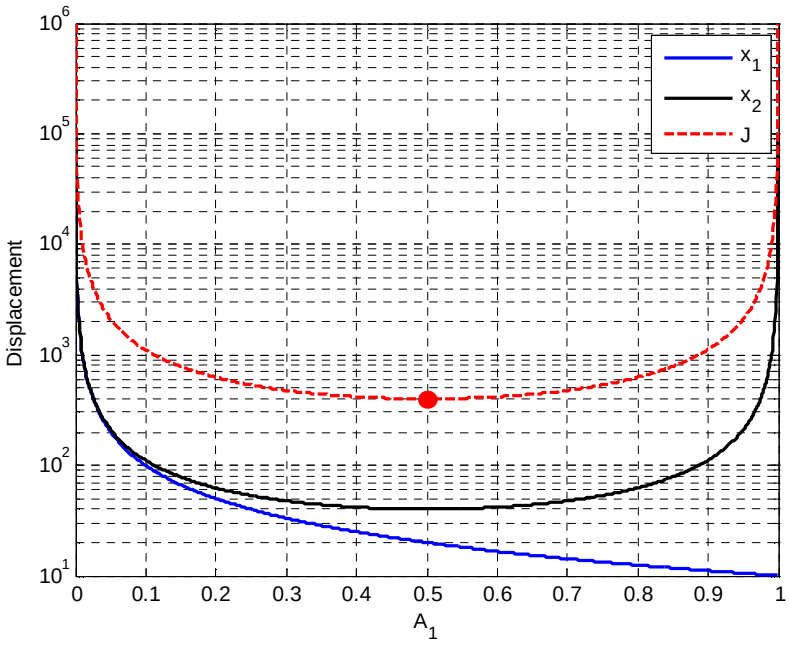


**Figure 2.2:** Displacement with respect to $A_1$.

Next, the case that the loading is static and the quantity to be minimized is the weighted sum of the displacements of both masses is considered. As it shown in Figure 2.3, the optimal value for the cross sectional area of the first member is equal to $A_1 = 0.5856$ and therefore the value of the cross sectional area for the second member is equal to $A_2 = 0.4144$.

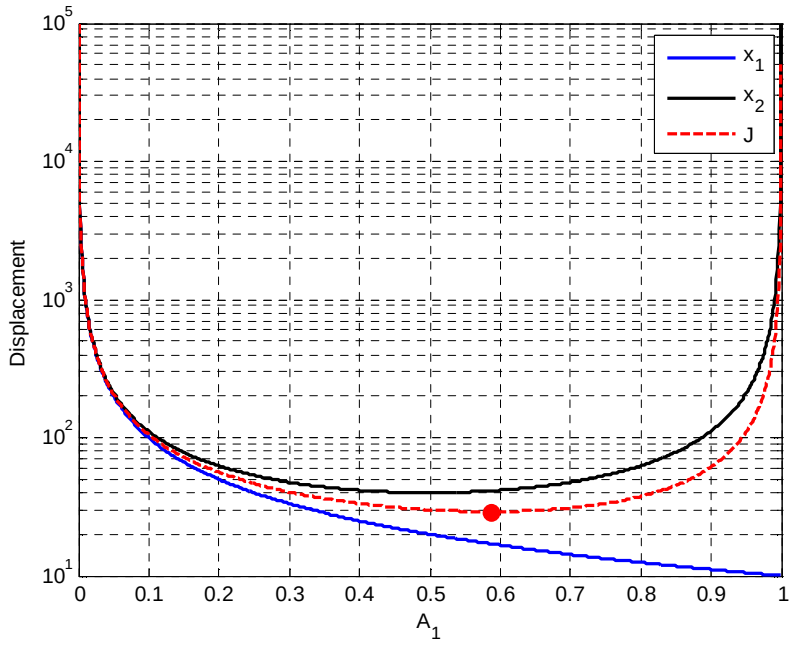


**Figure 2.3:** Displacement with respect to $A_1$.

### 2.6.2 Displacement – Based Optimal Design under Stochastic Dynamic Loads

In Figure 2.4 the results of the exhaustive search for the optimization problem are presented for the dynamic case, and for nodal masses selected to be $m = 0$. That is the value of the covariance of the mass displacement, as well as the value of the objective function are calculated with respect to the optimization parameter $A_1$. In order to evaluate the objective function for the case of minimum nodal displacements, the matrices $C$ and $W$ are given by

$$C = \begin{bmatrix} 1 & 0 \\ 0 & 1 \end{bmatrix} \tag{2.145}$$

$$W = \begin{bmatrix} 0.5 & 0 \\ 0 & 0.5 \end{bmatrix} \tag{2.146}$$

It is observed that the optimal value of the optimization parameter is $A_1 = 0.513$ and using (2.144) one has $A_2 = 0.487$. Next, in Figure 2.5, the same results are presented but for nodal masses selected to be $m = 30\rho AL$, where $A$ and $L$ are equal to one. It is seen that a 3% difference appears at the optimal solution, as the optimum value of the optimization parameter is $A_1 = 0.529$.

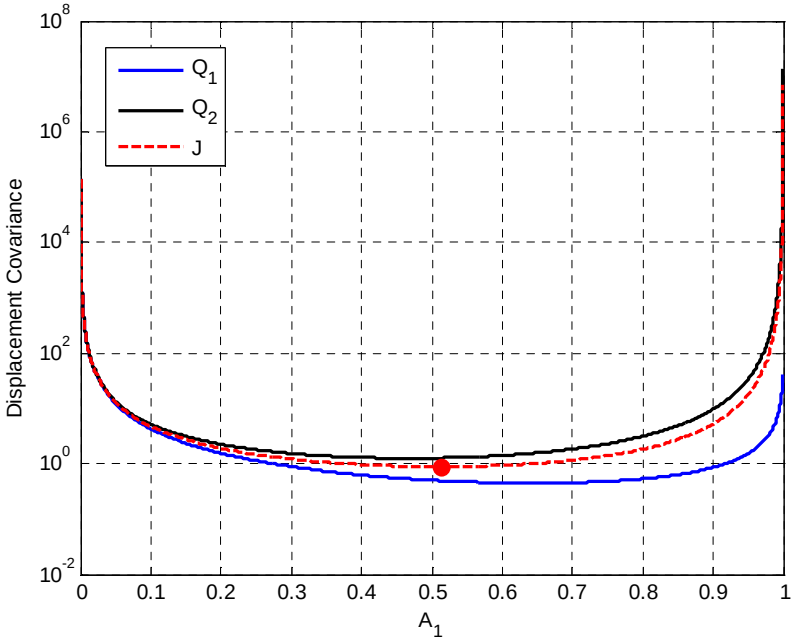


**Figure 2.4:** Covariance with respect to $A_1$ for $m = 0$.

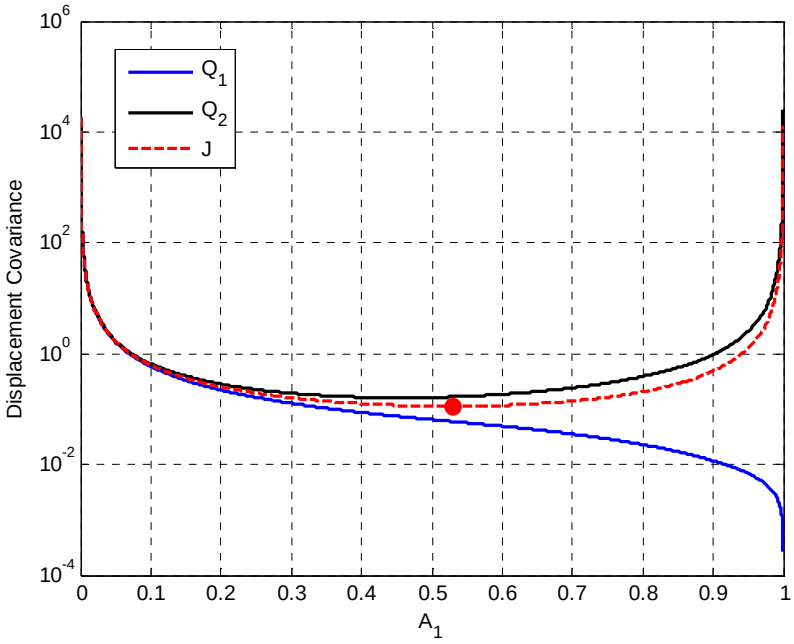


**Figure 2.5:** Covariance with respect to $A_1$ for $m = 30\rho AL$.

Finally, in Figure 2.6, the optimal value of $A_1$ and $A_2$ as a function of the value of the nodal mass $m$. The parameter $\alpha$ denotes the factor that multiplies the quantity $\rho AL$ so that

$$m = \alpha \rho AL \tag{2.147}$$

It is observed that as the mass $m$ increases from 0 to 30, the optimal solution tends to increase the cross sectional area of the first truss $A_1$, whereas the cross sectional area of the second truss $A_2$ decreases equivalently, following the relationship (2.144).

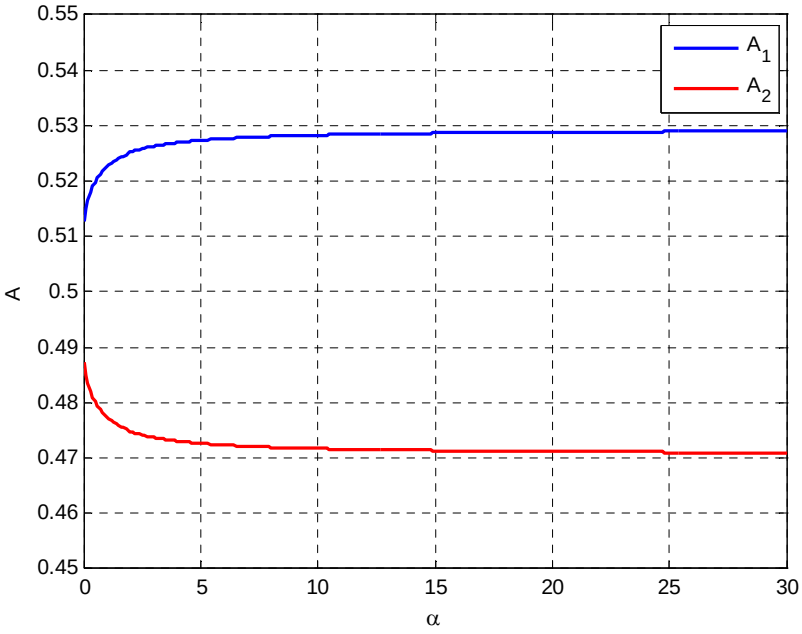


**Figure 2.6:** Optimal value of $A_1$ and $A_2$ with respect to $\alpha$.

### 2.6.3 Stress – Based Optimal Design under Stochastic Dynamic Loads

In Figure 2.7 the results of the exhaustive search for the optimization problem are presented for the dynamic case, and for $m = 0$. That is the value of the variance of the stresses, as well as the value of the objective function are calculated with respect to the optimization parameter $A_1$. In order to evaluate the objective function for the case of minimum truss stresses, the matrices $C$ and $W$ are given by

$$C = \frac{E}{L}\begin{bmatrix} 1 & 0 \\ 1 & -1 \end{bmatrix} \tag{2.148}$$

$$W = \begin{bmatrix} 0.5 & 0 \\ 0 & 0.5 \end{bmatrix} \tag{2.149}$$

where $E$ is the Young modulus of the material. It is observed that the optimal value of the optimization parameter is $A_1 = 0.477$ and using (2.144) one has $A_2 = 0.523$. Next, in Figure 2.8, the same results are presented but for $m = 30\rho AL$, where $A$ and $L$ are equal to one. It is seen that the optimal solution changes about 9%, as the optimum value of the optimization parameter is $A_1 = 0.526$, whereas $A_2 = 0.474$.

Finally, in Figure 2.9, the optimal values of the cross sectional areas $A_1$ and $A_2$ as a function of the parameter $\alpha$ are shown. It is observed that as the mass $m$ decreases towards zero, the optimal solution tends to decrease the cross sectional area of the first truss $A_1$, whereas the cross sectional area of the second truss $A_2$ is increasing.

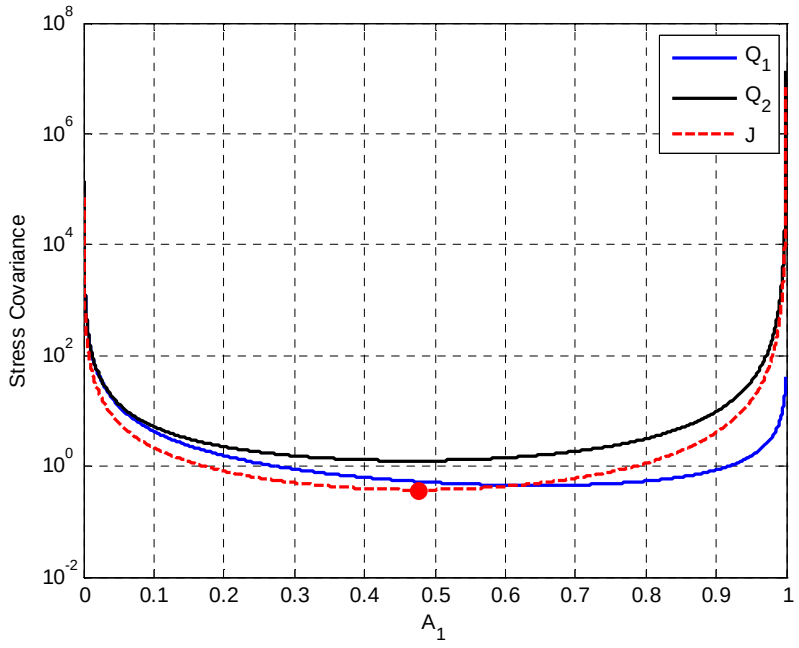


**Figure 2.7:** Variance with respect to $A_1$ for $m = 0$.

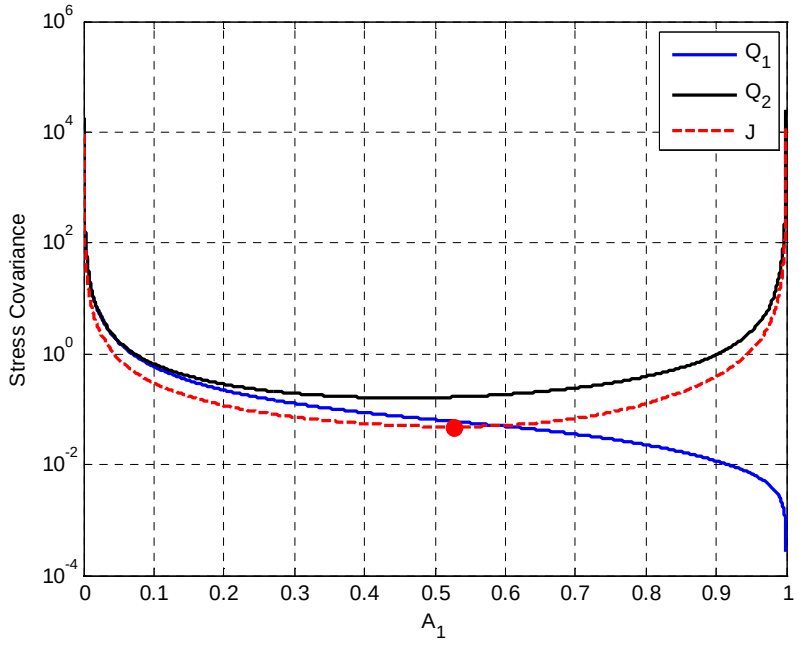


**Figure 2.8:** Variance with respect to $A_1$ for $m = 30\rho AL$.

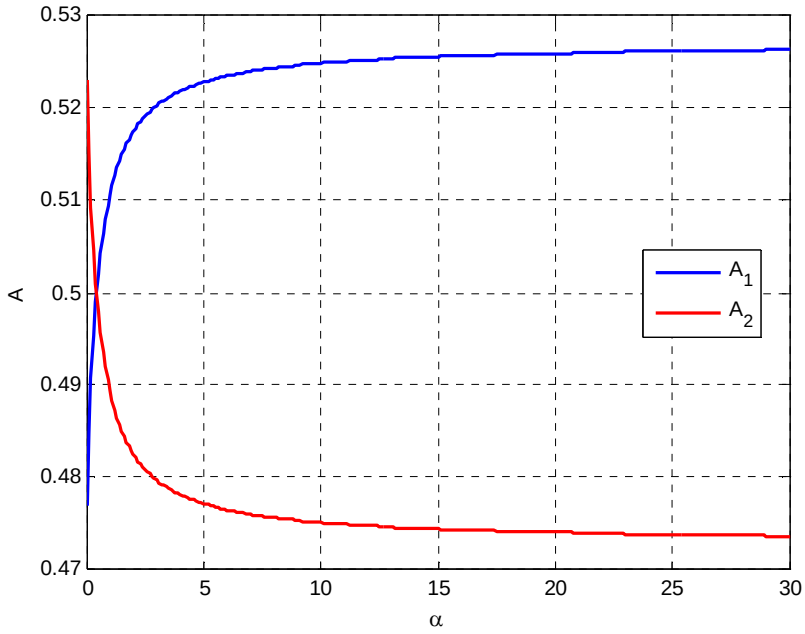


**Figure 2.9:** Optimal value $A_1$ with respect to $\alpha$.

## 2.7 Conclusions

In this chapter, an innovative methodology for the optimization of the performance of multi-degree-of-freedom systems, under stochastic dynamic excitations has been presented. The performance of the system response is quantified by using different measures of the response, such as the weighted sum of the variance of the nodal displacements or the weighted sum of the variance of the developed stresses in the structural parts. The variance of the response quantities have been estimated very efficiently by solving the Lyapunov equation of the system. Additionally, the adjoint method is used in order to efficiently and accurately estimate the sensitivities of the objective function with respect to the design variables, thus minimizing the computational effort needed to estimate the derivatives of the objective function numerically. The formulation of the optimization problem has been presented for both Gaussian white noise excitation and filtered white noise excitation.

Next, the proposed methodology has been extended to the modal space, in order to take advantage of the efficiency of modal analysis, by using a limited number of contributing modes for the estimation of the system response. The adjoint method is also used in this case of modal analysis in order to calculate the derivatives of the objective function with respect to the design variables. Similarly, the proposed methodology has been formulated for white and filtered noise excitation. Finally, the proposed methodology has been applied on the sizing optimization of a simple 2DOF bar – mass system in order to illustrate its applicability. It has been shown that the optimal results for different cases of performance functions are slightly different for this simple one dimensional system.

# CHAPTER 3 Size and Topology Optimization of Truss Structures

## 3.1 Introduction

The design optimization methodologies proposed in Chapter 2 are applied in the sizing and topology optimization of truss structures. Such problems are stated as follows. Given a set of loads, static or dynamic, find the topology and size of a truss structure to withstand these loads, so that the performance is optimum and the constrains are not violated. The effectiveness of the proposed design methodology is demonstrated using a specific class of two dimensional truss structures.

In this chapter, results for all the cases of loading on a two-dimensional truss structure are presented. The truss structure consists of base parts, as the one shown in Figure 3.2. The final truss structure is built by several connecting base parts together. The total length of the system is considered to be fixed, and equal to 4m, whereas the total height is also fixed and equal to 2m. The three nodes at the left side of the structure are considered to be pinned and the loading is considered to be applied on the middle node at the right edge of the structure at distance 4m from the left end. Furthermore, the value of the material density $\rho$ is chosen to be equal to 7850 kg/m$^3$, the Young modulus is equal to $2 \cdot 10^{11}$ Pa and

the Rayleigh damping matrix is chosen such that the damping ratio is equal to 2% at the first and the fifth mode in the case of dynamic loading. The set of the optimization parameters $\underline{\theta}$ is chosen to be the cross-section area of each truss of the structure. The configurations of the truss with one, two, four, and six base parts are shown in Figure 3.2.

First, after a short description of the truss structure, an iterative process for the size and topology optimization of such systems is described. Next, the methodology for the deterministic static case is applied on the truss structure, using as performance function a combination of the displacement at the nodes and thus obtaining the optimal configurations for the structure. Subsequently, results for the case of stochastic dynamic loading are presented using the output displacements as performance function. The optimal configurations are presented and compared with the optimal results for the case of deterministic static loading. Stress-base design optimization applied on the truss structures for both deterministic static and stochastic dynamic loading follows. The optimal configurations are presented, along with a comparison between the static and dynamic case, as well as between the stress-based and displacement-based design optimization. Finally, the design optimization using the modal space approach is applied on the aforementioned truss structures, along with the displacement-based performance function. The results using limited amount of modes are presented and the effect of modal contribution in the optimal results is discussed.

## 3.2 Iterative Process for Size and Topology Optimization of Trusses

From the topology optimization point of view, the objective is to find the optimal number of base parts needed for the truss to curry the static or dynamic load. From the sizing optimization point of view, the objective is to find the optimal values of the cross-sectional areas for the optimal number of base parts selected. This sizing and topology optimization problem is solved as follows. First, the sizing optimization problem is solved for a truss structure corresponding to a selected number $n_b$ of base parts. Then the procedure is repeated by varying $n_b$ from one up to a selected number. Finally, the objective values of the optimal structures for different number of base parts are compared and the optimal truss structure is the one corresponding to the number of base parts with the minimum objective value. If $N_b$ is the maximum number of base parts used, then the process requires the solution of $N_b$ constrained optimization problems.

In order to find the final optimal shape of each structure, an iterative process is applied. At the first step of this process, the vector of the design parameters $\underline{\theta}$ contains all the cross sectional areas of the initial structure, as shown in Figure 3.2. A gradient-based optimization algorithm is the used in order to find the optimal values of the parameters. At the next step, the parameters with optimal values that are close to zero are removed from the design set, thus changing the shape of the structure. Note that if the value of the cross sectional area of the truss becomes equal to zero during the optimization process, the stiffness matrix becomes singular, causing problems to the optimization process. To overcome such problems, lower bounds are introduced for the design parameters associated with the cross sectional area. Such lower bound is denoted by $A_0$ and is taken to be the same for design parameters in $\underline{\theta}$. Given the volume $V_0$, the value of the lower bound $A_0$ is selected to be a very small percentage of the average cross sectional area corresponding to $V_0$ for the $n_t$ active members of the truss structure. Note that the total volume of the structure is given by

$$V_0 = \sum_{i=1}^{n_t} A_i L_i \tag{3.1}$$

Under the assumption that all the cross sectional areas of all the members are equal to $A$, one has $V_0 = A\sum_{i=1}^{n_t} L_i$, resulting in

$$A = \frac{V_0}{\sum_{i=1}^{n_t} L_i} \tag{3.2}$$

Therefore, a good estimation of the average cross sectional area of the members of the truss structure can be the total volume divided by the total length of the members of the structure. The lower value of $A_0$ is selected to be

$$A_0 = \alpha \frac{V_0}{\sum_{i=1}^{n} L_i} \tag{3.3}$$

where $\alpha$ is the fraction of the average cross sectional area, chosen to be equal to $10^{-3}$. Consequently, the members of the optimal solution that have cross sectional area close to the lower value are removed, and the process progresses to the next step, where the optimization procedure continues using the new reduced parameters set. If the optimal result of this iteration contains no truss members with cross sectional areas close to the lower bound, then the iterative process stops

and the result is accepted as the optimum structure. If the optimal result contains truss members with cross sectional areas close to the lower bound the iteration process continues.

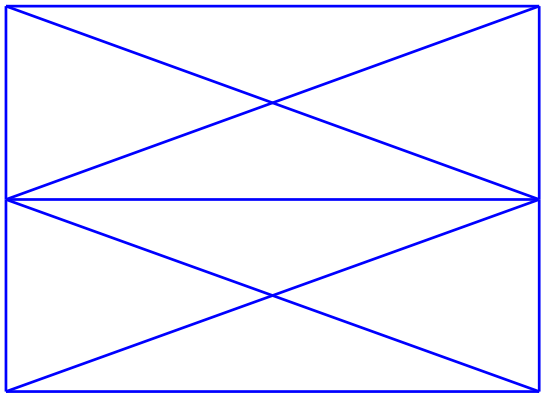

**Figure 3.1:** Schematic diagram of a base part.

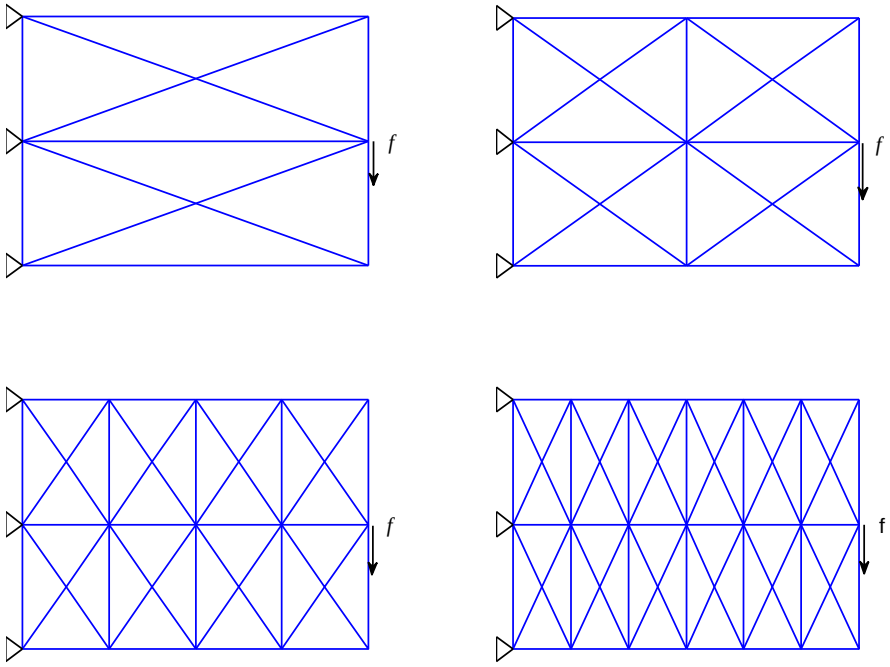


**Figure 3.2:** Ground structures of (a) one, (b) two, (c) four and (d) six base parts.

## 3.3 Displacement – Based Optimal Design under Static Loads

Two cases, denoted as Case A and Case B are considered. In the Case A, the performance function is selected to be the variance of the displacement of the truss along the degree of freedom on which the load is applied. In Case B, the performance function is selected to be the weighted sum of the variances of the displacements at all degrees of freedom, with all weights chosen to be equal. For static loads Case A is the most commonly used in the bibliography.

In Case A of static loading, the optimization problem is stated in (2.1) - (2.4). In Case B of static loading, the optimization problem is stated in (2.23) - (2.26). For both cases the volume constant $V_0$ is chosen to be equal to $10^{-5}\,\mathrm{m}^3$ and the value of the static force is considered to be 1000N.

The optimal truss structures that consist of one up to ten base parts $N_b$ are presented in Figure 3.3 to Figure 3.12. The Figures denoted with (a) refer to Case A, whereas the Figures denoted with (b) refer to Case B. The number next to each truss member is the ratio of the truss member's volume over the total volume of the structure. Additionally, in Table 3.1 and in Table 3.2 are shown the optimal values of the objective function $J$ for the different structures of one up to ten base parts, information which also plotted in Figure 3.13 and Figure 3.14 for Case A and B respectively. Note that in Table 3.2 an additional column with the values of the objective function $J^*$ is shown for the Case B. The objective function $J^*$ is chosen to be equal to the objective function $J$ defined for Case A. This definition is very useful when one needs to compare the optimal solutions of structures with different number of base parts. This comparison is impossible using the objective function $J$ for Case B, as the degrees of freedom at the optimal solution change with respect to the number of base parts, thus the number of terms in the summation is also different. Therefore, in order to define the optimal solution between the optimal solutions with different number of base parts, the objective function $J^*$ should be used. It is observed that the structure with the minimum value of the objective function for both cases, consists of two base parts, that is the optimal structure for static loading for these specific dimensions is the structure that is shown in Figure 3.4a and in Figure 3.4b for the Case A and B respectively.

For Case A, it is observed that the optimization trend is to eliminate all the vertical members, except for the cases of two base parts in Figure 3.4, where two vertical members are not eliminated. Furthermore, the middle horizontal members are also eliminated, whereas the bottom and top edge horizontal members are kept

in place. In addition, a symmetric, with respect to the middle horizontal axis, optimal truss is obtained, as it should be expected, due to the overall truss configuration and the symmetry of the applied load. It should be noted that for all the base parts considered, the values of the top and bottom horizontal members are decreasing, as one moves from the left towards the right side of the structure. In contrast, the diagonal members that are maintained during the optimization process, do not show this decreasing behavior. Specifically, the cross sectional area and thus the volume ratio remains constant.

Figure 3.16 shows an additional optimal solution for two base parts, which corresponds to a local optimum in the optimization process, in relation to the global optimum presented in Figure 3.4a. This is confirmed by noting that the value of the objective function for the optimal solution in Figure 3.16 is equal to 162, which is significantly larger than 112.5, the value of the objective function for the global optimal solution in Figure 3.4a. It should be noted, however, that the local optimal solution in Figure 3.16 has topology that is consistent with the global optimal solutions obtained for all trusses with numbers of parts different from two.

Also, it is worth pointing out interesting results that are obtained for the structure that consists of four base parts. In this case, several global/local optima are obtained. Two such optimal solutions are presented in Figure 3.17 and in Figure 3.18. The values of the objective function are 128.015 and 128 for the first and the second optimal solution respectively, whereas the value for the global solution is 127.99. From the practical point of view and considering numerical errors in the optimization process, these three optimal solutions can be all considered to be global optimal solutions. The optimal solutions in Figure 3.17 and in Figure 3.18 for four base parts are similar in topology with the optimal solution in Figure 3.4a. An exhaustive search has not been undertaken in this study to verify the existence of multiple global solutions for other cases of one to ten base parts of the truss structure. However, the local optimal solution in Figure 3.16 provides clear evidence that if such multiple optimal truss topologies exist, then these solutions are not necessarily global solutions.

For Case B, it is observed that the optimization trend is also to eliminate all the vertical members, except for the cases of two base parts. Furthermore, the middle horizontal members are also eliminated, whereas the top and bottom edge horizontal members are kept in place. Also, as expected, all the optimal structures are symmetric with respect to the middle horizontal axis. It should be noted that for all base parts considered, the values at the top and bottom horizontal members

are decreasing as one moves from the left towards the right side of the structure. Additionally, the values of the cross sections of the diagonal members that are kept in place also show this decreasing behavior, from the left towards the right side of the structure, in contrast to the case of the edge displacement.

Similar to Case A, a local optimal solution also exists for Case B for four base parts. This suboptimal topology is presented in Figure 3.19. The value of the objective function is equal to 0.00264 for the local optimal solution, whereas the value for the global solution is equal to 0.00255. The difference between the value of the objective function for the local and the global solution is less than 4%. This local optimal solution is similar in topology to the optimal solutions shown in Figure 3.4a and in Figure 3.18.

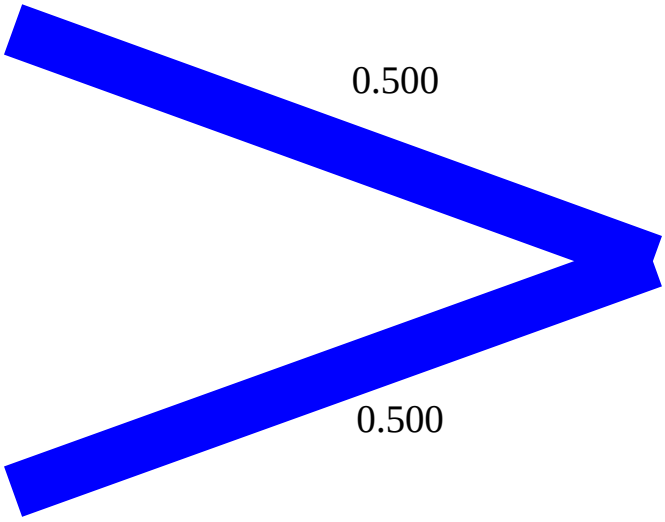


(a)

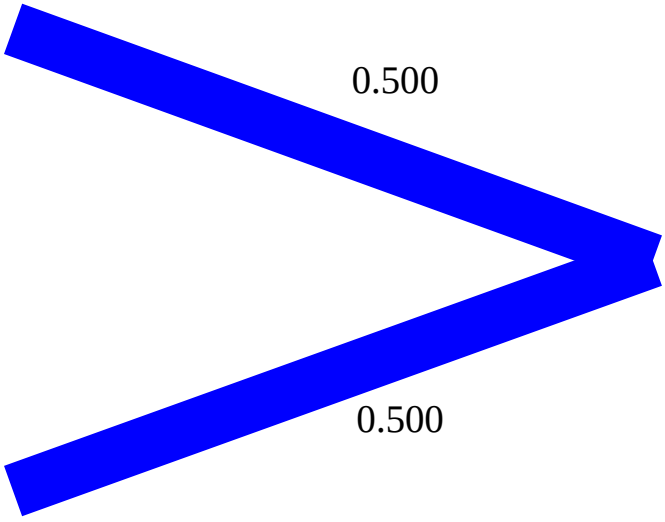


(b)

**Figure 3.3:** Optimal solution for one base part, (a) Case A, (b) Case B.

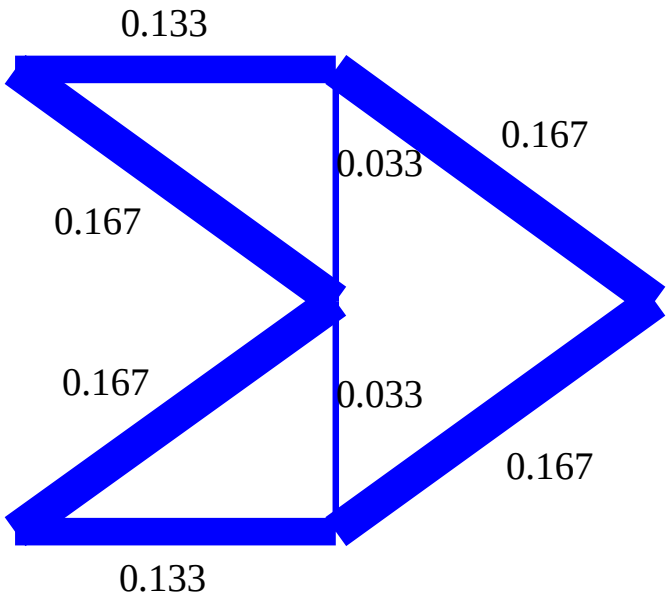


(a)

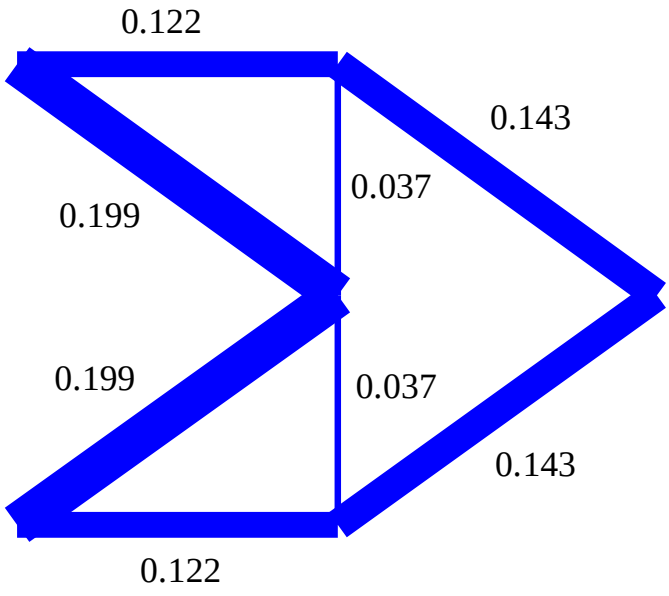


(b)

**Figure 3.4:** Optimal solution for two base parts, (a) Case A, (b) Case B.

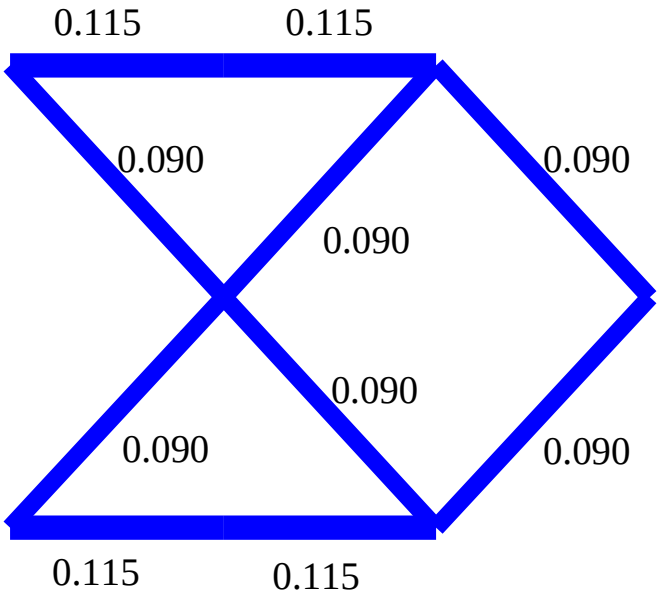


(a)

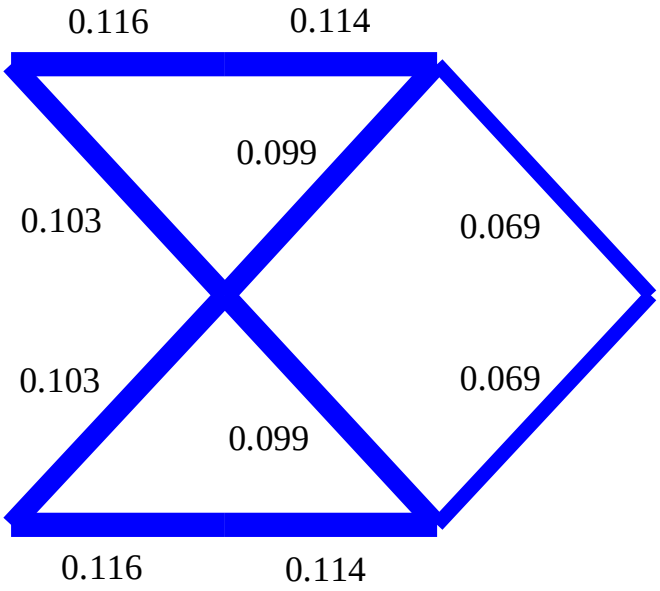


(b)

**Figure 3.5:** Optimal solution for three base parts, (a) Case A, (b) Case B.

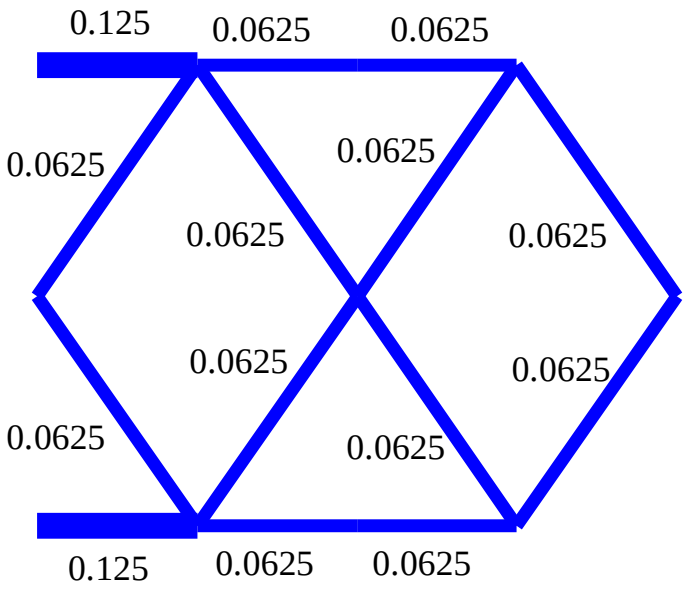


(a)

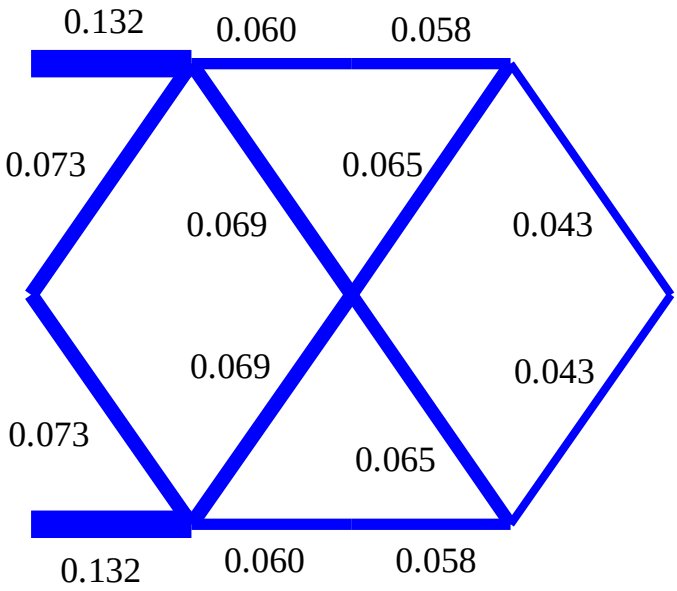


(b)

**Figure 3.6:** Optimal solution for four base parts, (a) Case A, (b) Case B.

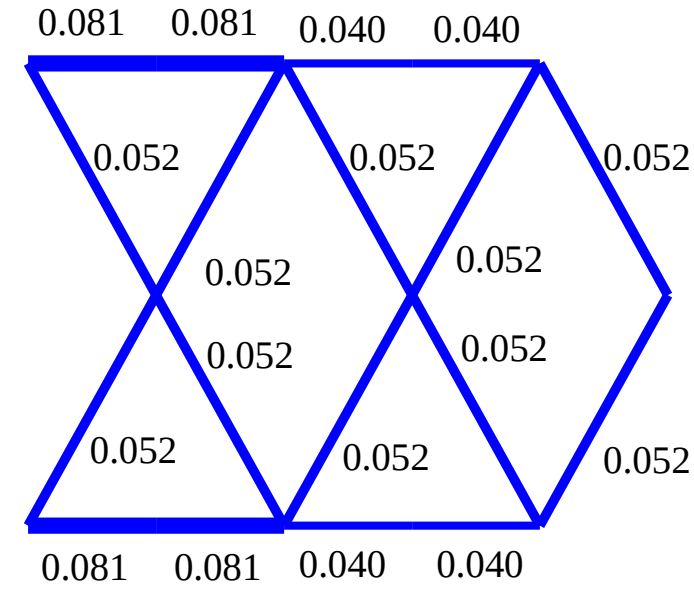


(a)

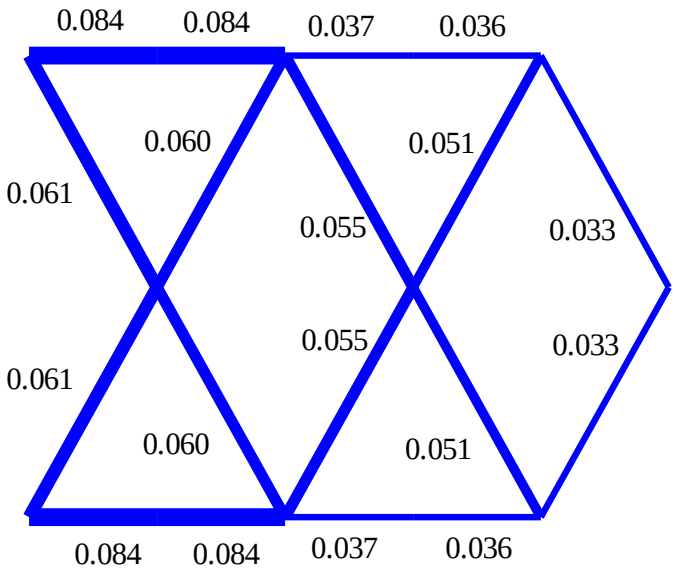


(b)

**Figure 3.7:** Optimal solution for five base parts, (a) Case A, (b) Case B.

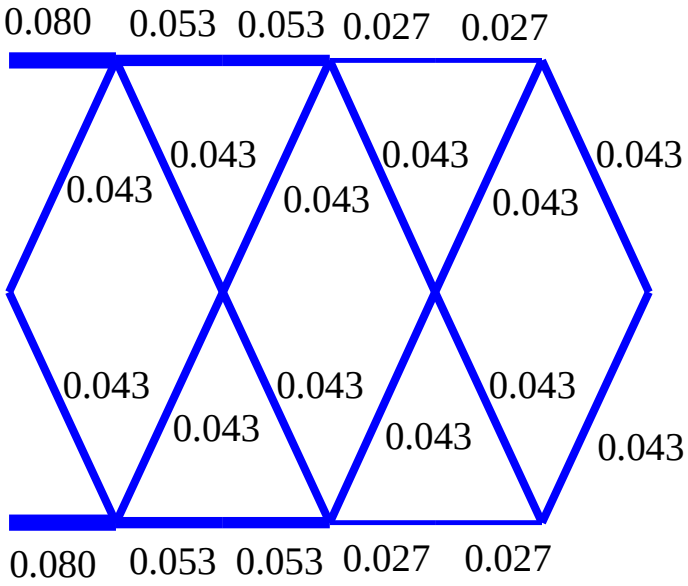


(a)

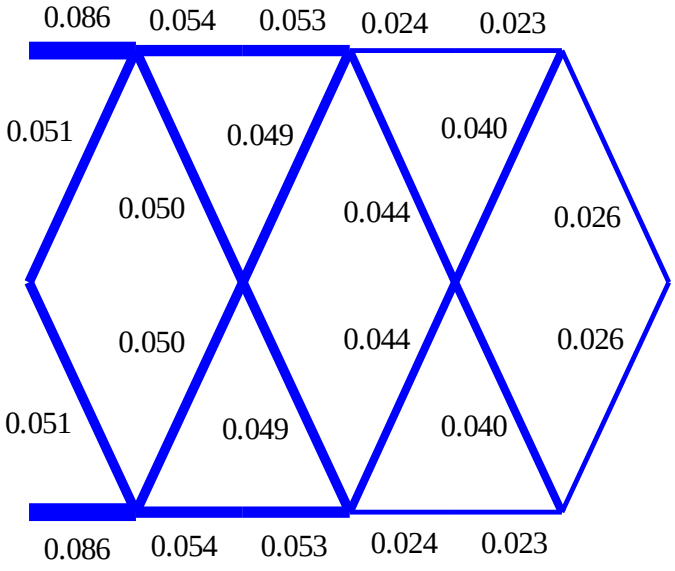


(b)

**Figure 3.8:** Optimal solution for six base parts, (a) Case A, (b) Case B.

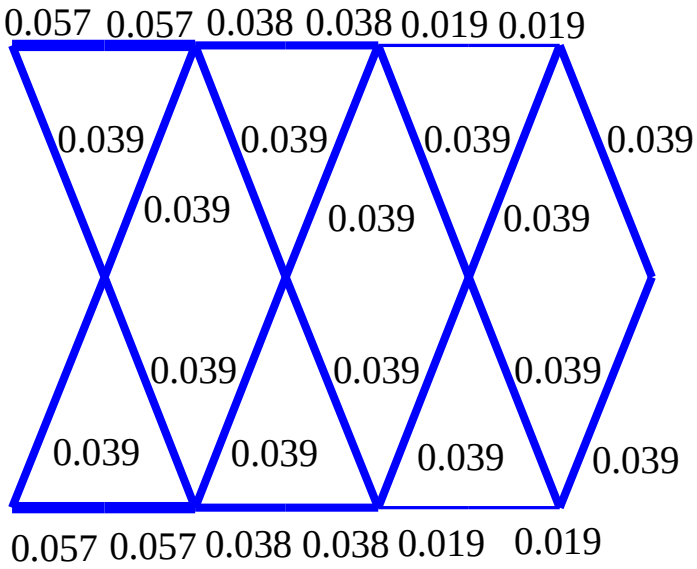


(a)

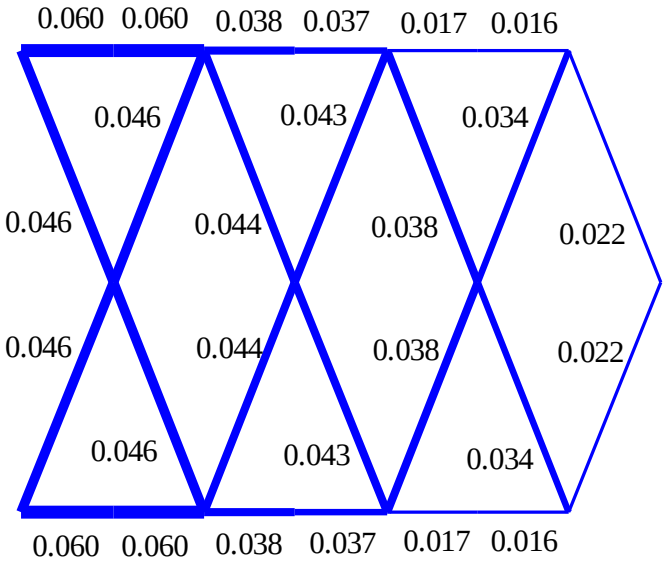


(b)

**Figure 3.9:** Optimal solution for seven base parts, (a) Case A, (b) Case B.

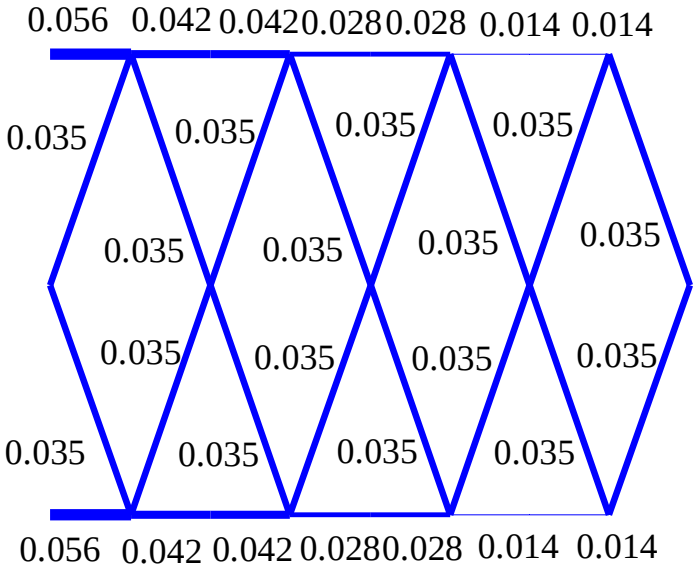


(a)

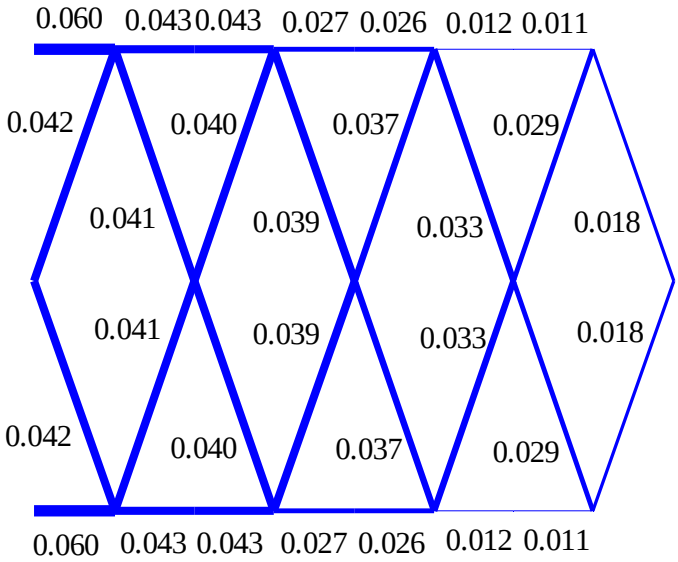


(b)

**Figure 3.10:** Optimal solution for eight base parts, (a) Case A, (b) Case B.

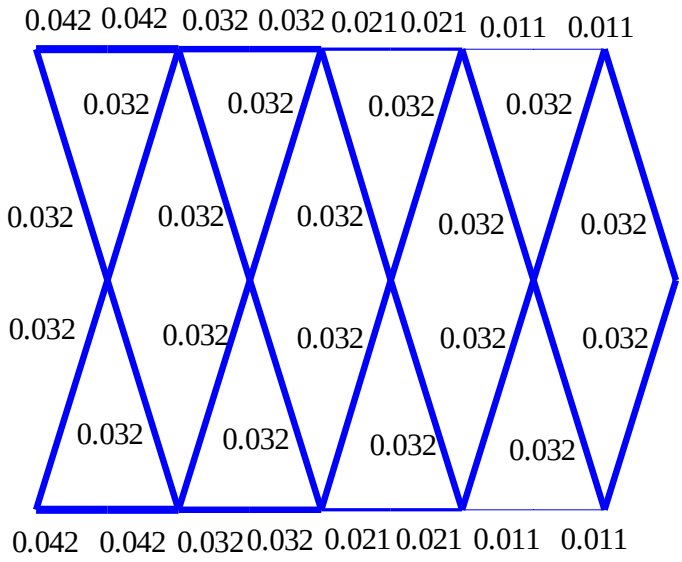


(a)

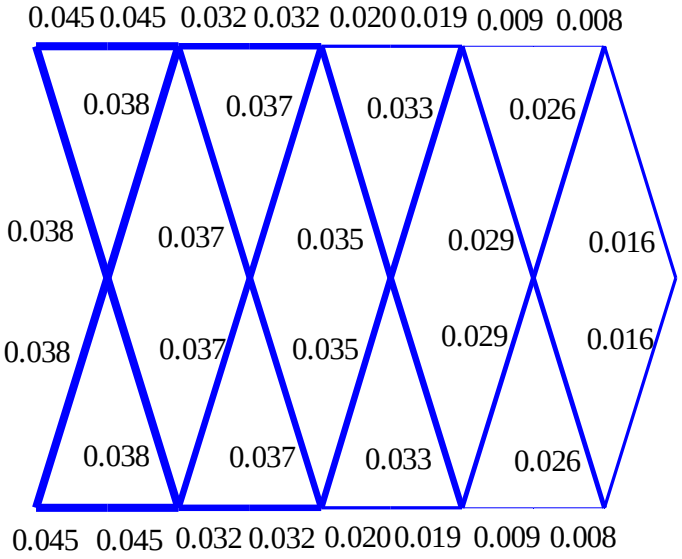


(b)

**Figure 3.11:** Optimal solution for nine base parts, (a) Case A, (b) Case B.

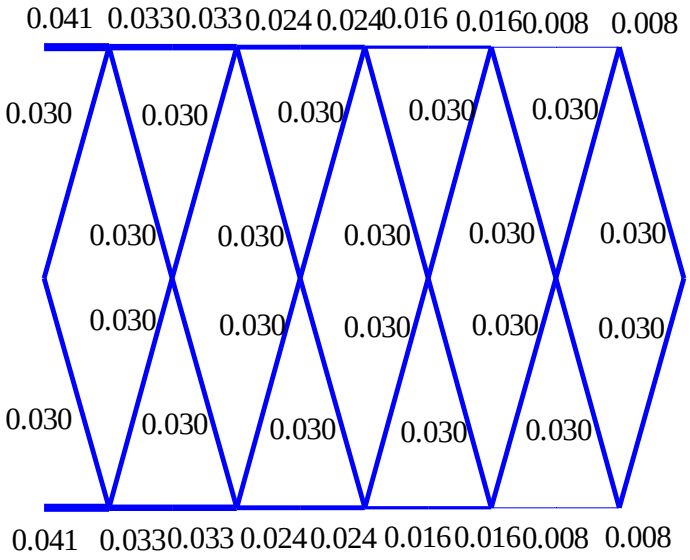


(a)

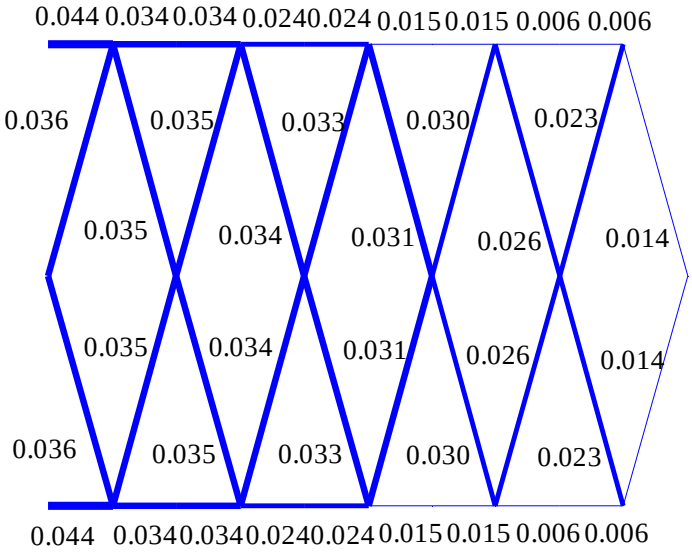


(b)

**Figure 3.12:** Optimal solution for ten base parts, (a) Case A, (b) Case B.

**Table 3.1:** Values of the objective function for one to ten base parts, for Case A.

| Parts | $J$ |
|---|---|
| 1 | 144.5 |
| 2 | 112.5 |
| 3 | 119.3 |
| 4 | 128.0 |
| 5 | 126.1 |
| 6 | 138. 9 |
| 7 | 146.6 |
| 8 | 162.0 |
| 9 | 174.5 |
| 10 | 192.1 |

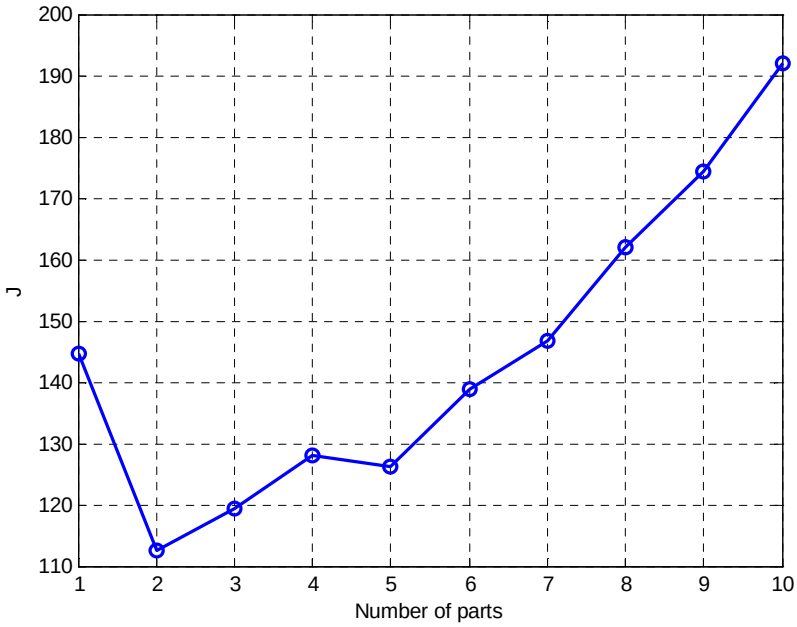


**Figure 3.13:** Optimal values of the objective function $J$ with respect to the number of the base parts of the structure, for Case A.

**Table 3.2:** Values of the objective function for one to ten parts for Case B.

| Parts | $J$ | $J^*$ |
|---|---|---|
| 1 | 0.01044 | 144.5 |
| 2 | 0.00221 | 114.9 |
| 3 | 0.00248 | 121.4 |
| 4 | 0.00255 | 131.1 |
| 5 | 0.00222 | 129.6 |
| 6 | 0.00258 | 143.5 |
| 7 | 0.00273 | 152.1 |
| 8 | 0.00326 | 168.8 |
| 9 | 0.00367 | 182.4 |
| 10 | 0.00439 | 201.6 |

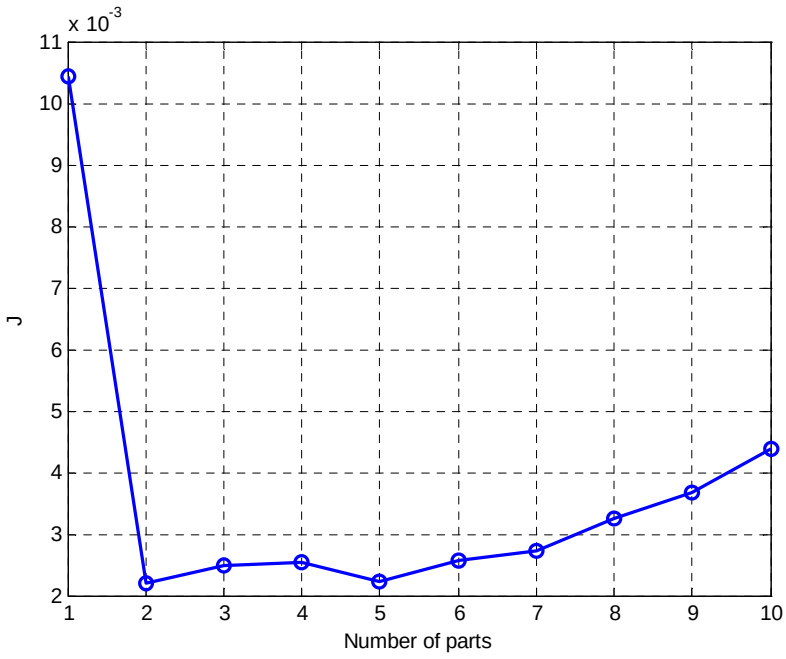


**Figure 3.14:** Optimal values of the objective function $J$ with respect to the number of the parts of the structure, for Case B.

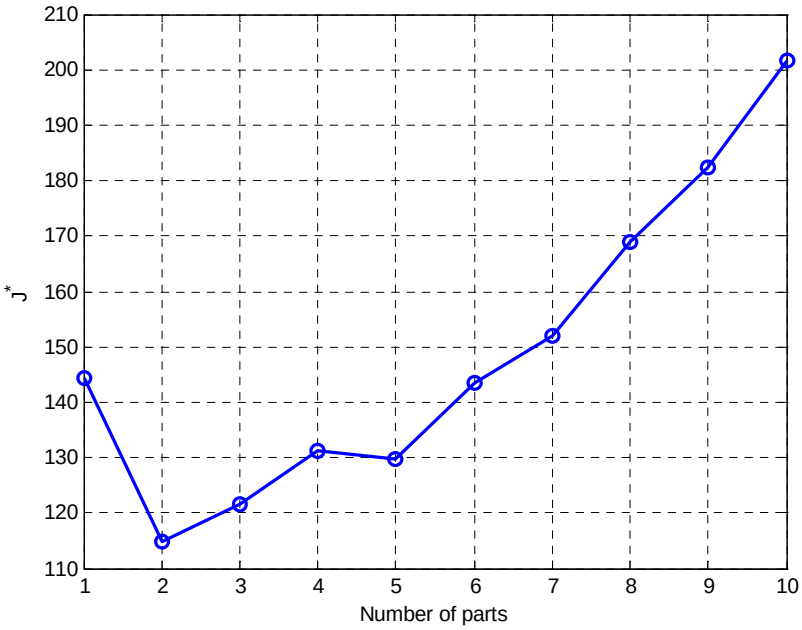


**Figure 3.15:** Optimal values of the objective function $J^*$ with respect to the number of the parts of the structure for, Case B.

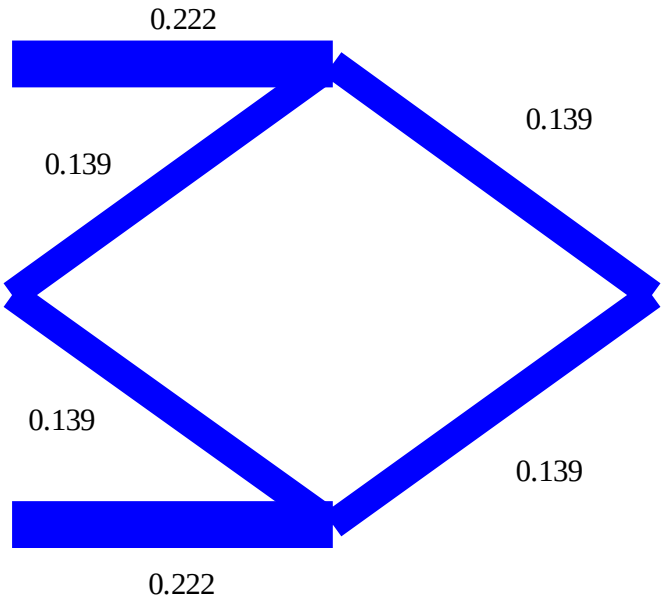


**Figure 3.16:** Local optimal solution for two base parts, for Case A.

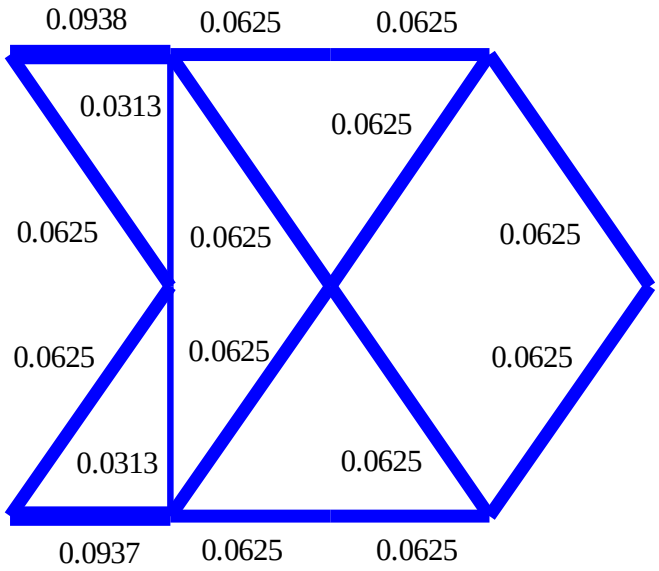


**Figure 3.17:** Optimal solution for four base parts, for Case A.

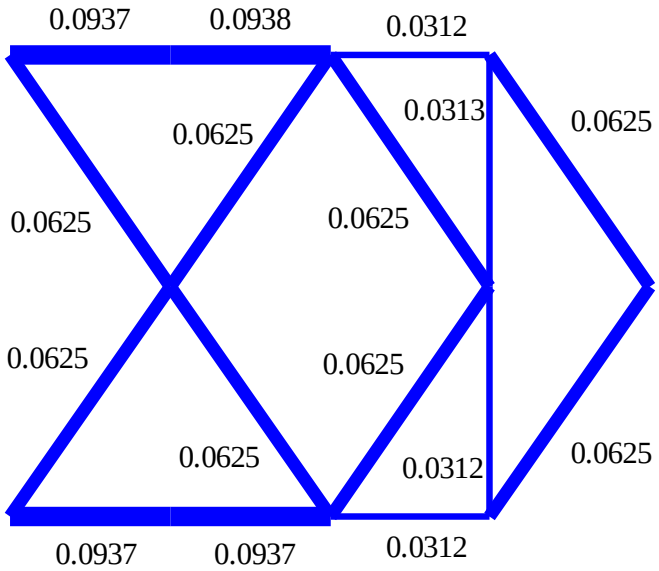


**Figure 3.18:** Optimal solution for four base parts, for Case A.

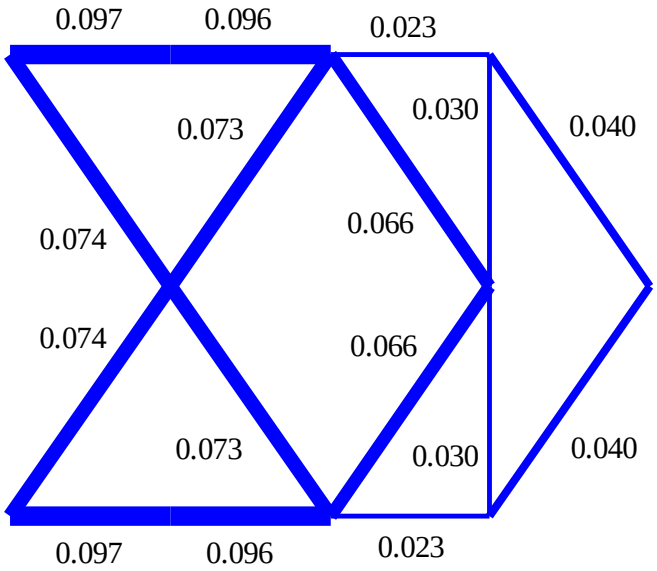


**Figure 3.19:** Local optimal solution for four base parts, for Case B.

## 3.4 Displacement-Based Optimal Design under Stochastic Dynamic Loads

Results for the case of stochastic dynamic loading on a truss structure are presented. The excitation is considered to be white noise, with power spectral density equal to 1000. The performance function is related to the displacements. First, the performance function is selected to be the variance of the displacement of the truss along the degree of freedom on which the load is applied, multiplied by the power spectral density of the white noise excitation. In this case, the optimization problem is stated in (2.35) - (2.38) and the matrix $\Sigma$ is given by (2.85). The total volume of the structure $V_0$ is chosen equal to $10^{-5}\,\mathrm{m}^3$. For this specific case, an additional nodal mass equal to 5kg divided by the degrees of freedom of each system is added at all the nodes of the truss structure. The aforementioned study case is denoted as Case C.

In Figure 3.20 and in Figure 3.21 are presented the optimal structures for one and two base parts respectively. The results for these two cases are quite similar to the results obtained for the static loading (Case A and Case B). On the other hand, the results for three base parts are unexpected. This is due to fact that the optimal

structure obtained is asymmetrical as shown in Figure 3.22(a), and consequently the mirrored structure with respect to the horizontal middle axis is also a solution of the topology optimization as shown in Figure 3.22(b). The value of the objective function is equal to 2.43 for these two topologies. The value of the objective function for the symmetrical solution was found to be equal to 3.60, which is more than 50% higher than the asymmetrical solution. The symmetrical optimal solution was obtained by imposing the cross sectional areas of the truss members that are symmetric with respect to the horizontal middle axis to be equal. The solution of this case is presented in Figure 3.23.

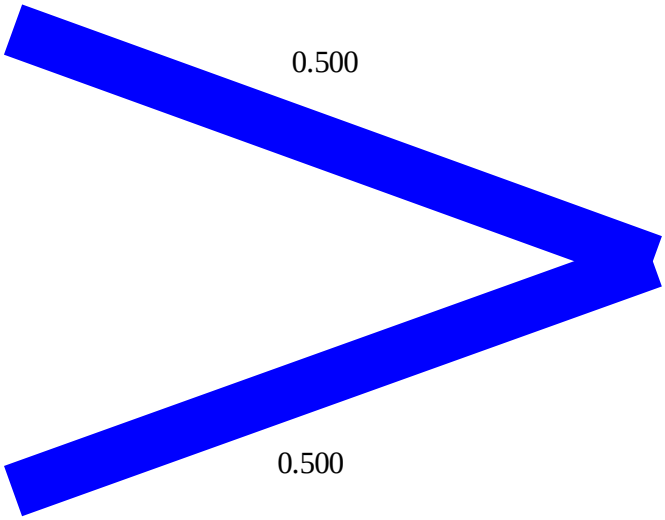


**Figure 3.20:** Optimal solution for one base part, for Case C.

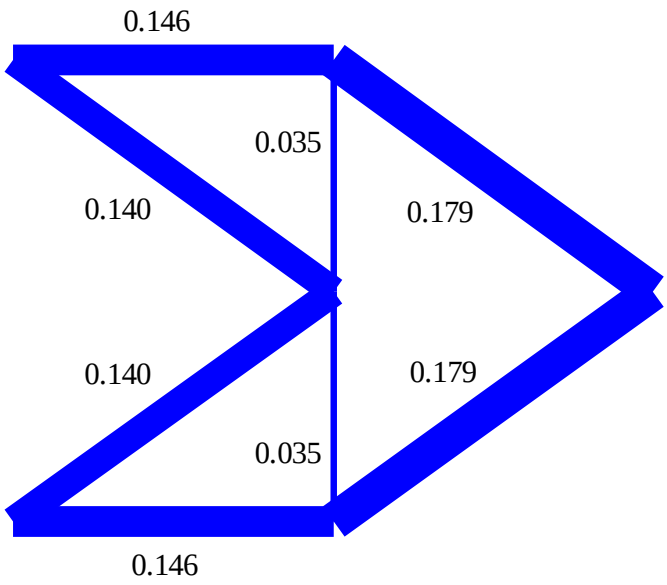


**Figure 3.21:** Optimal solution for two base parts, for Case C.

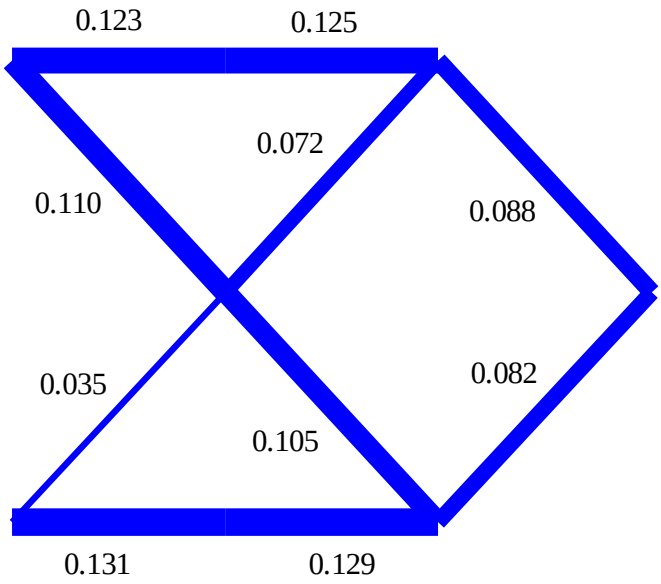


(a)

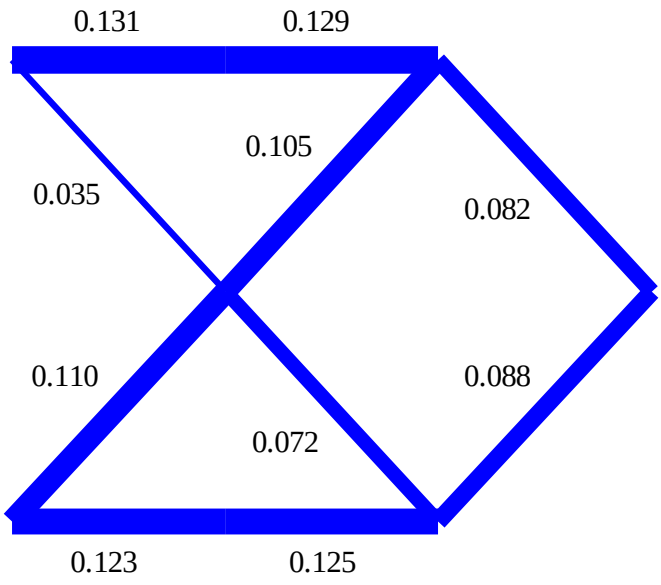


(b)

**Figure 3.22:** Asymmetrical local optimal solutions (a) and (b) for three base parts, for Case C.

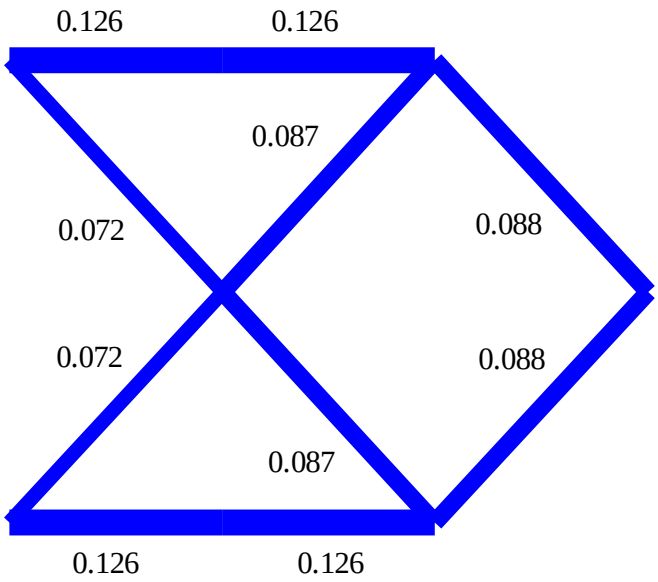


**Figure 3.23:** Symmetrical local optimal solution for three base parts, for Case C.

Next, the performance function is selected to be the weighted sum of the variances of the displacements at all the degrees of freedom of the structure, with all the weights chosen to be equal. In this case, the optimization problem is stated in (2.35) - (2.38), the matrix $\Sigma$ is given by (2.75). Two cases are considered, denoted by Case D and Case E. In case D an additional nodal mass equal to 1kg is added at all the nodes of the truss structure. On the other hand, in Case E, an additional nodal mass equal to 5kg divided by the degrees of freedom of each system is added at all the nodes of the truss structure. For both cases, the volume constant $V_0$ is chosen to be equal to $10^{-5}\,\mathrm{m}^3$ and the value of the power spectral density of the white noise excitation is chosen to be equal to 1000.

The optimal truss structures that consist of one up to ten base parts $N_b$ are presented in Figure 3.24 to Figure 3.33. The Figures denoted with (a) refer to Case D, whereas the Figures denoted with (b) refer to Case E. Additionally, in Table 3.3 and in Table 3.4 are shown the optimal values of the objective function $J$ for the different structures of one up to ten base parts, information which is also plotted in Figure 3.34 and in Figure 3.36, for Case D and E respectively. Note that in Table 3.3 and in Table 3.4 an additional column with the values of the

objective function $J^*$ are shown. The objective function $J^*$ is chosen to be equal to the objective function $J$ defined for Case C. This definition is very useful when one needs to compare the optimal solutions of structures with different number of base parts. This comparison is impossible using the objective function $J$ for the cases D and E, as the degrees of freedom at the optimal solution change with respect to the number of base parts, thus the number of terms in the summation is also different. Therefore, in order to define the optimal solution between the optimal solutions with different number of base parts, the objective function $J^*$ should be used. It is observed that the structure with the minimum value of the objective function for both cases, consists of two base parts, that is the optimal structure for static loading for these specific dimensions is the structure that is shown in Figure 3.25a and in Figure 3.25b for the Case D and E respectively.

It is observed that the optimal configurations for the two cases are exactly the same. For both cases, it is observed that the optimization trend is to eliminate all the vertical members, except for the cases of two base parts in Figure 3.25, where two vertical members are not eliminated. Furthermore, the middle horizontal members are also eliminated, whereas the bottom and top edge horizontal members are kept in place. In addition, a symmetric, with respect to the middle horizontal axis, optimal truss is obtained, as it should be expected, due to the overall truss configuration and the symmetry of the applied load. It should be noted that for all the base parts considered, the values of the top and bottom horizontal members are decreasing, as one moves from the left towards the right side of the structure. Additionally, the values of the cross sections of the diagonal members that are kept in place also show this decreasing behavior, from the left towards the right side of the structure, in contrast to the case of the edge displacement. It is therefore observed that the optimal results show similar trends with the optimal configurations obtained in Case B of static loading. Nevertheless, there are differences in the size of the corresponding truss members (values of the volume ratio), that is some truss members are reinforced, whereas others are weakened.

Also, it is worth pointing out interesting results that are obtained for the structure that consists of four base parts, similarly to the Case A and B. In these cases, several global/local optima are obtained. Two such optimal solutions are presented in Figure 3.38 and in Figure 3.39. In Case D, the values of the objective function are 0.0011 and 0.0012 for the first and the second optimal solution respectively, whereas the value for the global solution is 0.00109. On the other

hand, in Case E, the corresponding values of the objective function are 0.0019 and 0.0021 for the first and the second optimal solution respectively, whereas the value for the global solution is 0.0017. From the practical point of view and considering numerical errors in the optimization process, these optimal solutions can be all considered to be global optimal solutions.

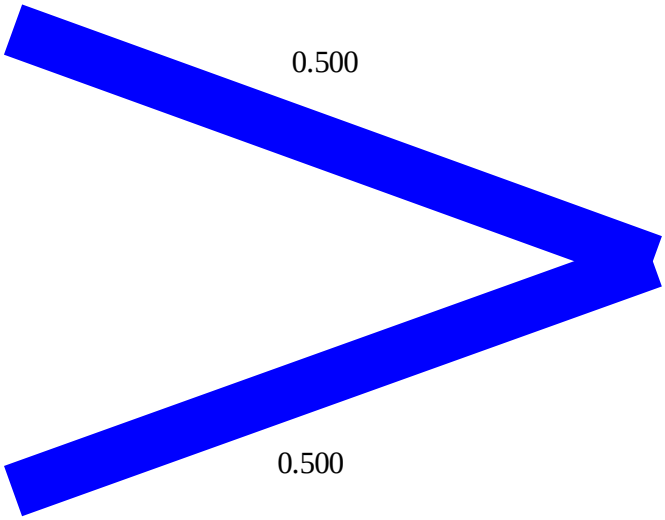


(a)

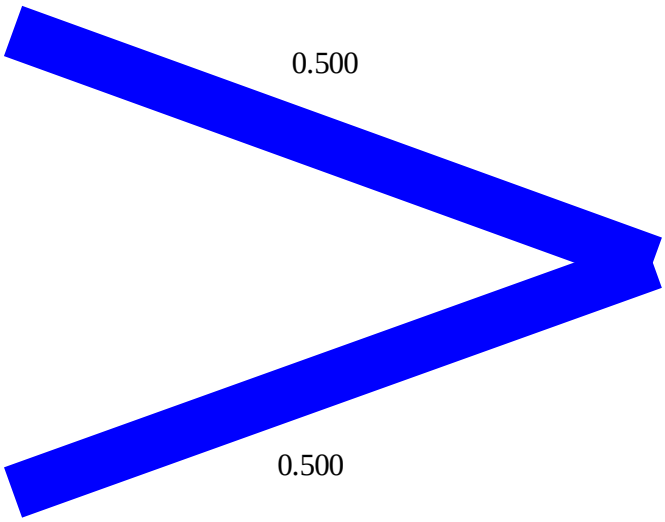


(b)

**Figure 3.24:** Optimal solution for one base part, (a) Case D, (b) Case E.

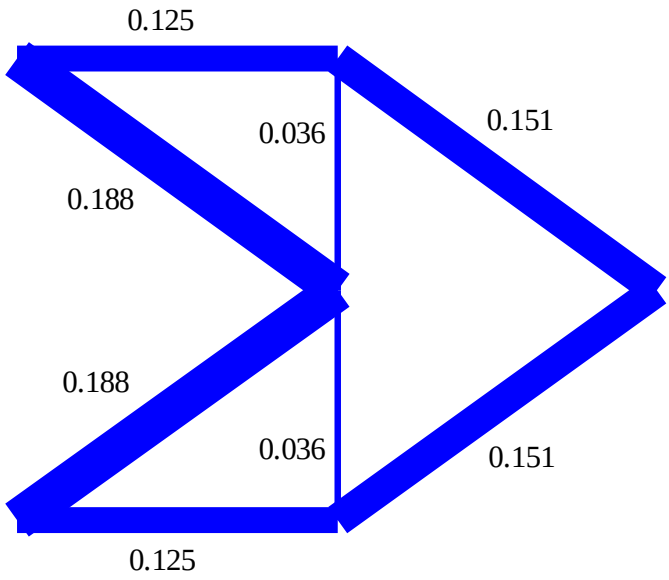


(a)

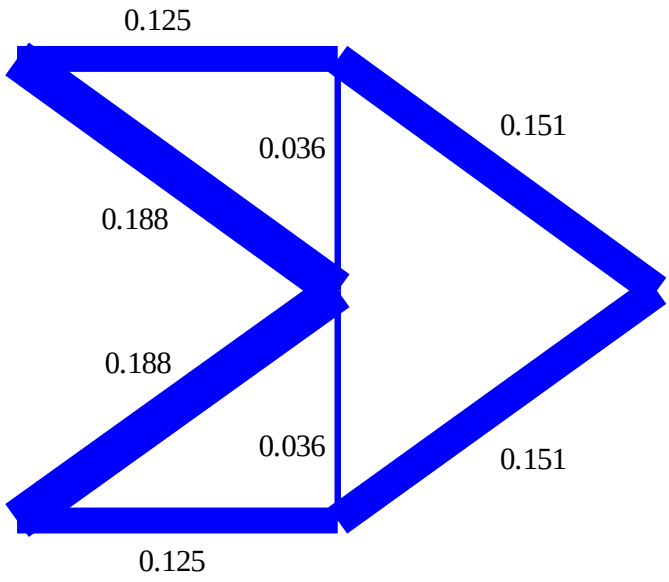


(b)

**Figure 3.25:** Optimal solution for two base parts, (a) Case D, (b) Case E.

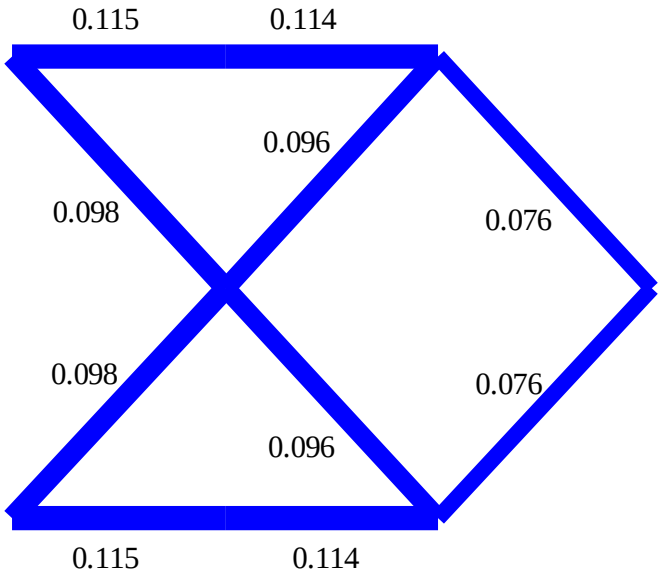


(a)

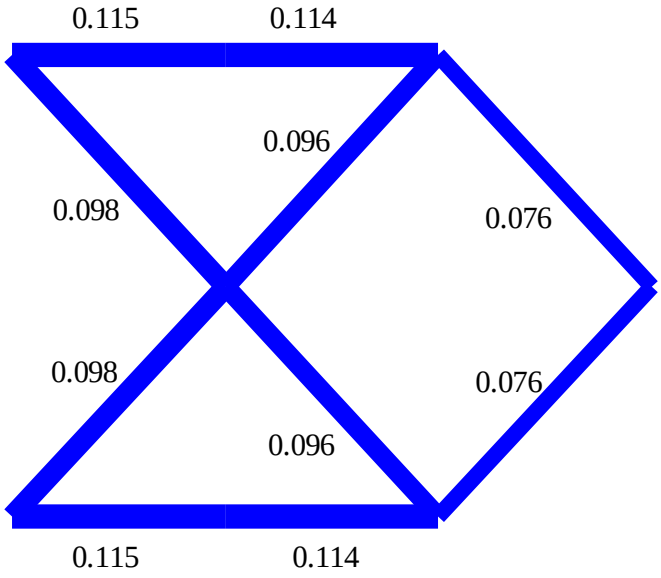


(b)

**Figure 3.26:** Optimal solution for three base parts, (a) Case D, (b) Case E.

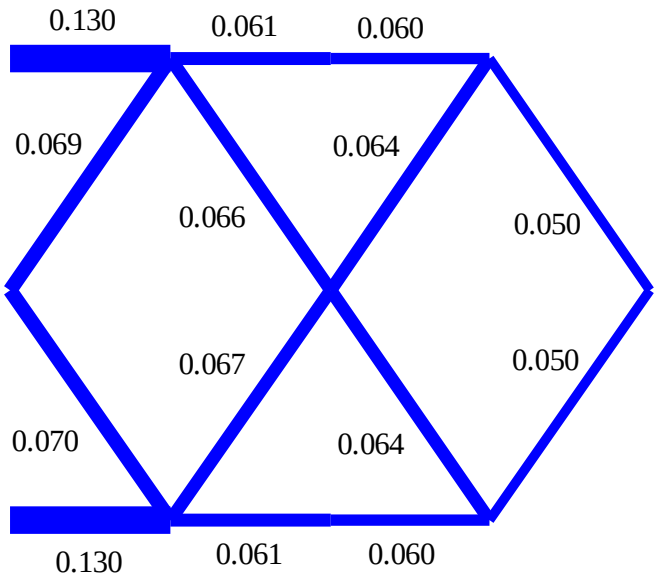


(a)

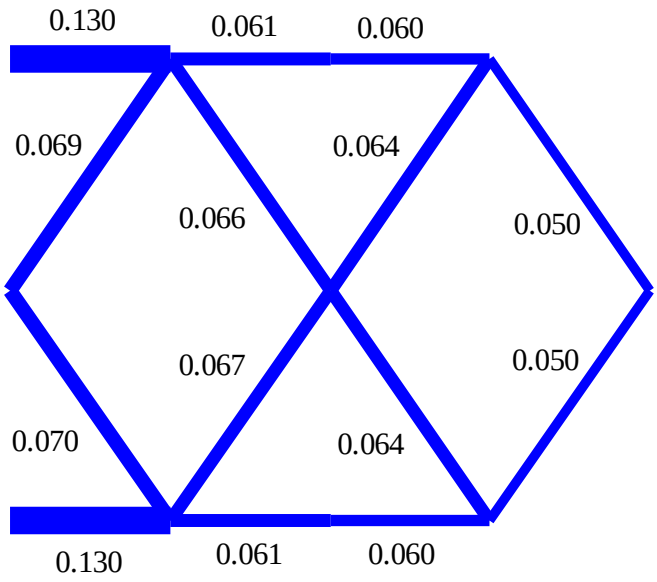


(b)

**Figure 3.27:** Optimal solution for four base parts, (a) Case D, (b) Case E.

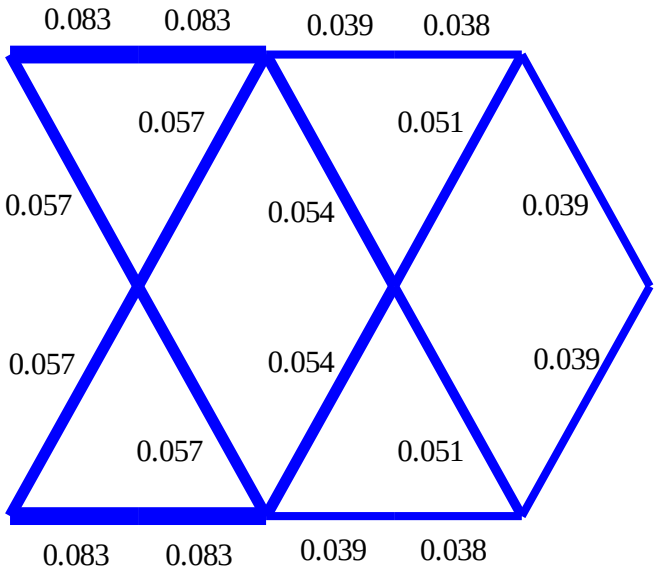


(a)

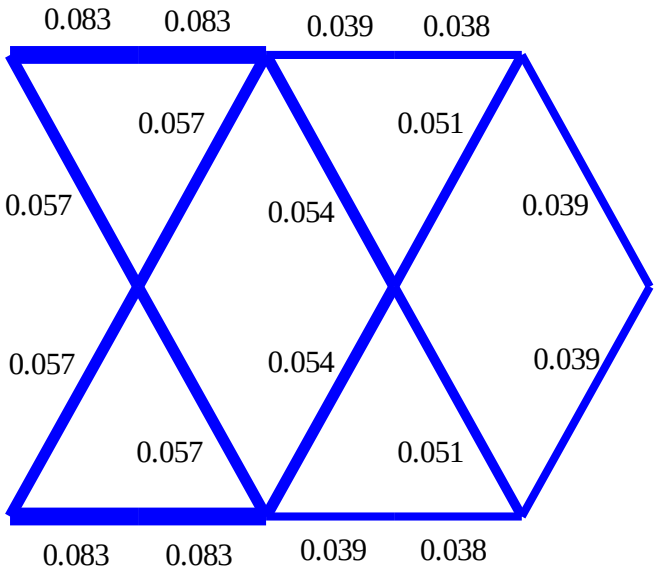


(b)

**Figure 3.28:** Optimal solution for five base parts, (a) Case D, (b) Case E.

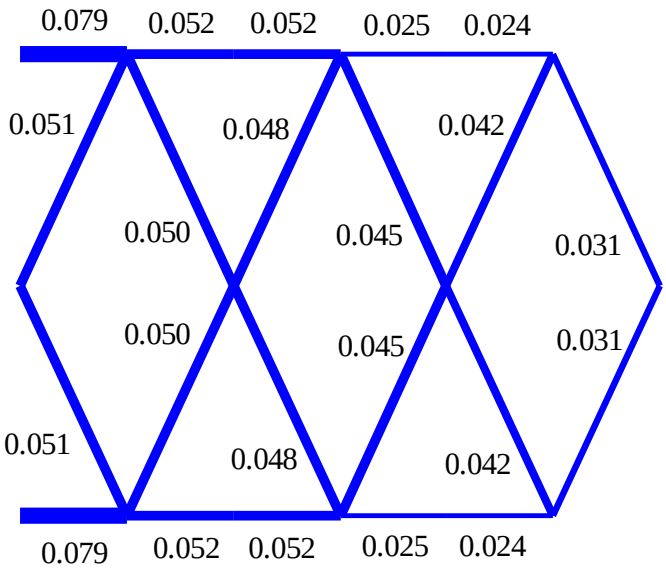


(a)

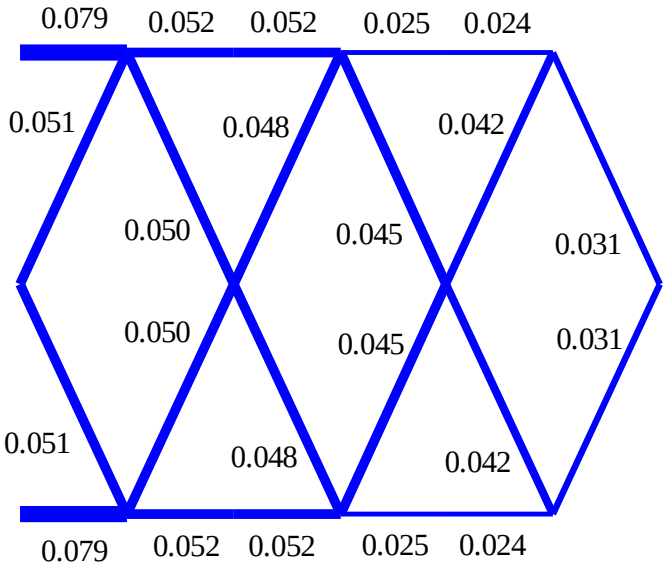


(b)

**Figure 3.29:** Optimal solution for six base parts, (a) Case D, (b) Case E.

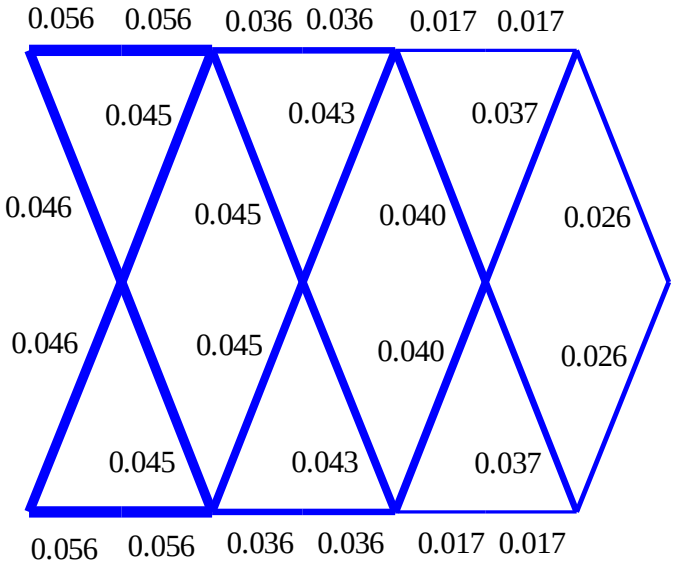


(a)

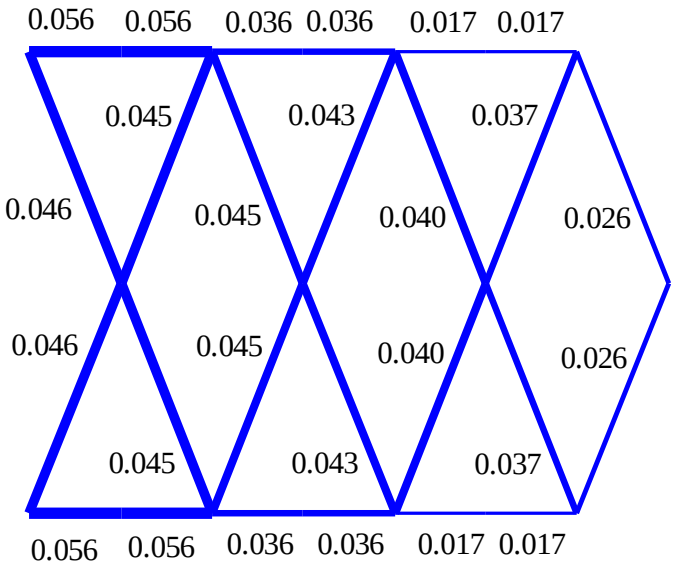


(b)

**Figure 3.30:** Optimal solution for seven base parts, (a) Case D, (b) Case E.

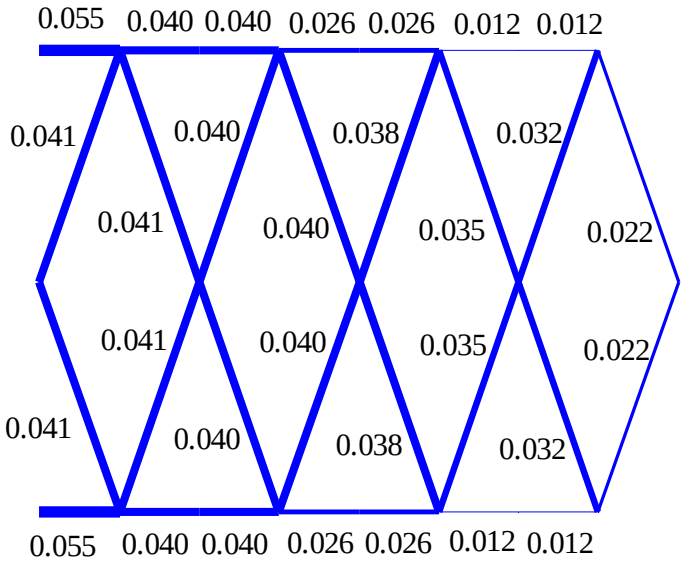


(a)

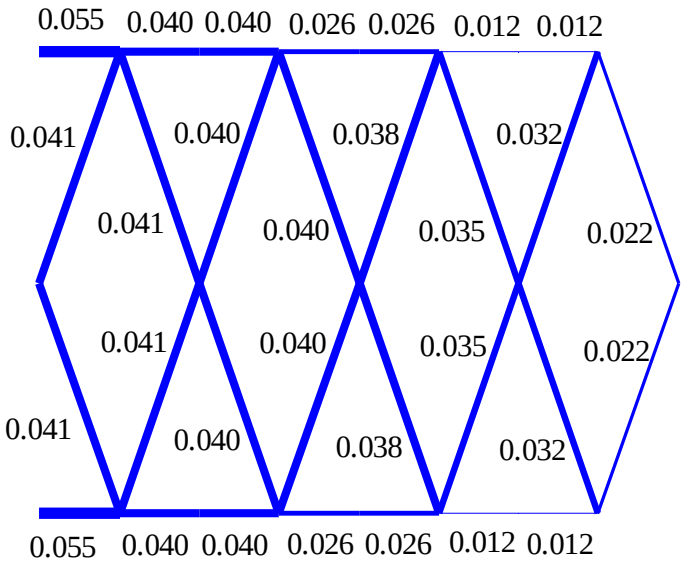


(b)

**Figure 3.31:** Optimal solution for eight base parts, (a) Case D, (b) Case E.

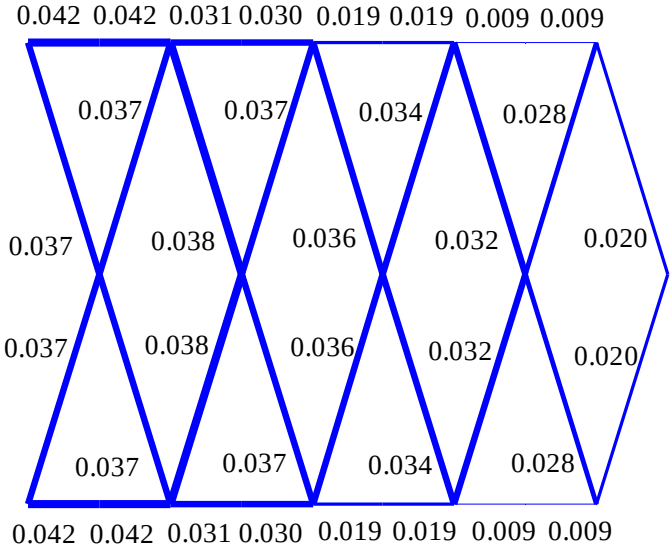


(a)

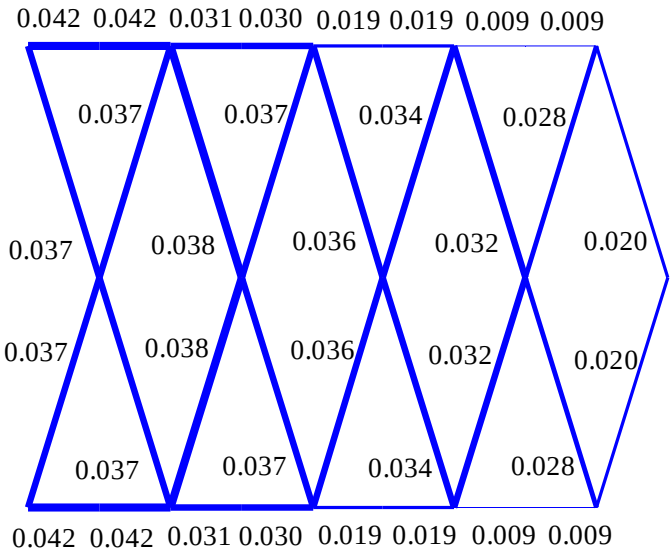


(b)

**Figure 3.32:** Optimal solution for nine base parts, (a) Case D, (b) Case E.

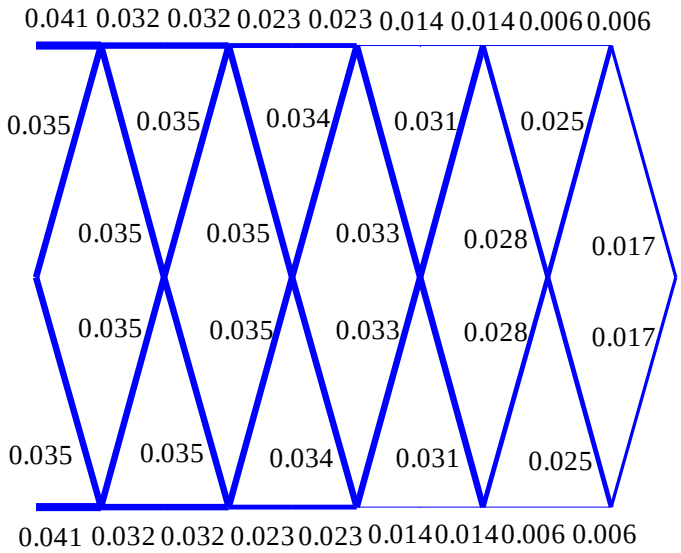


(a)

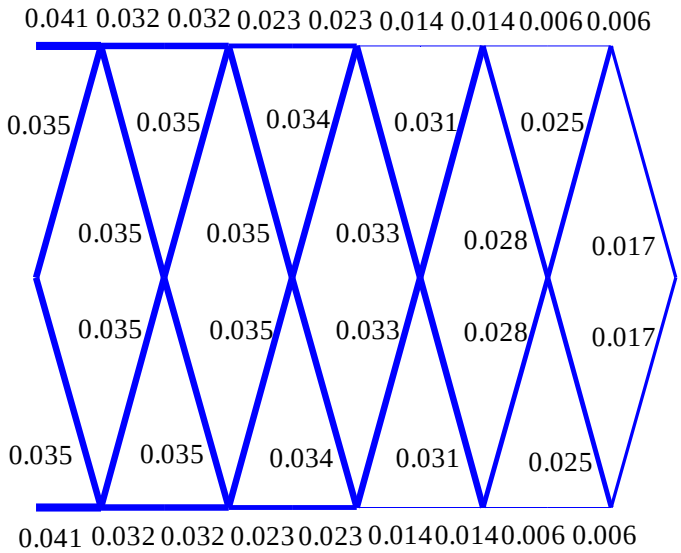


(b)

**Figure 3.33:** Optimal solution for ten base parts, (a) Case D, (b) Case E.

**Table 3.3:** Values of the objective function for one up to ten base parts, for Case D.

| Parts | $J$ | $J^*$ |
|---|---|---|
| 1 | 0.00357 | 21.43 |
| 2 | 0.00148 | 8.957 |
| 3 | 0.00118 | 10.49 |
| 4 | 0.00109 | 10.18 |
| 5 | 0.00092 | 9.101 |
| 6 | 0.00095 | 9.605 |
| 7 | 0.00088 | 9.131 |
| 8 | 0.00109 | 11.35 |
| 9 | 0.00118 | 12.40 |
| 10 | 0.00134 | 13.94 |

**Table 3.4:** Values of the objective function for one up to ten base parts for Case E.

| Parts | J | $J^*$ |
|---|---|---|
| 1 | 0.00228 | 13.66 |
| 2 | 0.00187 | 11.28 |
| 3 | 0.00166 | 14.77 |
| 4 | 0.00183 | 16.93 |
| 5 | 0.00173 | 17.12 |
| 6 | 0.00199 | 19.92 |
| 7 | 0.00149 | 15.38 |
| 8 | 0.00266 | 27.45 |
| 9 | 0.00306 | 31.90 |
| 10 | 0.00364 | 37.89 |

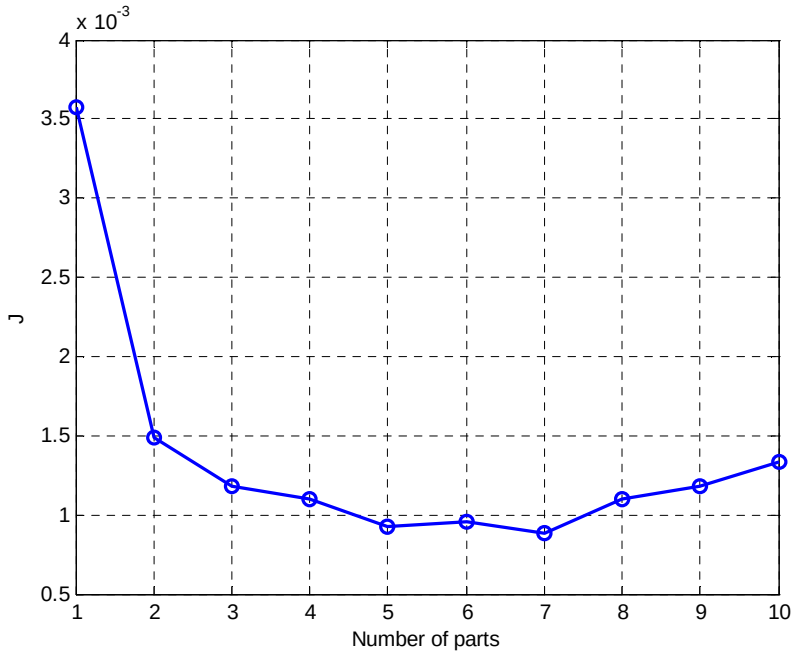


**Figure 3.34:** Optimal values of the objective function $J$ with respect to the number of base parts of the structure, for Case D.

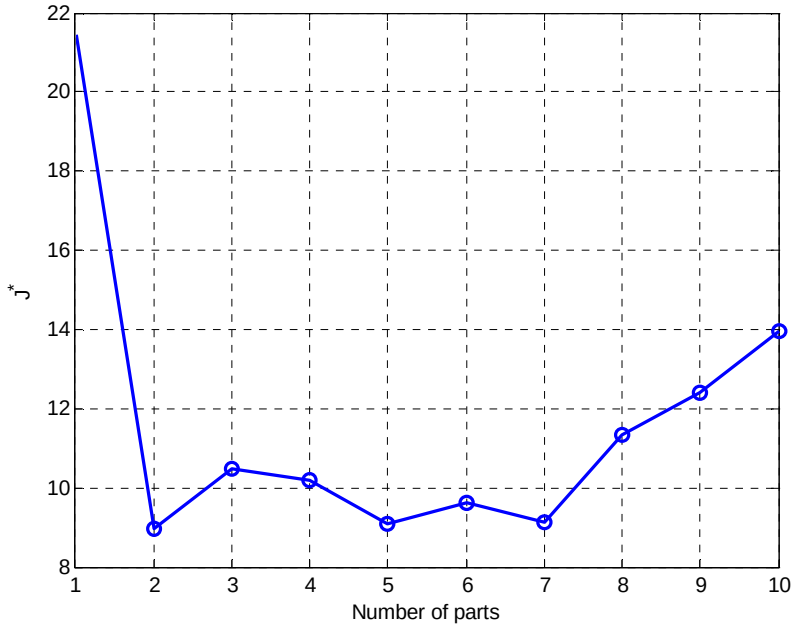


**Figure 3.35:** Optimal values of the objective function $J^*$ with respect to the number of base parts of the structure, for Case D.

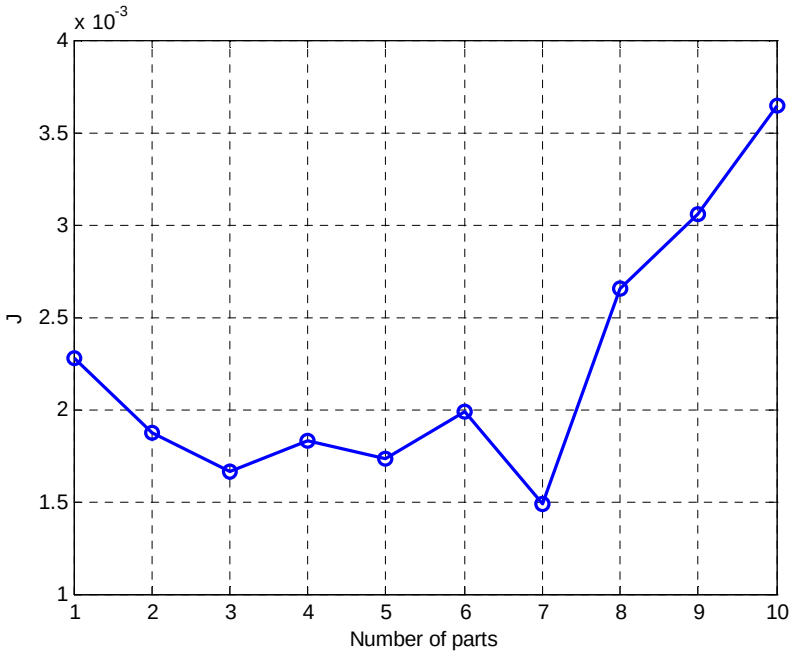


**Figure 3.36:** Optimal values of the objective function $J$ with respect to the number of base parts of the structure, for Case E.

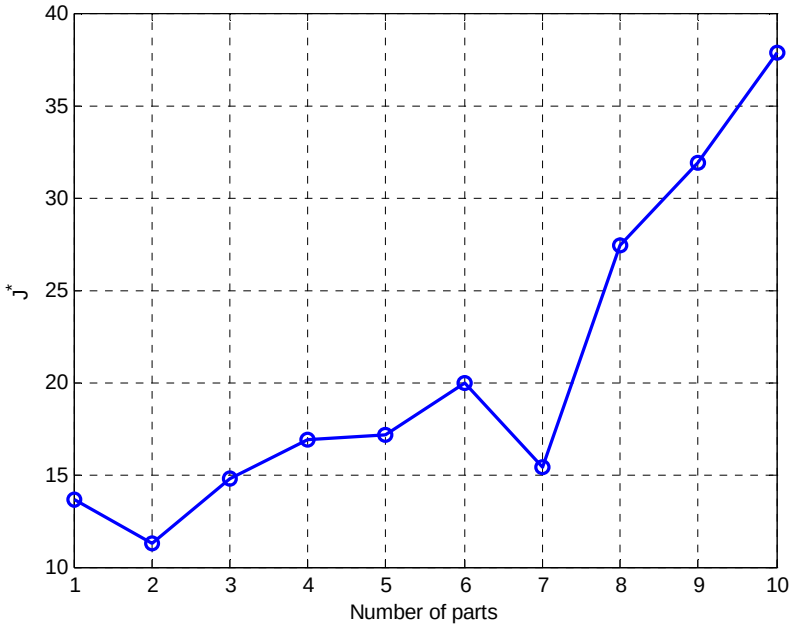


**Figure 3.37:** Optimal values of the objective function $J^*$ with respect to the number of base parts of the structure, for Case E.

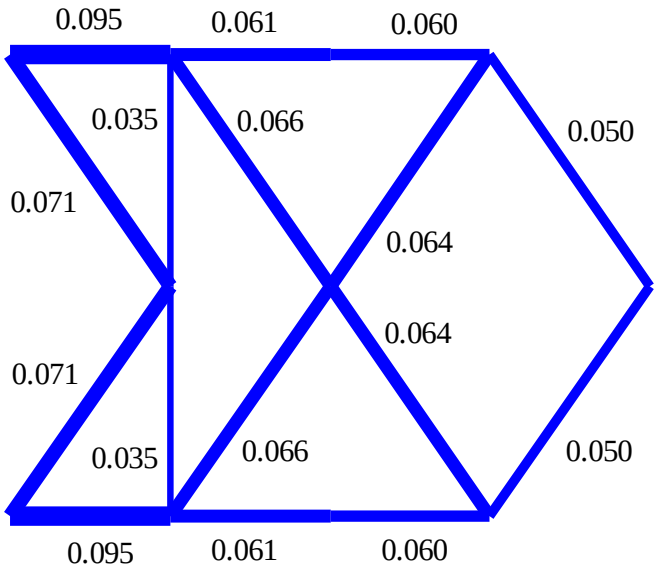


(a)

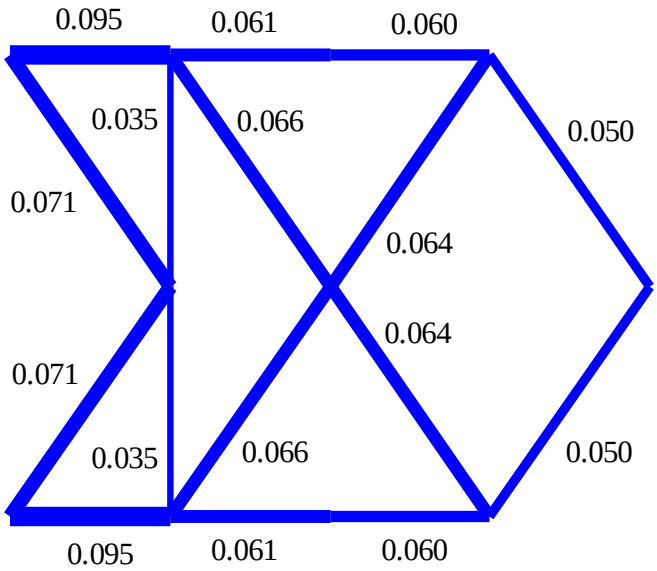


(b)

**Figure 3.38:** Local optimal solutions for four base parts, (a) Case D, (b) Case E.

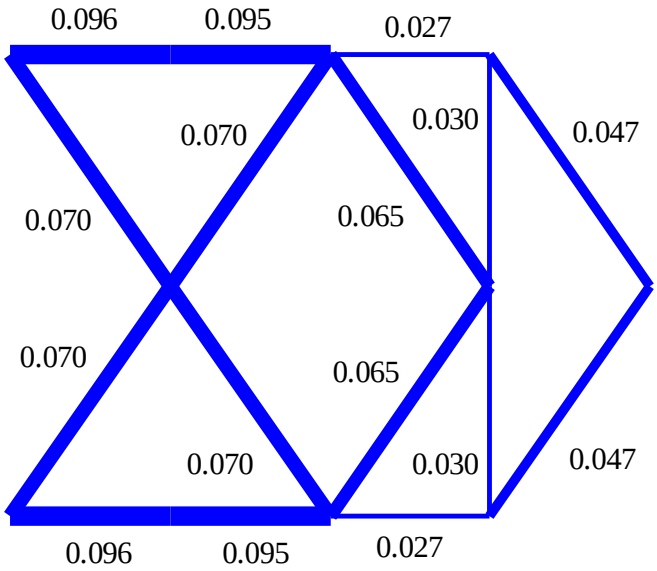


(a)

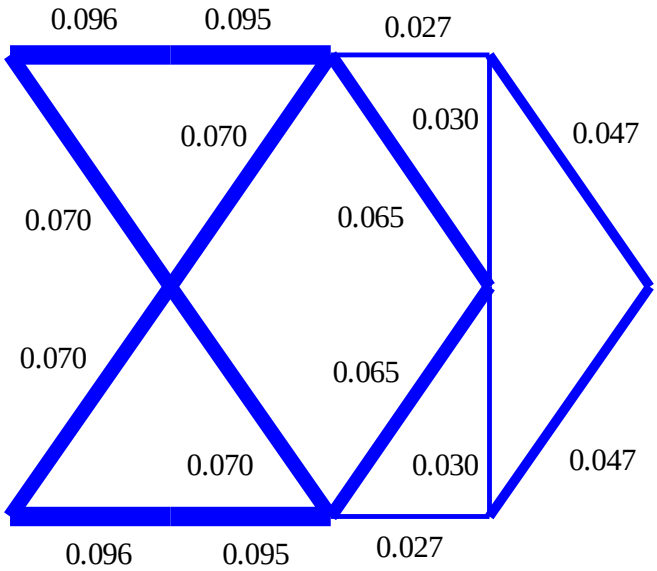


(b)

**Figure 3.39:** Local optimal solution for four base parts, (a) Case D, (b) Case E.

## 3.5 Stress-Based optimal Design under Static and Stochastic Dynamic Loads

Next, two cases are considered, denoted as Case F and Case G. In Case F, the performance function is selected to be the weighted sum of the variances of the stresses developed in the truss members of the structure, with all the weights chosen to be equal, under static deterministic loading. In this case, the optimization problem is stated in (2.23) - (2.26), the matrix $\Sigma$ is given by (2.75). In Case G, the performance function is selected to be the weighted sum of the variances of the stresses developed in the truss members of the structure, with all the weights chosen to be equal, under stochastic dynamic loading. In this case, the optimization problem is stated in (2.35) - (2.38), the matrix $\Sigma$ is given by (2.75). Additionally, an additional nodal mass equal to 5kg divided by the degrees of freedom of each system is added at all the nodes of the truss structure. For both cases, the volume constant $V_0$ is chosen to be equal to $10^{-5}\,\mathrm{m}^3$. The value of the power spectral density of the white noise excitation in Case G is chosen to be equal to 1000, whereas the value of the static load in Case F is chosen to be 1000.

It should be noted that in the case that the output state vector $\underline{y}$ is considered to be the stresses at the elements of the system, then the matrices $\hat{C}$ and $D$ in the observation equation (2.45) are given by

$$\hat{C} = [R_{N_{el}n} \quad 0_{N_{el}n}] \tag{3.4}$$

$$D = 0_{N_{el}n} \tag{3.5}$$

where $N_{el}$ is the number of the elements of the system, and $R$ is a matrix that each row corresponds to an element of the system and has only four non-zero elements which correspond to the four degrees of freedom of the truss elements edge nodes. The non-zero elements in $R$ are obtained by developing the relation between the stress in a truss member and the displacements of the elements nodes. Let $x_i$, $y_i$ and $x_j$, $y_j$ be the coordinates of the nodes of a given truss element and $u_i$, $v_i$ and $u_j$, $v_j$ the corresponding displacements. The uniaxial stress component of this element is given by

$$\begin{aligned}\sigma_{ij}(t) &= E_{ij}\varepsilon_{ij} = \frac{E_{ij}}{L_{ij}}\delta_{ij} \\ &= \frac{E_{ij}}{L_{ij}}\Big[\big(u_j(t)-u_i(t)\big)\cos\theta_{ij} + \big(v_j(t)-v_i(t)\big)\sin\theta_{ij}\Big]\end{aligned} \tag{3.6}$$

where $L_{ij}$ is the length, $E_{ij}$ is the elasticity modulus, $\varepsilon_{ij}$ is the uniaxial strain and $\delta_{ij}$ is the elongation of the truss element. The angle $\theta_{ij}$ is given by

$$\theta_{ij} = \tan^{-1} \frac{y_j - y_i}{x_j - x_i} \tag{3.7}$$

whereas the length can be calculated using

$$L_{ij} = \sqrt{\left(x_j - x_i\right)^2 + \left(y_j - y_i\right)^2} \tag{3.8}$$

The optimal truss structures that consist of one up to ten base parts $N_b$ are presented in Figure 3.40 to Figure 3.49. The Figures denoted with (a) refer to Case F, whereas the Figures denoted with (b) refer to Case G. Additionally, in Table 3.5 and in Table 3.6 are shown the optimal values of the objective function $J$ for the different structures of one up to ten base parts, information which is also plotted in Figure 3.50 and in Figure 3.52, for Case F and G respectively. Note that in Table 3.5 and in Table 3.6 an additional column with the values of the objective function $J^*$ is shown. The objective function $J^*$ is chosen to be equal to the maximum stress across the stresses developed at the truss elements for the Case F, whereas it is equal to the maximum variance of the stresses developed at the truss members. This definition is very useful when one needs to compare the optimal solutions of structures with different number of base parts. This comparison is impossible using the objective function $J$ for the cases F and G, as the number of the truss members at the optimal solution change with respect to the number of base parts, thus the number of terms in the summation also changes. Therefore, in order to define the optimal solution between the optimal solutions with different number of base parts, the objective function $J^*$ should be used. Also, note that, for computational issues, the estimation of the matrix $\hat{C}$ in (3.4) is performed by choosing the Young's modulus to be equal to one. The values of the objective function $J^*$ that correspond to the optimal solutions are presented in Figure 3.51 and in Figure 3.53, for Case F and G respectively. It is observed that the structure with the minimum value of the objective function for Case F, consists of two base parts, that is the optimal structure for static loading is the structure that is shown in Figure 3.41a. On the other hand, the structure with the minimum value of the objective function for Case G consists of one part, that is the optimal structure for stochastic dynamic loading is shown in Figure 3.40b.

For Case F, it is observed that the optimization trend is similar to the optimization trend observed in Case A. That is to eliminate all the vertical members, except for

the cases of two and four base parts, as shown in Figure 3.41a and Figure 3.43a, where two vertical members are not eliminated in each case. Furthermore, the middle horizontal members are also eliminated, whereas the bottom and top edge horizontal members are kept in place. In addition, a symmetric, with respect to the middle horizontal axis, optimal truss is obtained, as it should be expected, due to the overall truss configuration and the symmetry of the applied load. It should be noted that for all the base parts considered, the values of the top and bottom horizontal members are decreasing, as one moves from the left towards the right side of the structure. In contrast, the diagonal members that are maintained during the optimization process do not show this decreasing behavior. Specifically, the cross sectional area and thus the volume ratio remains constant.

Additionally, it is worth pointing out interesting results that are obtained for the structure that consists of four base parts. In this case, several global/local optima are obtained, as in previous cases. Two such optimal solutions are presented in Figure 3.54 and in Figure 3.55. The values of the objective function are $2.49\times10^{18}$ and $2.5\times10^{18}$ for the first and the second optimal solution respectively, whereas the value for the global solution is $2.45\times10^{18}$. From the practical point of view and considering numerical errors in the optimization process, these three optimal solutions can be all considered to be global optimal solutions.

For Case G, it is observed that the optimization trend is also to eliminate all the vertical members, except for the cases of two base parts. Furthermore, the middle horizontal members are also eliminated, whereas the top and bottom edge horizontal members are kept in place. It should be noted that for all base parts considered, the values at the top and bottom horizontal members are decreasing as one moves from the left towards the right side of the structure. Additionally, the values of the cross sections of the diagonal members that are kept in place also show this decreasing behavior, from the left towards the right side of the structure, until a minimum value is reached and then they increase, in contrast to the static case.

Similar to Case F, local optimal solutions also exist for Case G for four base parts. These local optimal topologies are presented in Figure 3.56 and in Figure 3.57. The values of the objective function are equal to $4.07\times10^{-5}$ and $3.27\times10^{-5}$ for the local optimal solutions respectively, whereas the value for the global solution is equal to $3.27\times10^{-5}$.

It is also worth noting that the configurations of the optimal structures for seven to ten base parts for Case G are not presumable. This is due to fact that the optimal

structures obtained are asymmetrical. Consequently, the mirrored structure with respect to the horizontal middle axis is also a solution of the topology optimization. One such mirrored optimal structure is shown in Figure 3.59 for the case of eight base parts, noting that the value of the objective function is equal to the initial solution shown in Figure 3.85b. On the other hand, optimal symmetrical solution can be obtained by imposing the cross sectional areas of the truss members that are symmetric with respect to the horizontal middle axis to be equal. One such solution is shown in Figure 3.58 for the case of seven base parts. The value of the objective function in this case is equal to $2.70\times10^{-5}$, whereas the value of the objective function for the asymmetrical solution is equal to $2.65\times10^{-5}$.

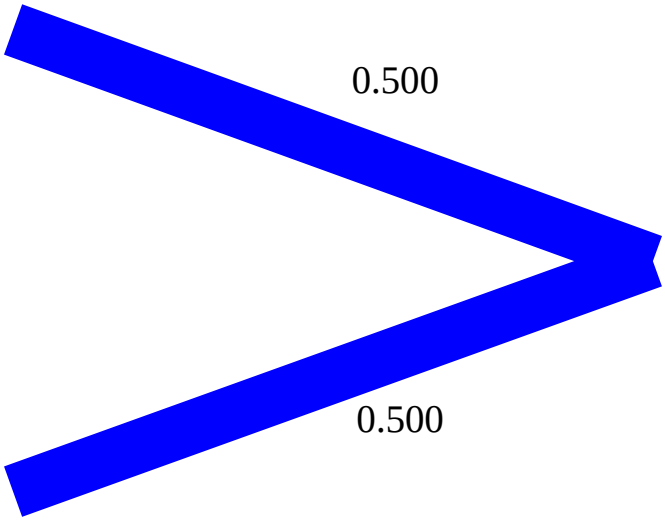


(a)

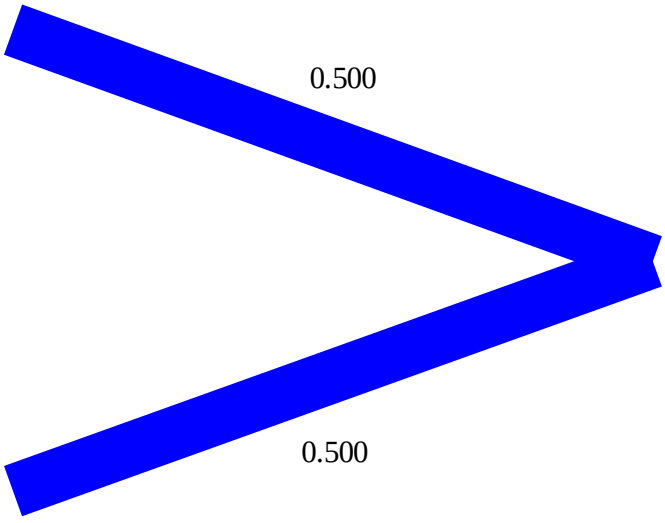


(b)

**Figure 3.40:** Optimal solution for one base part, (a) Case F, (b) Case G.

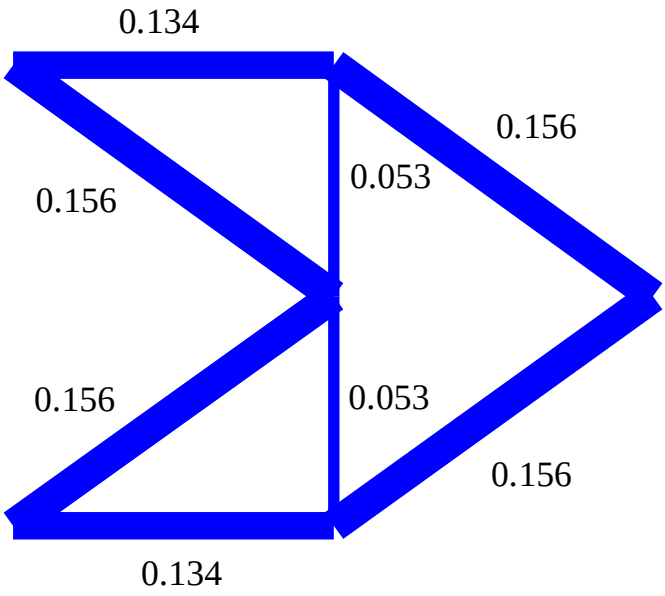


(a)

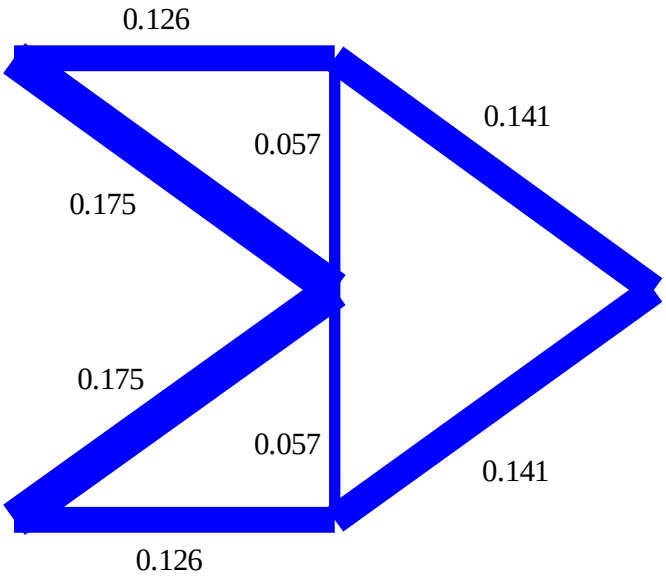


(b)

**Figure 3.41:** Optimal solution for two base parts, (a) Case F, (b) Case G.

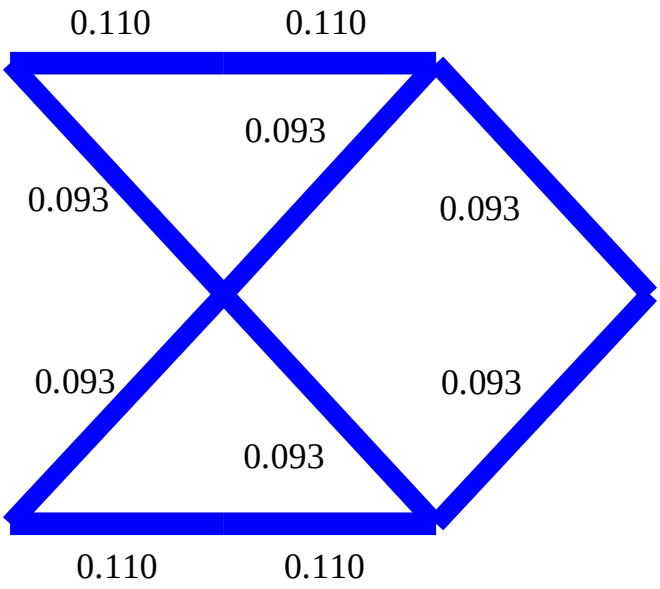


(a)

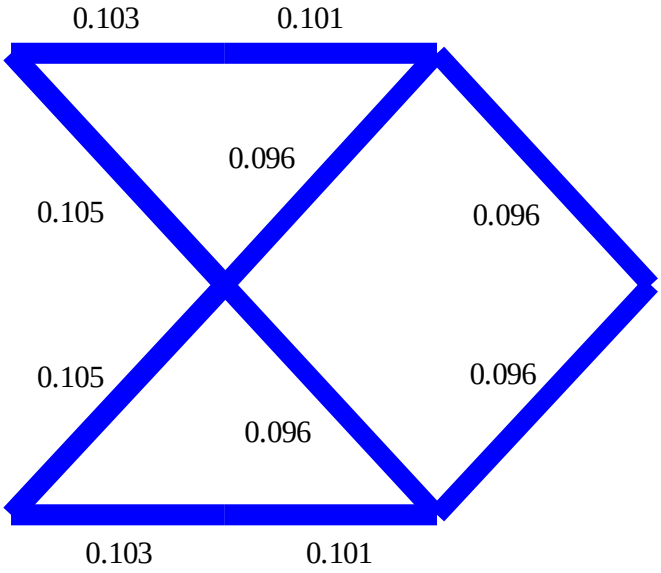


(b)

**Figure 3.42:** Optimal solution for three base parts, (a) Case F, (b) Case G.

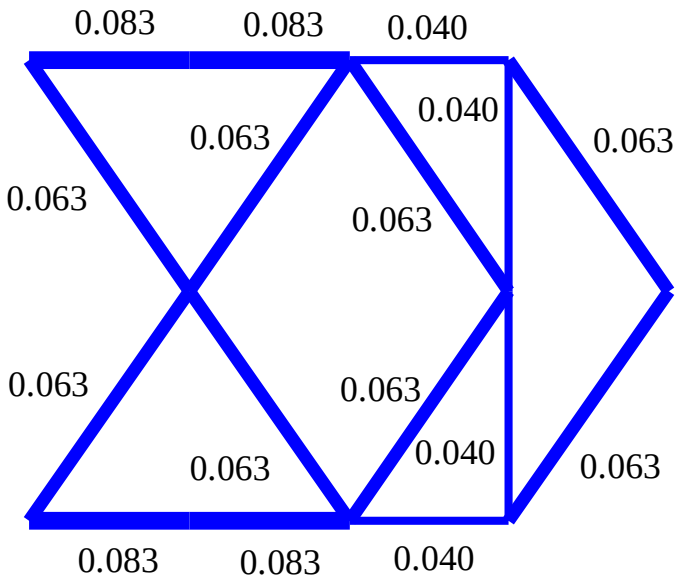


(a)

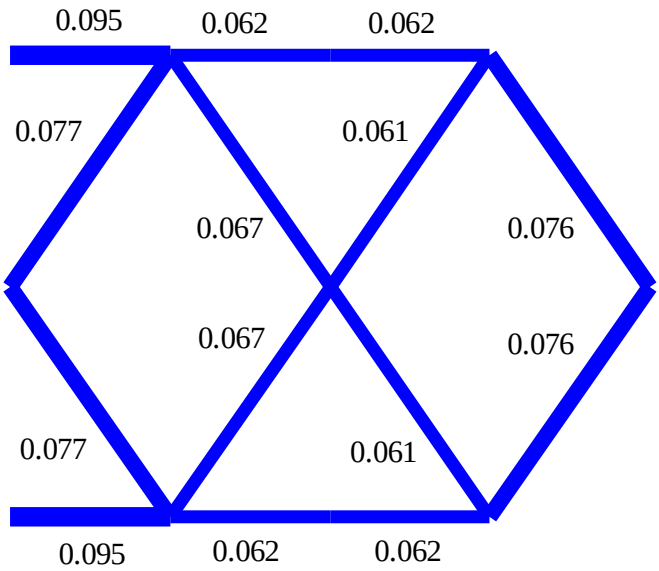


(b)

**Figure 3.43:** Optimal solution for four base parts, (a) Case F, (b) Case G.

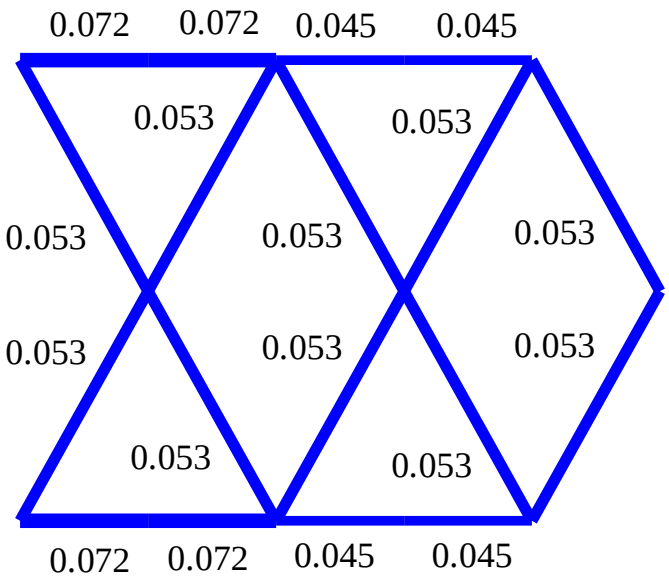


(a)

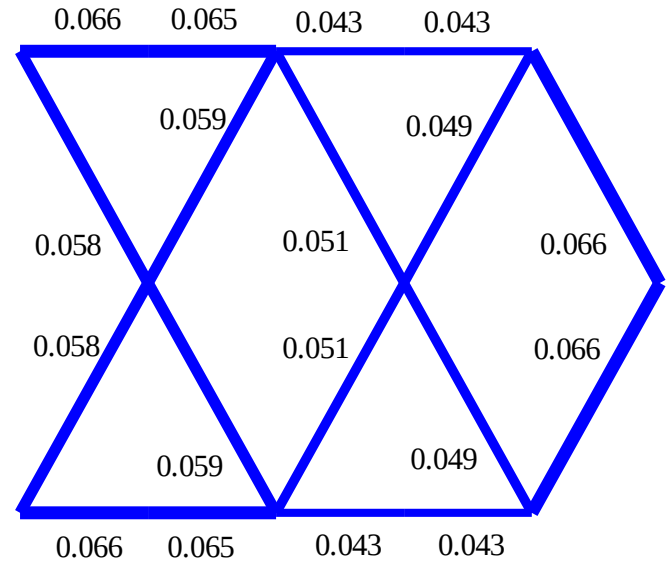


(b)

**Figure 3.44:** Optimal solution for five base parts, (a) Case F, (b) Case G.

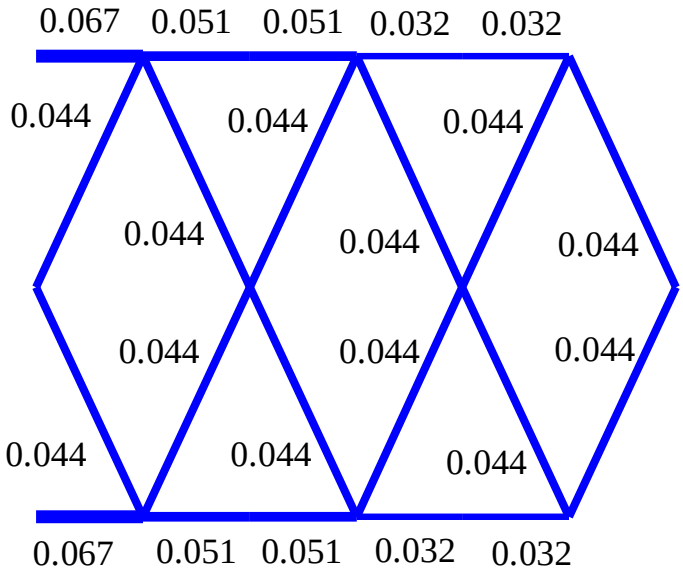


(a)

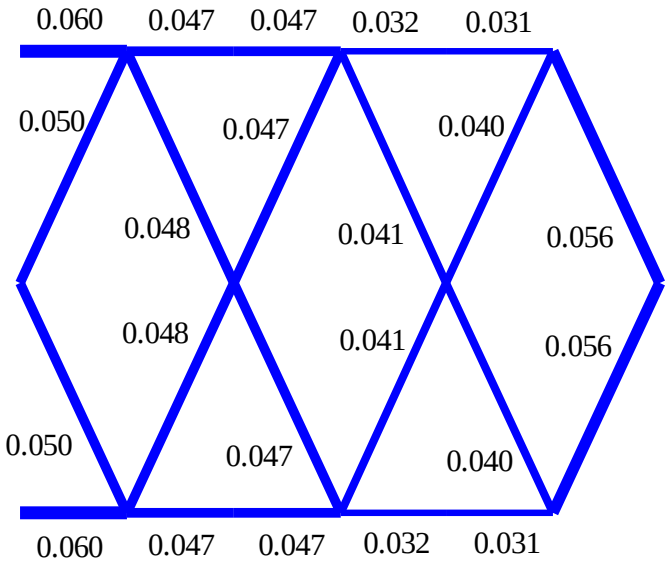


(b)

**Figure 3.45:** Optimal solution for six base parts, (a) Case F, (b) Case G.

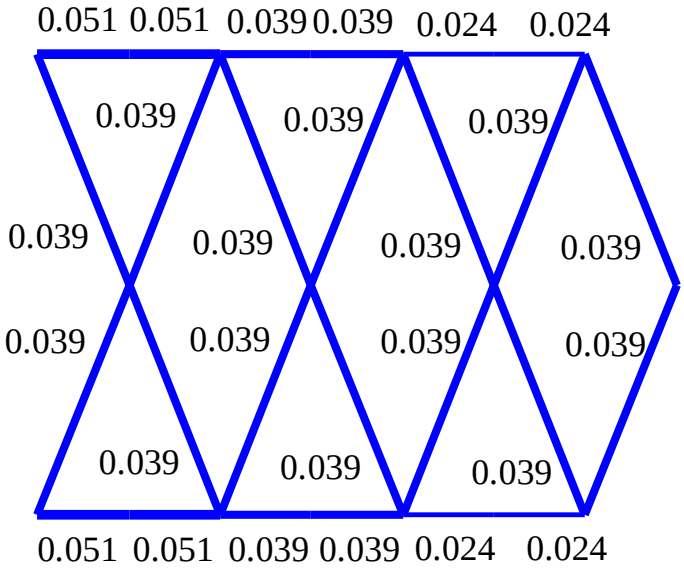


(a)

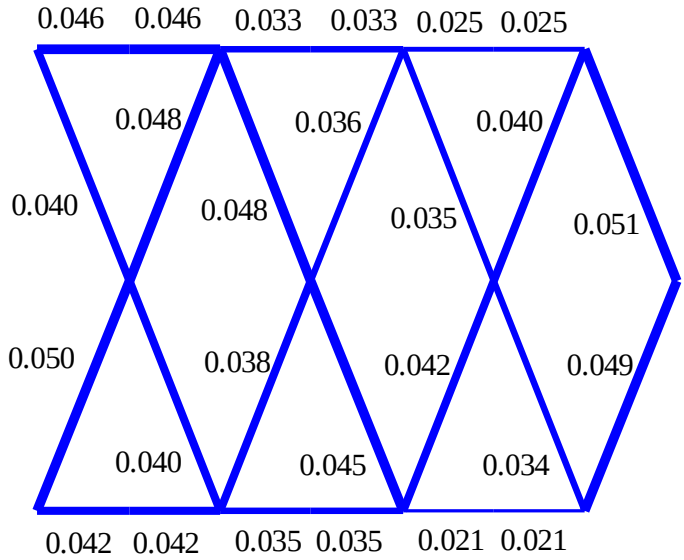


(b)

**Figure 3.46:** Optimal solution for seven base parts, (a) Case F, (b) Case G.

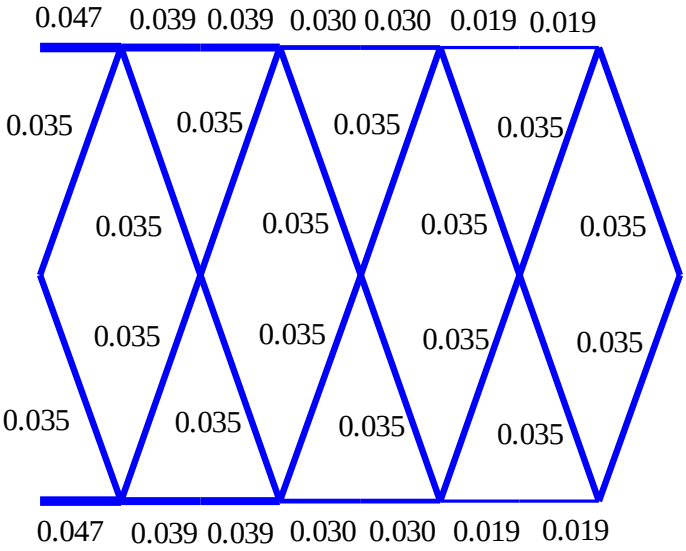


(a)

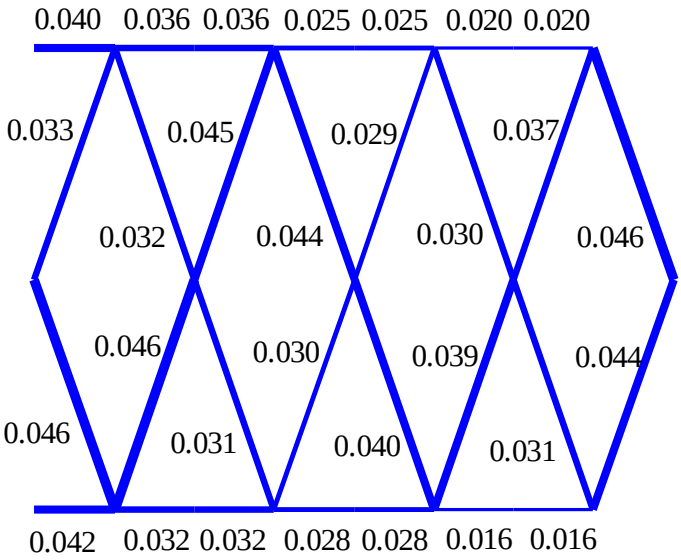


(b)

**Figure 3.47:** Optimal solution for eight base parts, (a) Case F, (b) Case G.

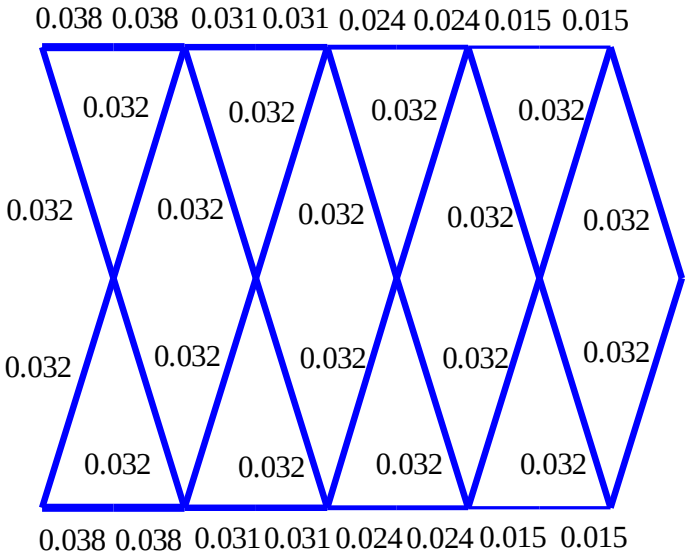


(a)

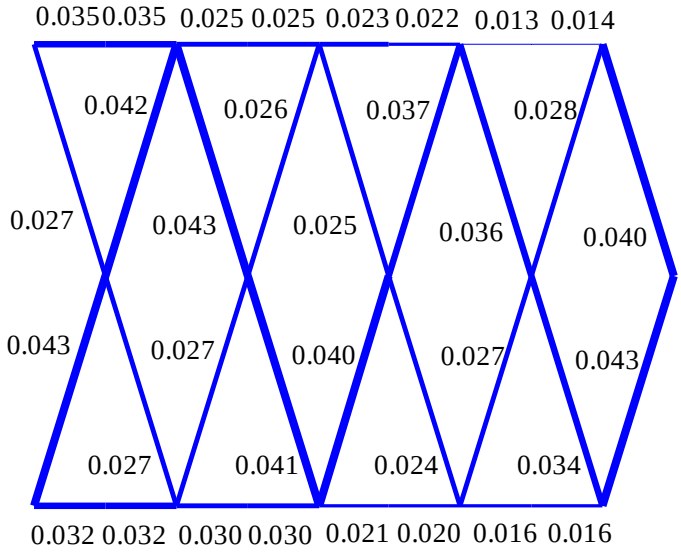


(b)

**Figure 3.48:** Optimal solution for nine base parts, (a) Case F, (b) Case G.

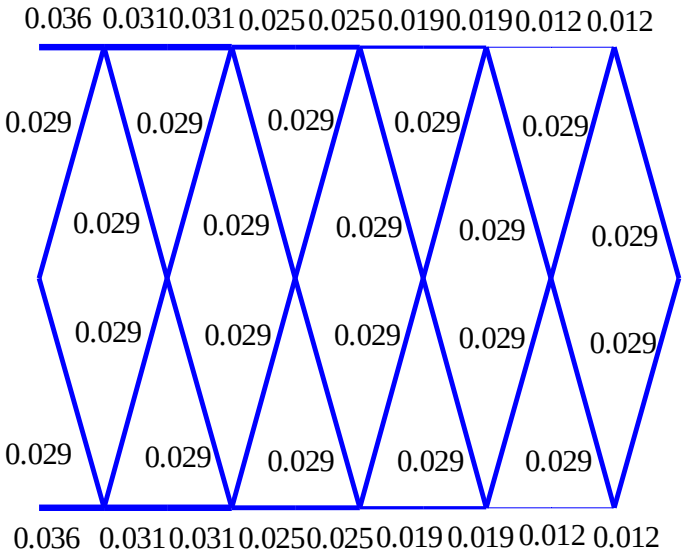


(a)

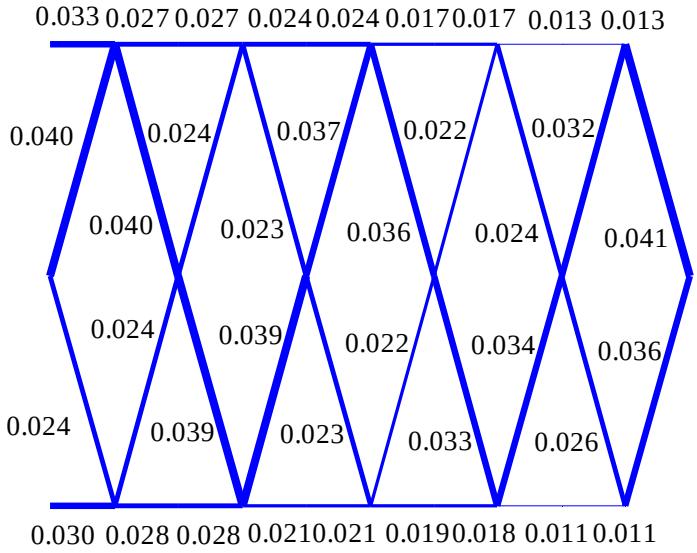


(b)

**Figure 3.49:** Optimal solution for ten base parts, (a) Case F, (b) Case G.

**Table 3.5:** Values of the objective function for one to ten base parts, for Case F.

| Parts | $J\ (\times 10^{18})$ | $J^{*}(\times 10^{9})$ |
|---|---|---|
| 1 | 2.890 | 1.7000 |
| 2 | 2.055 | 1.4069 |
| 3 | 2.373 | 1.5393 |
| 4 | 2.447 | 1.5519 |
| 5 | 2.472 | 1.5670 |
| 6 | 2.700 | 1.6354 |
| 7 | 2.852 | 1.6806 |
| 8 | 3.134 | 1.7594 |
| 9 | 3.367 | 1.8225 |
| 10 | 3.686 | 1.9045 |

**Table 3.6:** Values of the objective function for one to ten base parts, for Case G.

| Parts | $J\ (\times 10^{-5})$ | $J^{*}(\times 10^{-5})$ |
|---|---|---|
| 1 | 0.859 | 4.727 |
| 2 | 2.961 | 7.402 |
| 3 | 2.890 | 8.382 |
| 4 | 3.269 | 8.868 |
| 5 | 3.495 | 9.125 |
| 6 | 3.684 | 9.377 |
| 7 | 2.654 | 6.634 |
| 8 | 4.350 | 1.073 |
| 9 | 4.781 | 1.167 |
| 10 | 5.240 | 1.269 |

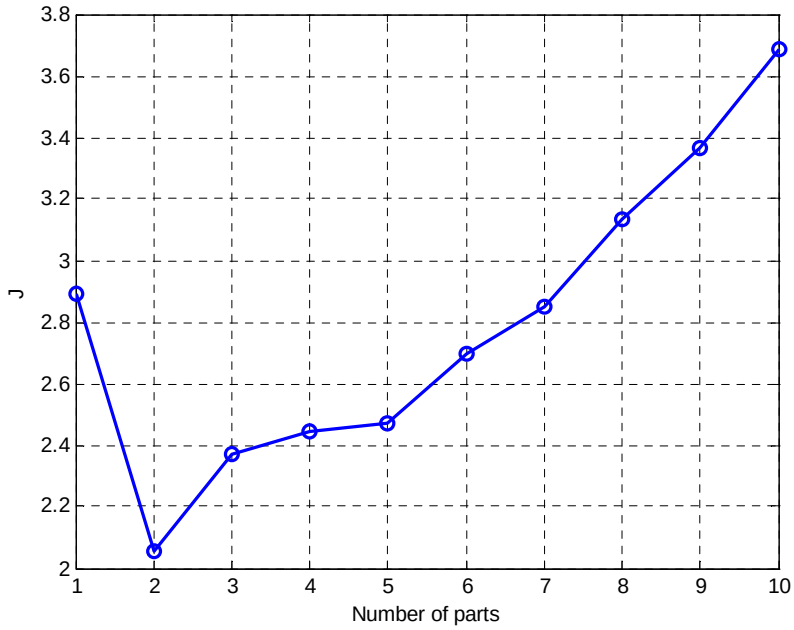


**Figure 3.50:** Optimal values of the objective function $J$ with respect to the number of base parts of the structure, for Case F.

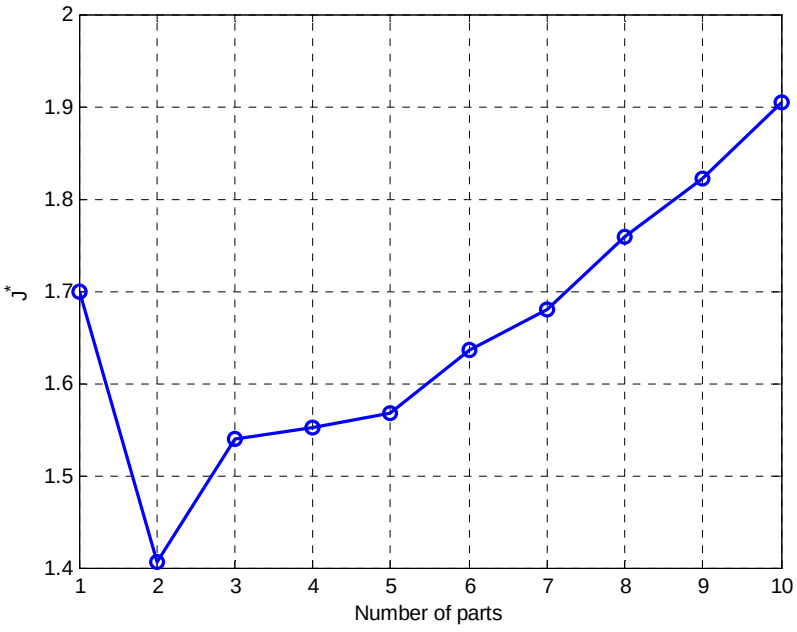


**Figure 3.51:** Optimal values of the objective function $J^*$ with respect to the number of base parts of the structure, for Case F.

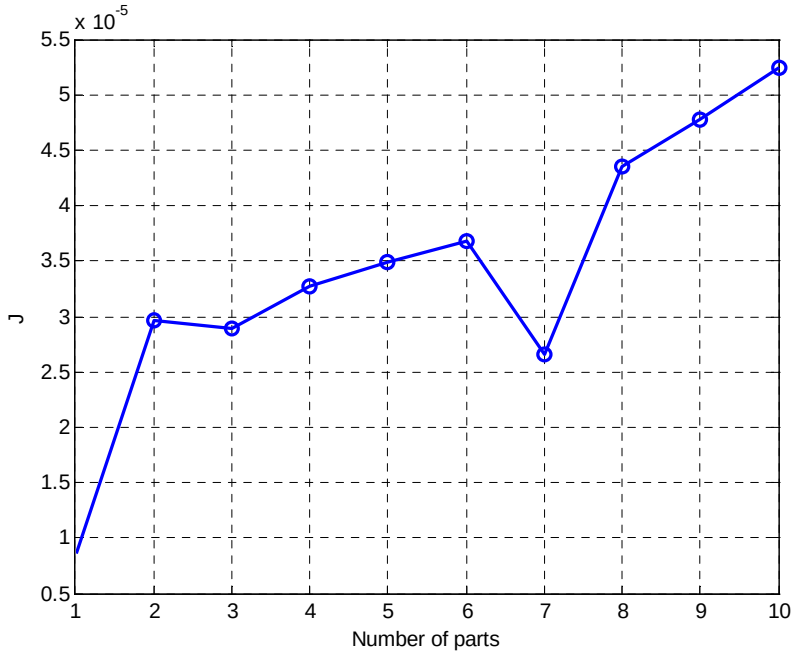


**Figure 3.52:** Optimal values of the objective function $J$ with respect to the number of base parts of the structure, for Case G.

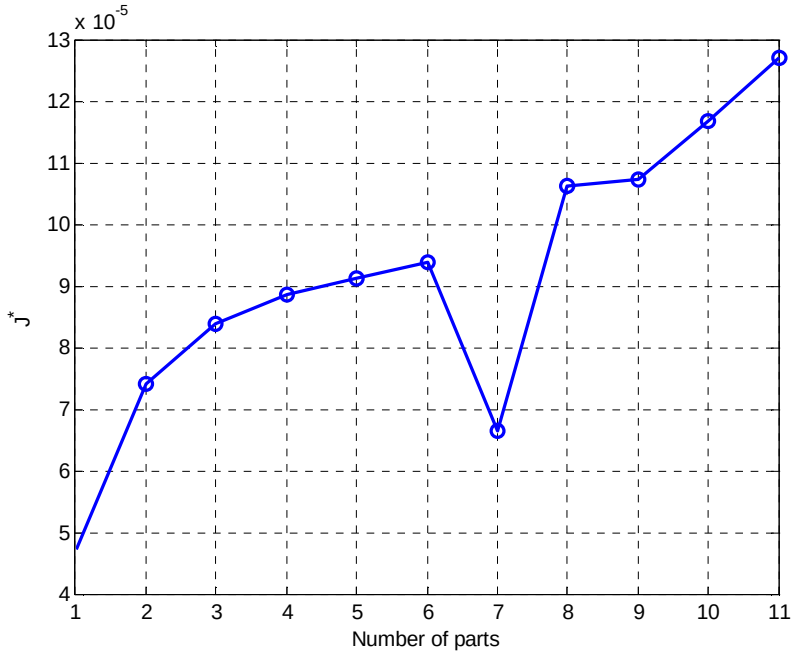


**Figure 3.53:** Optimal values of the objective function $J^*$ with respect to the number of base parts of the structure, for Case G.

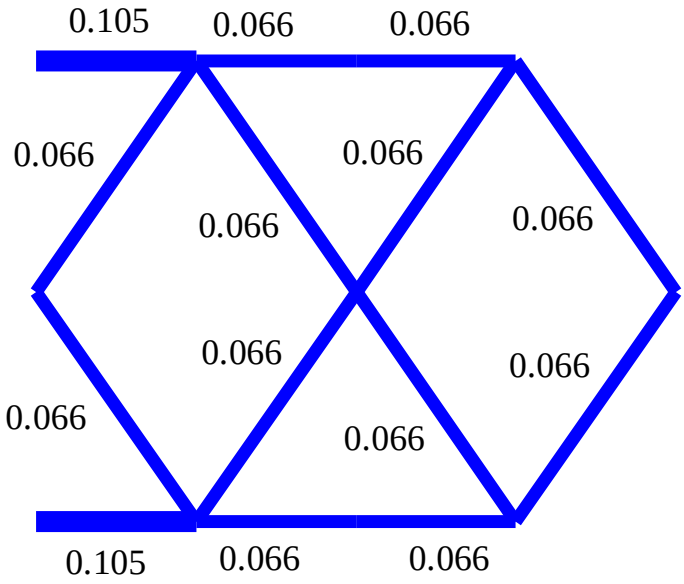


**Figure 3.54:** Optimal solution for four base parts, for Case F.

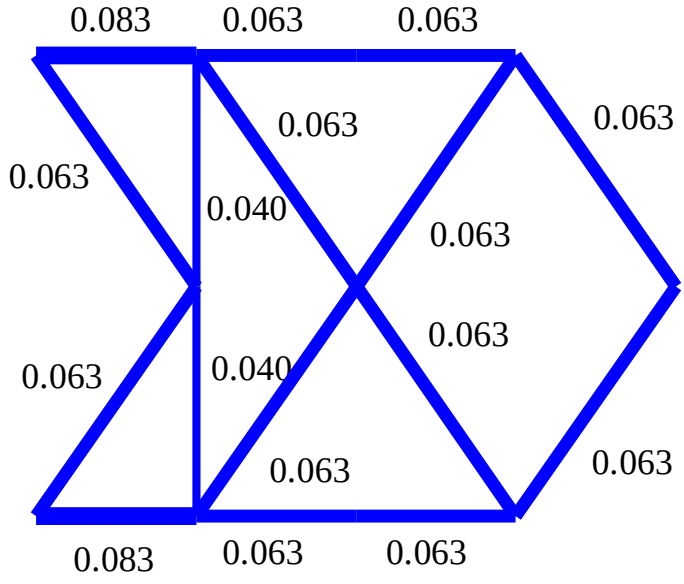


**Figure 3.55:** Optimal solution for four base parts, for Case F.

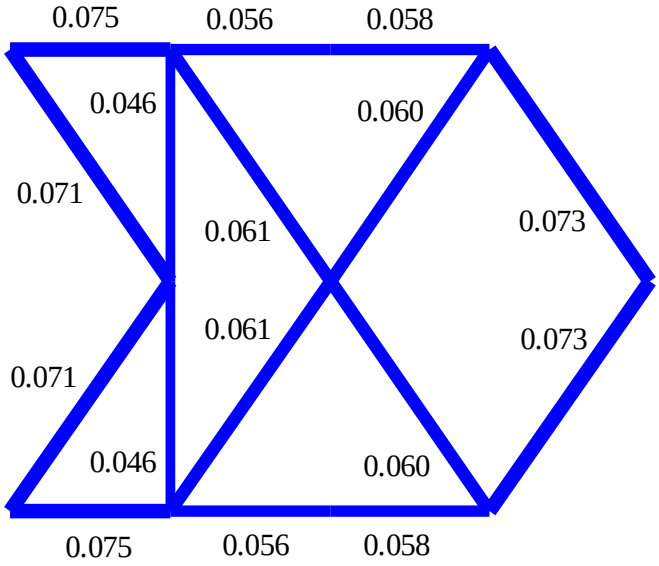


**Figure 3.56:** Local optimal solution for four base parts, for Case G.

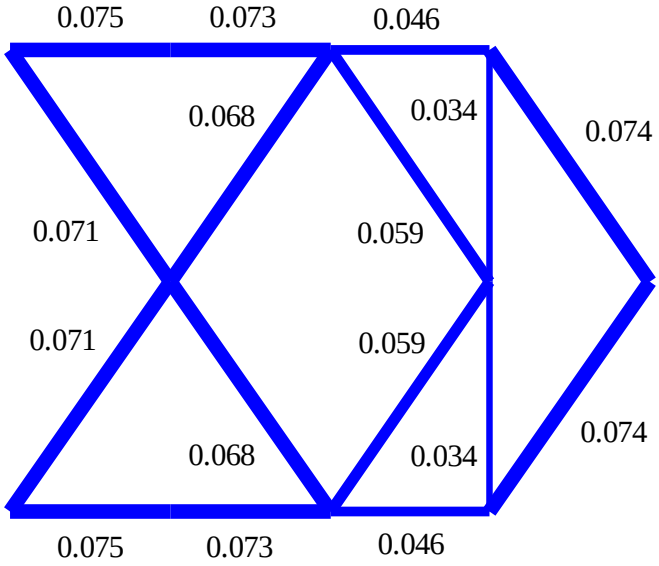


**Figure 3.57:** Local optimal solution for four base parts, for Case G.

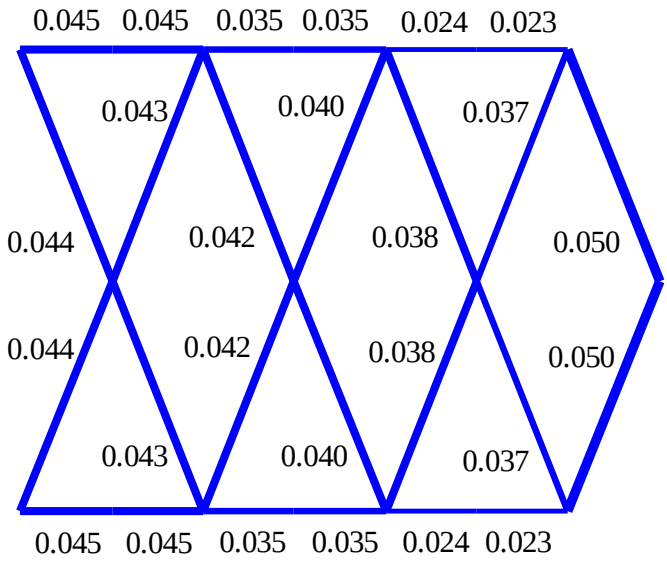


**Figure 3.58:** Symmetrical solution for seven base parts, for Case G.

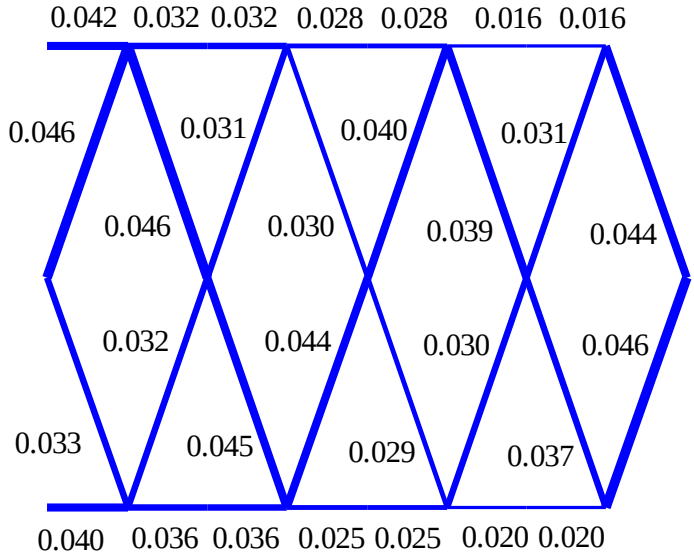


**Figure 3.59:** Asymmetrical solution for eight base parts, for Case G.

## 3.6 Optimal Design under Dynamic Loads Using Limited Number of Contributing Modes

In this section, results for the case of stochastic dynamic loading using the modal space approach are presented. The case under investigation is Case E, with the difference that the contribution of $m$ ($m \leq n$) modes is considered for estimating the dynamic response of the system. Four cases, denoted as Case E1, Case E2, Case E10 and Case En are considered. In Case E1, only the lowest mode is considered ($m=1$), whereas in Case E2 and E10 the first two and ten modes are considered, respectively ($m=2$, $m=10$). Finally, in Case En, all the modes of each system are considered for the estimation of the dynamic response. For these cases, the optimization problem is stated in (2.35) - (2.38), and the matrix $\Sigma$ is given by (2.75). Additionally, the volume constant $V_0$ is chosen to be equal to $10^{-5}\,\mathrm{m}^3$ and the value of the power spectral density of the imposed white noise excitation is considered to be 1000.

It should also be noted that the values of the objective function $J^*$ for the optimal structure are presented. This objective function is defined equivalently as in Case E, that is it is chosen to be equal to the objective function $J$ defined for Case C. This definition is very useful when one needs to compare the optimal solutions of structures with different number of base parts. This comparison is impossible using the objective function $J$, as the degrees of freedom at the optimal solution change with respect to the number of base parts, thus the number of terms in the summation is also different. Therefore, in order to define the optimal solution between the optimal solutions with different number of base parts, the objective function $J^*$ should be used.

### 3.6.1 Optimal Design Using the Lowest Mode

In the following paragraph the optimal topologies of the multi-base truss structure are presented using only the first mode ($m=1$) of each structure in order to calculate the covariance of the response. In Figure 3.60 up to Figure 3.63 are shown the optimal structures for one up to four base parts. It is observed that the results for one up to three base parts are quite satisfactory compared to the results obtained on the equivalent Case E of time domain approach. The difference at the volume percentage of each truss member is less than 5%. But, as the number of the base parts increases, and therefore the number of the degrees of freedom of the system increases, it becomes obvious that the information acquired by only the lowest mode is not enough to satisfactorily estimate the system response. This fact can be observed at Figure 3.63 up to Figure 3.65, where the optimal and the local

optimal solutions for the structure that consists of four base parts are presented. Note that the structure in Figure 3.63 is asymmetrical, something that stems from the lack of information in using only the lowest mode. The values of the objective function $J$ for the two local optimal solutions are 0.00187 and 0.002, respectively, whereas the value of the objective function for the asymmetrical optimal solution is equal to 0.00155. It also becomes clear that for higher number of base parts, it is impossible for the algorithm to converge, due to this lack of information. Finally, in Table 3.7 and in Table 3.8 are shown the values of the objective functions $J$ and $J^*$ for the optimal structures and the corresponding eigenfrequencies respectively.

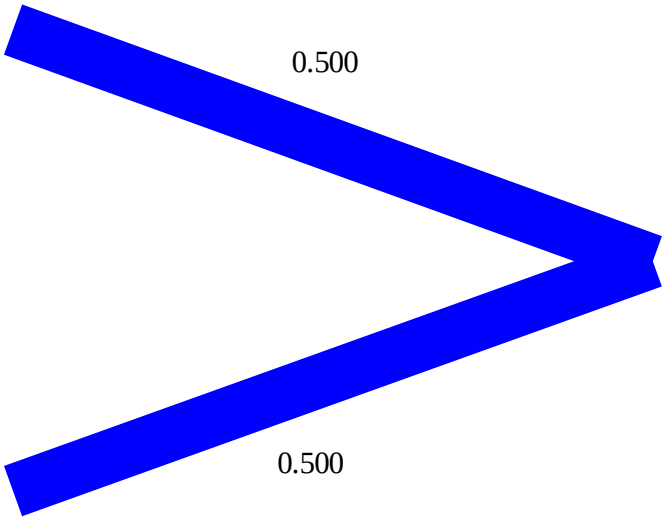


**Figure 3.60:** Optimal solution for one base part, for Case E1.

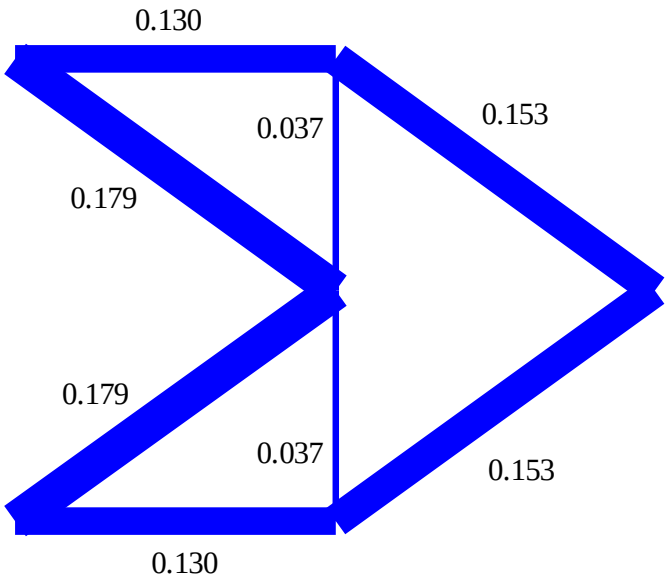


**Figure 3.61:** Optimal solution for two base parts, for Case E1.

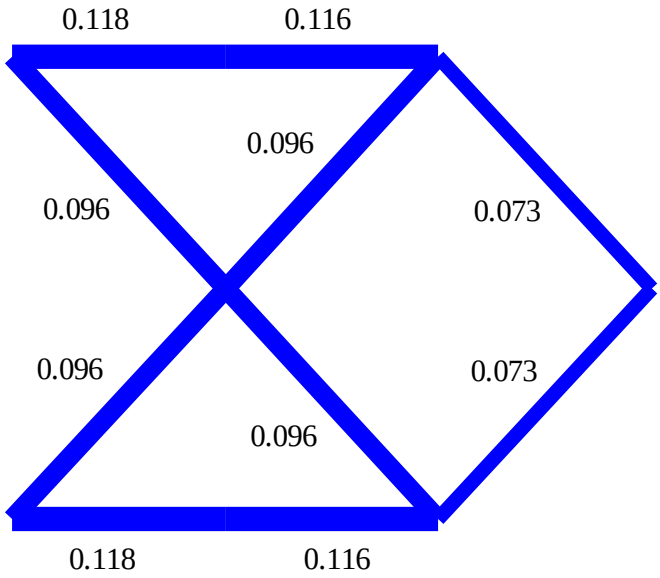


**Figure 3.62:** Optimal solution for three base parts, for Case E1.

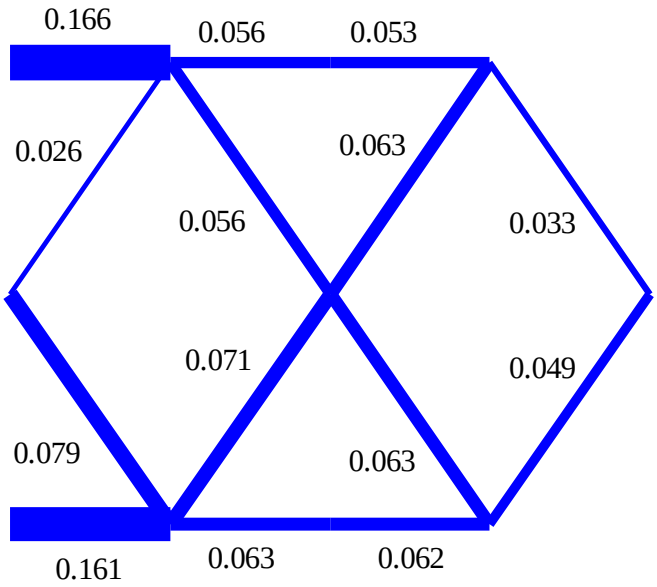


**Figure 3.63:** Optimal solution for four base parts, for Case E1.

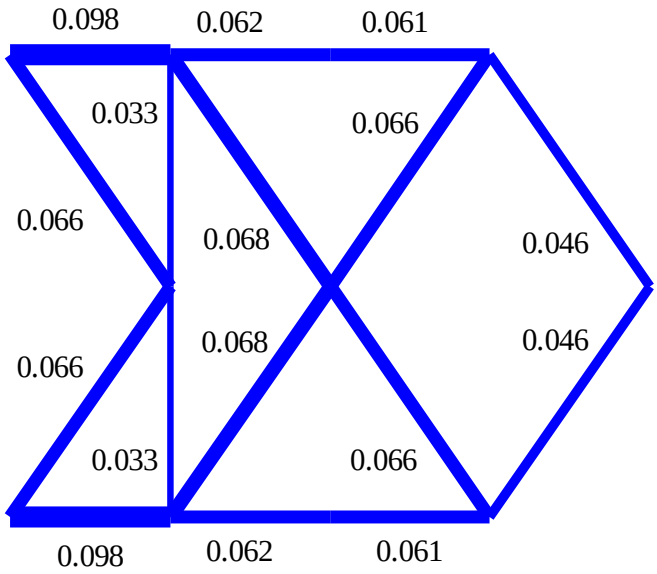


**Figure 3.64:** Local optimal solution for four base parts, for Case E1.

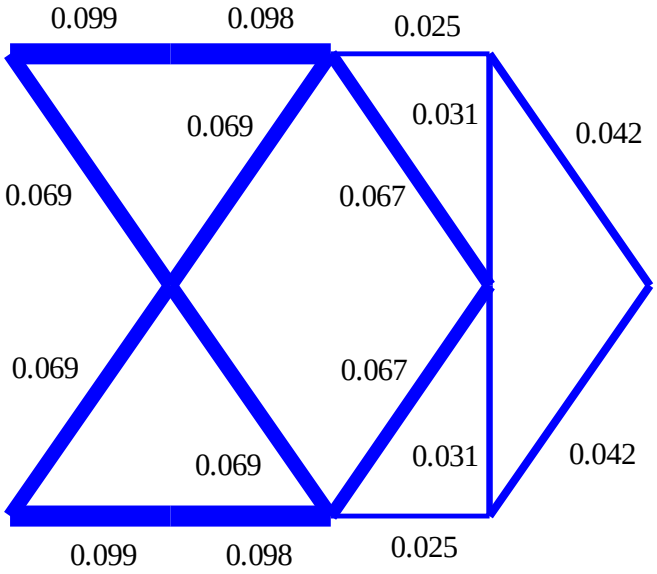


**Figure 3.65:** Local optimal solution for four base parts, for Case E1.

**Table 3.7:** Values of the objective function for one up to four base parts, for Case E1.

| Parts | $J$ | $J^*$ |
|---|---|---|
| 1 | 0.00228 | 13.661 |
| 2 | 0.00163 | 9.8117 |
| 3 | 0.00161 | 14.558 |
| 4 | 0.00155 | 8.6572 |

**Table 3.8:** Eigenfrequencies of the optimal structure (Hz), for Case E1.

| mode / parts | 1 | 2 | 3 | 4 | 5 | 6 | 7 | 8 | 9 | 10 |
|---|---|---|---|---|---|---|---|---|---|---|
| 1 | 8.330 | 33.32 | | | | | | | | |
| 2 | 14.74 | 27.93 | 36.84 | 53.82 | 67.59 | 71.86 | 87.84 | 99.5 | | |
| 3 | 14.99 | 17.07 | 42.10 | 48.15 | 68.76 | 78.12 | 84.99 | 101.2 | 137.1 | 138.3 |
| 4 | 13.40 | 16.89 | 33.08 | 39.05 | 61.36 | 68.92 | 71.13 | 82.02 | 103.2 | 110.5 |
| 4 | 16.10 | 20.74 | 36.59 | 42.74 | 68.90 | 72.37 | 78.91 | 82.06 | 85.68 | 106.5 |
| 4 | 14.71 | 24.10 | 36.42 | 41.07 | 58.51 | 61.72 | 76.44 | 76.86 | 97.26 | 105.6 |

### 3.6.2 Optimal Design Using the Lowest Two and Ten Modes

In the following paragraph the optimal topologies of the multi-base truss structure are presented using only the first two and ten modes ($m=2$, $m=10$) of each structure in order to calculate the covariance of the response. The case of two modes is denoted as Case E2 and the case of ten modes is denoted as Case E10. In Figure 3.66 to Figure 3.75 are shown the optimal structures for one up to ten base parts. It is observed that the structure with the minimum value of the objective function for both cases, consists of two base parts, as expected in comparison with the results obtained in Case E. That is the optimal structure is the structure that is shown in Figure 3.67 for both Case E2 and Case E10.

As far as the Case E2 is concerned, it is observed that all the results are quite satisfactory compared to the results obtained on the equivalent case of time domain approach (Case E). The difference at the volume percentage of each truss member between these two cases is less than 3%. Finally, in Table 3.9 and in Table 3.11 are shown the values of the objective functions $J$ and $J^*$ for the optimal structures and the corresponding eigenfrequencies, respectively.

Similarly, for Case E10, it is observed that all the results are even closer to the results obtained on the equivalent case of time domain approach (Case E), due to the fact that more modes are used to describe the system response and therefore the estimation is better. It should be stressed that for the cases of one and two base parts the modes of the optimal structure is less than ten, therefore the results have been obtained using all the available modes for each structure. The difference at the volume percentage of each truss member between these two cases is less than 2%. Finally, in Table 3.10 and in Table 3.12 are shown the values of the objective functions $J$ and $J^*$ for the optimal structures and the corresponding eigenfrequencies respectively.

Also, it is worth pointing out interesting results that are obtained for the structure that consists of four base parts, similarly to the Case E. Two such optimal solutions are presented in Figure 3.80 and in Figure 3.81 for both Case E2 and Case E10. For the Case E2 the values of the objective function are 0.00187 and 0.002 for the first and the second local optimal solution respectively, whereas the value for the global solution is 0.00178. For the Case E10 the values of the objective function are 0.00194 and 0.0021 for the first and the second local optimal solution respectively, whereas the value for the global solution is 0.00182.

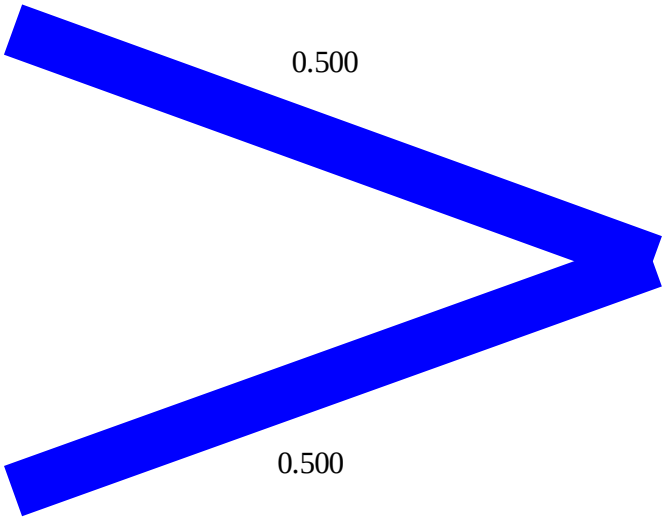


(a)

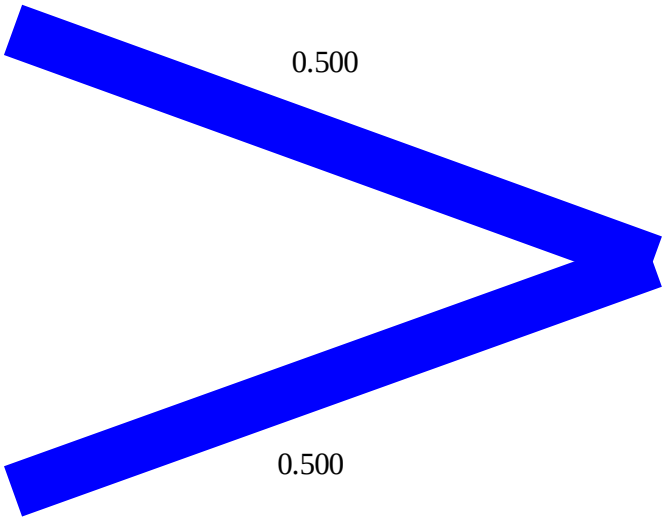


(b)

**Figure 3.66:** Optimal solution for one base part, (a) Case E2, (b) Case E10.

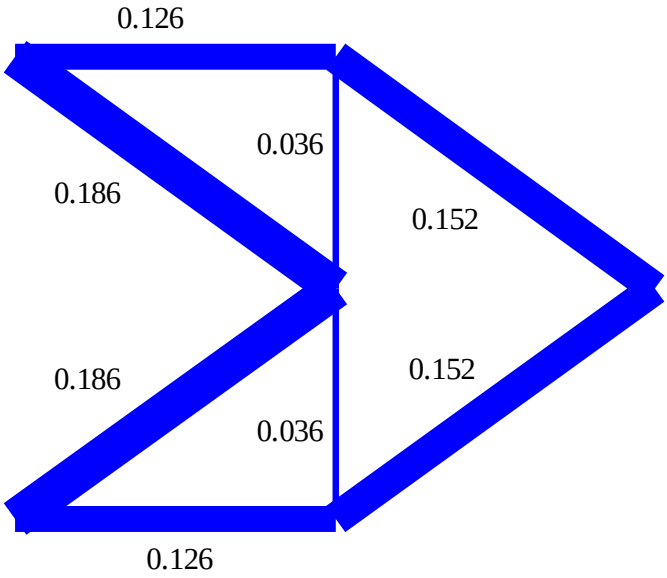


(a)

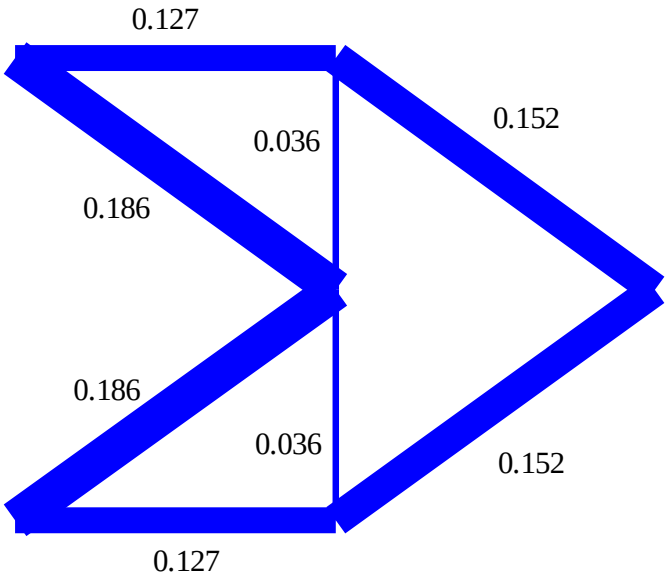


(b)

**Figure 3.67:** Optimal solution for two base parts, (a) Case E2, (b) Case E10.

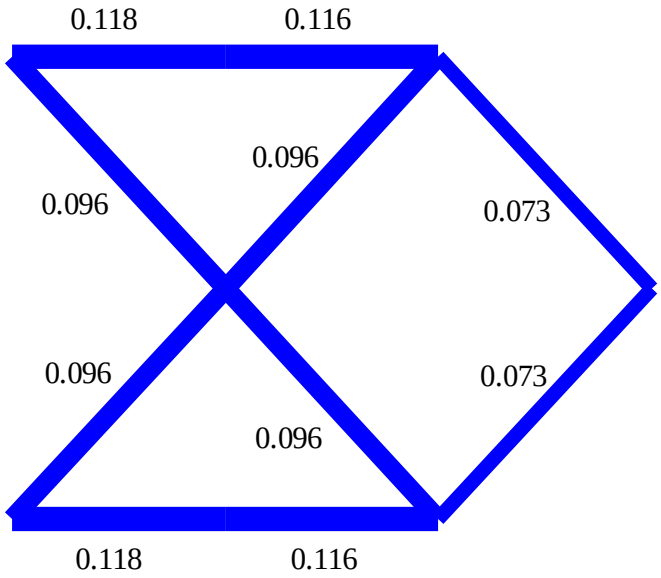


(a)

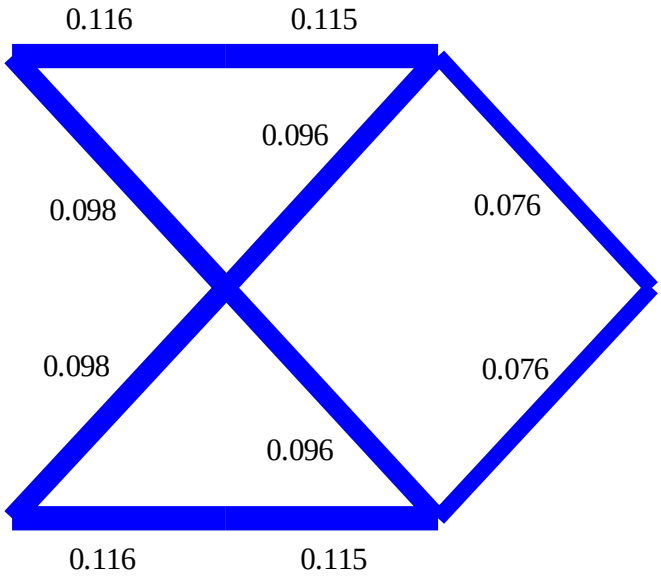


(b)

**Figure 3.68:** Optimal solution for three base parts, (a) Case E2, (b) Case E10.

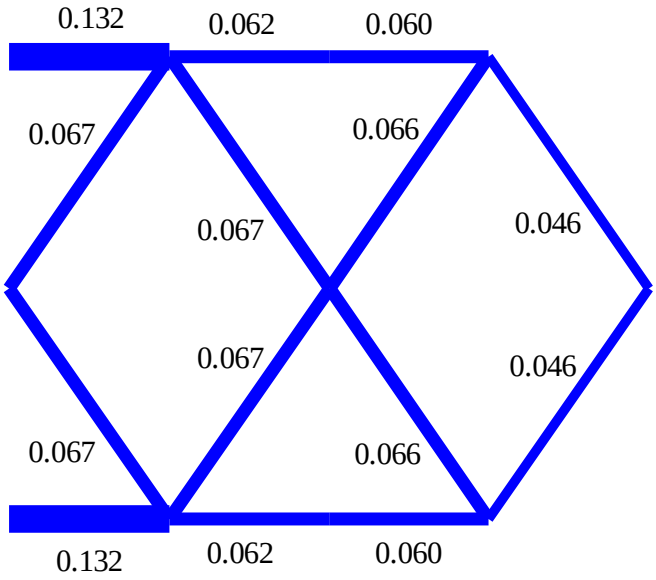


(a)

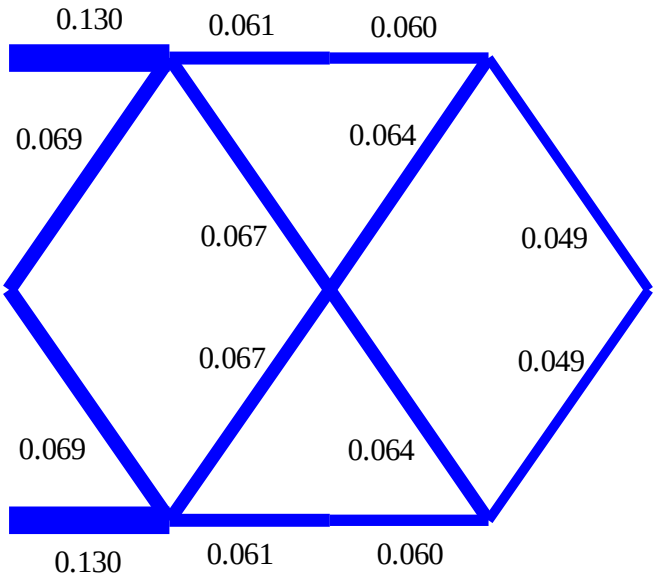


(b)

**Figure 3.69:** Optimal solution for four base parts, (a) Case E2, (b) Case E10.

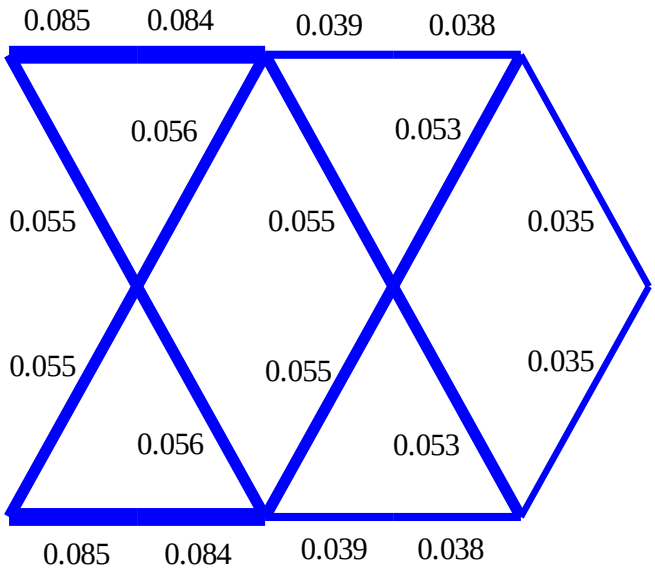


(a)

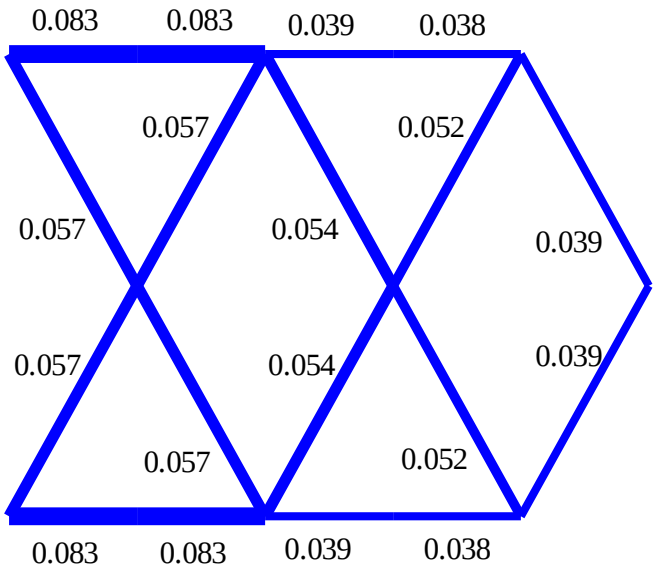


(b)

**Figure 3.70:** Optimal solution for five baser parts, (a) Case E2, (b) Case E10.

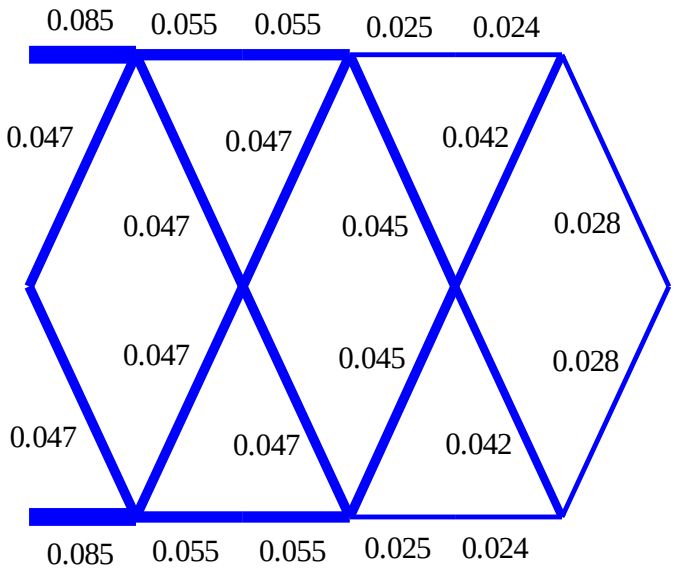


(a)

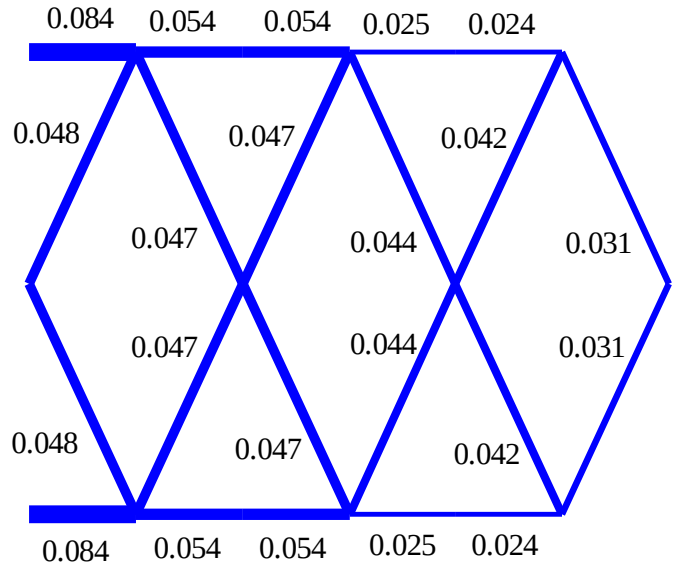


(b)

**Figure 3.71:** Optimal solution for six base parts, (a) Case E2, (b) Case E10.

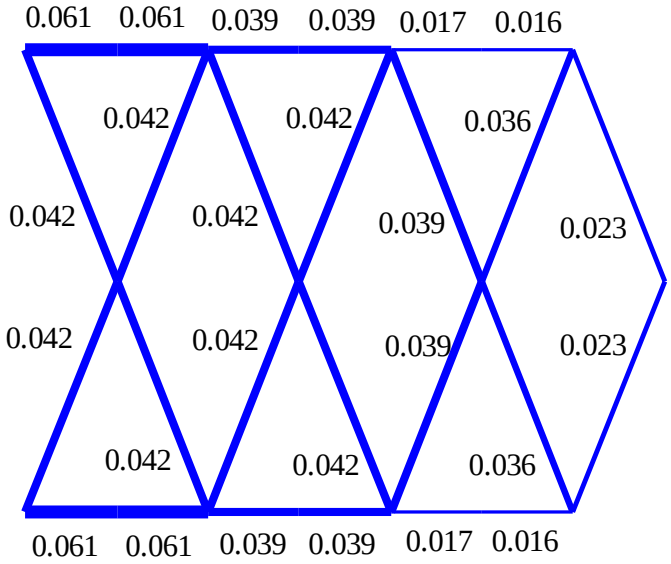


(a)

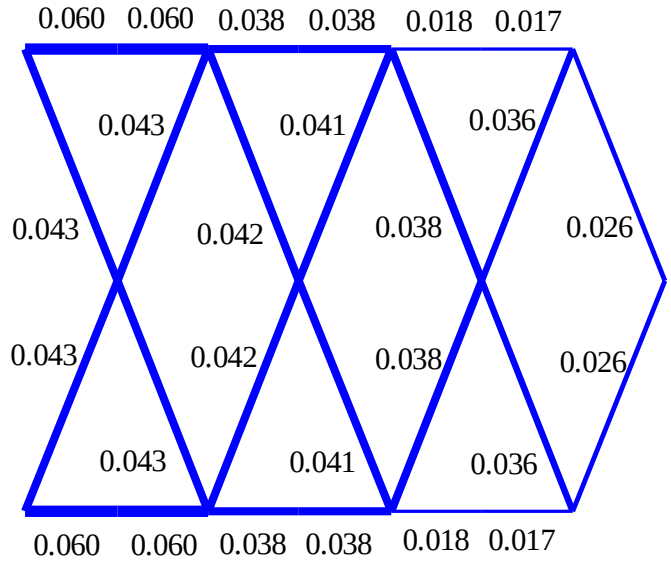


(b)

**Figure 3.72:** Optimal solution for seven base parts, (a) Case E2, (b) Case E10.

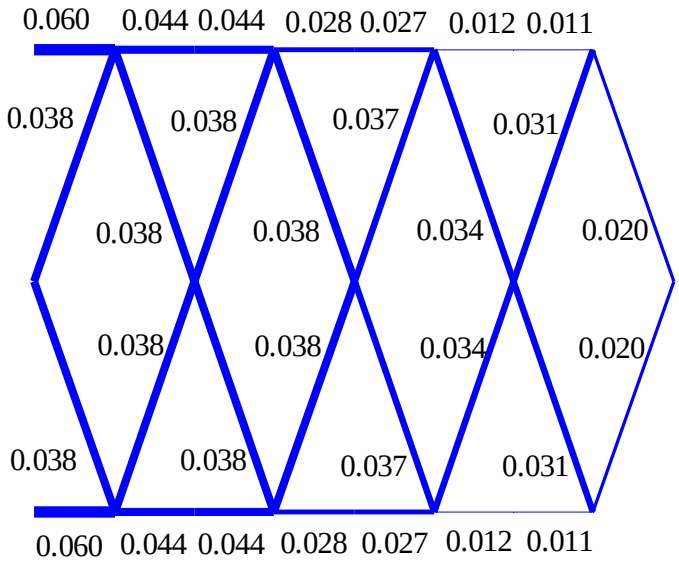


(a)

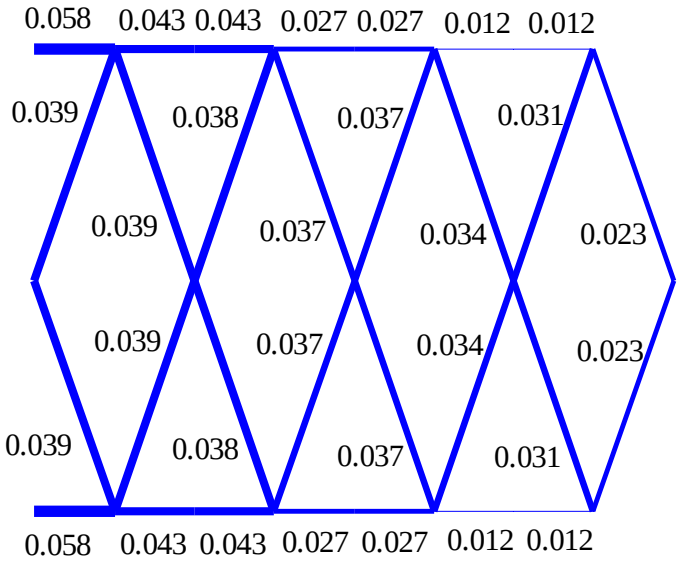


(b)

**Figure 3.73:** Optimal solution for eight base parts, (a) Case E2, (b) Case E10.

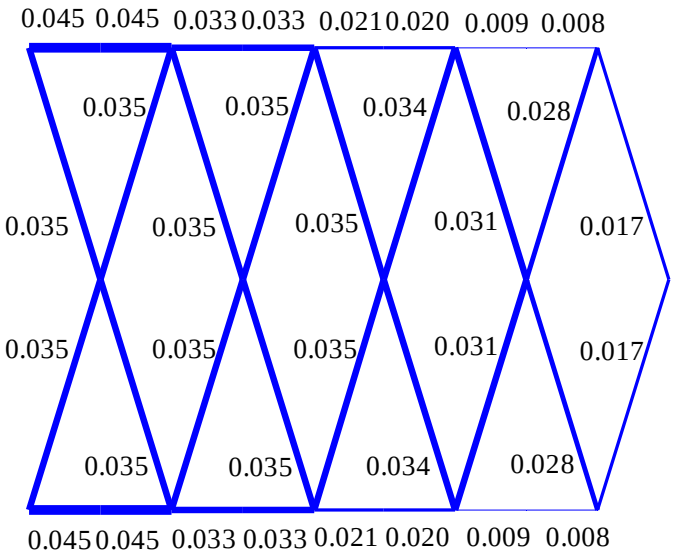


(a)

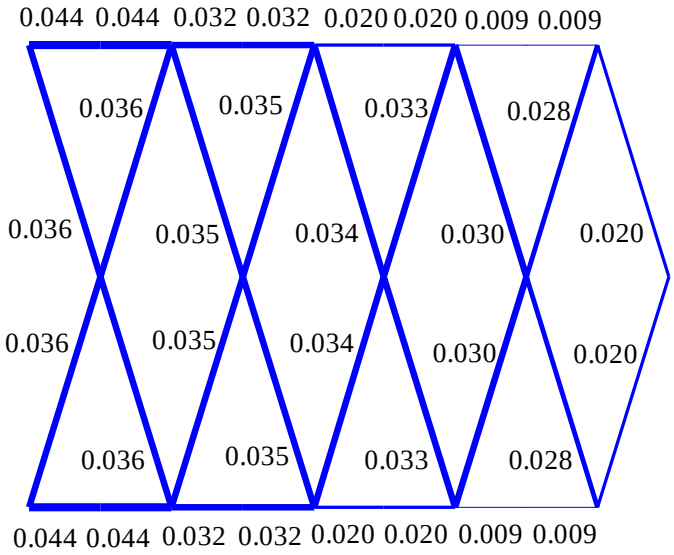


(b)

**Figure 3.74:** Optimal solution for nine base parts, (a) Case E2, (b) Case E10.

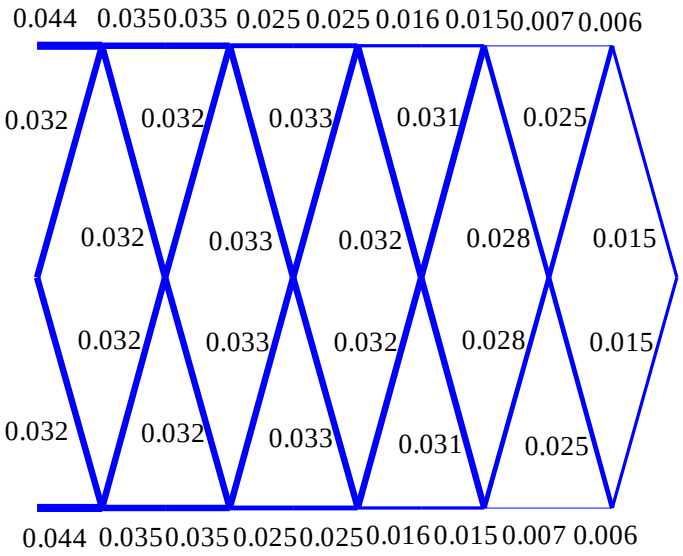


(a)

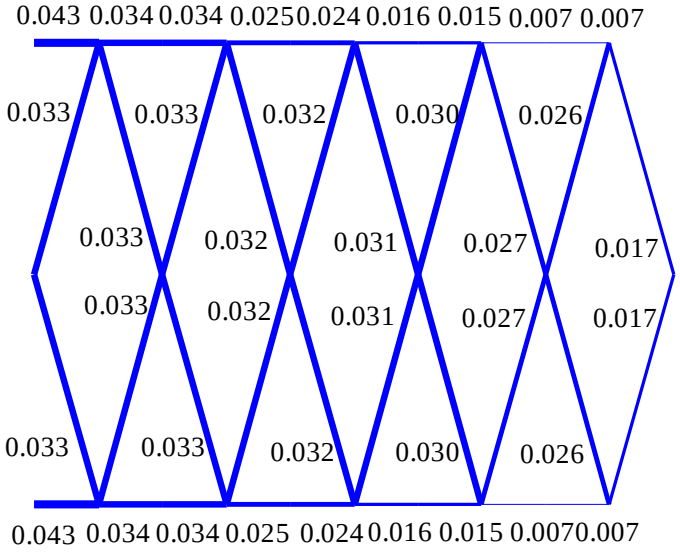


(b)

**Figure 3.75:** Optimal solution for ten base parts, (a) Case E2, (b) Case E10.

**Table 3.9:** Values of the objective function for one to ten base parts, for Case E2.

| Parts | $J$ | $J^*$ |
|---|---|---|
| 1 | 0.00228 | 13.661 |
| 2 | 0.00181 | 10.961 |
| 3 | 0.00161 | 14.558 |
| 4 | 0.00177 | 16.627 |
| 5 | 0.00168 | 16.808 |
| 6 | 0.00192 | 19.364 |
| 7 | 0.00137 | 14.156 |
| 8 | 0.00236 | 24.272 |
| 9 | 0.00261 | 27.007 |
| 10 | 0.00299 | 30.871 |

**Table 3.10:** Values of the objective function for one to ten base parts, for Case E10.

| Parts | $J$ | $J^*$ |
|---|---|---|
| 1 | 0.00228 | 13.661 |
| 2 | 0.00182 | 10.959 |
| 3 | 0.00166 | 14.725 |
| 4 | 0.00182 | 16.905 |
| 5 | 0.00173 | 17.123 |
| 6 | 0.00199 | 19.706 |
| 7 | 0.00142 | 14.418 |
| 8 | 0.00245 | 24.825 |
| 9 | 0.00271 | 27.685 |
| 10 | 0.00312 | 31.734 |

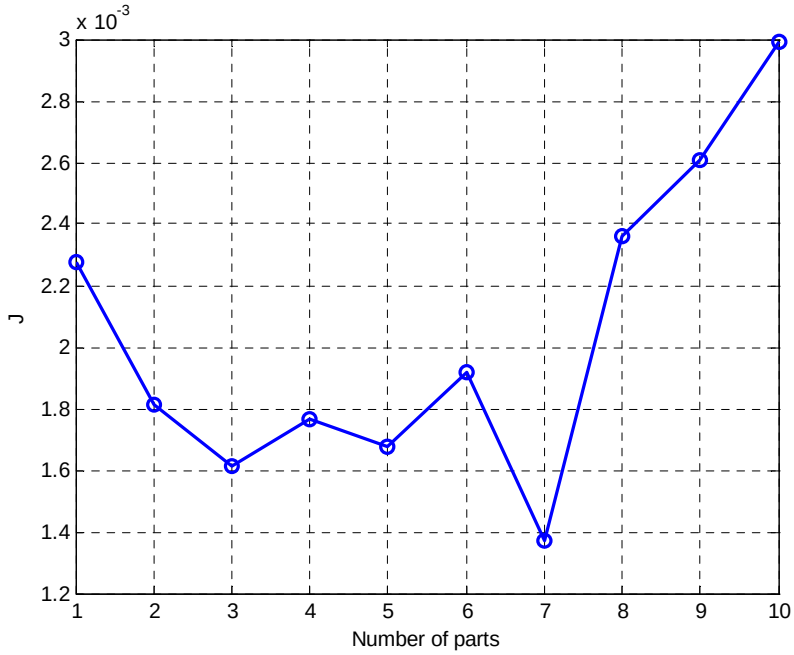


**Figure 3.76:** Optimal values of the objective function $J$ with respect to the number of base parts of the structure, for Case E2.

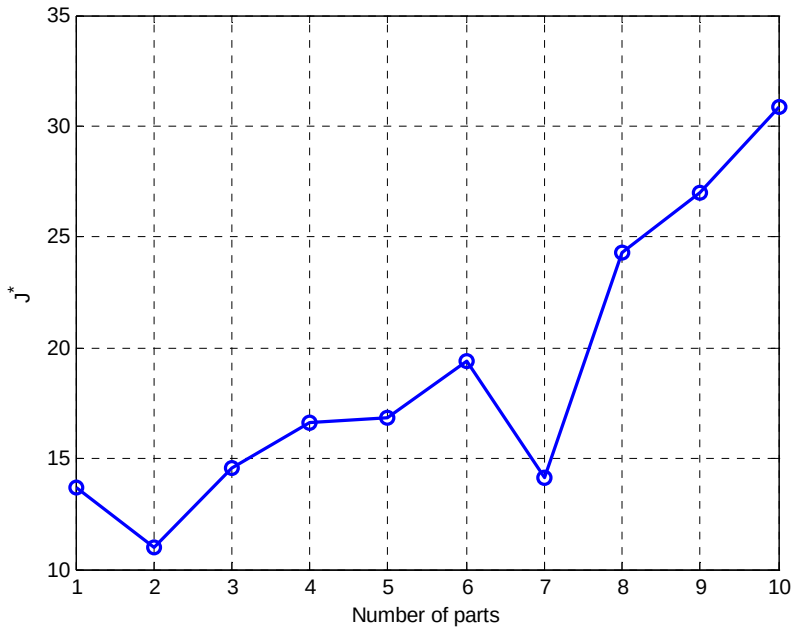


**Figure 3.77:** Optimal values of the objective function $J^*$ with respect to the number of base parts of the structure, for Case E2.

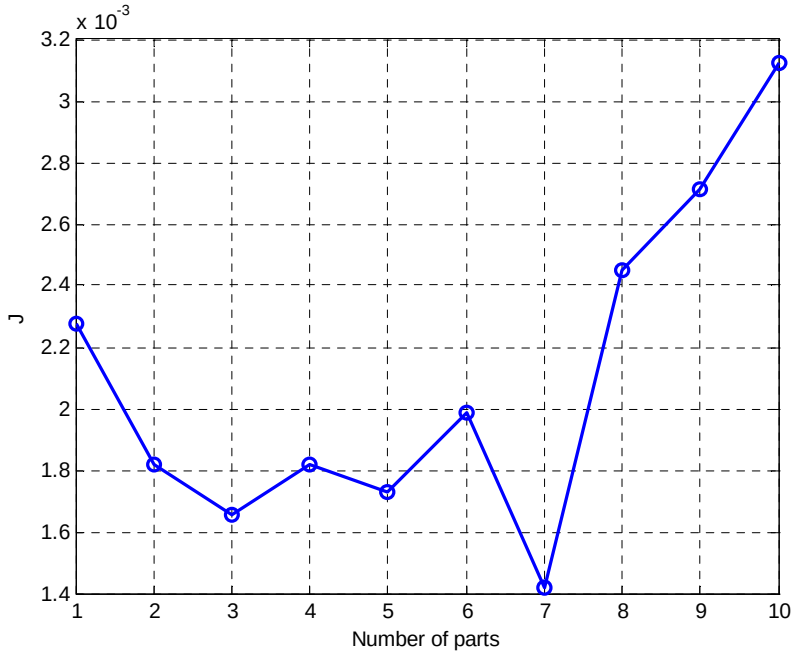


**Figure 3.78:** Optimal values of the objective function $J$ with respect to the number of the parts of the structure, for Case E10.

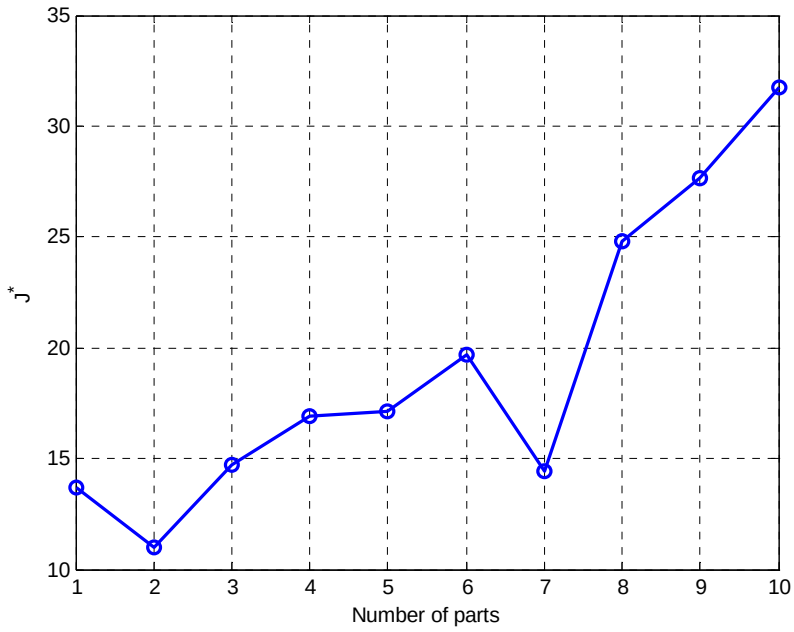


**Figure 3.79:** Optimal values of the objective function $J^*$ with respect to the number of base parts of the structure, for Case E10.

**Table 3.11:** Eigenfrequencies of the optimal system (Hz), for Case E2.

| mode / parts | 1 | 2 | 3 | 4 | 5 | 6 | 7 | 8 | 9 | 10 |
|---|---|---|---|---|---|---|---|---|---|---|
| 1 | 8.330 | 33.32 | | | | | | | | |
| 2 | 14.87 | 27.79 | 36.33 | 52.81 | 68.83 | 71.21 | 87.27 | 97.91 | | |
| 3 | 14.99 | 17.07 | 42.10 | 48.15 | 68.76 | 78.13 | 84.99 | 101.2 | 137.1 | 138.3 |
| 4 | 15.24 | 17.73 | 34.96 | 41.98 | 69.04 | 69.36 | 79.28 | 79.59 | 106.1 | 112.3 |
| 5 | 16.13 | 17.08 | 33.25 | 42.19 | 60.98 | 74.47 | 83.94 | 85.15 | 105.6 | 110.3 |
| 6 | 15.33 | 15.64 | 33.15 | 40.93 | 45.79 | 71.26 | 81.22 | 82.82 | 96.48 | 101.2 |
| 7 | 9.153 | 10.40 | 21.71 | 26.60 | 26.70 | 45.79 | 46.34 | 53.80 | 57.05 | 71.71 |
| 8 | 12.07 | 14.90 | 29.94 | 37.32 | 38.21 | 53.64 | 65.46 | 77.96 | 79.89 | 103.8 |
| 9 | 10.69 | 14.51 | 27.38 | 35.29 | 36.81 | 46.68 | 62.72 | 68.45 | 74.91 | 79.20 |
| 10 | 9.42 | 13.88 | 24.87 | 32.80 | 35.41 | 42.24 | 55.89 | 59.36 | 72.12 | 74.55 |

**Table 3.12:** Eigenfrequencies of the optimal system (Hz) , for Case E10.

| mode / parts | 1 | 2 | 3 | 4 | 5 | 6 | 7 | 8 | 9 | 10 |
|---|---|---|---|---|---|---|---|---|---|---|
| 1 | 8.331 | 33.32 | | | | | | | | |
| 2 | 14.87 | 27.80 | 36.36 | 52.80 | 68.81 | 71.23 | 87.25 | 97.87 | | |
| 3 | 14.99 | 17.05 | 42.28 | 48.22 | 69.49 | 79.05 | 84.87 | 101.2 | 136.3 | 137.6 |
| 4 | 15.23 | 17.77 | 34.95 | 42.23 | 69.18 | 69.21 | 81.14 | 81.61 | 105.8 | 111.7 |
| 5 | 16.12 | 17.16 | 33.22 | 42.42 | 61.11 | 74.04 | 86.54 | 87.12 | 105.8 | 111.6 |
| 6 | 15.41 | 15.62 | 33.26 | 41.11 | 45.81 | 71.04 | 83.98 | 84.31 | 97.68 | 103.5 |
| 7 | 9.204 | 10.40 | 21.92 | 26.63 | 26.76 | 46.22 | 46.38 | 54.43 | 58.45 | 72.57 |
| 8 | 12.15 | 14.89 | 30.41 | 37.11 | 38.39 | 54.11 | 65.31 | 78.95 | 81.94 | 105.3 |
| 9 | 10.75 | 14.50 | 27.89 | 35.12 | 37.04 | 47.00 | 62.69 | 69.28 | 75.81 | 80.64 |
| 10 | 9.468 | 13.87 | 25.37 | 32.79 | 35.63 | 42.53 | 56.22 | 59.36 | 73.04 | 75.81 |

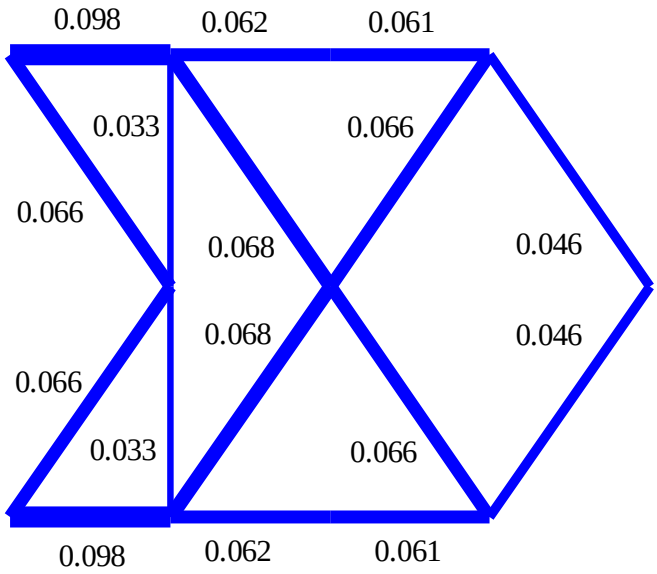


(a)

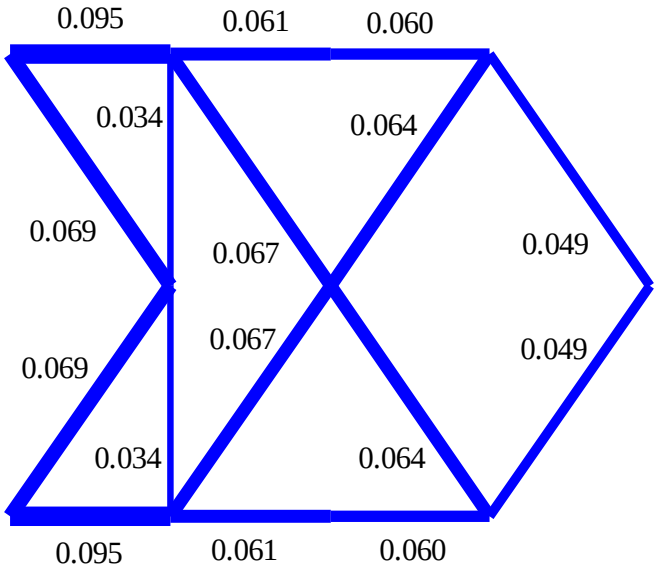


(b)

**Figure 3.80:** Local optimal solution for four base parts, (a) Case E2, (b) Case E10.

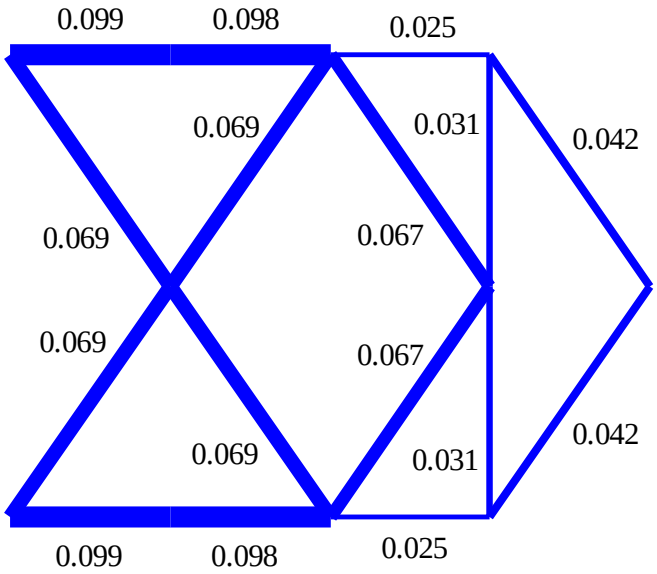


(a)

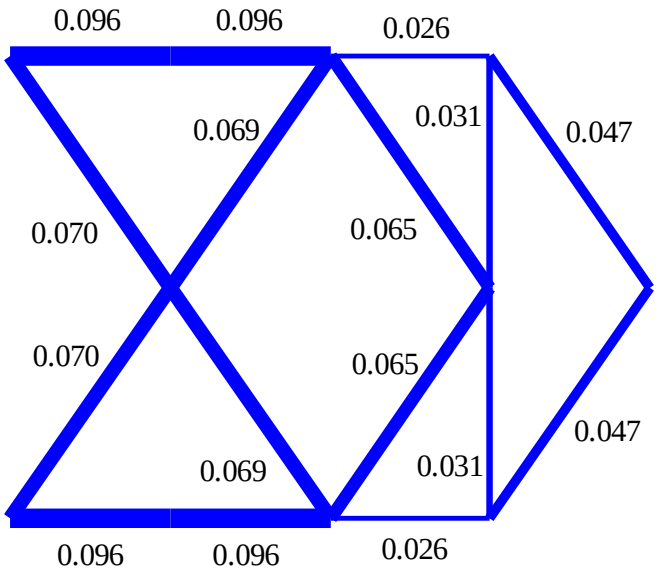


(b)

**Figure 3.81:** Local optimal solution for four base parts, (a) Case E2, (b) Case E10.

### 3.6.3 Optimal Design Using Contribution from All Modes

In the following paragraph the optimal topologies of the multi-base truss structure are presented using all the modes ($m = n$) of each structure in order to calculate the covariance of the response. This case is denoted as Case $E_n$. In Figure 3.82 to Figure 3.86 are shown the optimal structures for one up to ten base parts. It is observed that the structure with the minimum value of the objective function for Case $E_n$, consists of two base parts, as expected in comparison with the results obtained in Case E. That is, the optimal structure is the structure shown in Figure 3.82(b).

It is also observed that all the results are almost identical to the results obtained on the equivalent Case E of time domain approach. Specifically, for the case of one base part, the results are identical due the fact that the systems are exactly the same. As far as all the other systems are concerned, the very small differences at the truss volume percentage stem from the difference at the damping of the system. In the case of the analysis in modal space the damping ratio is equal to 2% at all modes, whereas in the previous analysis, Rayleigh damping was assumed, with damping ratio equal to 2% at the first and the fifth mode, less than 2% at the second, third and fourth mode, and higher than 2% at all the higher modes. In Table 3.13 and in Table 3.14 are shown the values of the objective functions $J$ and $J^*$ for the optimal structures and the corresponding eigenfrequencies, respectively.

Also, it is worth pointing out interesting results that are obtained for the structure that consists of four base parts, similarly to the Case E. Two such optimal solutions are presented in Figure 3.89 and in Figure 3.90. The values of the objective function are 0.00194 and 0.0021 for the first and the second local optimal solution respectively, whereas the value for the global solution is 0.00182.

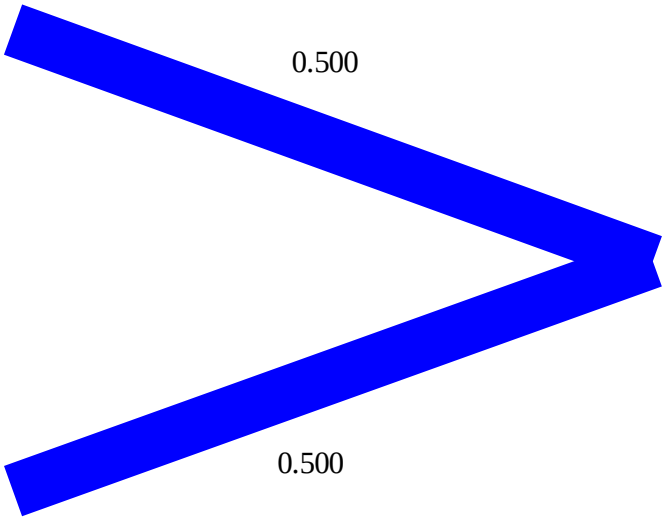


(a)

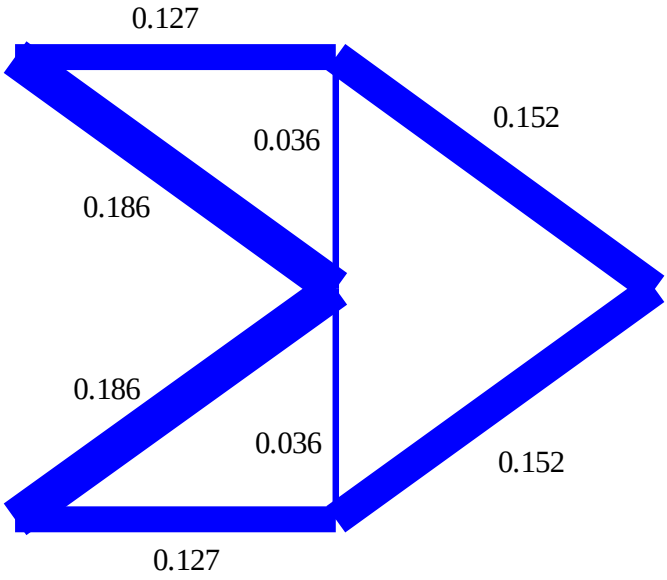


(b)

**Figure 3.82:** Optimal solution for (a) one and (b) two base parts, for Case $E_n$.

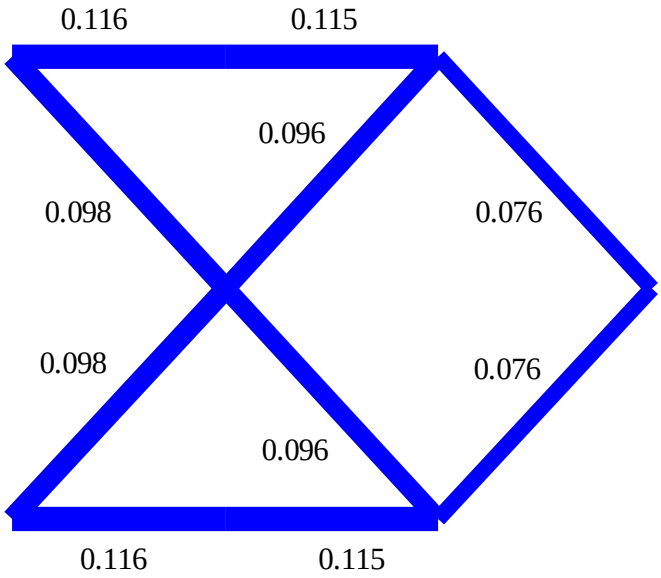


(a)

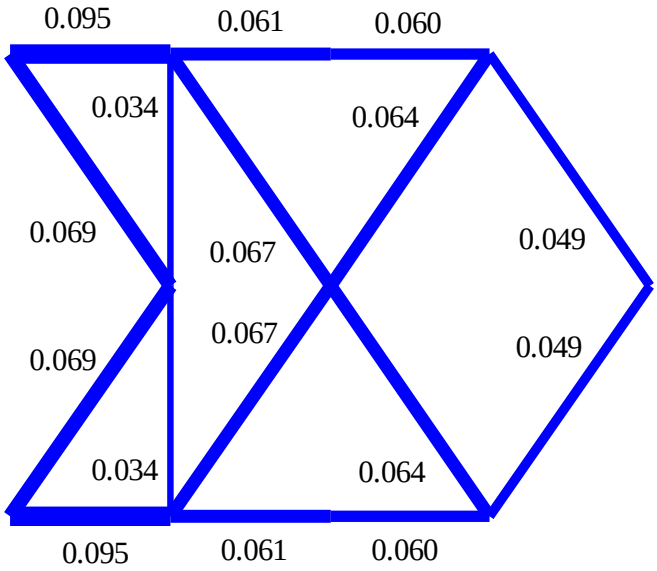


(b)

**Figure 3.83:** Optimal solution for (a) three and (b) four base parts, for Case $E_n$.

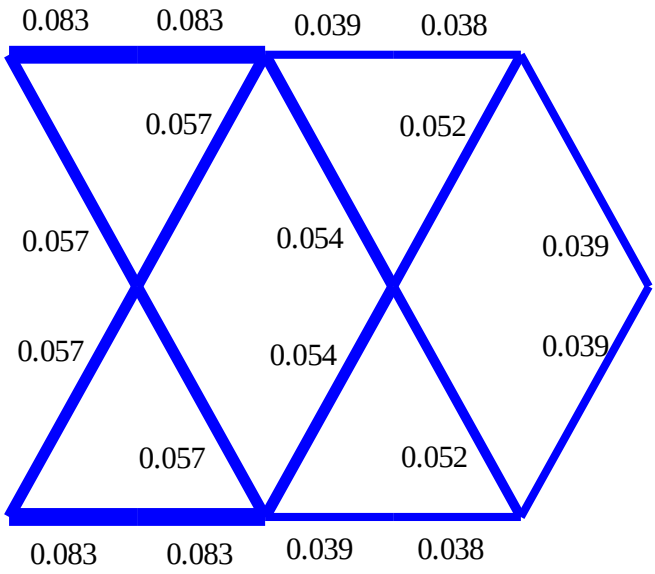


(a)

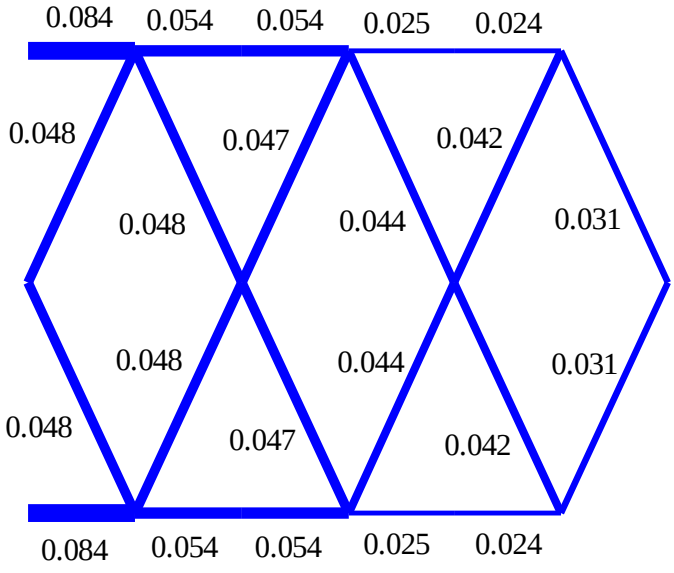


(b)

**Figure 3.84:** Optimal solution for (a) five and (b) six base parts, for Case $E_n$.

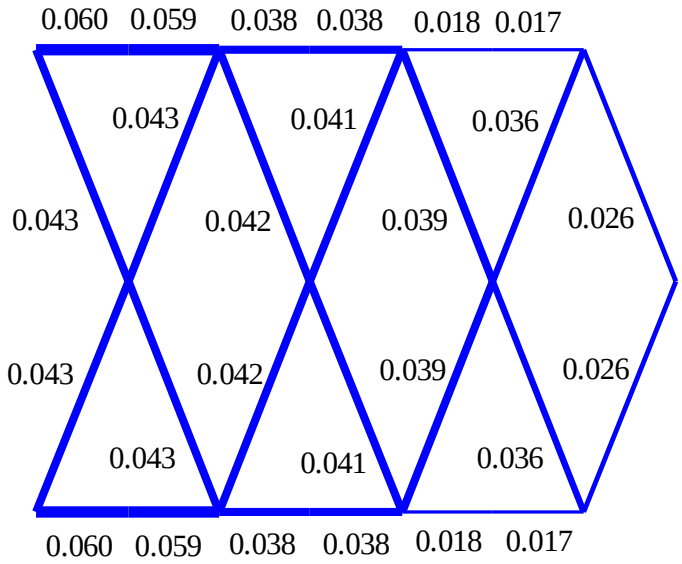


(a)

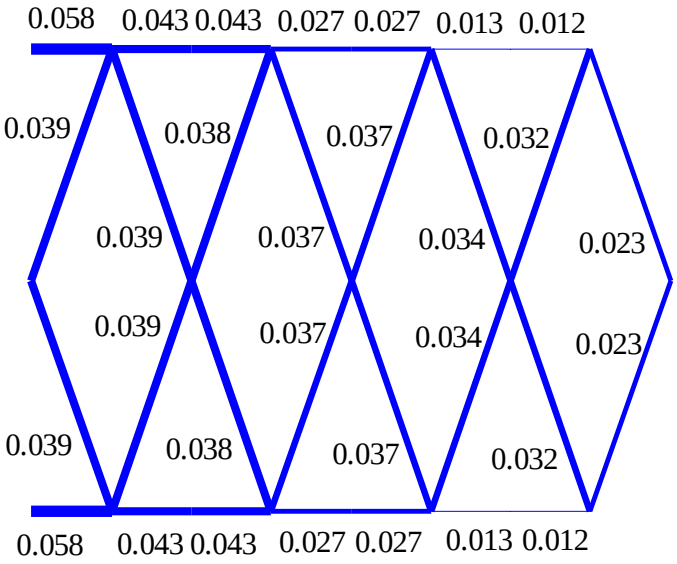


(b)

**Figure 3.85:** Optimal solution for (a) seven and (b) eight base parts, for Case $E_n$.

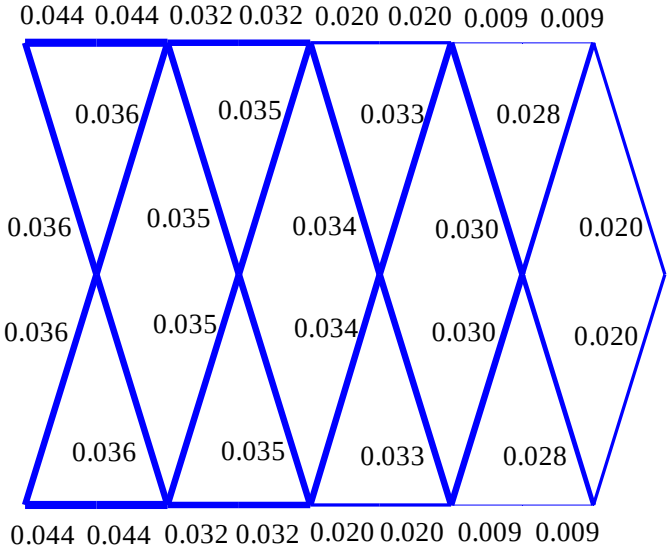


(a)

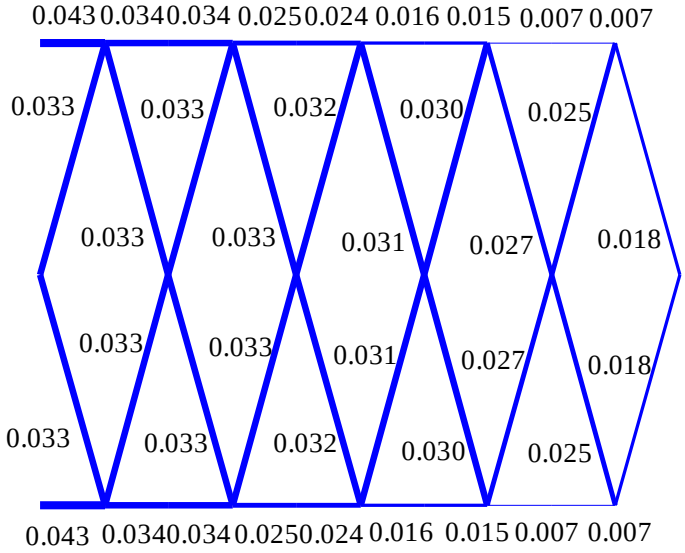


(b)

**Figure 3.86:** Optimal solution for (a) nine and (b) ten base parts, for Case $E_n$.

**Table 3.13:** Values of the objective function for one up to ten base parts, for Case $E_n$.

| Parts | $J$ | $J^*$ |
|---|---|---|
| 1 | 0.00228 | 13.661 |
| 2 | 0.00182 | 10.959 |
| 3 | 0.00166 | 14.724 |
| 4 | 0.00182 | 16.905 |
| 5 | 0.00173 | 17.124 |
| 6 | 0.0019 | 19.740 |
| 7 | 0.00142 | 14.469 |
| 8 | 0.00246 | 24.938 |
| 9 | 0.00272 | 27.842 |
| 10 | 0.00314 | 31.884 |

**Table 3.14:** Eigenfrequencies of the system (Hz)

| mode / parts | 1 | 2 | 3 | 4 | 5 | 6 | 7 | 8 | 9 | 10 |
|---|---|---|---|---|---|---|---|---|---|---|
| 1 | 8.331 | 33.32 | | | | | | | | |
| 2 | 14.87 | 27.80 | 36.36 | 52.80 | 68.81 | 71.23 | 87.25 | 97.87 | | |
| 3 | 14.99 | 17.05 | 42.28 | 48.22 | 69.49 | 79.04 | 84.88 | 101.2 | 136.2 | 137.6 |
| 4 | 15.23 | 17.76 | 34.95 | 42.23 | 69.18 | 69.21 | 81.14 | 81.61 | 105.8 | 111.7 |
| 5 | 16.12 | 17.15 | 33.22 | 42.42 | 61.11 | 74.04 | 86.53 | 87.12 | 105.8 | 111.6 |
| 6 | 15.41 | 15.63 | 33.28 | 41.14 | 45.80 | 71.06 | 83.59 | 84.17 | 97.49 | 103.2 |
| 7 | 9.210 | 10.39 | 21.92 | 26.63 | 26.75 | 46.26 | 46.40 | 54.47 | 58.55 | 72.68 |
| 8 | 12.14 | 14.89 | 30.46 | 37.10 | 38.42 | 54.09 | 65.37 | 78.97 | 81.95 | 105.4 |
| 9 | 10.75 | 14.49 | 27.93 | 35.10 | 37.02 | 47.05 | 62.67 | 69.34 | 75.88 | 80.87 |
| 10 | 9.472 | 13.86 | 25.43 | 32.79 | 35.61 | 42.58 | 56.27 | 59.33 | 73.10 | 76.08 |

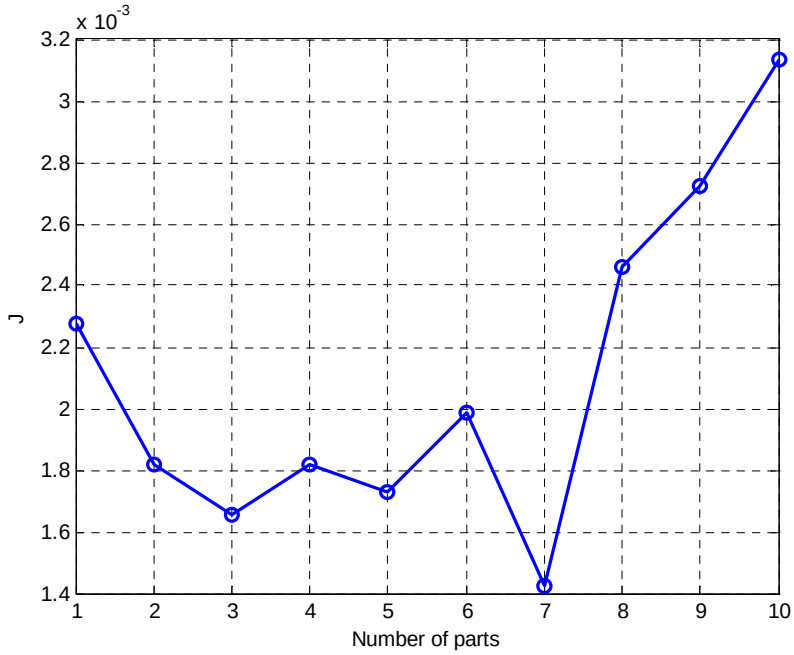


**Figure 3.87:** Optimal values of the objective function $J$ with respect to the number of base parts of the structure, for Case $E_n$.

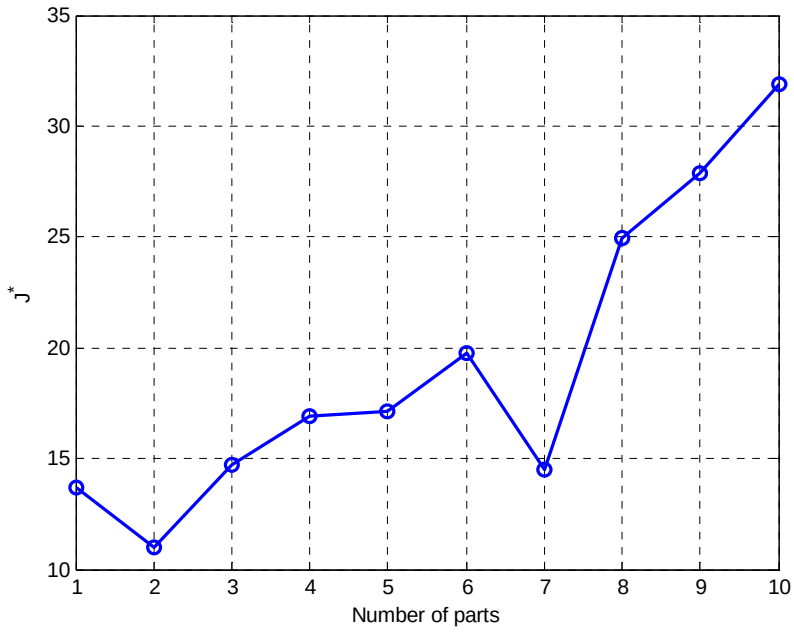


**Figure 3.88:** Optimal values of the objective function $J^*$ with respect to the number of base parts of the structure, for Case $E_n$.

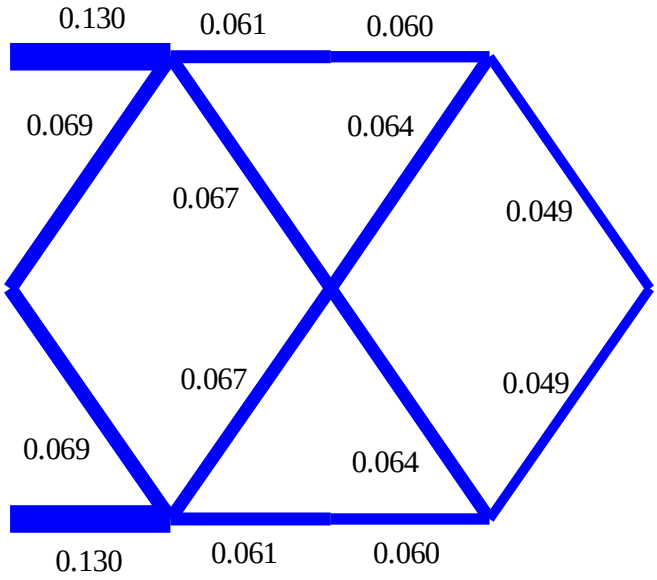


**Figure 3.89:** Local optimal solution for four base parts, for Case $E_n$.

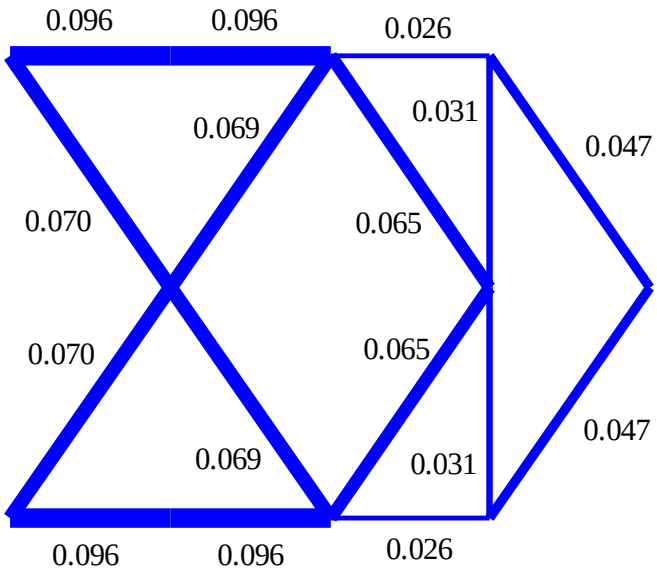


**Figure 3.90:** Local optimal solution for four base parts, for Case $E_n$.

## 3.7 Conclusions

In this chapter, the proposed methodology for design optimization of structures under stochastic dynamic excitations has been applied on the sizing and topology optimization of two dimensional truss structures. An iterative method for the simultaneous optimization of the size and the topology of trusses has been described. Different types of performance functions have been used, such as the weighted sum of the variance of the nodal displacements or the weighted sum of the variance of the developed stresses. The design variables have been chosen to be the cross sectional areas of the truss member, the location and number of nodes o the structure. First, the methodology of design optimization under deterministic static load has been considered using as performance functions the displacement of the system along the degree of freedom on which the loading is imposed and the weighted sum of the displacements at all the degrees of freedom. The optimal results have been presented and discussed, showing similar trends with slight differences between the two cases, as far as the cross sectional areas are concerned. It has also been shown that local optimal solutions may appear for specific cases, which complicate the search for the global optimal solution using gradient – based optimization algorithms.

Next, the sizing and topology optimization of the structure under white noise dynamic excitations has been considered. First, the variance of the displacement across the degree of freedom on which the loading is imposed, has been chosen as performance function. It is shown that as the degrees of freedom of the system is increasing, the information needed for the design optimization is insufficient and therefore the results are inaccurate. Next, the performance function has been considered the weighted sum of the variance of the displacements at the degrees of freedom. The optimal results have been presented and compared to the results obtained for the deterministic static case, showing similar trends, but quantitative differences between the two cases, as far as the cross sectional areas of the optimal solutions are concerned. Similarly to the previous case, it has been shown that local optimal solutions may appear for specific cases, complicating the search for the global optimum.

Additionally, the weighted sum of the variance of the of the developed stresses at the truss members has been chosen as performance function for the dynamic case. The results have been compared with the static load case for which the performance function is also chosen to be the weighted sum of the of the developed stresses. The optimal results for these two cases have been presented and compared with the results obtained for the displacement based optimization.

The optimal configurations show similar trends, but the stress – based optimal structures have shown a slight reinforcement at the truss members close to the location where the dynamic loading is imposed.

The modal space approach has also been applied on the sizing and topology optimization of the truss structure, in order to examine how the use of limited number of contributing modes in the estimation of the variance of the response affects the optimal solutions. It has been shown that, in some cases, a small fraction of contributing modes in relation to the degrees of freedom of the structure can lead to quite satisfactory results compared to the optimal results obtained in the previous cases. In particular, for the example case considered, for ten contributing modes, the optimal results are almost identical to the optimal structures obtained at the previous case. This fact can lead to a significant reduction of the computational cost of the optimization in many cases. Finally, it has been shown that if all the modes of each system contribute to the estimation of the variance of the response, the results are identical to the results obtained for the time domain method, with minor differences been attributed to the different models used for of the system damping.

# CHAPTER 4 Fatigue of Multi-Dimensional Vibratory Degrading Systems under Stochastic Loading

## 4.1 Introduction

In this chapter the basic methodology for the fatigue reliability assessment of randomly vibrating multi-degree of freedom systems is presented within the coupled response-degradation model. The fatigue process in the system components is quantified by the fatigue crack growth equations, which - via the stress range - are coupled with the system response. Simultaneously, the system dynamics are affected by fatigue process via its stiffness degradation so that it provides the actual stress values to the fatigue growth equation. In addition to the general coupled response-degradation analysis, its special case of non-coupled fatigue crack growth is treated as well for the wide-band stationary applied stress by the use of its first four spectral moments and the approximate, empirically motivated, Dirlik's (Dirlik 1985) probability distribution for the stress range. Both, the general analysis and the illustrating exemplary problems elaborated in the paper provide the route to the fatigue reliability estimation in complex–hierarchical vibratory systems under random loading.

First, the general stochastic differential equations, as well as the equations of the specific case of stiffness degrading systems, are presented. Next, the fatigue induced stiffness degradation is described, along with two ways of characterizing the random stress range: using second order moments and using a spectrum distribution. Three methodologies for crack growth prediction for hierarchical systems are proposed next. First a methodology that takes into account the stiffness degradation of the system along with the crack length growth, second a method that uses the second order spectral moments and assumes that the response is uncoupled from the degradation and finally a non-coupled response-degradation method using a spectrum distribution. Specifically, the spectrum distribution used is the empirical approximation proposed by Dirlik. Finally, the proposed approaches of the stochastic fatigue problem are applied on two hierarchical systems, first a single degree of freedom system and subsequently a three degrees of freedom system. Illustrative results of all the cases are shown and compared for the different approaches.

## 4.2 Response-Degradation Models

### 4.2.1 General Governing Stochastic Differential Equations

Stochastic governing equations for many engineering dynamical systems should be represented in the form, which accounts for both – the system dynamics and degradation process, taking place in the system. In the case of mechanical/structural systems these are, above all, the elastic-plastic vibratory systems (under severe random loadings) in which the restoring force has a hereditary nature (Lin and Cai 1995, Wen 1986) and elastic systems with stiffness degradation due to fatigue damage.

In general, a coupled response-degradation model for nonlinear vibratory systems with random excitation (parametric and/or external) can be formulated in the following vectorial form:

$$\boldsymbol{M}\ddot{\boldsymbol{y}}(t)+\boldsymbol{C}\dot{\boldsymbol{y}}(t)+\boldsymbol{R}[\boldsymbol{y}(t),\dot{\boldsymbol{y}}(t),\boldsymbol{d}(t),\boldsymbol{X}_1(t,\gamma)]=\boldsymbol{P}\boldsymbol{X}_2(t,\gamma) \tag{4.1}$$

$$\mathcal{F}\{\boldsymbol{y}(t),\dot{\boldsymbol{y}}(t),\boldsymbol{d}(t),\boldsymbol{X}_1(t,\gamma)\}=\boldsymbol{0} \tag{4.2}$$

$$\boldsymbol{y}(t_0)=\boldsymbol{y}_0,\ \dot{\boldsymbol{y}}(t_0)=\boldsymbol{y}_{1,0},\ \boldsymbol{d}(t_0)=\boldsymbol{d}_0 \tag{4.3}$$

where $\boldsymbol{M}$ and $\boldsymbol{C}$ represent the constant mass and damping matrices, respectively, $\boldsymbol{y}(t)=[y_1(t),y_2(t),...,y_N(t)]$ is an unknown response vector process, $\boldsymbol{R}$ characterizes a nonlinear restoring force depending on $\boldsymbol{y}$ and $\dot{\boldsymbol{y}}$, and on the

process $\boldsymbol{d}(t)=[d_1(t),d_2(t),...,d_M(t)]$, $M$ < $N$, which characterizes a process responsible for degradation phenomena; $\boldsymbol{X}_1(t,\gamma)$, $\boldsymbol{X}_2(t,\gamma)$ are given random processes symbolizing parametric and external excitations, respectively. The variable $\gamma$ is an element of the space of elementary events in the basic scheme $(\Gamma,F,P)$ of probability theory (Sobczyk 1991). $\mathcal{F}\{\cdot\}$ denotes a relationship between degradation and response processes; its specific mathematical form depends on the particular physical/mechanical situation. It is clear that $\boldsymbol{y}_0,\boldsymbol{y}_{1,0},\boldsymbol{d}_0$ are given initial values of the response $[\boldsymbol{y}(t),\dot{\boldsymbol{y}}(t)]$ and degradation $\boldsymbol{d}(t)$ processes, respectively.

It should be noted, that in the cases when the original system is of a continuous type (e.g. beam, plate, shell) governed by partial differential equations, the model (4.1)–(4.3) is a spatially discretized version (e.g. via Galerkin or finite element methods) of the original equations and it describes the system response-degradation as a function of time at fixed spatial points. It is also worth noticing that the meaning of $\mathcal{F}\{\cdot\}$ in (4.2) can be quite different in specific situations; it can be a differential operator, and also a functional defined on $[\boldsymbol{y}(t),\dot{\boldsymbol{y}}(t)]$. It is natural to assume that $\boldsymbol{d}(t_0)=\boldsymbol{0}$. During the dynamical process vector $\boldsymbol{d}(t)$ approaches, as time increases, the unsafe state symbolized by the boundary $\tilde{B}$. Each $\boldsymbol{d}\in\tilde{B}$ denotes a critical level of degradation. Set $B$ of the admissible values of $\boldsymbol{d}(t)$ – being a part of the first quadrant – constitutes a quality space. Therefore, the reliability of the system in question is defined as the probability that process $\boldsymbol{d}(t)$ will belong to $B$ i.e.

$$\mathcal{R}(t)=\Pr\{\boldsymbol{d}(t)\in B,\quad \tau\in[t_0,t]\} \tag{4.4}$$

### 4.2.2 Specific Vibratory Systems with Stiffness Degradation

An important class of vibration-degradation model (4.1) has the form:

$$\boldsymbol{M}\ddot{\boldsymbol{y}}(t)+\boldsymbol{C}\dot{\boldsymbol{y}}+\boldsymbol{R}[\boldsymbol{y},\boldsymbol{k}(\boldsymbol{d})]=\boldsymbol{P}\boldsymbol{X}(t,\gamma) \tag{4.5}$$

where $\boldsymbol{M}=diag(m_p)\in\mathbb{R}^{N\times N}$, $p=1,2,...,N$, $\boldsymbol{C}\in\mathbb{R}^{N\times N}$, $\boldsymbol{k}(\boldsymbol{d})=[k_1(d_1),\cdots,k_N(d_N)]^T\in\mathbb{R}^N$, with $k_p(d_p)$ be a function (empirically identified) characterizing dependence of $p$-th stiffness element on the degradation mode $d_p$ (e.g. it can be fatigue crack size, amount of wear, etc.), $\boldsymbol{R}$ is the nonlinear restoring force depending on $\boldsymbol{y}$ and the degrading stiffness $\boldsymbol{k}(\boldsymbol{d})$, $\boldsymbol{P}\in\mathbb{R}^{N\times M}$ is a matrix that associates the external loads in $\boldsymbol{X}(t,\gamma)=[X_1(t,\gamma),X_2(t,\gamma),...,X_N(t,\gamma)]^T\in\mathbb{R}^M$ to

the degrees of freedom of the structure. In the linear case, the vector function $\boldsymbol{R}[\boldsymbol{y},\boldsymbol{k}(\boldsymbol{d})]$ is a linear combination of the components $y_p$ of $\boldsymbol{y}(t)$.

In particular, model (4.5) includes the special class of multi DOF hierarchical system, shown in Figure 4.1. This class consists of a "perpendicular chain" of oscillatory systems axially subjected to random loading. The system in Figure 4.1 consists of $N$ bodies with the $p-th$ body having mass $m_p$. The $p-1$ and the $p$ bodies are connected by elastic plate elements which provide the stiffness $k_p$ to the system. It is assumed that in each plate element a fatigue crack develops perpendicular to the direction of the motion as shown in Figure 4.1. The initial crack size of the plate element $p$ is $2L_{p,0}$. In general, it can be assumed that the axial stiffness provided by each plate depends on the crack size $L_p$. This dependence is introduced by letting the stiffness $k_p(L_p)$ be a function of the crack size $L_p$. The model in Figure 4.1 can be used as a simplified model for a *p*-story shear building subjected to some lateral external excitation such as wind forces or base earthquake acceleration (with various rates of damage growth at each level). Also, the two degree of freedom version of Figure 4.1 can be used to represent the dynamics of quarter car models with linear or nonlinear stiffness and damping characteristics (Papalukopoulos and Natsiavas 2007). Therefore, in what follows, such "hierarchical" systems will be of our main concern.

To represent Eqs. (4.5) in the state space form we define the $2N$-dimensional state vector:

$$\boldsymbol{z}(t)=[y_1(t),y_2(t),...,y_N(t),\dot{y}_1(t),\dot{y}_2(t),...,\dot{y}_N(t)]^T=[\boldsymbol{y}^T\ \dot{\boldsymbol{y}}^T]^T \tag{4.6}$$

Equations (4.5) can now be written in the form of a system of $2N$ equations of first order. This system can be written in the vectorial form as

$$\dot{\boldsymbol{z}}=\begin{Bmatrix}\begin{bmatrix}\boldsymbol{0}_{N,N} & \boldsymbol{I}_{N,N}\end{bmatrix}\boldsymbol{z}\\ -\boldsymbol{M}^{-1}\begin{bmatrix}\boldsymbol{0}_{N,N} & \boldsymbol{C}\end{bmatrix}\boldsymbol{z}-\boldsymbol{M}^{-1}\boldsymbol{R}[\boldsymbol{z},\boldsymbol{k}(\boldsymbol{d})]\end{Bmatrix}+\begin{Bmatrix}\boldsymbol{0}_{N,M}\\ \boldsymbol{M}^{-1}\boldsymbol{P}\end{Bmatrix}\boldsymbol{X} \tag{4.7}$$

where $\boldsymbol{0}_{N,M}\in\mathbb{R}^{N\times M}$ is a matrix of zeroes and $\boldsymbol{I}_{N,N}\in\mathbb{R}^{N\times N}$ is the identity matrix.

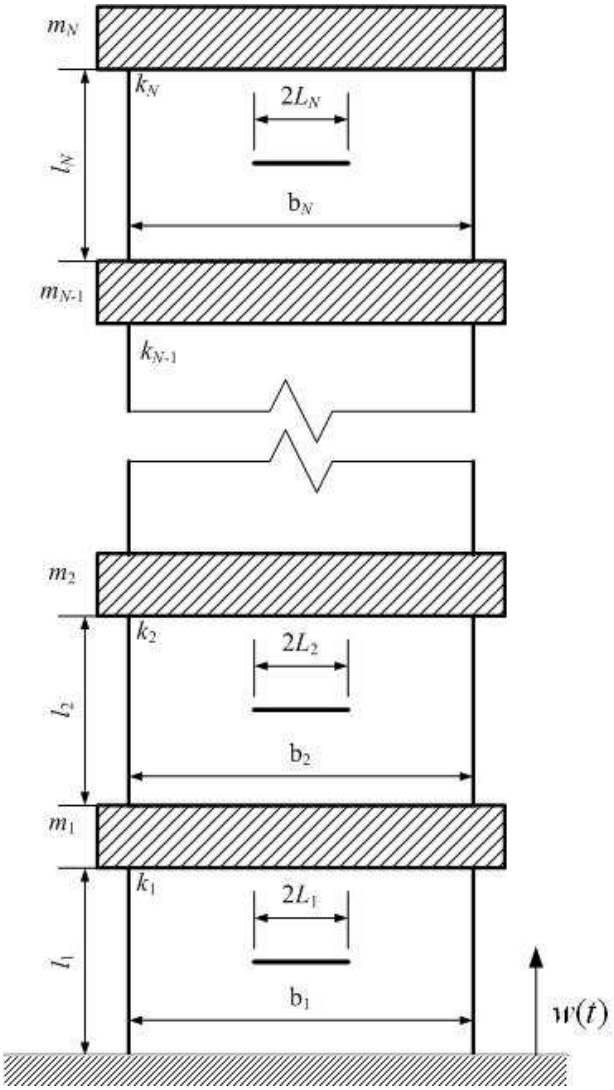


**Figure 4.1:** MDOF system with cracks

Let us confine our analysis in this paper to the linear relationships between the system components. In this situation, system (5) is linear, with $\boldsymbol{R}[\boldsymbol{y},\boldsymbol{k}(\boldsymbol{d})] = \boldsymbol{K}[\boldsymbol{k}(\boldsymbol{d})]\boldsymbol{y}$, where $\boldsymbol{K}[\boldsymbol{k}(\boldsymbol{d})]$ is the stiffness matrix of the structure that depends on the individual degrading stiffnesses $\boldsymbol{k}(\boldsymbol{d})$, the equations (4.5) and (4.7) are linear, and the general vectorial equation of motion is:

$$\dot{\boldsymbol{z}}(t) = \boldsymbol{A}\boldsymbol{z}(t) + \boldsymbol{B}\boldsymbol{X}(t,\gamma) \tag{4.8}$$

where the matrix $\boldsymbol{A}$ is composed of the constant damping matrix $\boldsymbol{C}$ and the degrading stiffness vector $\boldsymbol{k}(\boldsymbol{d})$, as follows

$$\boldsymbol{A} \equiv \boldsymbol{A}(\boldsymbol{C}, \boldsymbol{k}(\boldsymbol{d})) = \begin{Bmatrix} \boldsymbol{0}_{N,N} & \boldsymbol{I}_{N,N} \\ -\boldsymbol{M}^{-1}\boldsymbol{K}[\boldsymbol{k}(\boldsymbol{d})] & -\boldsymbol{M}^{-1}\boldsymbol{C} \end{Bmatrix} \tag{4.9}$$

and $\boldsymbol{B}$ is the matrix

$$\boldsymbol{B} = \begin{bmatrix} \boldsymbol{0}_{N,M} \\ \boldsymbol{M}^{-1}\boldsymbol{P} \end{bmatrix} \tag{4.10}$$

As a specific case, assuming linear elastic behavior of the plate elements in Figure 4.1, the stiffness matrix is

$$\boldsymbol{K}(\boldsymbol{d}) = \begin{bmatrix} k_1(d_1) + k_2(d_2) & -k_2(d_2) & \cdots & 0 \\ -k_2(d_2) & k_2(d_2) + k_3(d_3) & \cdots & \vdots \\ \vdots & \vdots & \ddots & -k_N(d_N) \\ 0 & \cdots & -k_N(d_N) & k_N(d_N) \end{bmatrix} \tag{4.11}$$

The stiffness elements in $\boldsymbol{k}(\boldsymbol{d})$ are varying in time due to variability of $\boldsymbol{d}(t)$ in time. The analysis of the systems (4.8) - (4.11) depends crucially on the mechanisms of degradations $\boldsymbol{d}(t)$. Therefore, the considered vibrating system governed by equations (4.8) - (4.11) is a time-variant and, in general, the response $\boldsymbol{z}(t)$ is a non-stationary random process, even when $\boldsymbol{X}(t,\gamma)$ is stationary. It should be noted, however, that the stiffness degradation is a process much slower than that of the system dynamics. In what follows we assume that stiffness degradation is due to fatigue taking place in the system elements and manifesting itself in fatigue crack growth during the vibration process. Functions $k_p(d_p)$ are assumed to be non-increasing functions known from the empirical data (Sobczyk and Trebicki 1999).

## 4.3 Fatigue-Induced Degradation

In the analysis of response of vibrating systems with stiffness degradation due to fatigue it is natural to quantify the process $\boldsymbol{d}(t)$ in (4.1) by scalar processes $d_p(t)$ which are deliverable from the "kinetic" crack growth equations. These equations contain the stress intensity factor range $\Delta K = K_{\max} - K_{\min}$. A wide class of the fatigue crack growth models can be represented by the Paris equation (Sobczyk and Spencer 1992) governing the evolution of the crack length $L_p(t)$ at the plate $p$ as

$$\frac{dL_p}{dt} = C_p'(\Delta K)^{\mu_p} = C_p'\left[B_p(L_p)\right]^{\mu_p}\left[\Delta S_p\right]^{\mu_p} \tag{4.12}$$

where $\mu_p$, $C_p'$ are empirical constants; $B_p(L_p)$ is the factor which accounts for the crack length and shape of the specimen and crack geometry. In the problem considered here the "specimens with cracks" are the finite rectangular plates, so $B_p(L_p)$ can be taken in the form (Miannay 1998)

$$B_p(L_p) \approx \frac{1}{2b_p}\sqrt{\pi L_p}\left(\sqrt{\cos\frac{\pi L_p}{b_p}}\right)^{-1} \quad , \quad \frac{L_p}{b_p} < 0.7 \tag{4.13}$$

where $b_p$ is the width of the *p*-th plate element. The second factor in equation (12) is the stress range (generated in the vibrating element), i.e.

$$\Delta S_p = S_{p,\max} - S_{p,\min} \tag{4.14}$$

which has to be evaluated as a result of solving multidimensional vibration problem for $\boldsymbol{y}(t) = [y_1(t),\ldots,y_N(t)]^T$, since equations for $y_p(t)$, $p = 1,2,\cdots,N$ are coupled.

### 4.3.1 Characterization of Random Stress Range Using Second Moments

Characterization of the random stress range (4.14) constitutes a crucial part of the analysis. In the existing works, most often $\Delta S_p$ was characterized by the envelope of the stress generated by the response process and (for linear systems) the Rayleigh probability distribution. However, the concept of the envelope itself can not be defined for all random processes. Only for stationary narrow-band processes it has clear meaning, and when process in question is Gaussian, the probability density function of the envelope has the Rayleigh distribution. These are serious restrictions if one has in mind a wider class of practical applications. Due to these reasons our analysis here will rely on a simple characterization of the random stress range, which, although not completely satisfactory, seems to constitute an acceptable approximation and enhances the effectiveness of the analysis of real engineering problems. The characteristic which we have in mind is the mean range $S_{mr}$:

$$S_{mr} = \langle \Delta S \rangle = \langle S_{\max} \rangle - \langle S_{\min} \rangle \tag{4.15}$$

where $S_{\max} = m_S + P$, $S_{\min} = m_S - P$ and $P$ is a random height of peaks. Therefore the mean range is $S_{mr} = 2\langle P \rangle$. For the stationary and Gaussian processes it is as follows (Sobczyk and Spencer 1992):

$$S_{mr} = 2\sigma_S \sqrt{\frac{\pi}{2}\left(1-\varepsilon^2\right)} \tag{4.16}$$

where $\sigma_S$ is the root mean square of $S(t)$ and $\varepsilon$ is the spectral width parameter

$$\varepsilon = \left(1-\alpha^2\right)^{\frac{1}{2}},\ \alpha = \frac{\lambda_2}{\sqrt{\lambda_0 \lambda_4}} \tag{4.17}$$

and $\lambda_0$, $\lambda_2$, $\lambda_4$ are the spectral moments of $S(t)$ and $\sigma_S = \sqrt{\lambda_0}$. If the process is a narrow band one, then $\varepsilon \to 0$ and $S_{mr} = \sqrt{2\pi}\sigma_S$.

The spectral moments $\lambda_k$ are defined as an integral of the product of $\omega^k$ and the spectral density $g_S(\omega)$ of the stress process $S(t)$:

$$\lambda_k = \int_{-\infty}^{\infty} |\omega|^k g_S(\omega) d\omega \tag{4.18}$$

over infinite range. Thus, the spectral moments may not be finite. The moment $\lambda_{2k}$ is finite if and only if the correlation function $K_s(\tau)$, $\tau = t_2 - t_1$, possesses a derivative of order $2k$ at $\tau = 0$ (Cramer and Leadbetter 1967).

### 4.3.2 Characterization of Random Stress Range Using Spectrum Distribution

The averaged characteristics of the stress field (like $S_{mr}$) themselves do not reflect specific features of the stress spectrum (e.g. bi-modal spectral densities) nor the properties of the probability distribution of $\Delta S_p$ (for wide-band processes). However, as it has recently been shown by Dirlik (1985) (see also Bishop 1994; Benasciutti and Tovo 2005), the spectral moments $\lambda_0, \lambda_1, \lambda_2, \lambda_4$ can constitute a base for construction of the approximate closed-form formula for the probability density of the stress range (in the rain-flow cycle analysis). This semi-empirical probability density being a mixture of one exponential and two Rayleigh distributions has been derived by fitting the shape of a rain-flow range distribution via minimizing the normalized error between the rain-flow ranges and the above density model. Its form is as follows

$$p(\Delta S) = \frac{\frac{D_1}{Q} e^{-\frac{Z(\Delta S)}{Q}} + \frac{D_2 Z(\Delta S)}{R^2} e^{-\frac{Z^2(\Delta S)}{2R^2}} + D_3 Z(\Delta S) e^{-\frac{Z^2(\Delta S)}{2}}}{2\sqrt{\lambda_0}} \tag{4.19}$$

where

$$Z(\Delta S)=\frac{\Delta S}{2\sqrt{\lambda_0}} \tag{4.20}$$

and $D_1$, $D_2$, $D_3$, $R$ and $Q$ are specific algebraic functions of the spectral moments $\lambda_0$, $\lambda_2$, $\lambda_4$, given by

$$D_1=\frac{2\left(x_m-a_2^2\right)}{1+a_2^2},\qquad D_2=\frac{1-a_2-D_1+D_1^2}{1-R},\qquad D_3=1-D_1-D_2 \tag{4.21}$$

$$Q=\frac{1.25\left(a_2-D_3-\left(D_2R\right)\right)}{D_1},\qquad R=\frac{a_2-x_m-D_1^2}{1-a_2-D_1+D_1^2} \tag{4.22}$$

$$x_m=\frac{\lambda_1}{\lambda_0}\left[\frac{\lambda_2}{\lambda_4}\right]^{\frac{1}{2}}=\alpha_1\alpha_2,\qquad \alpha_1=\frac{\lambda_1}{\sqrt{\lambda_0\lambda_2}},\qquad \alpha_2=\frac{\lambda_2}{\sqrt{\lambda_0\lambda_4}} \tag{4.23}$$

This formula can be interpreted as “empirical” or simulation – inspired extension of the Rayleigh distribution to non-narrow band processes. It can be viewed as an effective tool for fatigue crack estimation under wide-band stationary applied stress. It will be shown in Sec. 4.3 that it can be used for fatigue predictions in the case of non-coupled response-degradation problem.

## 4.4 Crack Growth Prediction for Hierarchical Systems

The equations for the evolution of the crack length are given by the Paris law (4.12). Thus, the evolution of the crack length depends on the description of the stress range $\Delta S_p$. In the uncoupled case – when the stiffnesses $k_p$ in the vibratory components are regarded to be constant and the load is a stationary random process – the stress ranges $\Delta S_p$ will be described in terms of spectral moments by (4.16) or by making use of the Dirlik’s formula for the probability density of $\Delta S_p$. The required spectral moments are calculated from the solution of the governing vibratory equations.

Although characterization of fatigue loads/applied stress is usually based on stationary random processes, in the coupled response-degradation problem the response of vibratory system (due to variability of the stiffness) is generally non-stationary. So, instead of spectral moments, the stress range will be characterized by the time-varying root mean square, i.e. in equation (4.12) $\Delta S_p(t)=\sqrt{2\pi}\sigma_p(t)$. In the coupled problem the standard deviations $\sigma_p(t)$ occurring in fatigue crack growth equations (4.12) are coupled with the moment equations for the system

response, e.g. with the equations for the covariance $\boldsymbol{Q}_{\boldsymbol{z}}(t) = E\left[\boldsymbol{z}(t)\boldsymbol{z}^T(t)\right]$ of the state vector $\boldsymbol{z}$ governed by the system of first order equations (4.7).

In what follows, Section 4.1, presents the analysis for the prediction of fatigue for the coupled response – degradation case. Sections 4.2 and 4.3 present the analysis for the prediction of fatigue for the non – coupled response – degradation case via spectral moments and Dirlick's approximation of the stress range, respectively.

### 4.4.1 A Coupled Response-Degradation Problem

When stiffness degradation takes place during the vibration process, the linear system (8) has a time varying matrix $\boldsymbol{A} = \boldsymbol{A}(t)$ since

$$\boldsymbol{k}(\boldsymbol{d}) \equiv \boldsymbol{k}(\sigma_{S_p}(t)) \tag{4.24}$$

and thus, using (4.9)

$$\boldsymbol{A}(t) \equiv \boldsymbol{A}(\sigma_{S_p}(t)) \tag{4.25}$$

Assuming that the stress range $\Delta S_p(t)$ is characterized by the time varying root mean square as $\Delta S_p(t) = \sqrt{2\pi}\sigma_p(t)$, the evolution of the crack length $\boldsymbol{L}(t)$ obtained by solving (4.12) is a deterministic function of time. Thus, $\boldsymbol{A}(t)$ is also a deterministic function of time $t$.

Let us consider the situation when the vectorial load process $\boldsymbol{X}(t,\gamma)$ is a white noise with intensity $\boldsymbol{G}_0(t)$, i.e. $\boldsymbol{X}(t,\gamma) = \boldsymbol{W}(t,\gamma)$, where $\boldsymbol{W}(t,\gamma)$ has zero mean and covariance

$$\boldsymbol{R}_{\boldsymbol{W}}(t,s) = E[\boldsymbol{W}(t)\boldsymbol{W}^T(s)] = \boldsymbol{G}_0(t)\delta(t-s) = E[\boldsymbol{z}(t)\boldsymbol{z}^T(t)] \tag{4.26}$$

In this case, the covariance matrix $\boldsymbol{Q}_{\boldsymbol{z}}(t)$ of the state vector $\boldsymbol{z}(t)$ for $s = t$ is given by the following system of equations (called sometimes the Lyapunov equations) (Soong and Grigoriu 1993; Lutes and Sarkani 2003)

$$\frac{d\boldsymbol{Q}_{\boldsymbol{z}}(t)}{dt} = \boldsymbol{A}(\boldsymbol{L}(t))\boldsymbol{Q}_{\boldsymbol{z}}(t) + \boldsymbol{Q}_{\boldsymbol{z}}(t)\boldsymbol{A}(\boldsymbol{L}(t))^T + \boldsymbol{B}\boldsymbol{G}_0(t)\boldsymbol{B}^T \tag{4.27}$$

$$\boldsymbol{Q}_{\boldsymbol{z}}(t_0) = \boldsymbol{Q}_0$$

where $\boldsymbol{Q}_0$ is the covariance of stationary response matrix of the initial non-degraded state obtained by solving the system (4.27) for constant stiffness matrix $\boldsymbol{K}_0 = \boldsymbol{K}\left[\boldsymbol{k}(\boldsymbol{L}_0)\right]$. As it is seen from (4.25), the system (4.27) is coupled with the

system of degradation equations (4.12) for the $p$-th component, $p = 1,2,\ldots,N$. The initial conditions for the equations (4.12) are: $L_p(t_0) = L_{p,0}$, $p = 1,2,\ldots,N$.

It should be noticed that for the case of filtered white-noise excitation that can be modeled as the output of a system of linear differential equations to white noise input, the state vector $\boldsymbol{x}(t)$ can be augmented to include the states of the linear differential equations describing the non-white noise input and thus a similar Lyapunov set of equations of the form (4.27) holds for the combined system with states describing the structural response states and the filter states associated with the input.

The information required in equation (4.12) is the axial stress range perpendicular to the crack in $p$-th plate element, which for the linear hierarchical structure in Figure 4.1, can be written in the form $S_p(t) = k_p(L_p)[y_p(t) - y_{p-1}(t)]$. In compact form, the axial stress $S_p(t)$ can be written in terms of the response vector $\boldsymbol{y}(t)$ as $S_p(t) = (\boldsymbol{\delta}_p^T - \boldsymbol{\delta}_{p-1}^T)\boldsymbol{y}$, where $\boldsymbol{\delta}_p$ is a vector that has the $p$ element equal to one and all other elements equal to zero. Letting $\boldsymbol{S}(t) = [S_1(t)\cdots S_N(t)]^T$ be the vector of axial stresses in the elastic plate elements, one can relate the axial stress vector to the response vector $\boldsymbol{y}(t)$ from the compact relationship

$$\boldsymbol{S}(t) = \boldsymbol{F}(\boldsymbol{L})\boldsymbol{y} \tag{4.28}$$

where

$$\boldsymbol{F}(\boldsymbol{L}) = diag[\boldsymbol{k}(\boldsymbol{L})](\boldsymbol{I}_{N,N} - \boldsymbol{I}_{N,N}^*) \tag{4.29}$$

is a matrix that for stiffness degradation problems depends on the vector of the crack lengths $\boldsymbol{L}(t)$, $\boldsymbol{I}_{N,N} = [\boldsymbol{\delta}_1,\cdots,\boldsymbol{\delta}_N]^T$ is the identity matrix of dimension $N$ and $\boldsymbol{I}_{N,N}^* = [\boldsymbol{\delta}_0,\cdots,\boldsymbol{\delta}_{N-1}]^T \in \mathbb{R}^{N\times N}$ is a matrix having the entries immediately below the diagonal equal one and all other entries equal to zero. Since $\Delta S_p(t)$ in eq. (12) is characterized by the root mean square of the random stress, i.e. $\Delta S_p(t) = \sqrt{2\pi}\sigma_p(t)$, we need to obtain a direct relationship between $\sigma_p(t)$ and the components of the covariance matrix $\boldsymbol{Q}_z(t)$. This is achieved by using (4.28) and noting that $\sigma_p^2(t)$, $p = 1,...,N$, are the diagonal elements of the matrix

$$E[\boldsymbol{S}(t)\boldsymbol{S}^T(t)] = \boldsymbol{Q}_y(t) \tag{4.30}$$

where $\boldsymbol{Q}_y(t)$ is $N \times N$ upper left partition of the matrix $\boldsymbol{Q}_z(t)$.

It should be noted that for time varying $\boldsymbol{A}(t)$ the equation (4.18) for computing $\lambda_{4,p}(t)$ can still be used by replacing the spectral density $g_s(\omega)$ by the time varying spectral density $g_s(\omega,t)$. This can be accurate, provided that $\boldsymbol{A}(t)$ is slowly varying compared to the variation of the states $\boldsymbol{x}(t)$.

The system of $N$ crack growth equations (4.12) and the system (4.27) of the response covariance form a system of coupled nonlinear differential equations that have to be solved simultaneously since the crack length increase affects the stiffness of each element and therefore the covariance of the response. The set of equations (4.30) are auxiliary equations needed to compute the mean square of $\sigma_p^2(t)$ used in the characterization of the random stress range processes $\Delta S_p(t) = \sqrt{2\pi}\sigma_p(t)$, involved in (4.12), in terms of the covariance response matrix $\boldsymbol{Q}_z(t)$ derived from (4.27).

The system of coupled differential equations is stiff due to the slow evolution process associated with the crack growth and the fast evolution process associated with the dynamics of the structure. Thus, the solution of the system of coupled differential equations is obtained using the Gear numerical differentiation formula (Gear 1971) suitable for solving stiff differential equation problems.

### 4.4.2 Non-Coupled Response-Degradation Problem; via spectral moments

Next, it is assumed that crack growth does not significantly affect the axial stiffness of the plate elements so that the stiffnesses remain constant, independent of the crack size, that is $k_p(\boldsymbol{L}_p) = k_{p,0} = const$ or, equivalently, $\boldsymbol{k}(\boldsymbol{L}) = \boldsymbol{k}_0$ is a constant vector independent of the evolution of the vector $\boldsymbol{L}(t)$ of crack lengths. In this case the state space matrix $\boldsymbol{A}(t) \equiv \boldsymbol{A}$, as well as the matrix $\boldsymbol{F}(\boldsymbol{L}) \equiv \boldsymbol{F}$ is constant, independent of the crack sizes $L_p(t)$, $p = 1, \cdots, N$. Simply, it is assumed that the stress range $\Delta S_p$ in each plate element (in degradation equation (4.12)) is specified by (4.16) and (4.17). That is, the stress range is completely specified by the spectral moments of the stress process within each plate.

In this case, the equations (4.27) for the covariance response of the state vector of the system are uncoupled from the crack growth or degradation equations (4.12). Specifically, the solution for the crack growth proceeds as follows. The linear equations of motion in the state space form are used to obtain the covariance matrix $\boldsymbol{Q}_z = E\left[\boldsymbol{z}(t)\boldsymbol{z}^T(t)\right]$ of the state vector by solving the corresponding Lyapunov system of equations:

$$\dot{\boldsymbol{Q}}_{\boldsymbol{z}} = \boldsymbol{A}\boldsymbol{Q}_{\boldsymbol{z}} + \boldsymbol{Q}_{\boldsymbol{z}}\boldsymbol{A}^T + 2\pi\boldsymbol{B}\boldsymbol{G}_0(t)\boldsymbol{B}^T \tag{4.31}$$

with constant matrix $\boldsymbol{A}\left(\boldsymbol{L}\left(t\right)\right) \equiv \boldsymbol{A}$ corresponding to the constant non-degrading stiffness properties $k_{p,0}$, $p = 1, \cdots, N$, of the elastic plate elements. The solution can be carried out numerically using a differential equation solver. Noting that $\dot{\boldsymbol{S}}(t) = \boldsymbol{F}(\boldsymbol{L})\dot{\boldsymbol{y}}$ and

$$\ddot{\boldsymbol{s}}(t) = \boldsymbol{F}(\boldsymbol{L}(t))\ddot{\boldsymbol{y}} = \boldsymbol{F}(\boldsymbol{L}(t))[-\boldsymbol{M}^{-1}\boldsymbol{K}(\boldsymbol{L}(t))\boldsymbol{y} - \boldsymbol{M}^{-1}\boldsymbol{C}\dot{\boldsymbol{y}} + \boldsymbol{M}^{-1}\boldsymbol{P}\boldsymbol{X}(t)] \tag{4.32}$$

the elements of the covariance matrix are used to find the covariance $\boldsymbol{Q}_{\boldsymbol{\eta}}(t)$ of the vector $\boldsymbol{\eta}(t) = [\boldsymbol{S}^T(t)\ \dot{\boldsymbol{S}}^T(t)\ \ddot{\boldsymbol{S}}^T(t)]^T$ of the stress responses within each plate from the relationship

$$\boldsymbol{Q}_{\boldsymbol{\eta}}(t) = \boldsymbol{H}(\boldsymbol{L})\boldsymbol{Q}_{\boldsymbol{x}}(t)\boldsymbol{H}^T(\boldsymbol{L}) \tag{4.33}$$

where $\boldsymbol{H}(\boldsymbol{L})$ is given by

$$\boldsymbol{H}(\boldsymbol{L}) = \begin{bmatrix} \boldsymbol{F}(\boldsymbol{L}) & \boldsymbol{0}_{N,N} & \boldsymbol{0}_{N,M} \\ \boldsymbol{0}_{N,N} & \boldsymbol{F}(\boldsymbol{L}) & \boldsymbol{0}_{N,M} \\ -\boldsymbol{F}(\boldsymbol{L})\boldsymbol{M}^{-1}\boldsymbol{K} & -\boldsymbol{F}(\boldsymbol{L})\boldsymbol{M}^{-1}\boldsymbol{C} & \boldsymbol{F}(\boldsymbol{L})\boldsymbol{M}^{-1}\boldsymbol{P} \end{bmatrix} \tag{4.34}$$

The second moments $\lambda_{p,i}(t)$, $i = 0, 2, 4$ of the stress process involved in $\boldsymbol{Q}_{\boldsymbol{\eta}}(t)$ are then obtained and used in equations (4.12) to independently solve the crack growth equations.

For stationary response, the second moments $\lambda_{p,i}(t) = \lambda_{p,i}$, $i = 0, 2, 4$ are independent of time and the solution for the crack growth length $L_p(t)$ as a function of time can be straightforward computed by numerically solving the first order differential equations (4.12). Alternatively, for the stationary response, the equations for the spectral moments $\lambda_{p,i}(t) = \lambda_{p,i}$, $i = 0, 2, 4$ can be computed from the one dimensional integrals (4.18). This requires numerical integration to be carried out over an infinite domain of $\omega$ and is usually more tedious computationally.

It should be emphasized that the formulation in (4.33) - (4.34) is applicable for the case for which the excitation $\boldsymbol{W}(t)$ is a filtered white noise excitation given by a system of ordinary deferential equations in which case $\boldsymbol{y}$, $\dot{\boldsymbol{y}}$ and $\ddot{\boldsymbol{y}}$ are part of the state vector $\boldsymbol{z}$. For the white noise excitation $\boldsymbol{W}(t)$ the spectral moment $\lambda_{4,p}$ takes infinity values. The formulation still holds if the contribution of the spectral width parameter $\varepsilon(t)$ is ignored in (4.12) and (4.16) by setting $\varepsilon(t) = 0$. Finite

values of the spectral moments $\lambda_{4,p}$ can be obtained by using a process resembling white noise with constant spectral density in the interval $[-\omega_0, \omega_0]$ and zero spectral values outside this interval. This truncated white noise process is often used to carry out the integration in (4.18) with bounded limits $[-\omega_0, \omega_0]$ without affecting the values of the spectral densities $\lambda_{0,p}$, provided that $\omega_0$ is high enough.

For stationary response, the second moments $\lambda_{p,i}(t) = \lambda_{p,i}$, $i = 0, 2, 4$ are independent of time and the solution for the crack growth length $\boldsymbol{L}_p(t)$ as a function of time can be straightforward computed by solving (4.12) to obtain:

$$\boldsymbol{L}_p(t) \equiv \boldsymbol{L}_p(t; \Delta s_p) = \left[ \left(1 - \mu_p / 2\right) d_p (\Delta s_p)^{\mu_p/2} t + L_{p,0}^{\left(1-\mu_p/2\right)} \right]^{(1-\mu_p/2)^{-1}} \tag{4.35}$$

where $d_p$ is given by

$$d_p = C_p' \left(B_p\right)^{\mu_p} \left(\sqrt{\pi}\right)^{\mu_p} \tag{4.36}$$

for $p = 1, ..., N$, and $\Delta s_p = 2\pi\lambda_{0,p}(1 - \varepsilon_p^2)$. The above derivation assumes that $\frac{L_p}{b_p} << 1$, so that the geometry factor $B_p$ is approximated by

$$B_p(L_p) \approx \frac{\sqrt{\pi L_p}}{2b_p} \tag{4.37}$$

### 4.4.3 Non-Coupled Response-Degradation Problem; via Dirlik's Approximation of Stress Range

Let us consider now the fatigue crack growth prediction making use of Dirlik's formula (4.19) for the probability density function of $\Delta S_p$. For convenience, it is assumed that crack growth does not significantly affect plate element stiffness so that the stiffnesses remain constant and equal to $k_p(L_p) = k_{p,0}$. The pdfs for $\Delta S_p$ are completely defined from the spectral moments $\lambda_{0,p}$, $\lambda_{1,p}$, $\lambda_{2,p}$ and $\lambda_{4,p}$ of the axial stress response and its derivatives. These moments can also be computed by the integral in (4.18) which can be used with bounded limits $[-\omega_0, \omega_0]$ to compute $\lambda_4$ in the case of white noise input. Alternatively, the spectral moments $\lambda_{p,i}(t) = \lambda_{p,i}$, $i = 0, 2, 4$ involved in $\boldsymbol{Q}_{\boldsymbol{\eta}}$ can be directly computed by solving the

Lyapunov equation (4.31) for the covariance response $\boldsymbol{Q}_{\mathbf{z}}$ of the state vector and then using the relationship (4.33).

Given the pdfs for $\Delta S_p$ from the Dirlik formula, the predictions of the pdfs of the crack size $L_p(t) \equiv L_p(t;\Delta S_p)$ are obtained from the equations (4.12). These pdfs can then be used to obtain the characteristics of failure, such as the mean and the variance of failure time, the probability of failure at a given time, etc. For demonstration purposes, failure $F_p(t)$ in the plate is defined as the state in which the crack length $L_p\left(t;\Delta S_p\right)$ exceeds a critical value $L_{p,crit}$ in a given time interval $[0,t]$, that is,

$$F_p(t) = \left\{ L_p\left(t;\Delta S_p\right) > L_{p,crit} \right\} \tag{4.38}$$

The probability of failure $\Pr[F_p(t)]$ in the plate element $p$ is given by the integral

$$\begin{aligned} \Pr[F_p(t)] &= \int_{\alpha_p(t;\Delta S_p)\geq \alpha_{p,crit}} p(\Delta S_p)d(\Delta S_p) = \int_{\Delta S_p \geq \Delta S_{p,crit}(t)} p(\Delta S_p)d(\Delta S_p) \\ &= \int_{\Delta S_{p,crit}(t)}^{\infty} p(\Delta S_p)d(\Delta S_p) \end{aligned} \tag{4.39}$$

where $p(\Delta S_p)$ is the probability density function given by (4.19) and $\Delta S_{p,crit}(t)$ is the value of the stress range ("design point" in reliability terminology) that can be calculated for given time instant $t$ by solving the equation

$$L_p\left(t;\Delta S_p\right) = L_{p,crit} \tag{4.40}$$

with respect to $\Delta S_p$. A numerical scheme can be used to obtain the solution of equation (4.40) for each time $t$ with $L_p(t;\Delta S_p)$ given by the solution of (4.12). The integration in (4.39) is one-dimensional and can be carried out efficiently using available numerical algorithms.

Finally, it should be noted that for the case where $\frac{L_p}{b_p} << 1$ (assumption of small crack compared to the width of plate) the geometry factor $B_p(L_p)$ is given by (4.37) and the evolution equation of the crack length $L_p(t;\Delta s_p)$, given by (4.35) and the equation (4.40), can be solved analytically to yield

$$\Delta S_{p,crit}(t) = \frac{c_1}{t^{2/\mu_p}} \left[ L_{p,crit}^{1-\frac{\mu_p}{2}} - L_0^{1-\frac{\mu_p}{2}} \right]^{\frac{2}{\mu_p}} \tag{4.41}$$

where $c_1$ is a constant and is given by

$$c_1 = [\pi(1-\mu_p/2)^{2/\mu_p} C_p'^{\,2/\mu_p} B_p{}^2]^{-1} \tag{4.42}$$

## 4.5 Applications - Numerical Results

The methods proposed for the fatigue life predictions are applicable for the $N$ degree of freedom system shown in Figure 4.1. For demonstration purposes, the system is subjected to a base acceleration $\ddot{a}(t)$. The base excitation is assumed to be stationary white noise, i.e. $\ddot{a}(t) = w(t)$, with power spectral density equal to $10^{-2}$. In this case, the matrix $\boldsymbol{P}$ relating the excitation forces to the degrees of freedom of the systems takes the form $\boldsymbol{P} = -\boldsymbol{M}\mathbf{1}$, while the input excitation vector $\boldsymbol{X}(t)$ takes the form $\boldsymbol{X}(t) = \ddot{a}(t) = w(t)$, where $\mathbf{1}$ is defined to be a vector with all elements equal to one. For this mathematically defined white noise, the spectral parameter $\lambda_4$ is infinite.

From the computational point of view, the random excitation is considered to have a constant power spectral density over the frequency range $[-\omega_0, \omega_0]$ which contains the values of the frequencies of the main contributing modes of the system. The spectral moments are then computed using (4.18) with the domain of the integration to be $[-\omega_0, \omega_0]$ for sufficient high value of $\omega_0$. The results from the integration for $\lambda_0$, $\lambda_1$ and $\lambda_2$ are same as the ones obtained by solving the Lyapunov equation for the covariance response. The results of the integration for computing $\lambda_4$ depend on the value of $\omega_0$ indicating the range of spectral frequencies with significant energy.

In the numerical results presented, the methodologies used are termed “constant stiffness - SM” method referring to the non-coupled response-degradation problem in Section 4.2 using spectral moments (SM), “constant stiffness - SD” method referring to the non-coupled response-degradation problem based on Dirlik’s formula for the spectrum distribution (SD) of the stress in Section 4.3, and “stiffness degradation” method referred to the coupled response-degradation problem in Section 4.1.

### 4.5.1 Single Degree of Freedom System

The case of a single oscillator ( $N=1$) is first considered. The initial crack length is assumed to be equal to $L_0=10^{-2}$. Also the values of $C'$ and $\mu$, defining the degradation equations, are assumed to be $C'=1.03\cdot10^{-12}$, $\mu=3.89$. The mass and the plate properties without the crack are selected so that the natural frequency of the system is 10 Hz. The damping coefficient is selected so that the damping ratio of the system is 5%. The value of $\omega_0$, defining the domain of integration of the spectral moments in (4.18), is taken to be $\omega_0=30\,\text{Hz}$.

a) Constant Stiffness – Spectral Moments (SM)

Results for the crack length growth are first obtained for the "constant stiffness – SM" method. The evolution of the crack growth is obtained from (4.12), considering that the response has reached stationary state due to stationary white noise excitation. The results for the crack length growth predictions in the system are shown in Figure 4.2 for the cases of spectral width parameter $\varepsilon=0$ and $\varepsilon\neq0$. It can be seen that the inclusion of spectral width parameter $\varepsilon$ significantly affects the predictions of failure, prolonging the time of failure.

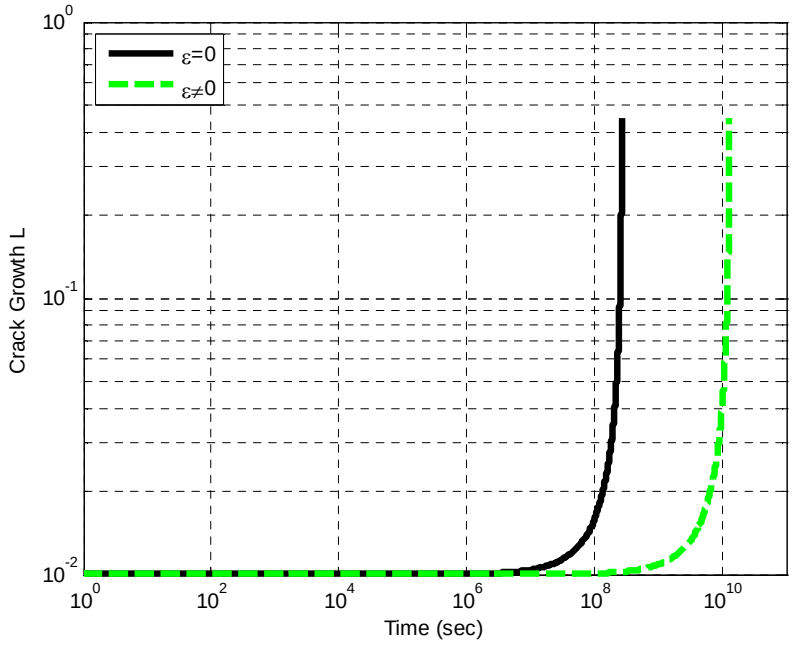


**Figure 4.2:** Crack size growth with respect to time for $L_{0,p}=10^{-2}$ using the "constant stiffness – SM" method for the system $N=1$.

b) Constant Stiffness – Spectrum Distribution (SD)

Next, results for the "constant stiffness – SD" method are presented using Dirlik's formula (4.19) for the probability density function of the stress range $\Delta S$. This probability density function for the $N=1$ system is shown in Figure 4.3. Using this pdf, the probability of failure of the system is calculated for a certain critical value of $L_{1,crit}=10^{-1}$ as shown in Figure 4.4 for different values of the initial crack size $L_0$. The results are also compared to the deterministic lifetime predictions provided by the "constant stiffness – SM" method for $\varepsilon=0$ and $\varepsilon\neq 0$.

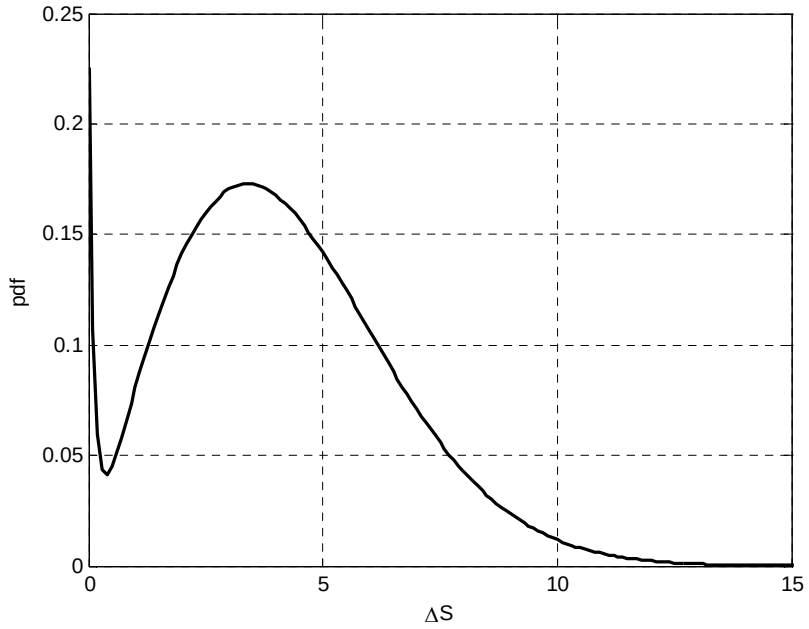


**Figure 4.3:** Probability density function of the stress range $\Delta S$.

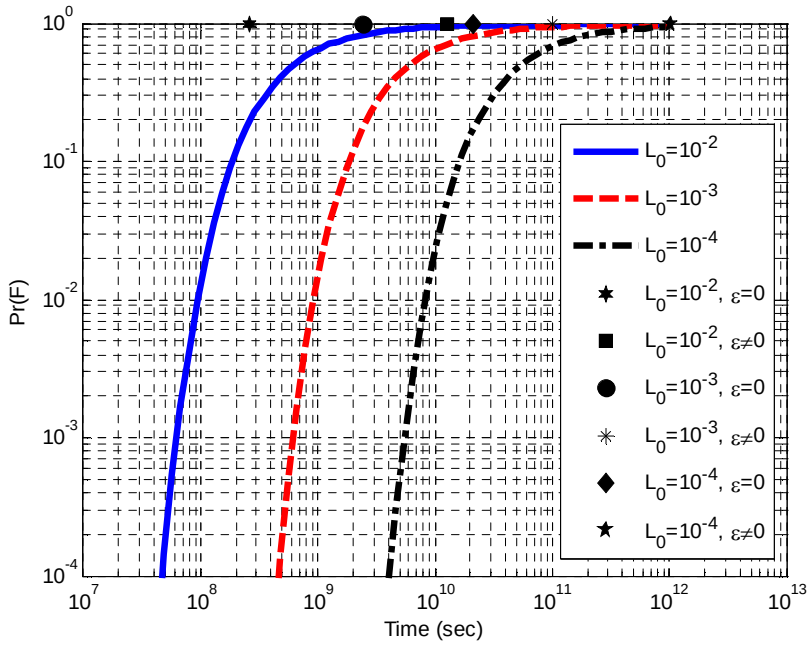


**Figure 4.4:** Probability of failure versus time for different initial crack sizes, along with comparisons of deterministic lifetime predictions from the "constant stiffness – SM" method for $\varepsilon = 0$ and $\varepsilon \neq 0$.

For demonstration purposes, consider the case in Figure 4.4 for which the initial crack size equals to $L_0 = 10^{-2}$. It can be seen that the failure time $t_{fail} = 1.26 \times 10^{10}$ sec predicted from the "constant stiffness – SM" method with $\varepsilon \neq 0$ corresponds to very high failure probability $\Pr(F) = 0.935$ predicted by the "constant stiffness – SD" method. Moreover, the "constant stiffness – SD" method predicts that the time of failure that corresponds to a smaller failure probability, say $\Pr(F) = 10^{-3}$, equals to $t_{fail} = 7 \times 10^{8}$ sec. Similar interpretations can be inferred comparing the other cases shown in Figure 4.4.

c) Stiffness Degradation

Finally, the stiffness degradation method is considered for which the crack length affects the stiffness of the structure, i.e. the case which $\boldsymbol{k}(L)$ depends on $L$. This effect can be introduced by employing the following empirical stiffness degradation function available in the literature (Sobczyk and Trebicki 1999)

$$k_p(L_p) = k_{0,p}\left[\beta_1 + \beta_2 \exp[-\beta_3(2L_p / b_p)^{\beta_4}]\right] \tag{4.43}$$

where $b_p$ is the width of the $p$ plate. The values of the coefficients are selected to be $\beta_1 = 0.5$, $\beta_2 = 0.5$, $\beta_3 = 1$ and $\beta_4 = 1$ such that $k_p(0) = k_{p,0}$, where $k_{p,0}$ is the initial stiffness of the uncracked plate.

Numerical results are presented assuming that the initial crack size equals to $L_{0,p} = 10^{-2}$. The crack growth predictions in this case are shown in Figure 4.5 for the case of $\varepsilon = 0$ and are compared to the corresponding crack growth predictions obtained from the "constant stiffness – SM". As expected, lifetime reduces when the effect of stiffness degradation due to crack growth is taken into account in the formulation. Results for the case of $\varepsilon \neq 0$ are not presented since they require the evaluation of $\lambda_4(t)$ from the integral (4.18) with finite limits $[-\omega_0, \omega_0]$. This numerical evaluation has to be performed for each time step $\Delta t$ used to integrate the coupled system of equations (4.12) and (4.27). This procedure is computationally time consuming due to the numerical integration involved.

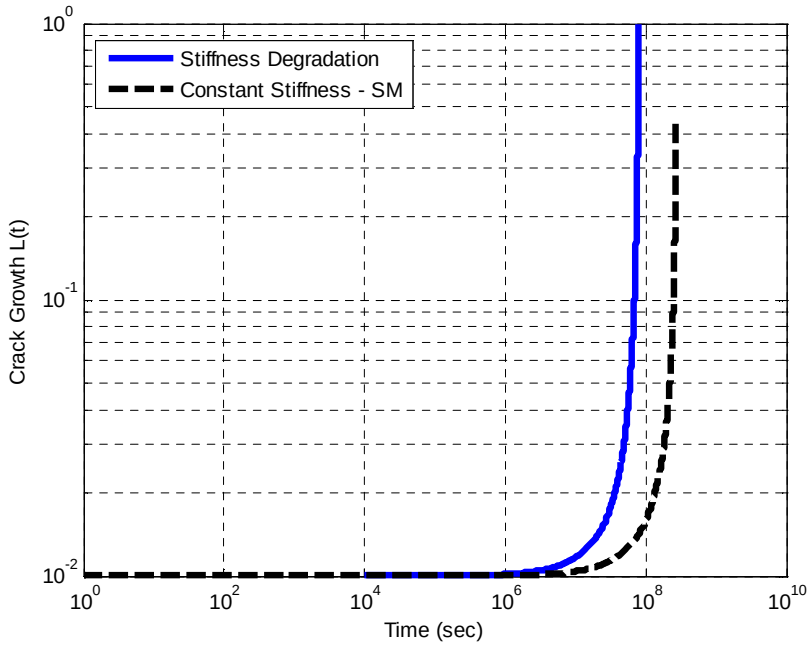


**Figure 4.5:** Comparison of crack growth prediction obtained from the "stiffness degradation" and the "constant stiffness – SM" methods ($\varepsilon = 0$).

The ratio $\sigma_S^2 / \sigma_{S,0}^2$ of the variance $\sigma_S^2(t)$ of the axial stress response $S(t)$ obtained from the stiffness degradation method to the constant variance $\sigma_{S,0}^2$ obtained from the "constant stiffness – SM" method (non-degrading structure) is given in Figure 4.6 as a function of time. Also, the stiffness reduction $k(L(t))$ with respect to time due to degradation $L(t)$ is shown in Figure 4.7. It can be seen that the variance ratio increases, indicating that the response of the structure increases due to degradation. This increase has a result of accelerating failure which, as shown in Figure 4.5, occurs earlier than the time expected for non-degrading constant stiffness structures.

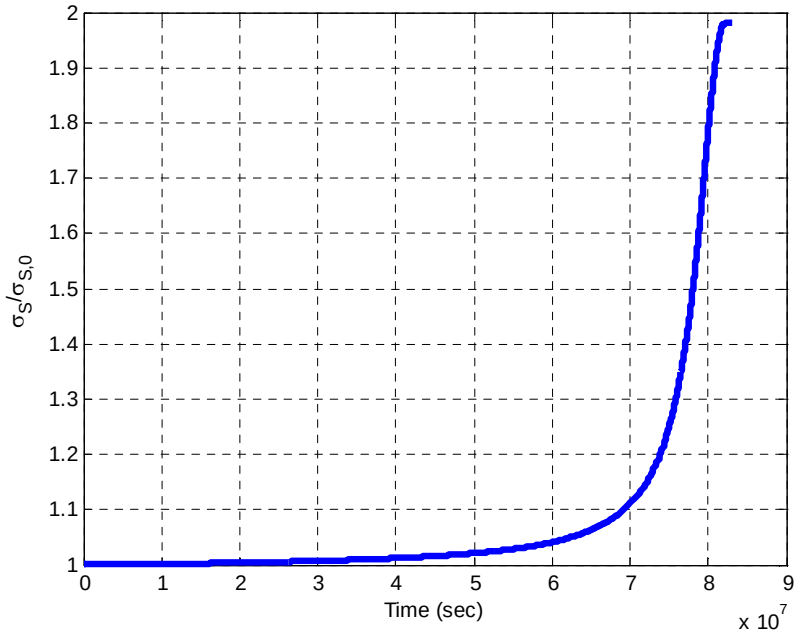


**Figure 4.6:** Variance ratio $\sigma_S^2 / \sigma_{S,0}^2$ of the stress response with respect to time.

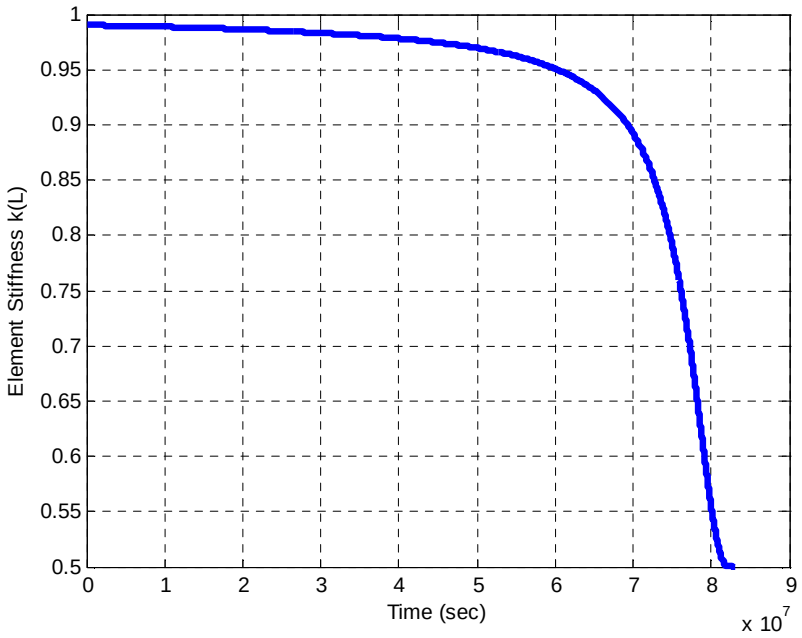


**Figure 4.7:** Stiffness decrease $k(L(t))$ with respect to time.

### 4.5.2 Multi Degree of Freedom System

The methodology is next applied to a three degree of freedom hierarchical system ($N=3$), shown in Figure 4.1. The initial crack length is assumed to be equal to $L_{0,p}=10^{-2}$ for the three subsystems. Also the values of $C_p'$ and $\mu_p$ are assumed to be $C_p'=1.03\cdot10^{-12}$ and $\mu_p=3.89$, $p=1,2,3$. For the mass and plate properties selected, the natural frequencies of the three degree of freedom system without cracks are 4.45 Hz, 12.47 Hz and 18.02 Hz. The damping matrix $\boldsymbol{C}$ is chosen assuming that the system is classically damped at its initial non-degrading state. Specifically, the damping matrix $\boldsymbol{C}$ is selected so that the values of the modal damping ratios corresponding to the un-cracked structure are 5% for all three modes. The value of the upper frequency $\omega_0$ needed in computing $\lambda_4$ using (4.18) is taken to be $\omega_0=30\,\text{Hz}$.

a) Constant Stiffness – Spectral Moments (SM)

Results for the crack growth at each plate element as a function of time for the "constant stiffness – SM" method are shown in Figure 4.8 for the three

subsystems and for the cases of $\varepsilon = 0$ and $\varepsilon \neq 0$. It can be seen that the crack grows faster on the first plate since the stresses in this plate takes higher values than the stresses in the other two plates. Also, the inclusion of the spectral width parameter $\varepsilon$ ($\varepsilon \neq 0$) in the formulation significantly affects predictions of failure, prolonging the time of failure for the first and third subsystem and accelerating the time of failure for the second subsystem.

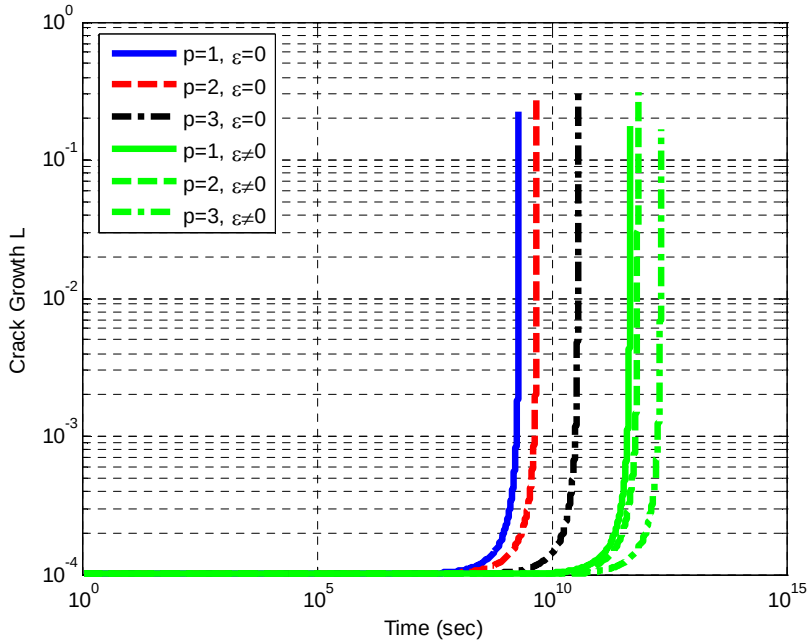


**Figure 4.8:** Crack size growth with respect to time for the three-DOF system ($N = 3$) using the "constant stiffness - SM" method.

b) Constant Stiffness – Spectrum Distribution (SD)

Finally, results for the "constant stiffness – SD" method are presented using Dirlik's formula (4.19) for the probability density functions of the stress ranges $\Delta S$. The probability density functions for all axial stress ranges $\Delta S_p(t)$ are shown in Figure 4.9. Using these pdfs, the probabilities of failure for the first, second and third subsystems are calculated for a certain critical value of $L_{p,crit} = 10^{-1}$, $p = 1, 2, 3$, as shown in Figure 4.10 for initial crack size values $L_{p,0} = 10^{-2}$. The results are also compared to the deterministic lifetime predictions provided by the "constant stiffness – SM" method for $\varepsilon = 0$ and $\varepsilon \neq 0$.

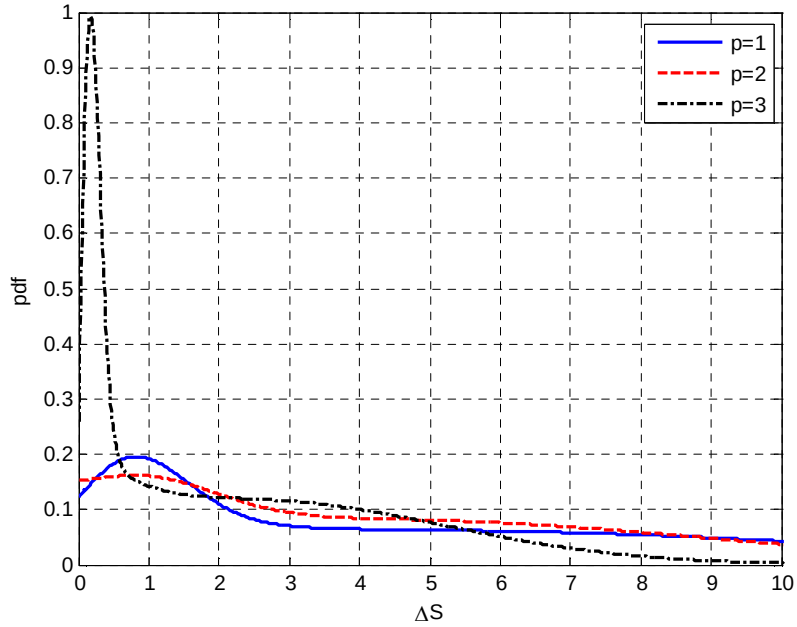


**Figure 4.9:** Probability density functions of the stress ranges $\Delta S_p$ at the three subsystems.

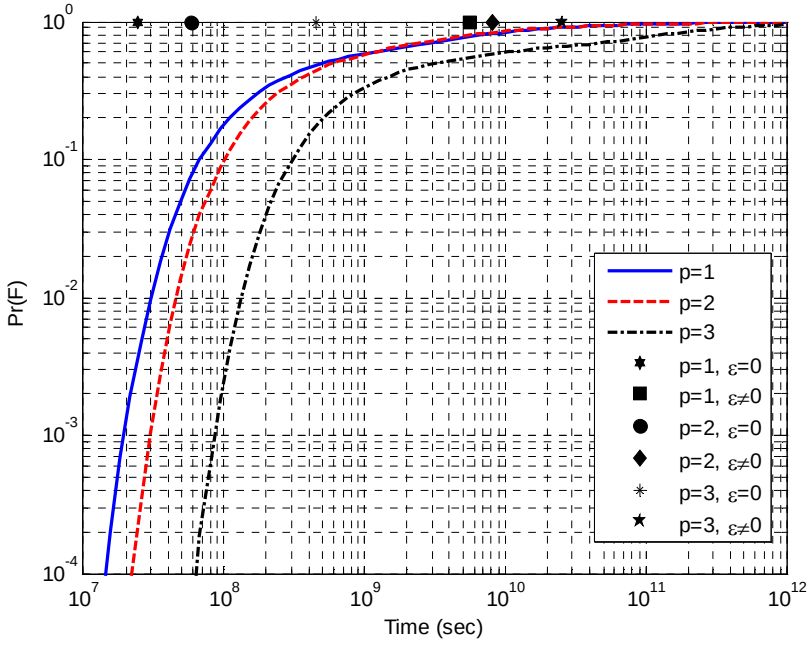


**Figure 4.10:** Probability of failure versus the time of failure for the three subsystems, along with comparison of deterministic lifetime prediction from the "constant stiffness – SM" method for $\varepsilon = 0$ and $\varepsilon \neq 0$.

For the predictions provided by the "constant stiffness – SD" method, it can be seen that for probability of failure of the system is controlled by the failure of the first subsystem since the time of failure for any probability level is is smaller than the time of failure for the other two subsystems. Also, it can be seen that the failure time $t_{fail} = 5.7 \times 10^9$ sec predicted from the "constant stiffness – SM" method with $\varepsilon \neq 0$ corresponds to very high failure probability $\Pr(F) = 0.78$ predicted by the "constant stiffness – SD" method. Moreover, the "constant stiffness – SD" method predicts that the time of failure that corresponds to a smaller failure probability, say $\Pr(F) = 10^{-3}$, equals to $t_{fail} = 1.95 \times 10^7$ sec. Similar interpretations can be inferred comparing the other cases shown in Figure 4.10.

c) Stiffness Degradation

Next, results are presented for the "stiffness degradation" method for which the crack length affects the stiffness of the structure. This effect is introduced by employing the empirical stiffness degradation function (4.43) for each of the three plate elements. Numerical results are presented using that the initial crack sizes are all equal to $L_{0,p} = 10^{-2}$, $p = 1,2,3$. The crack growth predictions in this case are shown in Figure 4.11 for the case of $\varepsilon = 0$ and are compared to the crack growth predictions obtained from the "constant stiffness – SM" method. As expected, it can be seen that the lifetime reduces when the effect of stiffness degradation due to crack growth is taken into account in the formulation.

The ratio $\sigma^2_{S,p} / \sigma^2_{S,p0}$, $p = 1,2,3$, of the variance $\sigma^2_{S,p}(t)$ of the axial stress response $S_p(t)$ obtained from the "stiffness degradation" method to the constant variance $\sigma^2_{S,p0}$ obtained from the "constant stiffness – SM" method (non-degrading structure) are shown in Figure 4.12 as a function of time. Also, the stiffness reduction $k(L_p(t))$ with respect to time due to degradation $L_p(t)$ is shown in Figure 4.13. It can be seen that the variance ratios increases for all axial stresses, indicating that degradation affects the response of the structure. The most pronounced increase is manifested in the first subsystem. This increase has a result of accelerating failure which occurs earlier for the first subsystem as compared to the time of failure expected for non-degrading structure.

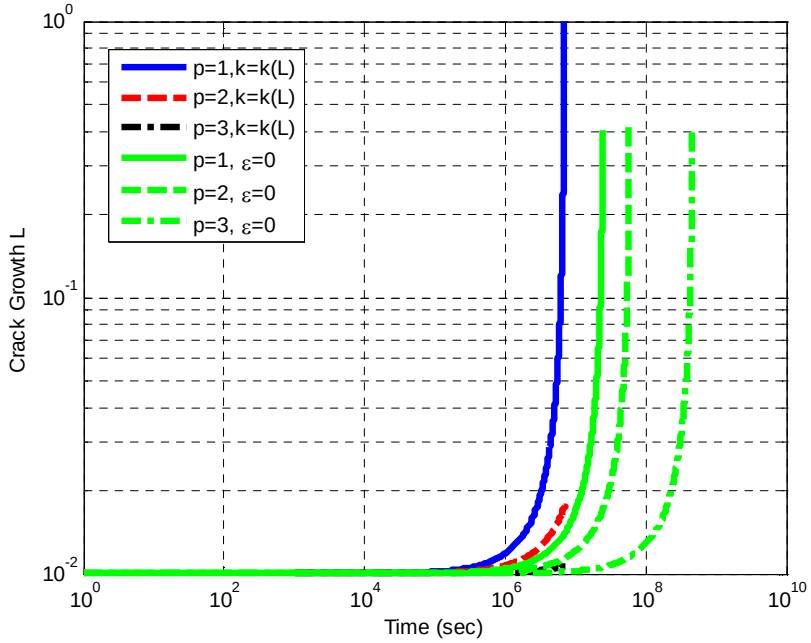


**Figure 4.11:** Comparison of crack growth prediction obtained from the "stiffness degradation" and the "constant stiffness – SM" methods ( $\varepsilon = 0$ ).

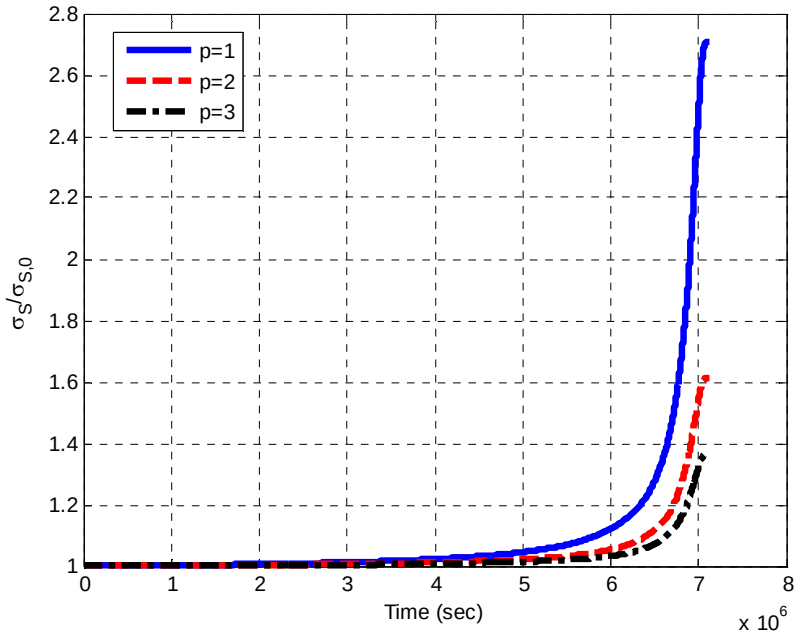


**Figure 4.12:** Variance ratio $\sigma^2_{S,p} / \sigma^2_{S,p0}$ of the stress response with respect to time.

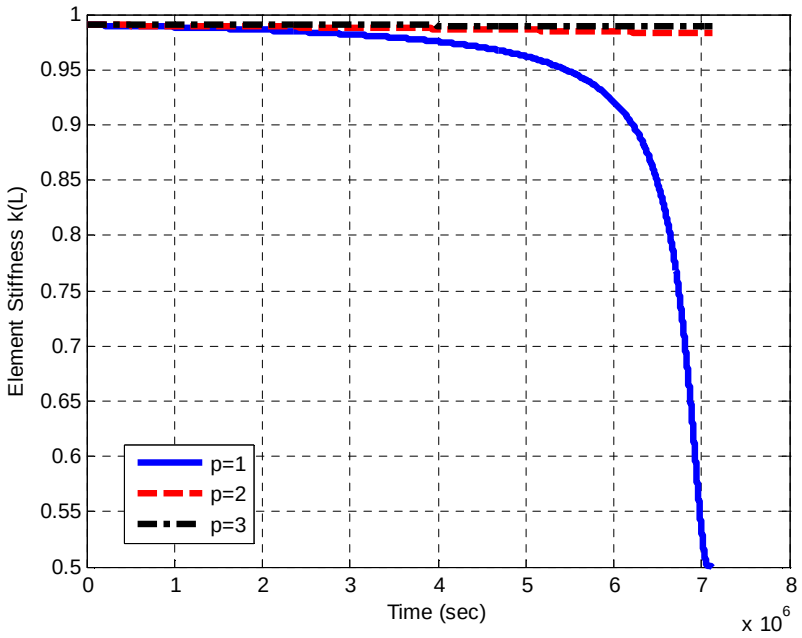


**Figure 4.13:** Stiffness decrease $k_p(L_p(t))$ with respect to time.

## 4.6 Conclusions

In this Chapter, a general formulation and an effective method for predicting the fatigue lifetime in randomly vibrating linear multi-degree-of-freedom systems/structures have been presented. The analysis is based on the coupled response-degradation model and it takes into account a wide-band spectrum of the stress process.

The fatigue process is characterized by crack growth in the structural components and is represented by Paris equation in which the stress range is evaluated form the multi-dimensional random response of the system. Both the stiffness degradation due to fatigue during the vibration, and non-degrading case are considered. The stress range was approximated by either the spectral moments or the empirically motivated and widely used Dirlik's probability distribution. The prediction capabilities of the proposed analyses were demonstrated using special classes of single and multi-degree of freedom structural systems. For the formulation based on spectral moments in the non-degrading case, it was demonstrated that the inclusion of the spectral width parameter in the model prolongs the time of failure of the system. For the formulation based on Dirlik's formula in the non-degrading case, more conservative estimates of failure times

corresponding to small failure probabilities were obtained than the estimates provided by the spectral moments which correspond to failure probabilities very close to one. Finally, it was demonstrated that stiffness degradation accelerates failure due to fatigue in the various structural components.

# CHAPTER 5 Fatigue-Based Design Optimization of Truss Structures

## 5.1 Introduction

In this Chapter, a methodology for design optimization of truss structures taking into account the fatigue lifetime, is proposed. Combining the methodology for system design optimization presented in Chapter 2 and the methodology for fatigue lifetime prediction presented in Chapter 4, one can optimize a dynamic system for maximum lifetime under the influence of loading uncertainties. The proposed methodology takes advantage of the simplicity of the solution for the crack length growth given in (4.35), assuming stationarity of the response and independence of the shape factor $B$ from the crack length, in order to construct an efficient objective function needed in formulating the performance function for the fatigue – based design optimization.

This Chapter is organized as follows. First, the general governing equations for the fatigue crack length growth in the case of stationary and broad band response are presented, along with the formulation of the design optimization problem based on fatigue. The similarities and differences with the case of stress – based design optimization presented in Chapter 3 are also underlined. Next, the sensitivities of the objective function with respect to the design variables are

obtained, using the adjoint method, in order to efficiently and accurately estimate the derivatives for the optimization problem. Finally, the proposed methodology is applied on the sizing and topology optimization of a two dimensional truss structure. The optimal configurations are presented and compared with the optimal configurations obtained for Case G of the stress – based performance function in Chapter 3.

## 5.2 Optimization Based on Fatigue

For the optimization of a structure for maximum fatigue lifetime, an efficient expression for the prediction of this lifetime has to be obtained. In order to achieve this, the following assumptions are be made. First, one assumes that the response is stationary and therefore the second moments $\lambda_{p,0}(t)=\lambda_{p,0}$ are independent of time. Second, independence of the shape factor $B$ from the crack length is assumed, which is valid for crack lengths that are relatively small compared to the width of the member.

Under these assumption, the crack growth length $L_p(t)$ as a function of time $t$ can be straightforward computed by solving (4.12) to obtain:

$$L_p(t)=\left[\left(1-\frac{\mu_p}{2}\right)d_p(\Delta s_p)^{\mu_p}t+L_{p,0}^{\left(1-\frac{\mu_p}{2}\right)}\right]^{(1-\frac{\mu_p}{2})^{-1}} \tag{5.1}$$

where $d_p$ is given by

$$d_p=C_p'B_p^{\mu_p}\pi^{\mu_p/2} \tag{5.2}$$

for $p=1,...,N$, and $\Delta s_p$ is given by

$$\Delta s_p=\sqrt{2\pi\lambda_0\left(1-\varepsilon_p^2\right)} \tag{5.3}$$

where $\varepsilon_p$ is the spectral width parameter $\varepsilon=\left(1-\alpha^2\right)^{1/2}$, $\alpha=\lambda_2/\sqrt{\lambda_0\lambda_4}$ and $\lambda_0$, $\lambda_2$, $\lambda_4$ are the spectral moments the stress process of $s_p(t)$ for the member $p$. Equivalently, the time $t_p$ corresponding to crack growth length $L_p(t;\Delta s_p)$ of member $p$ is given by:

$$t_p=\left(1-\frac{\mu_p}{2}\right)^{-1}d_p^{-1}\left(\Delta s_p\right)^{-\mu_p}\left\{\left[L_p(t;\Delta s_p)\right]^{\left(1-\frac{\mu_p}{2}\right)}-\left[L_{p,0}\right]^{\left(1-\frac{\mu_p}{2}\right)}\right\} \tag{5.4}$$

The time of failure $t_{p,cr}$ is computed as the time for which $L_p(t;\Delta s_p)$ approaches the critical crack length $L_{p,cr}$. Under the assumption that the initial crack length $L_{p,0}$ and the critical crack length $L_{p,cr}$ are analogous to the width of the plate, and therefore the cross sectional area $A_p$ for constant thickness, that is

$$L_{p,0} = aA_p \tag{5.5}$$

$$L_{p,crit} = bA_p \tag{5.6}$$

the equation (5.4) yields

$$t_{p,cr} = \left(1-\frac{\mu_p}{2}\right)^{-1} d_p^{-1}\left(\Delta s_p\right)^{-\mu_p}\left(a^{\left(1-\frac{\mu_p}{2}\right)} - b^{\left(1-\frac{\mu_p}{2}\right)}\right)A_p^{\left(1-\frac{\mu_p}{2}\right)} \tag{5.7}$$

and by substituting $\Delta s_p$ by the equation (5.3) one derives that the critical time for failure is given by

$$t_{cr} = \left(1-\frac{\mu_p}{2}\right)^{-1} d_p^{-1}\left(2\pi\right)^{-\frac{\mu_p}{2}} \lambda_{0,p}^{-\frac{\mu_p}{2}}\left(1-\varepsilon_p^2\right)^{-\frac{\mu_p}{2}}\left(a^{\left(1-\frac{\mu_p}{2}\right)} - b^{\left(1-\frac{\mu_p}{2}\right)}\right)A_p^{\left(1-\frac{\mu_p}{2}\right)} \tag{5.8}$$

Given $a$ and $b$, the critical time for failure of a member $p$ depends on the second – order statistics $\lambda_0$, $\lambda_2$ and $\lambda_4$ of the stress response process and the cross – sectional area $A_p$ of the member $p$.

### 5.2.1 Objective Function

After obtaining a suitable expression for the prediction of fatigue lifetime, an equivalent objective function for the optimization of the lifetime of the structure can be formulated as the weighted sum of the inverse of the lifetime of the structural members, normalized by typical lifetimes of these member. Specifically, the design optimization problem is formulated as follows. Find the $\underline{\theta}$ values that minimize the objective

$$J(\underline{\theta}) = \sum_{p=1}^{N_\theta} \tilde{w}_p \frac{t_{p,0}}{t_{p,cr}(\underline{\theta})} \tag{5.9}$$

subject to

$$AQ + QA^T + BS^*B^T = \mathbf{0} \tag{5.10}$$

$$V \pounds V_0 \tag{5.11}$$

$$\underline{q}_{\min} \leq \underline{q} \leq \underline{q}_{\max} \tag{5.12}$$

where $t_{p,0}$ is a typical time of failure for each member $p$ of the structure and can be chose as the critical time of failure that corresponds to all members of the truss structure to have a pre-selected cross – sectional area equal to $A_{p,0}$. That is

$$t_{p,0} = \left(1-\frac{\mu_p}{2}\right)^{-1} d_p^{-1} (2\pi)^{-\frac{\mu_p}{2}} \lambda_{0,p}^{-\frac{\mu_p}{2}} \left(1-\varepsilon_p^2\right)^{-\frac{\mu_p}{2}} \left(a^{\left(1-\frac{\mu_p}{2}\right)} - b^{\left(1-\frac{\mu_p}{2}\right)}\right) A_{p,0}^{\left(1-\frac{\mu_p}{2}\right)} \tag{5.13}$$

where $\tilde{\lambda}_{0,p}$ and $\tilde{\varepsilon}_p$ are the second moment and spectral width parameters that correspond to cross sectional areas $A_{p,0}$.

By substituting the equations (5.8) and (5.13) in (5.9), the objective function yields

$$J(\underline{\theta}) = \sum_{p=1}^{N_\theta} J_p(\underline{\theta}) = \sum_{p=1}^{N_\theta} \tilde{w}_p \left(\frac{\lambda_{0,p}(\underline{\theta})}{\tilde{\lambda}_{0,p}}\right)^{\frac{\mu_p}{2}} \left(\frac{1-\varepsilon_p^2}{1-\tilde{\varepsilon}_p^2}\right)^{\frac{\mu_p}{2}} \left(\frac{A_p(\underline{\theta})}{A_{0,p}}\right)^{\frac{\mu_p-2}{2}} \tag{5.14}$$

Selecting the weights $\tilde{w}_p$ in the form

$$\tilde{w}_p = w_p \tilde{\lambda}_{0,p}^{-\frac{\mu_p}{2}} \left(1-\tilde{\varepsilon}_p^2\right)^{-\frac{\mu_p}{2}} A_{0,p}^{-\frac{\mu_p-2}{2}} \tag{5.15}$$

the objective function takes the form

$$J(\underline{\theta}) = \sum_{p=1}^{N_\theta} w_p \lambda_{0,p}^{\frac{\mu_p}{2}} \left(1-\varepsilon_p^2\right)^{\frac{\mu_p}{2}} A_p^{\frac{\mu_p-2}{2}} \tag{5.16}$$

that is the objective function for maximizing the fatigue lifetime of a structure is only a function of the variance of the stresses developed on each truss member, and the cross sectional area.

It is observed that, since the value of the constant $\mu$ is equal to 3.89 for steel, the exponent of the spectral moment $\lambda_0$ is close to two. Additionally, the exponent of the cross sectional area is close to unity. Therefore, the objective function for the fatigue optimization problem is a generalization of the objective function developed for the case of the optimization for the stresses in a dynamic system. In particular, the objective function for the design optimization based on the stresses is a special case of the objective function for the design optimization based on fatigue with $\varepsilon_p \to 0$, the exponent $\mu/2$ selected to be equal to one and the exponent $(\mu-2)/2$ selected to be equal to zero.

### 5.2.2 Derivatives of the Objective Function

The sensitivities of the objective function for the *p*-th member of the structure, assuming $\varepsilon_p \to 0$, with respect to the *j*-th design variable is given by

$$\frac{\partial J_p}{\partial \theta_j} = \frac{\mu_p}{2} w_p \lambda_{0,p}^{\frac{\mu_p - 2}{2}} \frac{\partial \lambda_{0,p}}{\partial \theta_j} A_p^{\frac{\mu_p - 2}{2}} + \frac{\mu_p - 2}{2} w_p \lambda_{0,p}^{\frac{\mu_p}{2}} A_p^{\frac{\mu_p - 4}{2}} \frac{\partial A_p}{\partial \theta_j} \tag{5.17}$$

Therefore, the derivative of the objective function is given by adding up the $N_\theta$ terms of (5.17)

$$\begin{aligned} \frac{\partial J}{\partial \theta_j} &= \sum_{p=1}^{N_\theta} \frac{\partial J_p}{\partial \theta_j} = \sum_{p=1}^{N_\theta} \frac{\mu_p}{2} w_p \lambda_{0,p}^{\frac{\mu_p - 2}{2}} \frac{\partial \lambda_{0,p}}{\partial \theta_j} A_p^{\frac{\mu_p - 2}{2}} + \frac{\mu - 2}{2} w_j \lambda_{0,j}^{\frac{\mu_p}{2}} A_j^{\frac{\mu_p - 4}{2}} = \\ &= tr\left( E \frac{\partial Q_\sigma}{\partial \theta} \right) + \frac{\mu_j - 2}{2} w_j \lambda_{0,j}^{\frac{\mu_j}{2}} A_j^{\frac{\mu_j - 4}{2}} \end{aligned} \tag{5.18}$$

where $E$ is a diagonal matrix with the *i*-th diagonal element given by

$$E_{ii} = \frac{\mu_i}{2} w_i \lambda_{0,i}^{\frac{\mu_i - 2}{2}} A_i^{\frac{\mu_i - 2}{2}} \tag{5.19}$$

and $\frac{\partial Q_\sigma}{\partial \theta_j}$ is the gradient of the matrix of the stresses in each member with respect to the parameter $\theta_j$. Noting that the covariance matrix of the stresses is connected to the covariance matrix of the displacements through the relationship

$$Q_\sigma = CQC^T \tag{5.20}$$

the derivative of the stress covariance matrix is given by

$$\frac{\partial Q_\sigma}{\partial \theta_j} = C \frac{\partial Q}{\partial \theta_j} C^T \tag{5.21}$$

By introducing the equation (5.21) in (5.18) one has

$$\begin{aligned} \frac{\partial J}{\partial \theta_j} &= tr\left( EC \frac{\partial Q}{\partial \theta_j} C^T \right) + \frac{\mu_j - 2}{2} w_j \lambda_{0,j}^{\frac{\mu_j}{2}} A_j^{\frac{\mu_j - 4}{2}} = \\ &= tr\left( C^T EC \frac{\partial Q}{\partial \theta_j} \right) + \frac{\mu_j - 2}{2} w_j \lambda_{0,j}^{\frac{\mu_j}{2}} A_j^{\frac{\mu_j - 4}{2}} = \\ &= tr\left( \Sigma \frac{\partial Q}{\partial \theta_j} \right) + \frac{\mu_j - 2}{2} w_j \lambda_{0,j}^{\frac{\mu_j}{2}} A_j^{\frac{\mu_j - 4}{2}} \end{aligned} \tag{5.22}$$

where

$$\Sigma = C^T EC \tag{5.23}$$

Following adjoint method presented in Chapter 2, the derivatives of the augmented objective function $J^*(\underline{\theta})$ with respect to the design variables $\theta_j$ are given by

$$\frac{\partial J^*}{\partial \theta_j} = -tr\left(\Lambda\left(\frac{\partial A}{\partial \theta_j}Q + Q\frac{\partial A^T}{\partial \theta_j}\right)\right) - tr\left(\Lambda\left(\frac{\partial B}{\partial \theta_j}S^*B^T + BS^*\frac{\partial B^T}{\partial \theta_j}\right)\right) + \\ + \frac{\mu_j - 2}{2} w_j \lambda_{0,j}^{\frac{\mu_j}{2}} A_j^{\frac{\mu_j - 4}{2}} \tag{5.24}$$

where $\Lambda$ satisfies the adjoint equation

$$\Lambda A + A^T \Lambda - \Sigma = 0 \tag{5.25}$$

defined in Chapter 2.

## 5.3 Design Optimization of Truss Structures under Stochastic Fatigue

In the following paragraph results for the case of design optimization under fatigue on truss structures, are presented. The structure that is optimized is the truss structure described in Chapter 3. In order to apply the proposed methodology, it is assumed that the width of each truss member is much greater than the thickness, and therefore each member behaves as plate. For demonstrating the effectiveness of the methodology, failure due to buckling of the members is neglected in the design optimization. However, such failure criteria could be introduced in the optimization. The performance function is selected to be the weighted sum of the expected fatigue lifetime of the truss members of the structure, with all the weights chosen to be equal. In this case, the optimization problem is stated in (5.9) - (5.12), Additionally, an additional nodal mass equal to 5kg divided by the degrees of freedom of each system is added at all the nodes of the truss structure. The volume constant $V_0$ is chosen to be equal to $10^{-5}\,\mathrm{m}^3$. The value of the power spectral density of the white noise excitation is chosen to be equal to 1000. For simplicity and illustration purposes, results are presented in for the case in $\varepsilon_p \to 0$ in (5.3). Also, the value of the Young's modulus is considered to be equal to one, when used in the estimation for the matrix $C$ in (5.20).

The optimal truss structures that consist of one up to ten base parts $N_b$ are presented in Figure 5.1 to Figure 5.10. Additionally, in Table 5.1 are shown the optimal values of the objective function $J$ for the different structures of one up to ten base parts, information which is also plotted in Figure 5.11. Note that in Table 5.1 an additional column with the values of the objective function $J^*$ is shown. The objective function $J^*$ is chosen to be equal to the maximum fatigue lifetime across the lifetimes calculated at the truss elements. This definition is very useful when one needs to compare the optimal solutions of structures with different number of base parts. This comparison is not useful using the objective function $J$, as the number of the truss members at the optimal solution change with respect to the number of base parts, thus the number of terms in the summation of the objective function $J$ also changes. Therefore, in order to define the optimal solution between the optimal solutions with different number of base parts, the objective function $J^*$ should be used. The values of the objective function $J^*$ that correspond to the optimal solutions are presented Figure 5.12. It is observed that the structure with the minimum value of the objective function $J^*$, consists of one base part, that is the optimal structure for loading is the structure that is shown in Figure 5.1.

It is observed that the optimization trend is similar to the optimization trend observed in Case G of the optimization using as performance function the weighted sum of the stresses in the truss members. That is all vertical members are eliminated, except for the case of two base parts, where two vertical members are not eliminated. Furthermore, the middle horizontal members are also eliminated, whereas the bottom and top edge horizontal members are kept in place. It should be noted that for all base parts considered, the values at the top and bottom horizontal members are decreasing as one moves from the left towards the right side of the structure. Additionally, the values of the cross sections of the diagonal members that are kept in place also show this decreasing behavior, from the left towards the right side of the structure. Similarly to the case of stress – based performance function, the cross sections of the diagonal elements close to the right end tend to increase.

Similar to Case G, local optimal solutions also exist for this case and for four base parts. These local optimal topologies are presented in Figure 5.13 and in Figure 5.14. The values of the objective function are equal to $0.06647\times10^{-6}$ and $0.06186\times10^{-6}$ for the local optimal solutions respectively, whereas the value for the global solution shown in Figure 5.4 is equal to $0.05739\times10^{-6}$.

It is also worth mentioning that up to six base parts the optimal structure is, as should be expected, symmetric with respect to the middle horizontal axis. However, for seven up to ten base parts such symmetry did not arise in the numerical optimization. In fact, an asymmetric structure was obtained, which is contrary to the expectations. The asymmetric solution can be considered to be a local solution. The global symmetric solution for such problems was not predicted numerically. In such cases of asymmetrical solutions, the mirrored structure with respect to the horizontal middle axis is also a solution of the topology optimization is also a local solution. One such mirrored optimal structure is shown in Figure 5.15 for the case of seven base parts, noting that the value of the objective function is equal to the initial solution shown in Figure 5.7.

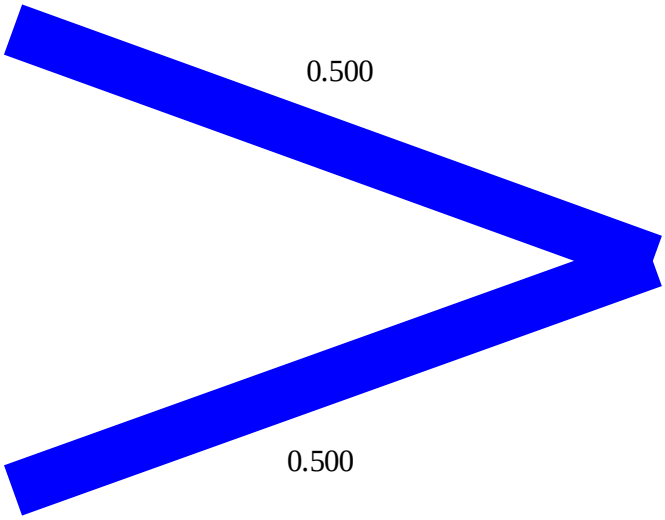


**Figure 5.1:** Optimal solution for one base part.

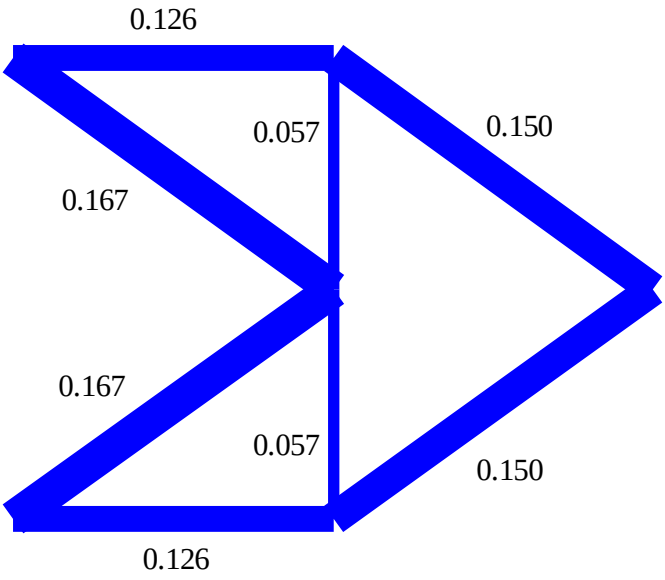


**Figure 5.2:** Optimal solution for two base parts.

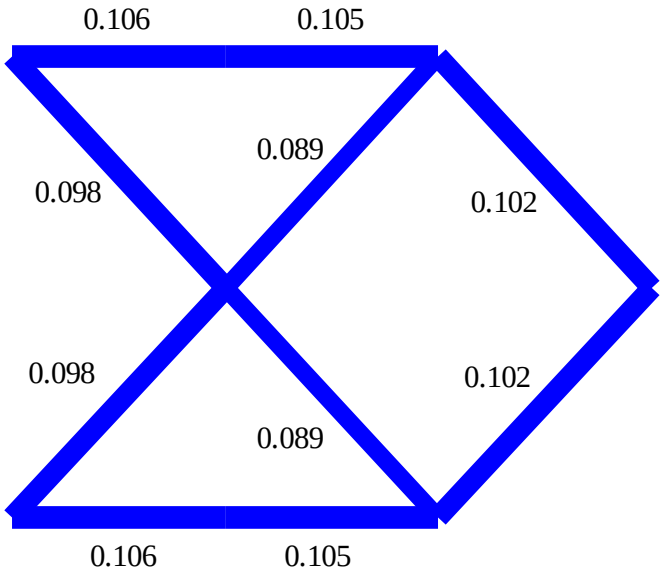


**Figure 5.3:** Optimal solution for three base parts.

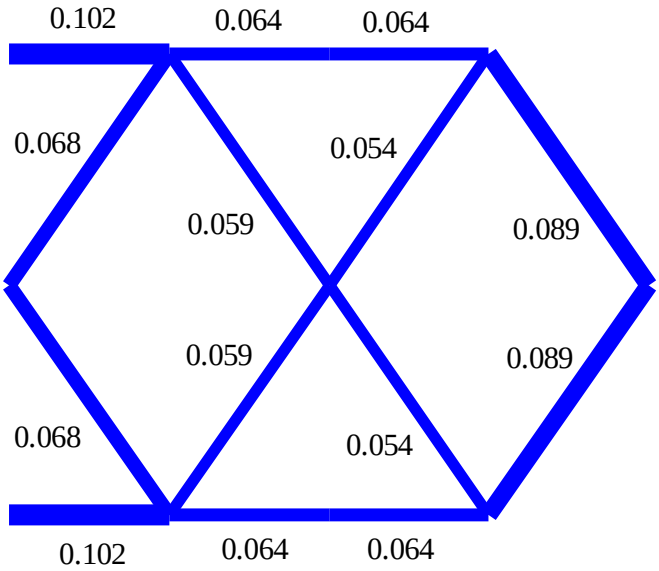


**Figure 5.4:** Optimal solution for four base parts.

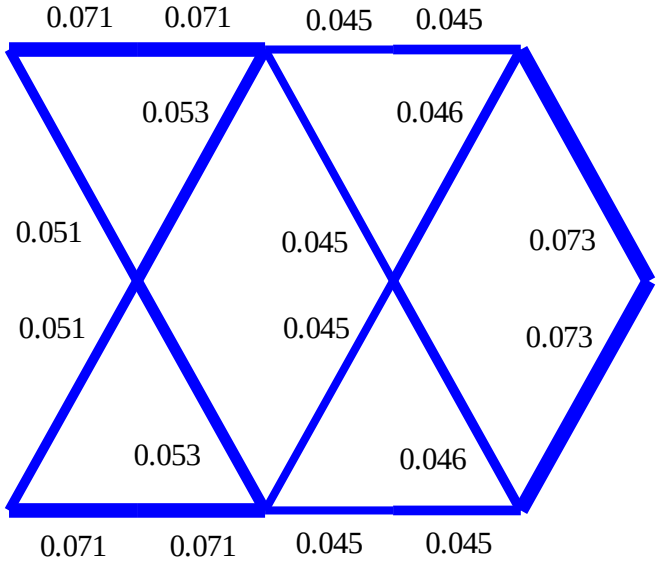


**Figure 5.5:** Optimal solution for five base parts.

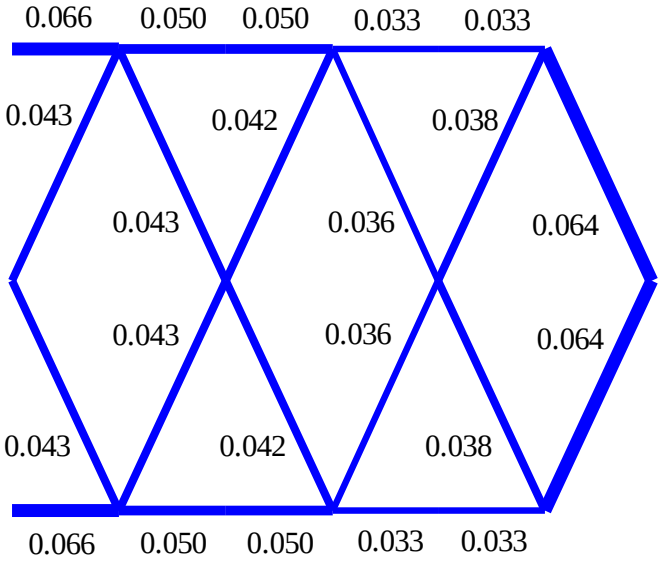


**Figure 5.6:** Optimal solution for six base parts.

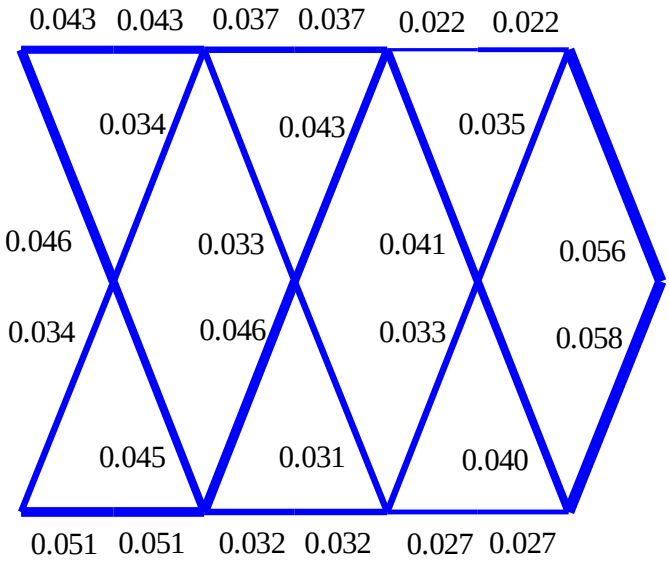


**Figure 5.7:** Optimal solution for seven base parts.

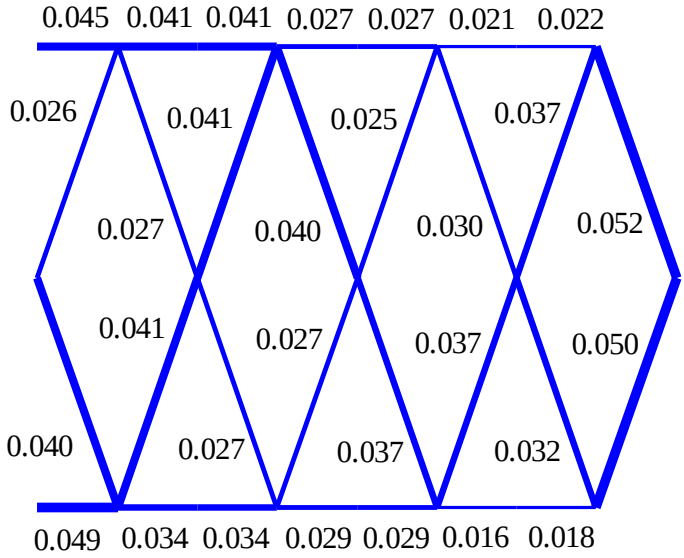


**Figure 5.8:** Optimal solution for eight base parts.

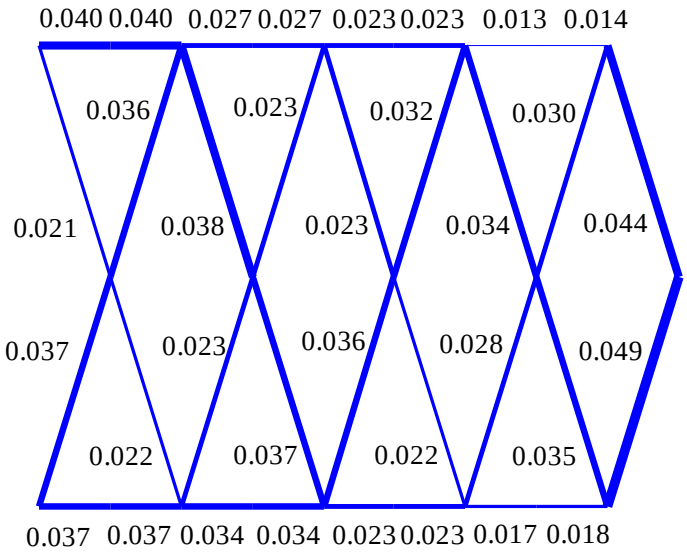


**Figure 5.9:** Optimal solution for nine base parts.

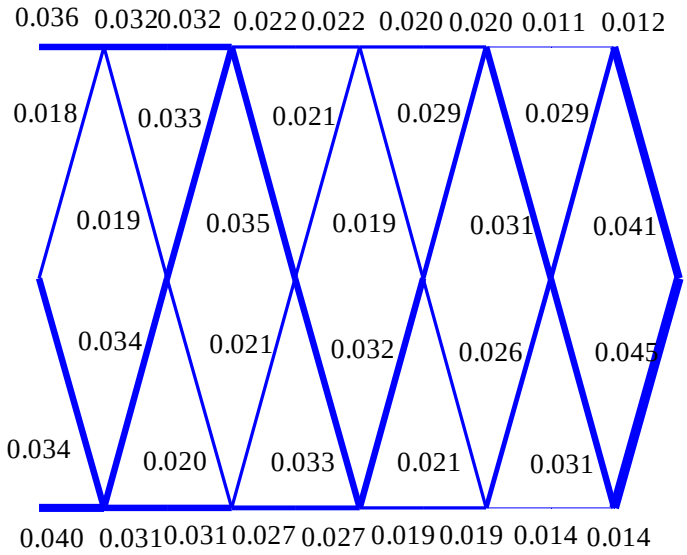


**Figure 5.10:** Optimal solution for ten base parts.

**Table 5.1:** Values of the objective function for one to ten base parts.

| Parts | $J\ (\times 10^{-6})$ | $J^{*}(\times 10^{-6})$ |
|---|---|---|
| 1 | 0.02489 | 0.00995 |
| 2 | 0.05866 | 0.2201 |
| 3 | 0.05417 | 0.1762 |
| 4 | 0.05739 | 0.2172 |
| 5 | 0.05764 | 0.2129 |
| 6 | 0.05840 | 0.2678 |
| 7 | 0.06008 | 0.3237 |
| 8 | 0.06425 | 0.3276 |
| 9 | 0.06775 | 0.3358 |
| 10 | 0.07160 | 0.3489 |

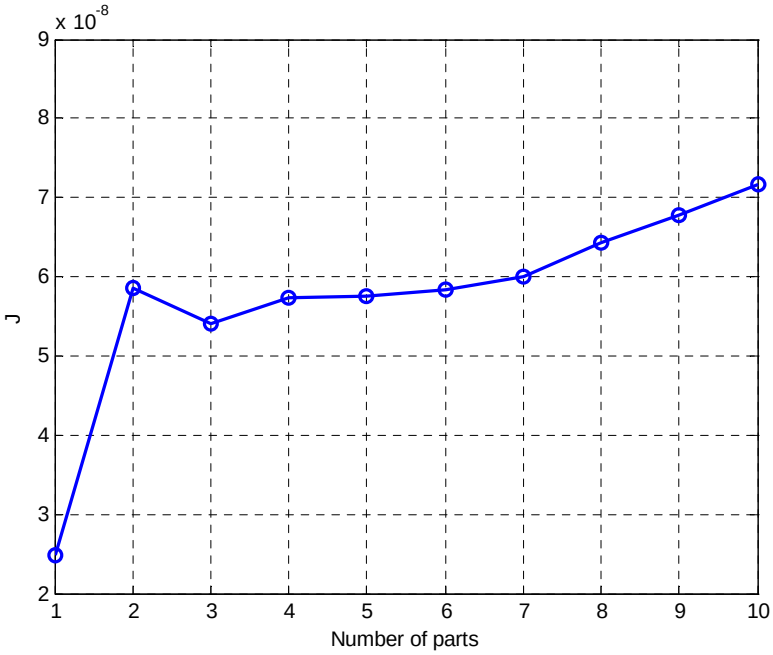


**Figure 5.11:** Optimal values of the objective function $J$ with respect to the number of base parts of the structure.

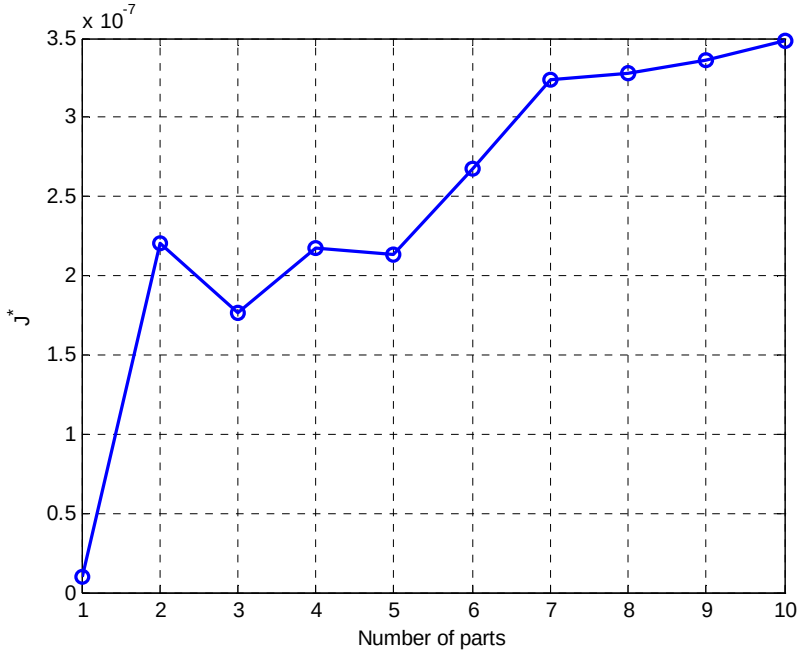


**Figure 5.12:** Optimal values of the objective function $J^*$ with respect to the number of the parts of the structure.

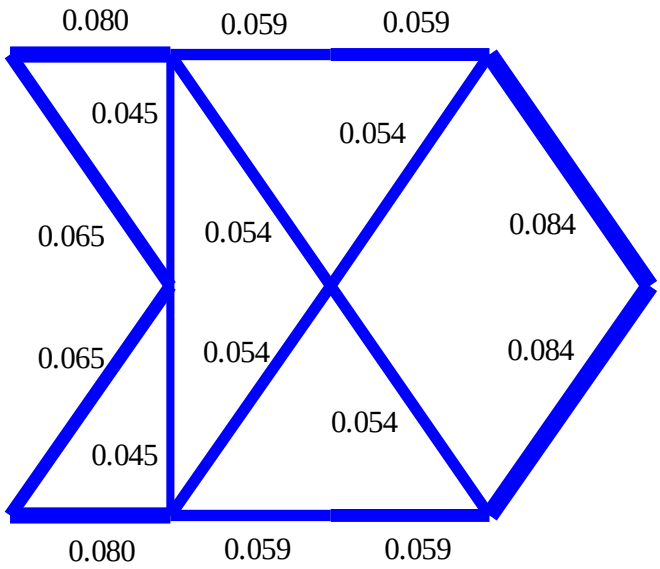


**Figure 5.13:** Local optimal solution for four base parts.

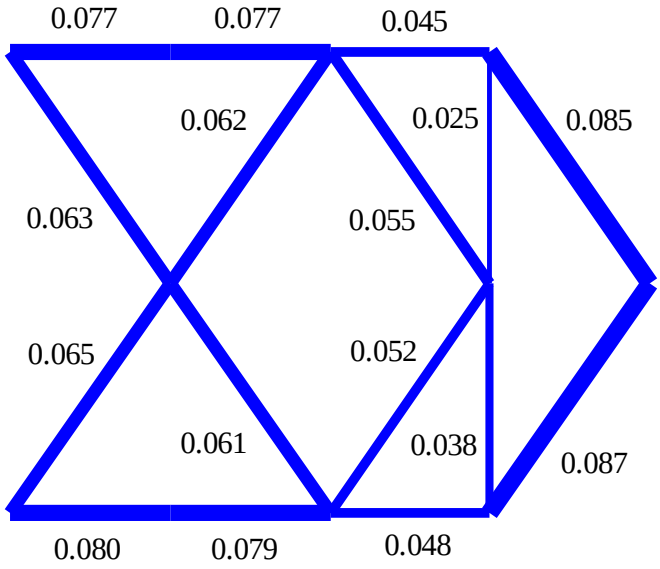


**Figure 5.14:** Local optimal solution for four base parts.

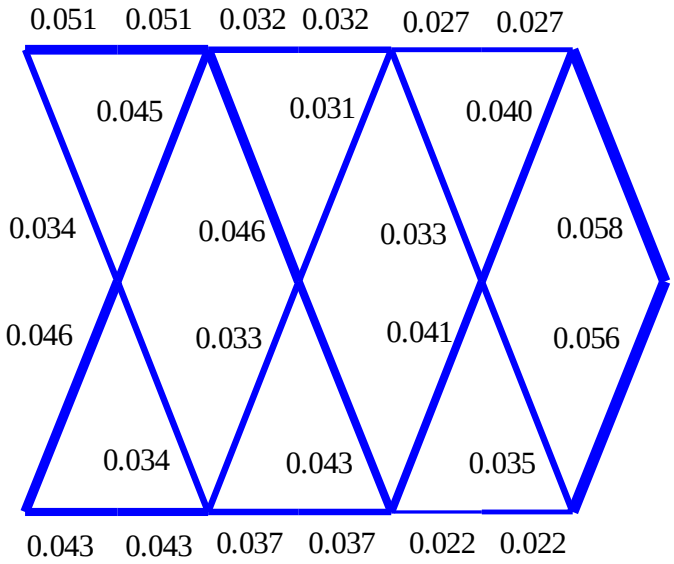


**Figure 5.15:** Asymmetrical solution for seven base parts.

## 5.5 Conclusions

A methodology is proposed for design optimization taking into account the fatigue lifetime of the system under the influence of stochastic dynamic loadings. Assuming independence of the shape factor $B$ from the crack length, an simple and efficient objective function for the optimization problem is constructed. Certain similarities between the fatigue – bases performance function and the stress – based performance function are revealed. It is shown that the stress – based performance function is a special case of the fatigue – based performance function, resulting by appropriately choosing the exponents arising in the formulation for the fatigue – based performance function. The derivatives of the objective function with respect to the design variables are shown that can be effectively estimated using the adjoint method. The proposed methodology is applied on the sizing and topology optimization of two dimensional truss structures, constructed with different number of base parts, under white noise excitation.

It is shown that the optimal configurations obtained for the truss structures are quite similar to the results obtained for Case G of the stress – based performance

function in Chapter 3, as expected, due to the fact that the performance functions for these two cases are proven to be similar. It is also shown that the optimal configuration in this case consists of one base part, as in Case G, despite the slight differences at the formulation of the objective function. Also, multiple local and global solutions may arise, as it was shown in the case of the structure that consists of four base parts. Such local solutions complicate the optimization problem and the search for the global optimum using gradient – based optimization algorithms. Additionally, asymmetrical solutions may also arise, along with the mirrored asymmetrical solution. These asymmetrical solutions were at first considered to be local optimal solutions. However, extensive numerical search using different initial values of the design variables has not yielded better symmetrical solutions. Therefore, these asymmetrical solutions where accepted as global optimal solutions.

# CHAPTER 6 Conclusions – Future Work

## 6.1 Conclusions

The problem of design optimization of dynamic systems under stochastic excitations was addressed in this thesis. Methodologies for design optimization of structures under stochastic dynamic loadings, were proposed. In addition, methodologies for the estimation of fatigue lifetime and reliability of structures were developed. The methodologies use second moments of the output stress process in order to efficiently estimate the fatigue lifetime, in a coupled or non – coupled response degradation framework. Finally, the fatigue lifetime prediction methodologies were incorporated into the design optimization methodology based on fatigue lifetime performance indices as well.

An innovative methodology for the optimization of the performance of multi-degree-of-freedom systems, under stochastic dynamic excitations was presented. The design optimization was formulated as a constrained optimization problem, with the objective function related to structural performance measures, the inequality constrains related to cost measures and the equality constrains related to the governing equations of motion of the system. The performance measures were associated with the second order statistics (e.g. variance). The performance of the system response was quantified by different measures of the response, such as the weighted sum of the variance of the nodal displacements or the weighted

sum of the variance of the developed stresses in the structural parts. The variance of the response quantities was conveniently obtained by solving the Lyapunov equation for the system. The adjoint formulation was used in order to efficiently and accurately estimate the derivatives of the objective function with respect to the design variables, thus minimizing the computational effort needed to estimate the derivatives numerically. The formulation of the optimization problem was presented for both Gaussian white noise excitation and filtered white noise excitation. The proposed methodology has been extended to the modal space, in order to take advantage of the efficiency of modal analysis, by using a limited number of contributing modes for the estimation of the system response, under white and filtered noise excitation. Finally, the proposed methodology was applied on the sizing optimization of a simple 2DOF bar – mass system in order to illustrate its applicability. It was shown that the optimal results for different cases of performance functions are slightly different.

The proposed methodology for design optimization of structures under stochastic dynamic excitations was applied on the sizing and topology optimization of truss structures. An iterative method for the simultaneous optimization of the size and the topology of trusses was developed. Different types of performance functions were used, such as the weighted sum of the variance of the nodal displacements or the weighted sum of the variance of the developed stresses in the structural members. The cross sectional areas of the truss members, as well as the location and the number of nodes were chosen as the design variables. First, the methodology of design optimization under deterministic static load was considered, using as performance function the displacement of the system along the degree of freedom on which the loading is imposed, and the weighted sum of the displacements at all the degrees of freedom. The optimal results presented, showed similar trends with slight differences between the two cases, as far as the optimal cross sectional areas are concerned. It has also been shown that local optimal solutions may appear for specific cases, that complicate the search for the global optimal solution using gradient based optimization algorithms.

The modal space approach was also applied on the sizing and topology optimization of truss structures, in order to examine how the use of limited number of contributing modes in the estimation of the variance of the response affects the optimal solutions. It was shown that, in many cases, a small fraction of contributing modes in relation to the DOF of the structure can lead to quite satisfactory results compared to the optimal results obtained in the previous cases. In particular, for the example case considered, for ten contributing modes, the

optimal results are almost identical to the optimal structures obtained at the previous case. This fact can lead to a significant reduction of the computational cost of the optimization in many cases. Finally, it was shown that if all the modes of each system contribute to the estimation of the variance of the response, the results are identical to the results obtained for the time domain method, with minor differences been attributed to the different models used for of the system damping.

A general formulation and an effective method for predicting the fatigue lifetime in randomly vibrating linear multi-degree-of-freedom systems/structures was also proposed. The analysis is based on the coupled response-degradation model and it takes into account a wide-band spectrum of the stress process. The fatigue process is characterized by crack growth in the structural components and is represented by Paris equation in which the stress range is evaluated form the multi-dimensional random response of the system. Both the stiffness degradation due to fatigue during the vibration, and non-degrading case were taken under consideration. The stress range was approximated by either the spectral moments or the empirically motivated and widely used Dirlik's probability distribution. The prediction capabilities of the proposed analyses were demonstrated using special classes of single and multi-degree of freedom structural systems. For the formulation based on spectral moments in the non-degrading case, it was demonstrated that the inclusion of the spectral width parameter in the model prolongs the time of failure of the system. As far as the formulation based on Dirlik's formula in the non-degrading case is concerned, more conservative estimates of failure times corresponding to small failure probabilities were obtained, than the estimates provided by the spectral moments, which correspond to failure probabilities very close to one. Finally, it was shown that stiffness degradation accelerates failure due to fatigue in the various structural components.

Finally, a methodology for design optimization taking into account the fatigue lifetime of the system under the influence of stochastic dynamic loadings, was proposed. Assuming stationary, broad - band response, a simple objective performance function for the optimization problem was constructed. The sensitivity of the objective function with respect to the design variables was shown that can be very effectively estimated using the adjoint formulation. The proposed methodology was also applied on the sizing and topology optimization of truss structures, under white noise excitation. As far as the sizing problem is concerned, it was shown that the optimal configurations obtained by optimizing the fatigue lifetime of the structure are quite similar to the optimal configurations

obtained minimizing the stresses. This is due to the fact that the performance functions for these two cases are proven to be closely related.

## 6.2 Future Work

In the future, this work can be extended to address the following issues:

- Include the uncertainty of the structural parameters. The problem of the uncertainty at the nodal coordinates can be addressed, as well as the uncertainty of the material properties, such as the Young's modulus and/or the density of the material. Both these cases require the calculation of the expected value of the stiffness and mass matrices of the system, as well as their sensitivities to the design variables in order to take advantage of the adjoint formulation for more efficient optimization.
- Extend the applications to optimize two or three-dimensional truss structures or general two or three-dimensional probabilistic systems, such as plates, shell, beams or solid finite element models.
- Extend the optimization framework to account for non stationary stochastic excitations models. Existing models which simulate ground motion could be used, such as the general non-stationary model proposed by Atkinson and Silva (2000).
- Generalize the fatigue lifetime prediction problem to account for biaxial and multi-axial stress states. In order to achieve this, a different measure of the stress range should be used. Such a measure could be the covariance of an equivalent stress, such as the Tresca or Von Misses equivalent stress. Additionally, structural uncertainty can also be included in the methodologies, such as uncertainty in the material properties.
- Apply all the aforementioned extensions in the design optimization under fatigue. Specifically, as a first step, broad band stochastic excitations can be included in the model, simply by allowing non-zero spectral width parameter $\varepsilon$ and recalculating the sensitivities of the objective function with respect to the design parameters. Furthermore, the fatigue-induced stiffness degradation of the structural parts that contain the crack can be introduced into the objective function. Additionally, the methodology can be augmented to include structures, that two or three dimensional stress fields are developed, by using as a measure of the stress range, the covariance of an equivalent stress, as discussed previously. On the other hand, in order to evaluate the expected fatigue lifetime for the optimization, available

frequency domain stochastic fatigue methods based on Palmgren-Miner damage rule, S-N fatigue curves can be used (Palmgren, 1924, Miner, 1945).

- Extend the performance function to account for failure probability instead of second order statistics.
- Incorporate in the design optimization framework, component mode synthesis techniques. Using such methodologies, one could optimally design a component of a complex structure, given the design of the other components.

## References

Au S.K., Papadimitriou C., Beck J.L., (1999), "Reliability of uncertain dynamical systems with multiple design points", *Structural Safety*, **21**, 113-133.

Atkinson, G. M., Silva W., (2000), "Stochastic modelling of California ground motions", *Bulletin of the Seismological Society of America*, **90(2)**, 255-274.

Baker J., Cornell C.A., (2003), "Uncertainty specification and propagation for loss estimation using FOSM methods," *PEER Technical Report* #2003-07.

Beck J.L., Chan E., Irfanoglu A., Papadimitriou C., (1999), "Multi-criteria optimal structural design under uncertainty," *Earthquake Engineering and Structural Dynamics*, **28**, 741-761.

Benasciutti D., Tovo R., (2005), "Spectral methods for lifetime prediction under wide-band stationary random processes", *International Journal of Fatigue*, **27**, 867-877.

Bendsoe M.P, Kikuchi N., (1988), "Generating optimal topologies in structural design using a homogenization method". *Computer Methods in Applied Mechanics and Engineering*, **71**, 197-224.

Bendsoe M.P, Sigmund O., (2003), "Topology Optimization: Theory, Methods and Applications", Berlin, Heidelberg: Springer-Verlag.

Bishop N., (1994), "Spectral methods for estimating the integrity of structural components subjected to random loading", Handbook of fatigue crack propagation in metallic structures, Elsevier Science, 1685-1720.

Bogdanoff, J.L., Kozin, F., (1985), "Probabilistic Models of Cumulative Damage", Wiley, New York.

Christiansen S., Patriksson M., Wynter L., (2001), "Stochastic bilevel programming in structural optimization", *Structural and Multidisciplinary Optimization*, **54**, 361-371.

Cramer H., Leadbetter M.R., (1967), "Stationary and Related Stochastic processes", John Willey & Sons, New York.

Dirlik T., (1985), "Applications of Computers to Fatigue Analysis", PhD Thesis, Warwick University.

Du J, Olhoff N. (2007), “Topological design of freely vibrating continuum structures for maximum values of simple and multiple eigenfrequencies and frequency gaps”, *Structural and Multidisciplinary Optimization*, **34**, 91-110.

Evgrafov A., Patriksson M., (2003), “Stochastic structural topology optimization: discretization and penalty function approach”, *Structural and Multidisciplinary Optimization*, **25**, 174-188.

Evgrafov A., Patriksson M., Petersson J., (2003), “Stochastic structural topology optimization: existence of solutions and sensitivity analysis”, *Z. Angew. Math. Mech.* **83**, 479-492.

Gear C.W., (1971), “Numerical Initial Value Problems in Ordinary Differential”, Prentice Hall.

Grigoriu M., (1990), “Reliability of degrading systems”, *Structural Safety*, **8**, 345-351.

Guest J.K., Igusa T., (2008), “Structural optimization under uncertain loads and nodal locations”, *Computer Methods in Applied Mechanics and Engineering*, **198(1)**, 116-124.

Kosaka I., Swan C.C., (1999), “A symmetry reduction method for continuum structural topology optimization”. *Computers and Structures*, **70**, 47-61.

Krajcinovic, L.M., (1986), “Introduction to Continuum Damage Mechanics”, Martinus Nijhoff. Pub.

Lin Y.K. and Cai G.Q., (1995), “Advanced Probabilistic Dynamics”, Mc-Graw Hill, New York.

Liou H.Y., Wu W.F., Shin, C.S., (1999), “A modified model for the estimation of fatigue life derived from random vibration theory,” *Probabilistic Engineering Mechanics,* **14,** 281-288.

Lutes L.D., Sarkani S., (2003), “Random Vibrations: Analysis of Structural and Mechanical Systems”, Butterworth-Heinemann.

Ma Z.D., Cheng H.C., Kikuchi N., (1995), “Topological design for vibrating structures”, *Computer Methods in Applied Mechanics and Engineering*, **121**, 259-280.

Miannay D.P., (1998), “Fracture Mechanics”, Springer, New York.

Miner M.A., (1945), "Cumulative damage in fatigue", *Applied Mechanics Transactions, ASME*, **12(3)**, 159-164.

Morrow J.D., (1986), "The effect of selected subcycle sequences in fatigue loading histories", *Random Fatigue Life Prediction, ASME Publications*, **72**, 43-60.

Nelson R.B., (1976), "Simplified calculation of eigenvector derivatives", AIAA Journal, **14 (9)**, 1201-1205.

Ntotsios E., Papadimitriou C. (2008). "Multi-objective Optimization Algorithms for Finite Element Model Updating", *ISMA2008 International Conference on Noise and Vibration Engineering*, September 15-17, 2008, Leuven, 1895-1909.

Palmgren A., (1924), Die Lebensdauer von Kugallagern, VDI-Zeitschrift, **68(14)** 339-341.

Papadimitriou C., Katafygiotis L.S., Au S.K., (1997), "Effects of structural uncertainties on TMD design: A reliability-based approach," *Journal of Structural Control*, **4(1),** 65-88.

Papalukopoulos C., Natsiavas S., (2007), "Dynamics of large scale mechanical models using multilevel substructuring", *Journal of Computational and Nonlinear Dynamics*, **1**, 40-51.

Pedersen N.L., (2000), "Maximization of eigenvalues using topology optimization", *Structural and Multidisciplinary Optimization*, **20**, 2-11.

Porter K.A., Beck J.L., Shaikhutdinov R.V., (2002), "Investigation of sensitivity of building loss estimates to major uncertain variables for the Van Nuys testbed", Report to PEER Center, Berkeley. 41pp.

Ravilly E., (1938), "Contribution a l' etude de la rupture des fils metalliques soumis a des torsion alternees," *Publications Scientifiques et Techniques du Ministere de L' Air*, **120**, 52-70.

Roberts J. B., (1978), "The response of an oscillator with bilinear hysteresis to stationary random excitation", *ASME Journal of Applied Mechanics*, **45**, 923-928.

Rozvany G., Zhou M., Birker T., (1992), "Generalized shape optimization without homogenization", *Structural Optimization*, **4**, 250-252.

Shlyannikov V.N., Braude N.Z., (1992), "A model for prediction crack growth rate for mixed mode fracture under biaxial loads", *Fatigue and Fracture of Engineering Materials and Structures*, **15(9)**, 825-844.

Sigmund O., (1997), "On the design of compliant mechanisms using topology optimization", *Mechanics of Structures and Machines*, **25(4)**, 493-524.

Sigmund O, Petersson J., (1998), "Numerical instability in topology optimization: a survey on procedures dealing with checkerboards, mesh-dependencies and local minima", *Structural Optimization*, **16**, 68-75.

Sobczyk K., (1987), "Stochastic models for fatigue damage of materials," *Advances in Applied Probability*, **19**, 652-673.

Sobczyk K., (1991), "Stochastic Differential Equations with Applications to Physics and Engineering", Kluwer Acad. Publ., Dordrecht.

Sobczyk K. and Spencer B.F., (1992), "Random Fatigue: From Data to Theory", Academic Press, Boston.

Sobczyk K. and Trebicki J., (1995), "Modeling of curvilinear random fatigue crack growth", *Engineering Fracture Mechanics*, **52(4)**,703-715.

Sobczyk K. and Trebicki J., (1999), "Stochastic response of degrading stochastic systems", Rheology of Bodies with Defects (ed. R.Wang), Proc. IUTAM Symp., Kluwer Acad. Publ., Dordrecht.

Sobczyk K. and Trebicki J., (2000), "Stochastic dynamics with fatigue induced stiffness degradation", *Probabilistic Engineering Mechanics*, **15**, 91-99.

Soong T.T. and Grigoriu M., (1993), "Random Vibrations of Structural and Mechanical Systems", Prentice Hall, New Jersey.

Tenek L.H., Hagiwara I., (1994), "Eigenfrequency maximization of plates by optimization of topology using homogenization and mathematical programming", *JSME International Journal*, **37**, 667-677.

Wang M.Y., Wang X., Guo D., (2003), "A level set method for structural topology optimization", *Computer Methods in Applied Mechanics and Engineering*, **192**, 227-246.

Weibull W., (1939), "A statistical theory of the strength of materials," *Ingeneiors Vetenshaps Akademien Handlingar*, **151**, 1-29.

Wen Y.K., (1986), "Stochastic response and damage analysis of inelastic structures", *Probabilistic Engineering Mechanics*, **1**, 57-69.

Wohler A., (1870), “Versuche uber die festigheir der eisen-bahkwagen,” Achsen. *Zeitschrift fuer bauwesen*.

Xie Y.M., Steven G.P., (1993), “A simple evolutionary procedure for structural optimization”, *Computers and Structures*, **49**, 885-96.

Xie Y.M., Steven G.P., (1996), “Evolutionary structural optimization for dynamic problems”, *Computers and Structures*, **58,** 1067-1073.

Xie Y.M, Steven G.P. (1997), “Evolutionary Structural Optimization”, Springer, London.

Yang X.Y., Xie Y.M., Steven G.P., Querin O.M.. (1999a), “Bidirectional evolutionary method for stiffness optimization”. *AIAA Journal*, **37(11)**, 1483-1488.

Yang X.Y., Xie Y.M., Steven G.P., Querin O.M., (1999b), “Topology optimization for frequencies using an evolutionary method”. *Journal of Structural Engineering*, **125(12),** 1432-1438.

Zhao C, Steven G.P., Xie Y.M., (1997), “Evolutionary natural frequency optimization of two-dimensional structures with additional non-structural lumped masses”, *Engineering with Computers*, **14(2)**, 233-251.

Zhou M., Rozvany G., (1991), “The COC algorithm. Part II: Topological geometry and generalized shape optimization”, *Computer Methods in Applied Mechanics and Engineering*, **89**, 197-224.